Geometric Interpretation of Lunar Craters

GEOLOGICAL SURVEY PROFESSIONAL PAPER 1046–C

Prepared on behalf of the
National Aeronautics and Space Administration

GEOMETRIC INTERPRETATION OF LUNAR CRATERS

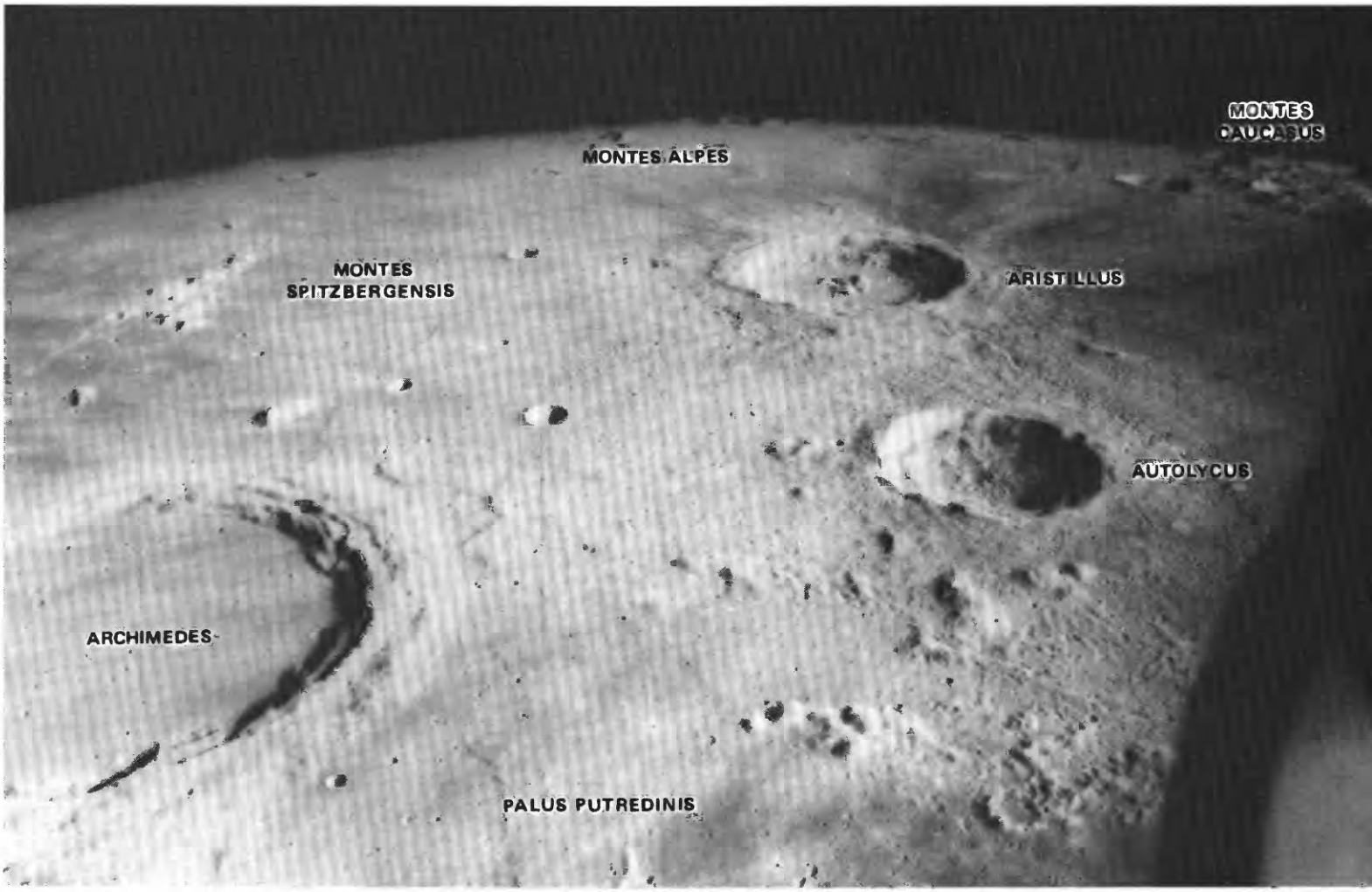

Impact craters and other features on the Moon, photographed by Apollo 15 crew while in orbit 106 km above surface on July 31, 1971. Oblique view is north across eastern Mare Imbrium. The horizon lies about 500 km from the lava-flooded 80-km-diameter crater Archimedes. Out-of-focus object in lower right corner is part of Command Service Module. Sun is to right. Apollo 15 mapping-camera photograph 1540.

Geometric Interpretation of Lunar Craters

By RICHARD J. PIKE

APOLLO 15–17 ORBITAL INVESTIGATIONS

GEOLOGICAL SURVEY PROFESSIONAL PAPER 1046–C

Prepared on behalf of the
National Aeronautics and Space Administration

UNITED STATES GOVERNMENT PRINTING OFFICE, WASHINGTON : 1980

UNITED STATES DEPARTMENT OF THE INTERIOR

CECIL D. ANDRUS, *Secretary*

GEOLOGICAL SURVEY

H. William Menard, *Director*

Library of Congress Cataloging in Publication Data

Pike, Richard J.
Geometric interpretation of lunar craters.

(Apollo 15-17 orbital investigation) (Geological Survey professional paper : 1046-C)
Bibliography: p. C60-C65.
Supt. of Docs. no.: I 19.16:1046-C
1. Lunar craters–Data processing. 2. Lunar craters– Statistical methods. I. Title. II. Series. III. Series: United States. Geological Survey. Professional paper ; 1046-C.
QB591.P73 559.9'1 79-607927

For sale by the Superintendent of Documents, U.S. Government Printing Office
Washington, D.C. 20402

CONTENTS

ILLUSTRATIONS

TABLES

GEOMETRIC INTERPRETATION OF LUNAR CRATERS

By RICHARD J. PIKE

ABSTRACT

Geometric properties of the Moon's craters between about 400 m and about 300 km across have been examined at a high and hitherto unattainable level of accuracy using new topographic measurements made on contour maps compiled from Apollo 15–17 photographs. Values of diameter, depth, rim height, rim width, rim-crest circularity, and (where applicable) floor diameter are tabulated here for 623 lunar craters belonging to 11 morphologic categories. Craters of the main sequence—the typical lunar craters customarily interpreted as having formed by impact—have remarkably similar morphologies, regardless of their location on the Moon. Craters on the far side do not differ in shape from near-side craters, and, except for evenness of the rim crest, craters on the maria are much like craters on the uplands. Nor is there any influence of lunar azimuth on the relative height of a crater rim, as once had been thought. Craterlets atop central peaks in large craters of the main sequence do not appear to be volcanic, and the enigmatic feature Linné is revealed as a quite ordinary impact crater.

The origin of the Moon's craters is treated as a formal problem in numerical taxonomy, using 11 types of lunar craters and 12 types of candidate terrestrial analogs. Lunar craters fall into two main morphologic and genetic categories—impact craters and volcanoes—according to a principal-components analysis and a cluster analysis of their surface dimensions. Main-sequence craters on the Moon most closely resemble terrestrial meteorite-impact craters and are much less like terrestrial maars or tuff rings. Terrestrial calderas are particularly poor analogs of the typical lunar craters. Smooth-rimmed lunar craters also resemble normal impact craters rather than calderas. Secondary-impact craters, craters atop lunar domes and cones, and dark-halo craters along some rilles all differ substantially in shape from main-sequence craters. The lunar domes and cones have the shapes of true central volcanoes, but dark-halo craters and secondary-impact craters—like terrestrial maars—are intermediate between the two main morphologic groups. Although single topographic variables such as depth/diameter and circularity cannot confidently indicate the genesis of any one crater of the Moon, multivariate statistical models constructed from several variables can distinguish consistently between volcanoes and large impact craters.

Eleven changes in the shape of fresh impact craters on the Moon occur within a diameter range of 10 to 30 km (average, 17.5 km) and mark the transition from simple small craters to large complex or modified craters. The seven ratio-level variations—those of rim-crest diameter with depth, rim height, flank width, rim-wall slope, floor diameter, circularity, and rim-crest evenness—all are defined for fresh-looking craters from the new Apollo data and expressed mathematically where practicable. These relations constitute a shape model that constrains interpretations of fresh craters on the Moon. The size-dependent changes reflect the occurrence of central peaks, rim-wall terraces, and a flat floor within craters over 10 to 20 km across. Interpretation of these features remains speculative. The threshold diameter probably is the maximum size reached by stable crater-landforms having only a simple morphology. The changes in crater shape may depend principally upon the manner in which the Moon's gravity and rock strength interact with the stresses and pressures generated by impact to control flowage, collapse, or elastic recoil of the target materials during crater formation. A similar interpretation probably applies to craters on other planets, but the threshold sizes at which craters change shape differ according to values of gravitational attraction and other properties.

INTRODUCTION

Rimmed circular depressions of a similar morphology dominate the landscape of the Moon at all scales. Indeed, the very monotony of crater shapes makes them at once both the most interesting and the least remarkable of all lunar surface features. Although interpretation of craters and other landforms preoccupied most observers throughout the long era of telescopic and photographic analysis before the Apollo program, establishment of seismic stations on the Moon and the availability of lunar rock samples and gravity and remotely sensed chemical data now have shifted overall emphasis in lunar science from solely geomorphology to include geophysics and geochemistry. This broader orientation can be expected to persist as a framework for further exploration of the planets, because the varied approaches complement one another. The development of lunar physics and chemistry has provided information that classical observers of the Moon could only speculate on, but this newly found emphasis has not displaced the importance of interpreting landforms. Indeed, the discovery of craters on other bodies has cast the Moon in the role of a planetary Rosetta Stone. Much of what can be learned from analysis of craters on the Moon, for which data are the

most abundant, applies elsewhere in the solar system on bodies for which data are sparse.

The Moon's craters are significant in many respects. First, the primary impact craters have been interpreted as recording a late stage or stages in the planet's formation (see review by Taylor, 1975, for example). From the observed population of lunar craters might be estimated the size-frequency distribution of the impacting bodies, from which in turn can be addressed the more difficult problems of accounting for their distribution and of locating the Moon's source within—or outside—the solar system (see discussion by C. R. Chapman, 1976). Second, the largest craters are vast basins that constitute the basic stratigraphic and structural-tectonic framework for most of the Moon (Howard and others, 1974). Material ejected from basins is voluminous and widespread across much of the planet. Topographic influences imparted by large basins, such as the "Imbrium sculpture" (Gilbert, 1893), have profoundly modified the lunar surface. Third, densities of impact craters per unit area record relative ages of various surfaces on the Moon (Hartmann, 1972a). When correlated with radiometric ages of lunar rock samples and with time-stratigraphy ascertained from photogeologic mapping, the relative chronologies obtained from cratering statistics can contribute toward reconstructing an accurate sequence of geologic events. Fourth, relative ages of (generally later) lunar surfaces also may be interpreted from the morphologies of impact craters displaying different degrees of preservation (Offield and Pohn, 1970; Boyce, 1976). In both of the preceding types of analysis, it is essential to exclude secondary-impact craters. Growing recognition of the importance of secondary impacts in creating landforms over much of the lunar surface is another recent development in lunar geology (Wilhelms, 1976). Fifth, systematic variations in crater shape with respect to crater size provide some clues to past lunar events and the operation of internal and external geologic processes (Quaide and others, 1965). Sixth, the harvest of descriptive data and geologic interpretations from the study of lunar craters provides a standard of comparison for craters on Mars and its satellites, Mercury, and other planets (Hartmann, 1972b; Cintala and others, 1976; Gault, Guest, and others, 1975; Burt and others, 1976; Schubert and others, 1977). Our understanding of the probable ancient craters on Earth also can be improved through analogy with the better preserved examples on the Moon. The current interest in extraterrestrial craters has prompted new interpretations of many important but heretofore enigmatic features and deposits in the terrestrial geologic record, such as the Sudbury, Canada, and Vredefort, South Africa, structures. Finally, a lively debate over the origin of lunar craters has continued for some 350 years. Although the issue now seems to be resolved to the satisfaction of most students of the Moon in favor of impact for craters throughout the entire size range, this interpretation is by no means accepted universally, especially for craters less than 5 km across (Schultz, 1976a). Regardless of whichever view one is inclined to accept, however, a few small craters almost certainly are true central volcanoes—probably lava shields and cinder cones—and some types of large impact craters appear to have been modified by post-impact volcanism (Pike, 1968; Schultz, 1976b).

Although there are several ways to learn more about the significance of lunar craters, geometric analysis is the principal approach applied here. The quantitative analysis of shape complements visual observation, photointerpretation, and size-frequency analysis in examining the Moon's craters. All four of these approaches, which evolved through the long history of telescopic work preceding the Apollo program, will continue to be essential to the interpretation of craters, even if detailed and protracted field study on the Moon becomes routine. Although no large craters were examined during any of the six Apollo landings from 1969 to 1972, the photographs taken from the Command Modules in orbit around the Moon on each of these missions have proved to be essential in upgrading the quality of less direct investigations of the craters. For an annotated selection of the best Apollo orbital pictures, see Masursky and others (1978). For quantitative analysis, by far the most useful materials are the orbital mapping-camera and panoramic photographs from the final three Apollo flights. Contour maps, topographic profiles, and other numerical data that accurately portray for the first time the surface geometry of lunar craters larger than about 400 m across have been prepared from these pictures. The principal results are the 1 : 250,000 Lunar Topographic Orthophotomaps (LTO) prepared by the Defense Mapping Agency Topographic Center in cooperation with the National Aeronautics and Space Administration (NASA), and obtainable through the Lunar and Planetary Programs Office, NASA Headquarters, Washington, D.C. 20546. Although map products portraying craters smaller than 400 m across are not plentiful, interpretations of the larger craters no longer need be compromised by topographic data of poor precision and unknown accuracy. Throughout the long pre-Apollo era, hypotheses dealing with the origin of lunar craters were put forth freely and frequently, and almost always without any hard descriptive information. Such unconstrained speculations will have little credibility unless they are consistent with accurate quantitative data, such as

those now available from Apollo orbital photographs.

The new topographic maps provide so much more accurate data than did older methods, notably measurement of lunar elevations from shadow lengths observed at the telescope, that several issues involving the Moon's craters need to be reassessed. First, the question of crater genesis can be tested more rigorously than in the past by comparing the shapes of different classes of lunar craters mathemetically with those of various types of terrestrial craters. Sceond, variations of crater shape with lunar geography can be measured. It is now possible to determine whether or not lunar craters that formed on the mare surfaces are similar to those formed on the uplands and to ascertain quantitatively any significant differences between them. Third, craters located on the far side of the Moon at last can be compared in detail with craters on the near side. Fourth, size-dependent differences in crater shape that were identified in older work can be defined more accurately, and additional differences of this type that did not show up in older less exact data now can be verified. Fifth, the geometric properties of lunar craters over a wide size range can be summarized by simple statistical models, such as exponential expressions for the depth/diameter relations. The resulting equations that related paired dimensions of craters furnish a rigorous basis for the comparison of lunar craters with craters elsewhere. The expressions also may be used, with appropriate caution, to model the geometry of multiring basins. Most of these points are addressed at some length in this paper. Several related areas might fruitfully be approached through analysis of the improved data on crater geometry, such as the changes in shape of a crater with time (Pike, 1968, 1971a), a reevaluation of the venerable Schröter's rule (Pike, 1967), and further development of various models of ejecta distribution (Pike, 1974a). I will not touch on these topics here.

ACKNOWLEDGMENTS

This report is one of four separately bound chapters presenting results of Apollo 15–17 orbital investigations of the following titles: "Stratigraphy of Part of the Lunar Nearside" (Chapter A), "Lunar Remote Sensing and Measurements" (Chapter B), "Geometric Interpretation of Lunar Craters" (Chapter C, this paper), and "Experimental Photogrammetry of Lunar Images" (Chapter D). It summarizes most of the research I did on behalf of the National Aeronautics and Space Administration under contract No. T–1167B (Experiment No. S–222) between July 1972 and December 1975. The manuscript was last revised in February 1977, except for tables 9 and 10, which were supplemented in November 1978 from later work done under NASA contract W13,130.

The advice and encouragement of H. J. Moore throughout the work are warmly appreciated. Many of the results described here were first published in several short papers; criticisms by reviewers and referees of those publications are acknowledged here. These and other contributions to various aspects of the research were made by D. W. G. Arthur, Joseph Ashbrook, Felix Chayes, M. R. Dence, Eric Eliason, R. H. Godson, J. W. Head, C. A. Hodges, K. A. Howard, R. M. Jordan, D. J. Milton, H. J. Moore, G. M. Nakata, Christopher Peebles, F. J. Schafer, P. H. Schultz, Paul Switzer, and S. S. C. Wu. I appreciate their help. Special thanks are due certain individuals, especially F. J. Doyle of the Geological Survey, who argued successfully for the inclusion of metric quality cameras aboard the Apollo 15, 16, and 17 spacecraft. Without their efforts, none of the data upon which this work was based would exist. D. C. Kinsler of the Lunar and Planetary Institute warrants special thanks for his continuing efforts in support of NASA's Lunar Cartographic Program. And finally, J. A. O'Keefe and S. K. Runcorn saw to it that I had the chance to present some of these results to the International Astronomical Union in Grenoble, France, in 1976. The report is dedicated to the memory of Thomas Logie MacDonald (1900–1974), former head of the Lunar Section, British Astronomical Association, and a pioneer analyst of the geometry of lunar craters. His statistical results, based upon data gathered by German astronomers in the last century, set the stage for the important breakthroughs made by Ralph Baldwin two decades later.

THE NEW DATA

Craters are so numerous on the Moon that no pretense can be made of examining them all, and a modest sample must suffice to represent the whole population. Previous experience shows that a few hundred craters usually are enough to obtain stable results (MacDonald, 1931; Baldwin, 1949; Pike, 1968; Schultz, 1976b). One of the outstanding contributions of the statistical studies by MacDonald (1929) and Baldwin (1963) is the list of all measurements used in their work; even if none of their analyses and interpretations were proved valid, the raw data would still provide useful information to another investigator. In an effort to continue this tradition, all topographic measurements—of rim-crest diameter and circularity, crater depth, rim height, and flank width (fig. 1)—that were made for the 623 lunar craters are tabulated in the back of this report, along with a detailed description of how they were made. Only 504 lunar craters

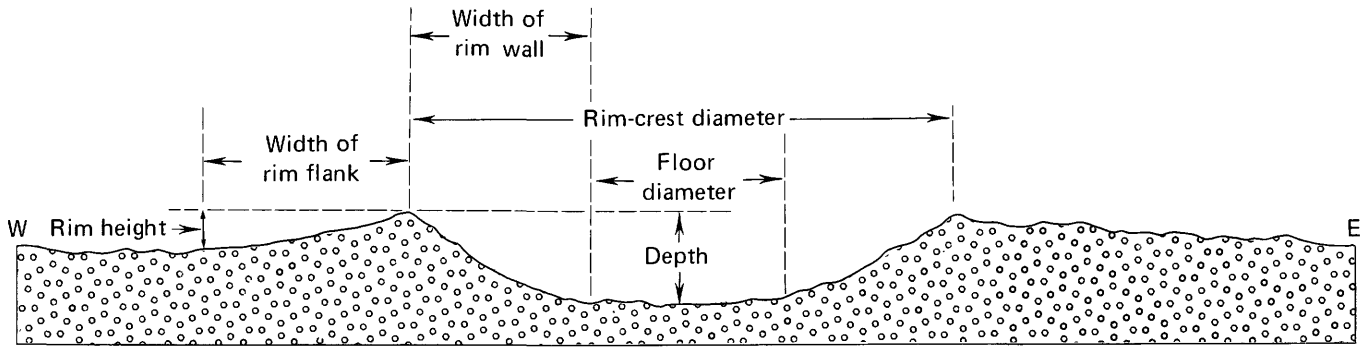

FIGURE 1.—Six crater dimensions. Topographic profile across crater Proclus (rim-crest diameter 28.5 km) from photogrammetry of Apollo 17 mapping-camera photographs. Corrected for planetary curvature. No vertical exaggeration. Compass directions are approximate.

were measured specifically for this study; 119 additional craters were included from later work. The data come from different sources and hence are not exactly uniform in quality. The sampled craters range generally from about 400 m to about 300 km in diameter and vary in appearance from very fresh to highly subdued. Most craters belong to the "main sequence" of Wilhelms and McCauley (1971), although a few less common varieties—such as rimless craters atop domes and cones—also are included. Some unusual types of craters, such as concentric-rimmed features, are omitted entirely. Despite efforts to include craters from the main sequence within a broad range of relative ages, the resulting sample is strongly skewed toward fresher craters. This bias was deemed necessary in order to establish a reliable geometric model for fresh, uneroded craters. More degraded craters can be added to the sample subsequently, as the need arises.

Although most measurements were made on the published 1 : 250,000 Lunar Topographic Orthophotomaps (LTO) (Defense Mapping Agency, 1974–1977), several contour maps and topographic profiles generated by stereoplotter at the Photogrammetric Unit of the U. S. Geological Survey Center for Astrogeology supplied data that could not be obtained from the LTO's. Relatively few fresh craters over 30 km across are portrayed on LTO's because the LTO series primarily covers the sparsely cratered mare regions. To make up the deficiency, topographic profiles and rim-crest outlines were prepared from Apollo 15–17 mapping-camera pictures for 11 large fresh craters in the far-side uplands (Pike, 1972a, 1973a). Crater measurements from these sources are only slightly less accurate than data obtained from the published maps. Conversely, the limitations of map scale and the 100-m contour interval preclude accurate measurements on the LTO's for craters much less than 3 km across. Adequate data on craters well under 1 km across were obtained from seven large-scale topographic maps that were compiled by the U.S. Geological Survey for small areas on the Moon from Apollo 15–17 panoramic-camera pictures. The contour interval on these maps is as small as 10 m. Topographic profiles and rim-crest outlines also were generated for various small craters (as small as 2 km across) of special interest, such as mare domes, possible volcanic cones, and the impact crater Linné. These large-scale data were supplemented by measurements from special 1 : 10,000 and 1 : 50,000 contour maps issued by the Defense Mapping Agency along with the LTO's, but the latter maps generally show few fresh impact craters suitable for statistical analysis.

Dimensions of about 100 additional craters were culled from the best pre-Apollo compilations of Lunar Orbiter and Earth-based measurements (Pike, 1968; Arthur, 1974). These craters were included for comparison with the Apollo data or because they were special types of features, such as summit craters on domes or smooth-rimmed craters, that are poorly represented by available photogrammetric data. At least two and typically about five relative-relief measurements (from shadow-length data) went into each estimate of crater depth and rim height; rim width and floor diameter were measured from Lunar Orbiter images; where possible, circularity was determined directly on rectified pictures, Lunar Aeronautical Charts (LAC) being used rarely as a last resort.

Some of the results in this paper were obtained partially from measurements other than those provided by the Apollo 15–17 pictures, shortly before all of the new LTO and other data became available. Overall agreement between older and newer crater measurements, with the important exception of depth/diameter for craters under 30 km across, is good. This agreement assures that the older results, especially those of a statistical nature as in the graphical comparison of large numbers of craters, are of the same satisfactory degree of confidence that is characteristic of the most recent findings. Table 1 (from Pike, 1974b) shows a sampling of extremes of differences between data from different sources. The crater-diameter differences between Lunar Orbiter images (mostly mission IV high-

TABLE 1.—*Depth and diameter measurements for a sampling of fresh lunar craters*

[From Pike (1974b)]

Crater	Diameter, D_r (m)		Depth, R_i (m)					
	LTO[1]	LO[2]−LTO / LTO	LTO	LO−LTO / LTO	LO−LAC[3]	LO−LAC / LAC	LTO−LAC	LTO−LAC / LAC
Bessel H	3,700	−0.05	670	−0.01	440	2.00	450	2.05
La Hire A	5,060	0	1,210	−.11	400	.59	530	.78
LeMonnier B	5,190	−.02	925	.04	550	1.34	515	1.26
Timocharis B	5,250	−.01	1,156	−.19	630	2.03	846	2.73
Bessel D	5,700	.01	1,065	−.07	620	1.68	695	1.88
Linné E	5,700	0	1,125	−.01	710	1.78	725	1.81
Sulpicius Gallus G	5,810	.02	1,215	−.16	620	1.24	715	1.43
Hadley C	5,880	−.01	1,195	−.04	620	1.24	695	1.39
Aratus B	7,000	0	933	−.14	300	.60	433	.87
Littrow B	7,000	.06	1,430	.01	730	1.04	730	1.04
Carlini B	7,120	.07	1,600	−.08	640	.77	770	.93
Bessel A	7,500	.01	1,730	−.04	1,010	1.55	1,080	1.66
Jansen L	7,570	−.05	1,494	−.03	350	.32	394	.36
Auwers A	7,630	−.01	1,635	−.06	230	.18	335	.26
Cauchy D	8,900	.06	1,905	0	1,000	1.11	1,005	1.12
Jansen F	8,940	.06	1,810	−.01	900	1.00	910	1.01
Hadley B	9,000	−.03	2,000	−.05	780	.70	880	.79
Angström	9,800	0	2,000	.02	860	.74	830	.71
Vitruvius E	10,900	.02	2,190	−.05	890	.74	990	.83
Taruntius E	11,500	−.02	2,200	−.04	520	.32	600	.38
Cauchy	12,800	−.03	2,673	−.02	810	.45	873	.49
Isidorus D	16,500	−.07	3,300	−.09	1,000	.43	960	.41
Diophantus	18,130	.02	3,020	−.02	385	.15	425	.16
Delisle	25,380	−.01	2,420	.06	140	.06	0	0
Mädler	28,000	−.01	2,830	−.06	950	.55	1,110	.65
Average		[4]−.01	------	[5]−.05	644	.91	701	1.00

[1]LTO—Photogrammetric data, principally from 1:250,000 Lunar Topographic Orthophotomaps.
[2]LO—Lunar Orbiter IV data (Arthur, 1974).
[3]LAC—Earth-based telescopic data, mainly from 1:1,000,000 Lunar Aeronautical Charts.
[4]Includes 24 additional craters not listed here.
[5]Includes 20 additional craters not listed here.

resolution pictures) and the new LTO's average a mere 0.01 of the crater diameter and are not systematic. However, contrasts between data obtained from Lunar Orbiter images, the LTO's, and the mainly Earth-based Lunar Aeronautical Charts (LAC) are both more serious and systematic for the depths of small craters. In particular, LAC depths average only half the LTO depths. This discrepancy is serious indeed, and Earth-based data on the depths of small craters have not been used here. Depth data from Lunar Orbiter images (Arthur, 1974) deviate much less from the Apollo measurements. Arthur's depths average only about 5 percent too low (table 1).

CRATER GEOMETRY AND CRATER GENESIS

COMPUTER CLASSIFICATION OF ANALOGS

Several aspects concerning the 350-year-old riddle of the origin of lunar craters persist despite six manned landings on the Moon and general acceptance of the impact hypothesis (Taylor, 1975). The problem has been compounded by the discovery of craters on Mars and its satellites, on Mercury, on Venus and on the satellites of Jupiter, and may well be complicated further when surfaces of the asteroids and the satellites of Saturn come under closer observation. Until geologic fieldwork on specific extraterrestrial craters again becomes feasible, approaches to solving the crater genesis problem will remain indirect. There are many such approaches (Pike, 1968): The oldest, analog analysis, compares craters of unknown origin with different types of craters whose origin is known. Given certain assumptions concerning magmatism, the availability of water, presence of an atmosphere, and the differences in gravitational acceleration, extraterrestrial craters that closely resemble terrestrial craters in morphology can be inferred to have had the same genesis. Most attempts to establish crater similitude have been made qualitatively, either at the telescope or through photointerpretation (Gilbert, 1893; Shoemaker, 1962).

Building upon morphometric work by T. L. MacDonald and earlier German astronomers, R. B. Baldwin reduced much of the subjectivity inherent in evaluating crater morphology by inspection. He compared lunar and terrestrial craters on logarithmic graphs of paired dimensions (for example, depth and diameter) that describe geometric characteristics common to all craters with raised rims (Baldwin, 1949, 1963). Subsequently, different groups of lunar craters were classified as either volcanoes or as various types of impact craters from the results of similarly graphed comparisons (Pike, 1967, 1972b; Guest and Murray,

1969; Smith, 1971). However, these and other such schemes run a serious risk of misclassifying individual craters, because only two of the several measurements required for a minimal expression of crater shape are examined on one graph simultaneously. The identical difficulty was identified in anthropology some time ago (Bronowski and Long, 1951). More recently, Siegal (1973), Siegal and Griffiths (1974), and myself (Pike, 1974c) have introduced multivariate techniques, which are not limited by the dimensional restrictions of graphical methods (Sokal, 1974), for comparing craters mutually with respect to several topographic variables. Because of this innovation, reservations about the geometric approach expressed by Shoemaker (1962) and Mutch (1970) with special reference to depth/diameter now are less warranted.

Multivariate classification requires a probabilistic comparison of crater morphology rather than the direct deterministic evaluation possible with graphical analysis. Genetic classifications of craters that are derived graphically from topographic variables all have been monothetic in concept (Sokal and Sneath, 1963). This means that each of the taxonomic criteria was required to uniquely specify the mutually exclusive classes, usually either volcanoes or impact craters. Individual parameters do not do this very well (see ranges of values in table 2); there is no simple "magic number." The statistical approach to crater classification adopted earlier (Pike, 1974c) and probed further here is inherently polythetic (Sokal and Sneath, 1963). It is an improvement over the monothetic mode because craters are grouped together only if they share in several but not necessarily all of the discriminating attributes expressed by the variables. In this way no one characteristic is vital to classifying a crater, nor can one alone place a crater in one group or another. The polythetic approach to crater analogs recognizes that the problem, like most in geomorphology, is inherently stochastic rather than physical in character (Leopold and Langbein, 1963).

The analytical procedures followed here also compare each crater to all other craters in the sample in each and all respects. The problem cannot be formulated as a simple choice between impact and explosion craters as one class and volcanoes as the other class, because there are several candidate terrestrial analogs and each differs in shape from the others. Nor has it been assumed beforehand that some terrestrial craters are better or worse analogs of lunar craters than others and thus must be grouped together or somehow accorded special consideration. The first question being asked here simply is this: Given the entire spectrum of (measurable) cratered landforms on the Earth and the Moon, regardless of their genesis, how can individual craters be grouped according to similarities in their gross topography? Other naive but useful queries follow: How many major groups of craters exist within the sampled universe of craters, and how are they related to each other? Do topographic differences and similarities evident in the resulting groups reflect recognized types of craters and particular modes of origin? If the last questions can be answered affirmatively, then various cratering processes are associated with specific crater shapes—as expressed by surface geometry—and an attempt can be made to set up numerical criteria for ascertaining the genesis of a given lunar crater from its topography.

The issue of crater genesis on the Moon is recast as a conventional problem in numerical taxonomy (Sokal and Sneath, 1963; Sokal, 1974). This experiment results in three rather similar solutions for 418 representative craters and seven original (four synthetic) descriptive variables. The classifications, which were constructed from a principal-components analysis and by a cluster analysis, closely resemble the results I obtained in a brief study using most of the same craters (Pike, 1974c). Contrary to conclusions reached by Siegal (1973), also on the basis of multivariate analysis although from quite different data, my results show that crater morphology is indeed an indicator of origin. A genetic scheme for classifying craters by morphology alone has been established for craters over 5 km in diameter. Interpretations focus on the relation of main-sequence lunar craters to three candidate terrestrial analogs: meteorite-impact craters, calderas, and maars. Detailed variations among lunar craters and among terrestrial volcanoes, which warrant separate study, are not treated in detail here (Pike, 1978a).

EXPERIMENTAL METHODS

Principal-components and cluster analyses are conventional quantitative approaches that have been used in many fields to recognize natural groups, more or less objectively, within a set of phenomena on which several observations have been made. The two techniques have been described sufficiently in the geologic literature so that this account need outline only the essentials of each procedure applied to the craters. Background material and details of the programmed algorithms are available elsewhere (Sokal and Sneath, 1963; Harman, 1967; Parks, 1969, 1970). All calculations were made by one computer run in about 10 minutes on an IBM360/65 machine. Compared to the costs incurred in measuring the craters and compiling the new data, which would have been needed even for a conventional graphical analysis, the expense of the machine time and data preparation was trivial.

Principal-components analysis is a statistical transformation for simplifying large unwieldy matrices of data with a minimum loss of information (Cattell, 1952; Harman, 1967). In many respects the technique resembles multiple-factor analysis, and results of the two procedures often are not very different (Harman, 1967). Principal-components analysis is performed on correlation coefficients relating all pairs of variables, which reduce to a few independent synthetic variables. These linear, uncorrelated combinations of the original variable are termed principal components. The number of significant components, which are extracted sequentially from the correlation matrix to explain successively diminished proportions of the total variance, is the number of independent aspects present in the data. Usually this number is substantially less than the number of original variables. Component scores, similar to the "factor loadings" resulting from a multiple-factor analysis (Harman, 1967), are calculated to show the correlation between variables and principal components as well as the makeup of each component in terms of original variables. The criteria on which a classification may be devised are a second set of scores which express the correlation of each crater with each component.

Cluster analysis arranges objects in a two-dimensional diagram, resembling a biologic family tree in appearance, on which any natural breaks between groups (clusters) of objects are evident by inspection (Sokal and Sneath, 1963). It has numerous applications to geologic problems (Parks, 1966; Harbaugh and Merriam, 1968; McCammon, 1969; Adam, 1974). The version of cluster analysis used here (Parks, 1969, 1970) begins with a principal-components transformation to simplify and orthogonalize the variables. The scores that were computed between each component and each crater are used to determine a statistical measure of similarity, known as the simple distance function, between each pair among the craters. In this experiment, the scores are weighted (multiplied) by the percentage of total variance accounted for by each component. Although the weighting of original variables or scores remains something of an art (Gower, 1970), the procedure used here at least assures that the clustering is not biased unduly toward the less important components. The distance function measures Euclidean rather than angular distance between any two craters in a multidimensional space: one dimension for each component. Its formula and properties are given by Parks (1966).

From an array of distance-function values, craters and subsequently groups of craters are cross-compared and then combined by a linkage procedure, one pair at a time, into hierarchical clusters. Craters with low values of the distance-function coefficient group first, and craters with similar shapes (similar values of the coefficient) group together, apart from differently shaped craters. Many linkage techniques, or sorting strategies, have been devised for cluster analysis (Sokal and Sneath, 1963). The procedure followed here (Parks, 1970) is a modification of the unweighted pair-group method, a well-known algorithm first described by Sokal and Michener (1958) and since used in many clustering applications. The resulting cluster diagram, or dendrogram, is printed automatically with the computer output in this case. Other types of graphic results, commonly involving an X–Y plotter, can be obtained as well (McCammon and Wenninger, 1970).

THE CRATER SAMPLE

In several respects, the data set assembled for this experiment is a marked improvement over crater samples that have been used for previous morphometric studies (Baldwin, 1949, 1963; Green and Poldervaart, 1960; Pike, 1967, 1972b; Katterfeld, 1967; Guest and Murray, 1969; Siegal, 1973; Smith, 1973; and Siegal and Griffiths, 1974). First, the 23 different categories better represent the variety of craters relevant to the analog problem (table 2). Older modified-looking lunar craters and secondary-impact craters are included along with the fresh primary craters that customarily are preferred for comparison with terrestrial craters: the bias toward fresh craters in the overall lunar sample has been eliminated for this analysis. Special attention is accorded terrestrial volcanoes, which have been neglected in most morphometric comparison, although the volcano data are not listed here but are published elsewhere (Pike, 1978a). Second, the sample is larger than previous samples, and so the resulting crater classifications are more likely to be statistically significant; most types of craters are well represented numerically. Third, the data are much more complete and systematic in that all seven variables were calculated for each crater. In earlier studies, graphs of different descriptive variables usually did not contain the same craters. Fourth, most of the basic measurements, including all rim widths and all rim-crest circularities, are new and surpass older data in accuracy. Photogrammetry of Apollo pictures furnished data for more than half of the lunar craters.

Terrestrial and extraterrestrial craters are equally represented (table 2). The 206 lunar craters range from 400 m to 275 km in diameter and include main-sequence Copernican and Eratosthenian and pre-Imbrian craters on the near-side uplands (Wilhelms and McCauley, 1971), craters on the maria, smooth-rimmed craters interpreted as possibly volcanic

TABLE 2.—*Statistical summary of untransformed variables 1–4 for 23 crater types*

[Entries under each variable are, from left to right, arithmetic mean, standard deviation, and range. ____, not calculated. These three statistics may be approximated for variables 5–7 from values given here for variables 2–4. Some statistics are for values of n (see Pike, 1974c) that differ slightly from those here]

Crater type, name	Type symbol	n	Variable 1—rim-crest circularity			Variable 2—rim height/crater depth			Variable 3—flank width/rim diameter			Variable 4—rim height/diameter		
Terrestrial craters														
Oceanic island (mainly tholeiitic basalt) caldera	KO	13	0.54	0.16	0.24–0.84	14.33	12.54	3.28–48.49	4.03	2.04	1.30– 6.82	0.623	0.335	0.156–1.167
Alkalic caldera	KA	18	.61	.13	.35– .75	4.50	2.92	1.22–12.89	2.61	2.01	.60– 8.00	.415	.424	.054–1.473
Calc-alkalic caldera	KC	26	.59	.14	.25– .78	4.71	7.50	.86–40.00	1.96	1.48	.61– 6.67	.198	.150	.013– .545
Potassic caldera	KP	6	.58	.14	.32– .68	5.80	9.03	.67–24.16	1.25	.54	.62– 2.13	.138	.077	.038– .237
Cratered ash-flow plain	AP	5	.36	.18	.14– .55	1.60	.41	1.05– 2.07	.82	.28	.59– 1.30	.048	.012	.033– .063
Maar	E	39	.59	.14	.23– .85	.39	.23	.08– 1.00	.37	.25	.11– 1.52	.042	.030	.005– .171
Tuff ring	T	20	.62	.15	.32– .85	1.58	1.04	.73– 4.95	.51	.25	.18– 1.18	.110	.066	.018– .253
Cinder cone	C	20	.70	.10	.52– .86	3.55	1.80	1.28– 6.74	1.15	.45	.50– 2.13	.483	.253	.103–1.107
Small lava shield	S	10	.48	.24	.19– .87	4.22	5.22	1.00–19.20	5.70	3.88	1.75–12.59	.539	.586	.043–1.655
Small lava dome	D	9	.58	.23	.25– .85	3.94	2.44	1.13– 9.00	1.91	1.22	.81– 4.20	.915	.580	.459–2.333
Meteorite-impact crater	M	20	.81	.06	.68– .92	.30	.11	.10– .59	.20	.04	.14– .30	.034	.016	.006– .067
Experimental-explosion crater	X	22	.85	.08	.66– .99	.18	.06	.10– 35	.26	.08	.12– .48	.040	.025	.005– .083
Lunar craters														
Mare-filled basin	MB	3	0.81	____	0.80–0.83	.0.41	____	0.32– 0.48	0.25	____	0.18– 0.31	0.003	____	0.002–0.003
Secondary impact crater	SC	29	.57	____	.34– .84	.22	____	.08– .51	.26	____	.13– .35	.025	____	.007– .041
Young mare crater	PM	40	.83	.05	.70– .92	.24	.07	.12– .40	.22	.05	.13– .33	.026	.009	.012– .051
Young upland crater	TY	23	.82	.07	.66– .91	.25	.09	.13– .52	.22	.05	.13– .35	.027	.011	.012– .052
Pre-Imbrian crater[1]	PI	40	.76	.08	.52– .88	.60	.20	.24– 1.29	.11	.04	.05– .21	.016	.008	.007– .038
Dark-halo crater within crater Alphonsus	DH	3	.56	____	.42– .64	.12	____	.07– .15	.53	____	.39– .68	.017	____	.009– .022
Mare-flooded crater	MF	17	.81	.06	.67– .88	.75	.19	.36– 1.00	.14	.04	.07– .22	.018	.007	.008– .029
Smooth-rimmed crater	IS	19	.78	.06	.66– .91	.49	.17	.25– .72	.12	.05	.06– .23	.022	.008	.010– .044
Isostatically compensated crater	IC	7	.79	.05	.74– .87	.69	.20	.36– 1.00	.10	.07	.05– .21	.011	.006	.005– .023
Cratered dome on mare surface	MD	15	.58	.20	.15– .88	2.25	1.39	.73– 6.07	2.25	1.31	.43– 6.35	.285	.224	.051– .851
Raised cone	RC	14	.55	.16	.28– .80	2.52	1.62	.73– 6.67	.85	.40	.35– 1.55	.255	.156	.077– .521

[1]Statistics omit Schiller and Wargentin.

(Wilhelms and McCauley, 1971), craters flooded with mare material or evidently affected by isostatic compensation, craters located atop domes on the mare surfaces, small raised cones located on mare surfaces or on the floors of fresh craters such as Copernicus and King, small dark-halo craters on the floor of the crater Alphonsus, and secondary-impact craters of Copernican age. Examples of most of these types of craters are illustrated in photographs throughout the report. The six martian craters and calderas included in the source multivariate classification have been removed (for later results, see Pike, 1978a), as have the unclassified craters on the lunar far side (Pike, 1974c). The latter omission is not important because near-side and far-side craters are similar in shape. Among the 212 terrestrial craters, which range in diameter from 1.3 m to 65 km, are calderas representing all the major petrographic associations, maars, cinder cones, tuff rings, small lava shields and domes, meteorite-impact craters, and experimental craters excavated by chemical and nuclear explosives. All these craters have been mentioned at one time or another as suitable analogs of lunar craters.

Seven dimensionless variables express the overall shape of each crater in plan and in profile. Rim-crest circularity, height/depth, width/diameter, height/diameter, depth/diameter, height/width, and depth/width provide the minimum geometric signature needed to identify and cross-compare the craters. Statistical properties of the first four variables have been summarized for all 23 types of craters (table 2). The circularity measure (C) is described in the back of this report (see also fig. 24). The last six variables are simply ratios of the four linear dimensions used by Baldwin (1963) to describe the basic profile shape of any rimmed crater: rim-crest diameter (D_r), depth (R_i), rim height (R_e), and rim width (W_e) (fig. 1).

The four profile dimensions are not used individually as variables, because they measure only crater size, an aspect that often is related to neither crater morphology nor crater genesis. Particularly in the case of lunar craters, which occupy at least six orders of magnitude, it is shape not size that reflects the fundamental mode of origin. Moreover, it has become customary in lunar analog work to compare any terrestrial crater with any lunar crater, regardless of the size disparity. Although the premise makes geologic sense only for those few types of terrestrial craters that could conceivably attain the great size of the larger lunar craters, it is interpreted liberally here—almost to the point of absurdity—to insure that the widest possible variety of potential analogs is fairly represented. For these reasons, size is eliminated as a morphologic discriminant. Failure to observe this practice in multivariate analysis can lead to incorrect or inconclusive results and interpretations (Siegal, 1973; Siegal and Griffiths, 1974). Although statistical problems can arise in applying correlation analysis to ratio data (Chayes, 1971; Atchley and others, 1976), forming ratios of linear dimensions is judged the most effective way to remove crater size from the analysis. Subsequent evaluation of the final results suggests that

ratio correlation has not produced a spurious outcome.

The multivariate techniques applied here can yield misleading results unless the input data conform to the normal or Gaussian statistical model. The frequency distributions of all seven variables are highly skewed, a condition brought about in part by combining 23 constituent distributions of very different craters that vary widely in mean, variance, and numbers of craters (table 2; see also older data in fig. 15). This is not the usual case, where mixing frequency distributions usually removes rather than generates skewness (F. Chayes, written commun., 1974). The circularity data are skewed negatively, toward slightly lower values, whereas the remaining six variables all are skewed positively, toward higher values (see older data in figs. 15, 16, and 17). Each variable was transformed to make its distribution as nearly symmetric as possible (table 3), but not to overcompensate (R. P. Chapman, 1976). Different transformations were required because the seven frequency distributions vary in their degree of skewness, especially in the distance of extreme values from the median. Although these simple transformations do not yield the Gaussian ideal, they eliminate the most disruptive effects of extreme values from the analysis (Sokal and Sneath, 1963; Lindqvist, 1976).

INTERPRETATION OF PRINCIPAL COMPONENTS

Correlation (both positive and negative) between the seven variables with respect to all 418 craters reveals that the variables are not equally interdependent. According to the matrix of similarity coefficients (table 3), height/depth, width/diameter, height/diameter, and depth/width are the most closely associated variables and describe a similar dominant pattern of covariance in the data.

The seven original variables reduce to four significant principal components (table 4), all of which can be interpreted in terms of crater morphology. The highest component scores correspond roughly to the highest absolute values of the similarity coefficients listed in table 3. The analysis is so nearly complete by the time four of the seven possible components are extracted that virtually no information is lost. This highly favorable outcome is evident in two respects. First, the variance (summed squares of the component scores) accounted for by the four components for each variable approximates unity. Second, and similarly, total variance accounted for by the seven variables for the first four components is 99.5 percent.

TABLE 4.—*Principal-components results for seven variables and 418 craters*

[Format after Harman (1967). Component scores are listed for each variable on the first four principal components (P_1–P_4) only. Including the last three components (not shown), total variance = 7.0 (the number of variables); four components yield an exceptionally complete solution]

Variable	Symbol	P_1	P_2	P_3	P_4	Variance
Circularity	C	−0.573	0.223	0.358	0.703	1.000
Height/depth	R_e/R_i	.924	−.053	.373	.026	.996
Width/diameter	W_e/D_r	.900	.072	−.334	.262	.995
Height/diameter	R_e/D_r	.863	.498	.019	.077	.999
Depth/diameter	R_i/D_r	−.003	.851	−.516	.082	.996
Height/width	R_e/W_e	.170	.772	.552	−.258	.997
Depth/width	R_i/W_e	−.805	.554	−.061	−.149	.980
Variance		3.412	1.932	.945	.665	6.954
Percentage of total variance		48.75	27.6	13.6	9.5	99.5

The first and dominant (49 percent of variance) principal component expresses the most important descriptive aspect present among the variables: size, position, and shape of the crater rim relative to that of the crater depression. The three highest scores in table 4 indicate its main constituents: height/depth, width/diameter, and height/diameter. Depth/width is somewhat less important and varies inversely; circularity also varies inversely and is even less significant. Scores of the various types of craters on the first principal component suggest that the component is oriented within the data to account for most of the variance resulting from the difference between volcanoes and craters usually attributed to impact (fig. 2). Terrestrial impact and experimental-explosion craters and fresh lunar craters typically have the lowest scores on the first component, whereas terrestrial shield volcanoes that contain either calderas or simple summit craters have the highest scores. These two extremes are only indicative of the dichotomous pattern within this component, which is interpreted accordingly as a good criterion of primary crater genesis.

TABLE 3.—*Matrix of similarity coefficients for principal-components analysis*

[Although technically these values were derived from the formula for the product-moment coefficient of correlation (r) between pairs of transformed variables, the numbers should be regarded as only indicators of similarity rather than as values of a testable statistic. Statistical tests of significance do not apply to these values because some correlation is inherent among ratios showing similar crater dimensions (Chayes, 1971)]

Variable	Transformation	Symbol	C	R_e/R_i	W_e/D_r	R_e/D_r	R_i/D_r	R_e/D_r	R_i/W_e
Circularity	x^3	C	1.00						
Height/depth	$\log \sqrt[3]{x}$	R_e/R_i	−.47	1.00					
Width/diameter	$\log \sqrt{x}$	W_e/D_r	−.44	.73	1.00				
Height/diameter	$\log \sqrt[3]{x}$	R_e/D_r	−.38	.77	.84	1.00			
Depth/diameter	$\log x$	R_i/D_r	.07	−.19	.29	.48	1.00		
Height/width	$\log x$	R_e/W_e	−.01	.29	−.01	.52	.41	1.00	
Depth/width	$\sqrt[3]{x}$	R_i/W_e	.46	−.79	−.68	−.40	.46	.31	1.00

The three remaining components are not clear-cut indicators of crater origin but represent other important descriptive attributes. The second principal component accounts for variance (28 percent) that is attributed to the next most important aspect of crater shape present in the data: slope of the crater depression (depth/diameter) and slope of the rim flank (height/width). Depth/width and height/diameter also contribute to this component, but not as much. Neither depth/diameter nor height/width is at all diagnostic of crater genesis (Green, 1959; Steinberg, 1969; Pike, 1972b), although both variables do reflect size-dependent differences in the shape of impact craters, as well as degradation of the crater rim with time and commensurate filling of the bowl. Depth/diameter correlates roughly with the relative age of many lunar craters (Baldwin, 1963; Pike, 1971a). Small steep features such as terrestrial volcanic domes and cones, as well as experimental-explosion craters, characteristically have the highest scores on the second component. Large gently sloping landforms such as mare-filled lunar basins and terrestrial ash-flow calderas have the lowest scores.

The third principal component, which explains 14 percent of the total variance within the data, is less amenable to a physical interpretation because none of the scores (table 4) is very high. This component reflects primarily the coincidence of a steep rim flank (height/width) with a shallow crater (depth/diameter). On Earth, this configuration is not very common among cratered landforms except for cinder cones (fig. 3). On the Moon, a relatively steep rim flank is more often associated with a shallow crater interior, especially where fresher, younger craters are filled or modified catastrophically and do not age gradually (for example, Archimedes, Taruntius). Conversely, low scores on the third component indicate exceptionally deep craters with low exterior rim flanks. These most often include dark-halo and secondary-impact craters on the Moon, as well as small lava shields (such as Burfell, in southwest Iceland) on Earth.

Although the fourth principal component contains only 9 percent of the total variance, it warrants interpretation by virtue of the relatively high score of circularity on it (table 4). To a limited extent, scores on this component by individual craters increase proportionately with circularity of the crater rim, but primarily the fourth component seems to account for variance arising from atypically high or low circularities. Highest scores on this component are made by craters that are nearly circular but have an overall profile geometry that is more characteristic of a volcano. On Earth, this configuration is found in many cinder cones (Wizard Island, in Crater Lake, Oregon), some maars (Ndubot in Tanzania), and in a few calderas (Volcán Darwin in the Galápagos Islands), but very high scores on this component are not typical of craters on the Moon. The lowest scores on the fourth principal component indicate highly acircular craters that have a profile geometry characteristic more of impact craters than volcanoes. Terrestrial craters of this sort tend to be irregular maars (Lojotipullur in Iceland). On the Moon, low scores on the fourth component often are found among secondary-impact craters and irregular or highly elongate main-sequence craters such as Zöllner, Daniell, Messier, and Schiller.

The 418 craters have been arranged and sorted into groups according to similarities and differences in shape, using the principal-components outcome in three of several possible ways (figs. 2 and 3 and pl. 1). The resulting classifications are similar overall—notably in the separation of most impact craters from most volcanoes—but differ in detail. Each grouping emphasizes some variations in crater shape that are not well shown in the others. The need for more than one graphic display for the principal-components outcome underscores the inherent difficulty of presenting results of a multivariate analysis in only two or three dimensions. The end product is always a compromise.

The three crater classifications are discussed in order of increasing complexity. The first is simply a plot of the scores of each crater (here grouped by types) on the first principal component (fig. 2). It emphasizes primary crater genesis without statistical "noise" from the last three components, which reflect postformational modification or less important variations in crater shape. An advantage of this kind of classification is the ease and directness with which individual craters can be compared (although labeling each crater is very awkward). However, figure 2 is oversimplified because the first component includes only half of the variance in the analysis and is incapable of breaking down the 418 craters into more than two large clusters. The information content of such a classification can be increased considerably by plotting the scores of individual craters on more than one principal component. The resulting diagrams are limited to only two or three components and can be virtually impossible to interpret if a great many craters are graphed. A triaxial plot (fig. 3) is a compromise, whereby 90 percent of the total variance in the analysis is represented and the craters are not graphed individually but are grouped by type. Although single craters cannot be compared in this diagram, relations among the different types are more fully and faithfully represented than they can be in figure 2. More than two major clusters of crater types can be distinguished. Finally, the 418 craters were grouped by a formal cluster analysis of all four (weigh-

ted) principal components (pl. 1). Largely prefigured by the dichotomous grouping evident in figure 2, the cluster sorting yields a more detailed and highly structured grouping of the 418 craters than do the first two classifications. Many subclusters are evident. All 100 percent of the variance is included, and all craters are labeled. A disadvantage of the cluster technique is that the dendrogram is confined to only two dimensions and some of the relations among crater types evident within the three-dimensional plot in figure 3 do not show up very well in plate 1.

CLASSIFICATION BY PRINCIPAL COMPONENTS

Scores on the first principal component classify the 23 crater types into two mutually exclusive and widely separated groups (fig. 2), with the conspicuous exception of terrestrial maars (E) and tuff rings (T) and lunar raised cones (RC). High scores indicate craters with high wide rims, floors lying well above the exterior datum, and (usually) highly acircular rim crests. The mare domes (MD) and most terrestrial volcanoes score over 0.250, whereas meteorite-impact (M) and experimental-explosion craters (X) and all other lunar craters except the raised cones usually score under 0.150. The two contrasting classes of crater shape reflect processes corresponding to one of two general modes of origin, excavation and accumulation. In excavational (mostly impact) craters, the rim is composed of material derived primarily from the crater bowl. In craters of net accumulation, or cratered edifices (most volcanoes), the rim material either comes from depth or is unrelated to formation of the present crater bowl. The three lunar dark-halo craters (DH) also are exceptions to the genetic dichotomy in figure 2: Their scores on the first principal component place them within the impact group—if only marginally—but their albedo and geologic setting on the floor of the larger crater Alphonsus (Carr, 1969) indicate an internal origin.

Terrestrial tuff rings (T) and maars (E) and lunar raised cones (RC) scatter widely and overlap both genetic clusters in figure 2. Considered as crater classes, maars and tuff rings resemble neither impact craters nor the more conventional volcanoes in shape, but rather bridge the two main groups. The transitional position of maars and tuff rings in figure 2 probably reflects a tendency for both excavational and accumulational processes to combine in forming specific craters. The difference between the two transitional classes of terrestrial craters in figure 2 suggests a sys-

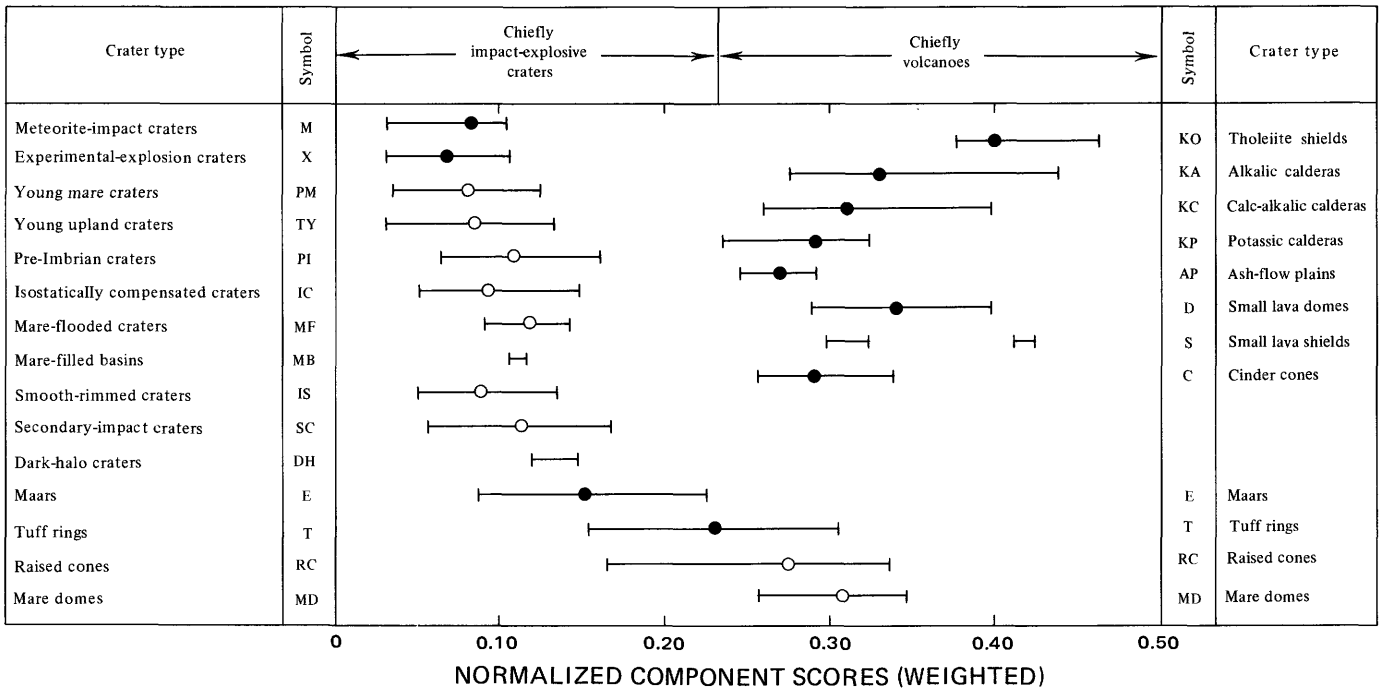

FIGURE 2.—Correlations of crater types with first principal component. Mean values and ranges of scores for 23 crater types listed in table 2. Closed circles, terrestrial craters; open circles, lunar craters. Normalization (transforming scores of each component to 0.0 to 1.0 scale) and weighting (see text) do not affect relative order of distribution. Mean scores omitted for mare-filled basins and dark-halo craters (too few) and for small lava shields (Icelandic shields group far to right of other small shields). Strongly dichotomous distribution of most crater types reflects fundamental contrasts between impact craters and most volcanoes and prefigures two-part cluster classification (pl. 1).

tematic mix of both mechanisms, maars being mostly excavational in origin and tuff rings being mostly accumulational. However, maars and tuff rings belong to a morphologic and genetic continuum, shared by cinder cones as well (Pike, 1978a), in which case this difference is only an artifact of the crater nomenclature. Most lunar raised cones (RC), which according to scores on the first component are shaped more like terrestrial cinder cones than tuff rings, are implied to be predominantly constructional landforms.

Classification of craters on the first principal component excludes terrestrial calderas of any type as acceptable topographic analogs of typical lunar craters. The most caldera-like of the main-sequence craters on the Moon are the badly battered pre-Imbrian crater Schröter (score 0.160) and the odd, boat-shaped crater Schiller (0.166). The evidently inundated crater Wargentin (0.137) is much less caldera-like in shape. Three of the secondary craters attributed to ejecta from Aristarchus also score over 0.160. The most lunar-like of the terrestrial calderas in this data set are Ilopango in El Salvador (0.240) and Suswa in Kenya (0.236). Meteorite-impact craters are the only natural features on Earth that consistently resemble all types of main-sequence lunar craters. Accordingly, these lunar craters probably formed by impact. Although many terrestrial maars (MacDougal Crater in the Pinacate volcanic field in Mexico; score 0.085) and a few tuff rings (Hverfjall in Iceland; 0.162) individually resemble some lunar craters—notably the more degraded types—as a class neither type of crater is consistently similar in shape to the lunar craters. Moreover, terrestrial maars and tuff rings rarely reach 1,500 m across and do not exceed 5 km in diameter, whereas impact craters appear to have no such upper limit in size (Gilbert, 1893; Shoemaker, 1962).

Ten types of craters make up the tightly clustered and low-scoring group attributed to impact or explosion (fig. 2). These types of craters vary systematically within the group, as reflected by average scores on the first principal component, according to degree of complexity of morphology and geologic history. The freshest and least modified craters have the lowest scores, in order of increasing mean scores: experimental-explosion craters (X), meteorite-impact craters (M), young mare craters (PM), and young upland craters (TY). Next come younger craters that either have slightly anomalous original shapes—smooth-rimmed craters (IS)—or else have been modified somewhat by isostatic rebound (IC). Clearly older main-sequence craters that have undergone much degradation (PI) are next, followed closely by mare-filled basins (MB). Secondary-impact craters (SC) and deeply flooded main-sequence craters (MF) both differ considerably in shape from fresh, young impact craters and are last. Dark-halo craters (DH) lie even farther to the right in figure 2 and thus do not really belong to the impact cluster, even on the basis of morphology. These craters occupy a mutually exclusive field with terrestrial meteorite-impact and experimental-explosion craters on figure 2 and are all but mutually exclusive with fresh craters on the lunar maria as well.

The scores of volcanoes scatter much more widely than do the scores of impact craters in figure 2. The disparity indicates that volcanoes intrinsically are more variable in overall shape than are impact craters. Certainly a more regular landform would be expected from the instantaneous and comparatively uniform impact mechanism than from volcanic central eruptions, which can vary considerably in duration, intensity, vent location, and in the chemistry and physical properties of their ejecta.

Some of the variance within the volcanic group (fig. 2) may have arisen from a connection between gross morphology of calderas and silica content of the erupted products and the percentage of pyroclastic material. First, most caldera-bearing tholeiite shield volcanoes (KO) (Hawaii) and those of the small shield volcanoes (S) of Iceland lie well to the right of other types of volcanoes. Average component scores also decrease systematically from tholeiite calderas (KO) through alkalic calderas (KA) to calc-alkalic calderas (KC), calderas of the potassic (Mediterranean) association (KP), and cratered ash-flow plains (AP). However, so much overlap occurs among the different caldera types that the dominant rocks of extraterrestrial caldera volcanoes, such as those on Mars, cannot be predicted with much certainty from this relation. Certainly the correlation is less substantial than that between petrography and geographic location of Cenozoic volcanoes (Chayes and Velde, 1965; Chayes, 1964). Moreover, although none of the mare domes (MD) occupy the same range of principal-component scores as do the large terrestrial tholeiite shields (KO) (fig. 2), the lunar mare basalts are more like tholeiite than any other type or terrestrial basalt. The lunar domes do coincide with about half of the smaller tholeiite shields (S), however, and in fact the lunar domes may more closely resemble this type of volcano than the others. I have pursued these problems in later work (Pike, 1978a).

The marked contrast between craters of excavation and cratered landforms of accumulation is again evident in a graph of crater scores on the first three principal components (fig. 3). Adding the second and third components has, if anything, enhanced and clarified the dichotomy. Weighted scores on each component were averaged for each crater type from scores of single

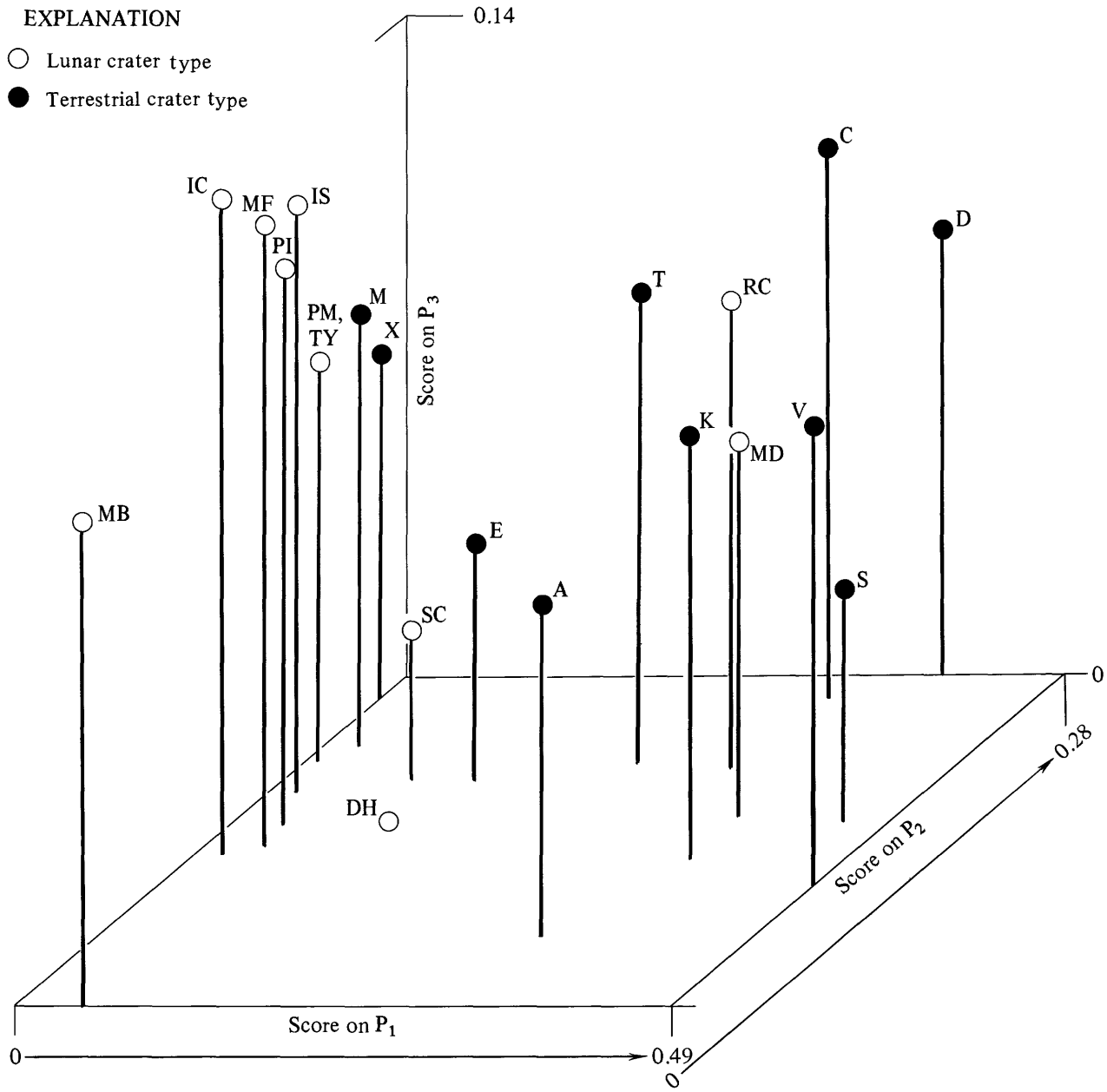

FIGURE 3.—Normalized scores of 21 crater types (table 2; pl. 1) on first three principal components (P_1, P_2, P_3), averaged from individual scores on 418 craters. For simplicity and clarity five categories of calderas in table 2 are reduced to three: calderas on shields (V), calderas on stratovolcanoes (K), and calderas surrounded by ash-flow sheets (A). Impact and explosively formed craters cluster in a tight linear distribution in upper left. They are arrayed from freshest to most degraded (declining scores on P_2 axis): experimental-explosion craters (X), meteorite-impact craters (M), fresh lunar impact craters (PM, TY), smooth-rimmed craters (IS), pre-Imbrian craters (PI), mare-flooded craters (MF), isostatically compensated craters (IC), and mare-filled basins (MB). Volcanoes cluster somewhat more loosely, on right. In addition to three types of calderas mentioned above, this group comprises tuff rings (T), mare domes (MD), raised cones (RC), small lava shields (S), cinder cones (C), and lava domes (D). A third loose grouping, comprising terrestrial maars (E), lunar dark-halo craters (DH), and secondary-impact craters (SC), is situated midway between the two primary clusters.

craters and plotted for 21 crater types: the fourfold chemical distinction among calderas is dispensed with. In figure 3 calderas are recognized on a somewhat simpler structural basis as being either on a shield volcano (V), atop a stratovolcano (K), or surrounded by an ash-flow sheet (A). Although the contrast between impact craters and volcanoes dominates the three-dimensional array of crater types in figure 3, some important relations concealed by the simpler method of data display in figure 2 also are evident.

Several observations may be made on both of the principal clusters of crater types in figure 3. The impact craters (M, PM, TY, PI, IS, IC, MF) cluster tightly together with experimental-explosion craters (X) as in figure 2, but the mare-filled basins (MB), secondary-impact craters (SC), and dark-halo craters (DH) here are detached from this group on the basis of significant differences expressed by the second and third principal components. Dark-halo craters (DH) are unique, by virtue of their negligible score on the third component, and form a loose cluster with secondary-impact craters (SC) and terrestrial maars (E). This cluster falls between the two principal groups but may be interpreted as a third major subdivision of the 21 crater types rather than as a satellite of one of the two larger groups. Judging from graphical distances between the grouped craters in figure 3, maars are not very good analogs of main-sequence craters on the Moon but easily could be confused with impact secondaries. Indeed, just this question arose concerning interpretation of the craters of Catena Davy (Oberbeck and Morrison, 1973). Differences among the seven types of impact and explosion craters with respect to components 2 and 3 seem to reflect systematic differences in relative age and state of degradation. This sequence starts with the experimental-explosion craters (X) and ends with the mare-flooded (MF) and isostatically compensated (or volcanically modified) craters (IC). According to distances between plotted points in figure 3, contrasts among these seven types are less than the contrasts between them as a group and any other type of crater; the impact interpretation of the lunar craters in this group remains compelling.

The volcanic craters scatter appreciably in figure 3, as they do in figure 2, but with some significant differences. The shallow calderas within ash-flow sheets (A) stand quite apart from the other volcanoes, a reasonable outcome for a shape classification in view of their unique morphologic characteristics and mode of origin. All three types of calderas are rather distinct from one another on the graph, presumably reflecting structural contrasts of the different kinds of volcanic edifices. Conversely, the two types of terrestrial shield volcanoes are fairly similar in figure 3. The mare domes (MD) seem to resemble more closely the calderas on large shields (K) than craters on small lava shields (S). However, the analysis presented here is restricted only to crater shape and does not take into account the disparity in size of the volcanic piles. Domes on the lunar mare surfaces still may resemble the smaller terrestrial shields. Raised cones (RC) on the Moon lie quite apart from lunar impact craters in figure 3, a distinction that is not made in figure 2. An interpretation of the mode of origin of the cones really cannot be extracted from either diagram, for these features have no clear-cut Earth analog. Terrestrial tuff rings (T), like maars (E), as a group still are transitional between most volcanoes and most impact craters with regard to morphology, but they do appear to lie closer to other types of volcanoes in figure 3 than they do in figure 2. Terrestrial cinder cones, tuff rings, and maars lie along a linear systematic trend in figure 3 that suggests a genetic, as well as morphologic, continuum of small pyroclastic volcanoes. This progression, which could reflect the relative abundance of ground or surface water in the crater-forming environment (Lorenz, 1973)—maars being the most dependent upon water—almost certainly is irrelevant to lunar volcanism. The great steepness of the terrestrial lava domes (D) and cinder cones (C) relative to other, mostly larger, types of volcanoes is clearly evident by their position in figure 3. This contrast sets the two types of craters apart from all other kinds of volcanoes, with respect to overall morphology.

CLASSIFICATION BY CLUSTER ANALYSIS

The overall dichotomous classification of craters that results from cluster analysis (pl. 1) differs only in minor detail from a cluster classification obtained in an earlier study of this kind (Pike, 1974c, fig. 2). Because most of the data are the same, it was judged unnecessary to test the new results. The stability of the earlier outcome, however, was tested several times because so few descriptive variables were used, because all clustering procedures do not necessarily yield similar or equally valid classifications of the same data (Anderson, 1971; Howarth, 1973), and because the analysis is based upon correlation of ratio data—a practice that is best avoided (Chayes, 1971). The craters first were divided evenly, and each subset was clustered separately by Parks' (1970) procedure. Next, the data were clustered by two quite different techniques that did not use the result of a principal-components analysis (Chernoff, 1973; Wishart, 1969). Finally, the 402 craters were increased to 420 and reclustered by Parks' program. In the latter two classifications (see also pl. 1), class I craters (Pike, 1974c, fig. 2, upper cluster) tended to separate into two groups each equal in rank to class II (Pike, 1974c, fig. 2, lower cluster). In all cases, some maars (E) and tuff rings (T) tended to shift back and forth between class I and class II depending upon the size and makeup of the crater sample, a clear indication that these craters fall between the two principal clusters and fit comfortably into neither. However, all five test outcomes agreed with the fundamental twofold division in plate 1 in that most class I craters differ markedly in shape from class II craters.

Although the cluster classification of 418 craters (redone for this report, pl. 1) generally preserves the same two major classes of crater shape evident in figures 2 and 3, many subclasses are distinguishable within the hierarchical structure of the dendrogram. Compositions of resulting subclasses by crater type may be determined from the letter code; these are summarized in table 5. The threefold division of caldera types has been carried over to plate 1 from figure 3, and in table 5 fresh lunar craters (PM, TY) have been combined and then divided into large craters (over 15 km across) and small craters. Average topographic differences between craters in the two principal classes, which also can be expressed by citing individual craters that have the same respective geometry, are very great indeed (fig. 4). The upper profile in figure 4 looks most like the terrestrial meteorite-impact crater Henbury No. 3, and the lunar craters Flamsteed and Aristillus. The lower profile in figure 4 most closely resembles the calderas Sete Cidades (Azore Is.), Black Peak (Aleutian Is.), and Nemrut Dagi (eastern Turkey). Although clusters I and II are very different on the average, certain craters in each group are quite similar; these tend to be tuff rings (T) and maars (E). The two most nearly alike craters in classes I and II, Potrillo maar (New Mexico, U.S.A.) and Laja maar (Tanzania), respectively, are

TABLE 5—*Composition of clusters in plate 1 by crater type*

Crater type (name)	Crater type (symbol)	N	Clusters								
			Craters of excavation				Craters of accumulation				Others
			IA	IB	IC	ID	IIA	IIB	IIC	IID	
All		418	120	29	67	44	53	30	26	24	25
Lunar craters											
Fresh mare and terra crater, small	PM, TY[1]	27	1	--	24	2	--	--	--	--	--
Fresh mare and terra crater, large	PM, TY[2]	36	26	--	9	1	--	--	--	--	--
Old lunar crater (pre-Imbrian)	PI	40	34	--	2	2	--	--	--	--	2
Isostatically compensated crater	IC	7	7	--	--	--	--	--	--	--	--
Mare-flooded lunar crater	MF	17	17	--	--	--	--	--	--	--	--
Mare-filled basin	MB	3	--	--	--	--	--	--	--	--	3
Smooth-rimmed crater	IS	19	16	--	2	1	--	--	--	--	--
Secondary-impact crater	SC	29	2	4	5	18	--	--	--	--	--
Dark-halo crater in Alphonsus	DH	3	--	--	--	2	--	--	--	--	1
Raised cone	RC	14	--	3	--	--	2	4	5	--	--
Cratered mare dome	MD	15	--	--	--	--	6	2	5	--	2
Terrestrial craters											
Experimental-explosion crater	X	22	1	--	14	6	--	--	--	--	1
Meteorite-impact crater	M	20	9	--	11	--	--	--	--	--	--
Shield volcano with caldera	V[3]	21	--	--	--	--	3	--	1	13	4
Stratovolcano with caldera	K[4]	38	--	--	--	--	26	1	6	4	1
Ash-flow plain with caldera	A[5]	9	--	--	--	--	7	--	--	--	2
Maar	E	39	7	12	--	12	--	--	--	--	8
Tuff ring, tuff cone	T	20	--	10	--	--	4	5	--	--	1
Cinder cone	C	20	--	--	--	--	--	16	3	1	--
Small lava shield	S	10	--	--	--	--	5	--	--	5	--
Cratered lava dome	D	9	--	--	--	--	--	2	6	1	--

[1]Under 15-km diameter.
[2]Over 15-km diameter.
[3]Type KO and some KA
[4]Type KA, KC, KP.
[5]Type AP and some KC.

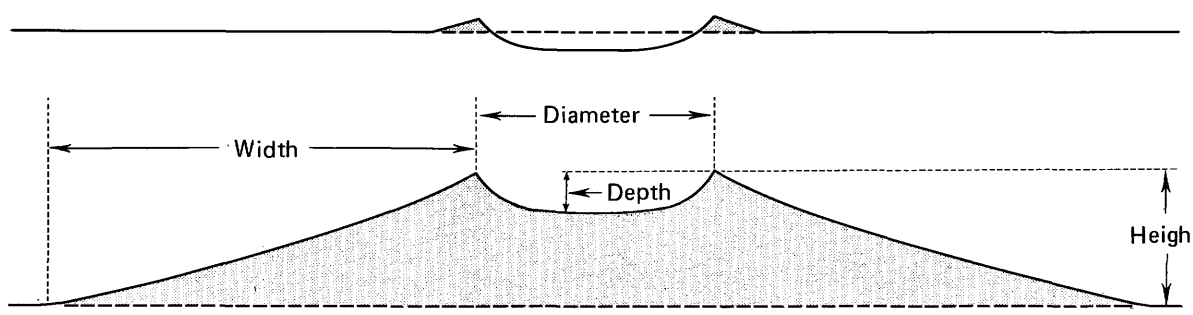

FIGURE 4.—Contrasting models illustrating overall geometric properties of two largest crater classes in plate 1. Dimensionless profiles, scaled to same rim-crest diameter, from averages of six of seven transformed variables for all 272 craters in class I (upper profile) and all 146 craters in class II (lower profile). Respective average values of circularity index are 0.78 and 0.64. Dashed line is exterior topographic datum, vertical exaggeration is 2×. Absence of transitional maars and tuff rings (fig. 2) would enhance contrast.

clearly transitional in topographic character and are not accommodated by a strict twofold division of the sample. In fact, both craters fall in small clusters that do not fit in very well with the other craters of the two major classes.

Further breakdown of the two resulting classes of craters is expressed by their subclasses, eight of which have been labeled in plate 1. Several minor subgroups have not been so designated. The selection of subgroups within a dendrogram is always somewhat subjective and largely depends upon the level of generalization appropriate to the interpretation. The subgroups shown here constitute a fairly general breakdown of classes I and II, commensurate with the nature of the 23 original crater types, most of which contain a wide variety of morphologies. A more detailed subdivision of plate 1 probably is not warranted by the data. Class I includes all terrestrial meteorite-impact and experimental-explosion craters, all but two maars, half of the tuff rings, the three mare-filled basins, and all lunar craters except those situated on the 15 domes and on 11 of the 14 raised cones. Like the craters with low scores in figure 2, most of these 272 craters have low narrow rims, a floor lying well below the exterior datum, and relatively high rim-crest circularity (fig. 4, upper profile). Most terrestrial craters in class I formed primarily by processes of excavation, in the case of natural craters either by meteorite impact or by maar volcanism. The lunar craters are implied to have formed similarly.

Subclustering within class I supports the interpretation evident from figures 2 and 3 that fresh lunar craters resemble terrestrial meteorite-impact craters more closely than maars. Most meteorite-impact craters group with the experimental-explosion craters and with small (under 15 km diameter) fresh lunar craters (Cauchy, Linné) throughout subclass IC and with larger and fresher lunar craters (Copernicus, Clavius) in subclass IA. On the other hand, most maars (along with lunar dark-halo craters and secondary-impact craters, which they resemble) group separately, in subclasses IB and ID. Tuff rings in class I occur only in subclass IB, which contains not one main-sequence lunar crater. There is not one maar in subclass IC. Only a few maars associate with main-sequence lunar craters, which tend to be the larger, older, or severely modified craters (McClure D, Capuanus, Briggs, Yerkes) in subclass IA, not the smaller fresh craters. A few terrestrial maars (Badillo, Bishoftu 4B, Kino, Lake Pawlo, and MacDougal; see Pike, 1978a) do indeed associate with meteorite-impact craters (Wolf Creek and Flynn Creek) and with some fresh main-sequence lunar craters in subclass IA (Theophilus, Aristillus, Plinius). However, postcrater sedimentation may have brought about even this minor agreement: both Lake Pawlo and Wolf Creek Crater are now known to be deeply filled with sediment (Fudali, 1979) and at least three of the remaining four maars have unknown thicknesses of postcrater fill. In plate 1 the differences between maars and impact craters substantially outweigh the similarities.

A possible tendency of cluster algorithms to misclassify transitional objects is evident in the arbitrary attachment of most maars, tuff rings, and lunar dark-halo craters to the impact craters of class I (pl. 1) rather than their separation into a third major class (as in fig. 3) or the inclusion of more of them in class II with the other volcanoes. The misclassification, if any, probably arises from three causes. First, the dendrogram is constrained to only two dimensions, and thus any tendency of subclasses IB or ID to separate from subclasses IA and IC cannot be shown effectively. Second, the "misclassified" craters were produced by explosive-excavational processes and belong in class I. Third, class II has much greater variance than does class I. This disparity, which shows up well in figure 2, evidently results in part from residual skewness not eliminated from the seven frequency distributions by the transformations. The difference in variance has placed the division between clusters I and II of the dendrogram at a higher value of the first principal-component score (0.225) than normally would be selected (0.200) from an inspection of figure 2 (Chayes and Velde, 1965). Shortcomings of this sort can be recognized by examining simple plots of principal-component scores (figs. 2 and 3) before attempting to interpret the more complex dendrograms.

However, the clustering procedure has correctly separated nearly all small (<15-km diameter) lunar craters (subclass IC) from both older and larger craters (subclass IA). The distinction probably was made on the basis of the second principal component. Smaller (simple or unmodified) lunar craters have long been known to differ from the larger (complex or modified) craters in being relatively deeper, in having relatively higher rims, and in lacking well-developed flat floors, rim terraces and central peaks (Gilbert, 1893; Quaide and others, 1965; Pike, 1967). These size-dependent contrasts appear to characterize impact craters on Earth and the other planets as well (Dence, 1968; Losej and Beales, 1975; Pike, 1971a; Hartmann, 1972b; Gault, Guest, and others, 1975).

Time-dependent, postformational effects also are reflected in the affiliation of craters with different subgroups within class I. The most evident of these effects is the shallowness of many older lunar craters in subclass IA, which contains most pre-Imbrian and smooth-rimmed craters and every one of the mare-

flooded and isostatically compensated craters. Postformational events also may have caused some of the unsystematic mixing of the types of lunar craters that make up class I; morphologies within the various crater types are by no means homogeneous. The most important processes evidently are isostatic adjustment, volcanic flooding of mare basins, ballistic erosion and sedimentation, and mass-wasting (Baldwin, 1963; Pike, 1971a, b; Ross, 1968; Howard, 1973; Schultz, 1976a).

Class II comprises the cratered mare domes, most of the raised lunar cones, and all terrestrial volcanoes except the maars and the remaining half of the tuff rings. It corresponds to the group of craters with high scores in figure 2. In contrast to the shapes of the craters in class I, these 146 craters typically have high wide rims, a floor situated well above the exterior datum, and relatively low rim-crest circularity (fig. 4, lower profile). All terrestrial craters in class II formed primarily by accumulation of erupted material rather than by processes of excavation. By implication, the cratered mare domes and raised cones also are volcanoes, a conclusion that is consistent with most other interpretations of the two types of features. Conspicuously absent from class II are such purportedly "volcanic" lunar craters as Schiller, Wargentin, Sabine, Ritter, and Kopff (Wilhelms and McCauley, 1971). The anomalous appearances of these craters, all of which associate with other main-sequence lunar craters in class I, have yet to be explained satisfactorily, although post-impact volcanism may have been at least partially responsible (Schultz, 1976b).

Although the four subgroups that are distinguished within class II (pl. 1) differ substantially from one another in crater geometry, their geologic and geomorphic interpretations are not as clear-cut as they are for the class I subgroups. The probable lunar volcanoes (RC, MD) neither cluster apart from terrestrial volcanoes nor predominate in any particular subclasses within class II (table 5). Some patterns are evident, however. The larger craters are in subclasses IIA and IID, whereas the smaller craters tend to occur in subclasses IIB and IIC. Mare domes (MD) and raised cones (RC) are all but mutually exclusive with large terrestrial tholeiite shield volcanoes (KO) and the smaller basalt shields (S). The highest concentrations of lunar domes are in subgroups IIA and IIC, whereas the lunar raised cones tend to occur in subgroups IIB and IIC. Most of the terrestrial lava domes are in subgroup IIC, but this may not be significant in terms of the origin of the lunar features. Terrestrial cinder cones (C) tend to occur only in subclass IIB, probably on the basis of their greater relative rim-steepness and crater depth. Too few lunar domes or cones are in this group to warrant any special interpretation. Subclasses IIA and IID, which comprise mostly terrestrial calderas, appear to be distinguished from each other by size of the crater relative to size of the host volcano. This difference seems to reflect both rock composition and the nature of caldera-forming eruptions: shield volcanoes dominate subclass IID, whereas most ash-flow calderas are located in subcluster IIA.

Given the scattered distribution of lunar domes and cones among the first three subgroups in plate 1, a good analogy cannot be drawn between probable lunar volcanoes and specific types of terrestrial volcanoes. Inasmuch as the topographic data on lunar domes and cones probably are the least accurate of all the measurements used here, detailed comparisons of this kind may be premature. The lunar domes probably are volcanoes and they appear to be some type of shield, but an exact interpretation remains problematical. The lunar raised cones are somewhat similar in shape to terrestrial cinder cones and lava domes, but their origin is not uniquely specified by analogy with terrestrial features, especially in view of possible effects of differing gravitational acceleration and energy of eruption (Wright and other, 1963; McGetchin and Head, 1973).

THE CALDERA ANALOGY

The inclusion of all terrestrial calderas exclusively within class II (pl. 1) and within the high-scoring group in figure 2—as well as their separation from all impact craters in figure 3—has clear-cut implications for genetic interpretation of most of the Moon's craters. Although calderas have been proposed repeatedly as terrestrial analogs of large main-sequence lunar craters since the time of Dana (1846), all three classifications based on the principal-components results verify the contention of Gilbert (1893) that caldera shapes differ dramatically from those of the lunar craters.

Large lunar craters usually are interpreted as volcanic calderas by inspection, on the basis of supposed morphologic similarities (such as flat floors, scalloped inner rims, and structural terraces and lineaments) that are presented in paired sketches and photographs of single lunar and terrestrial craters (Fielder, 1965; McCall, 1966; Moore and Cattermole, 1967; Peyve, 1969; Green, 1971; Firsoff, 1961; Erlich and others, 1974; Leonardi, 1976). Although minute details of the crater or caldera proper are discussed at great length in such comparisons, the form and extent of the overall structure are almost always ignored. The latter aspects are of critical importance. Two landforms so clearly different in gross surface geometry as terrestrial calderas and main-sequence lunar craters hardly can be

proved to be analogous on the basis of minor morphologic characteristics. Auxiliary geomorphic traits that previously were interpreted in terms of primary volcanic cratering on the Moon probably are either of exogenic origin or are secondary endogenic features superposed on initial impact landforms (Pike, 1971a). Many odd-shaped craters on the Moon are large basin-impact secondaries (Wilhelms, 1976; Oberbeck and Morrison, 1976). If any of the larger main-sequence craters on the Moon are of internal origin, then they have developed through volcanic processes and events distinctively unlike those that form terrestrial calderas. The close morphologic and geometric resemblance of the quite normal-looking calderas on Mars to their terrestrial counterparts (Carr, 1973; Pike, 1974c) suggests that such exceptional volcanic processes and events, whatever one might imagine them to be (Schultz, 1976a), have not formed any conspicuous craters on the Moon.

PREDICTING CRATER GENESIS

Whereas single topographic parameters can distinguish volcanoes as a class from impact craters as a class (Guest and Murray, 1969; Murray and Guest, 1970; Pike, 1972a, b; Oberbeck and others 1972), they cannot predict the mode of origin of individual craters with any certainty. Even if the lunar raised cones and the terrestrial maars and tuff rings are omitted, values of the first four morphologic variables (table 2)—taken one at a time—simply do not divide craters completely into two genetic groups (the last three variables are even poorer discriminants). Width/diameter data are only just mutually exclusive for the two main groups of craters (at an untransformed value of 0.49). Because the width of the rim flank often is difficult to measure accurately and can be in serious error when obtained from photointerpretation alone, especially of spacecraft images, a wider separation is needed. For all other variables, the two categories overlap to some extent. Although a height/depth value of about 0.93 would correctly separate most craters into either volcanoes or impact craters, rim height possibly is the least reliable of all crater measurements and should not be relied upon as the sole indicator of origin. Height/diameter (at a value of 0.053) would be an even less effective predictor of crater origin. Finally, the circularity data overlap so badly (centered at a value of 0.71) that this often-used parameter must not be regarded as a reliable genetic discriminant for individual craters. The considerable overlap explains the only moderate score for circularity on the first principal component (table 4) and the existence of the fourth component.

The chances of misclassifying an object decrease substantially as the number of taxonomic criteria increases and description of the object becomes more complete (Sokal and Sneath, 1963). The strength of the multivariate approach, when properly implemented, for classifying craters lies in its ability to combine several variables in a parsimonious statistical model that automatically emphasizes the most important properties present in the descriptive data. The adoption of shared attributes of crater geometry as a topographic signature eliminates the reliance on individual criteria, which are especially vulnerable to additional uncertainties resulting from unavoidable errors in measurement. Such errors can arise easily when the only sources of data are degraded spacecraft pictures.

The results of this experiment suggest a method for determining or at least narrowing the alternatives for the genesis of any large (over 5 km across), rimmed extraterrestrial crater on the basis of gross morphology. Five kilometers is the size of the largest terrestrial maar and a quite conservative cutoff diameter. As the original classification was based on the principle of indeterminacy, the genetic criterion too, must be stochastic. A suitable set of topographic measurements, preferably no fewer than the number used here, can be subjected to a multivariate analysis together with data for a representative sample of terrestrial craters whose origin is known. The origin of a given ("unknown") crater reflects that of the other ("known") craters in its cluster. Although this method appears to lack the exactness of the simple graphical criteria proposed previously (Pike, 1972b; Oberbeck and others, 1972; Smith, 1973), the chances of misclassifying craters are considerably less. The present investigation has developed three simple statistical models, illustrated in figures 2 and 3 and in plate 1, by which large craters may be tested for geometric similitude. Discriminant analysis—a multivariate technique by which "unknown" objects are assigned to one of several predetermined classes of "known" objects (Chayes and Velde, 1965; Griffiths, 1966)—offers yet a fourth approach for comparing a crater with craters belonging to the major types recognized here. Numerical criteria for determining the genesis of craters less than 5 km across using landform data continue to remain elusive, however, and may even prove to lie beyond the information content of the five basic topographic characteristics and their ratios.

THE LINNÉ CONTROVERSY RESOLVED

Apollo 15 pictures have both ended a century of controversy over the genesis of the lunar crater Linné (Pike, 1973b) and given us a new morphologic standard for simple impact craters on the Moon (fig. 5). Conflict-

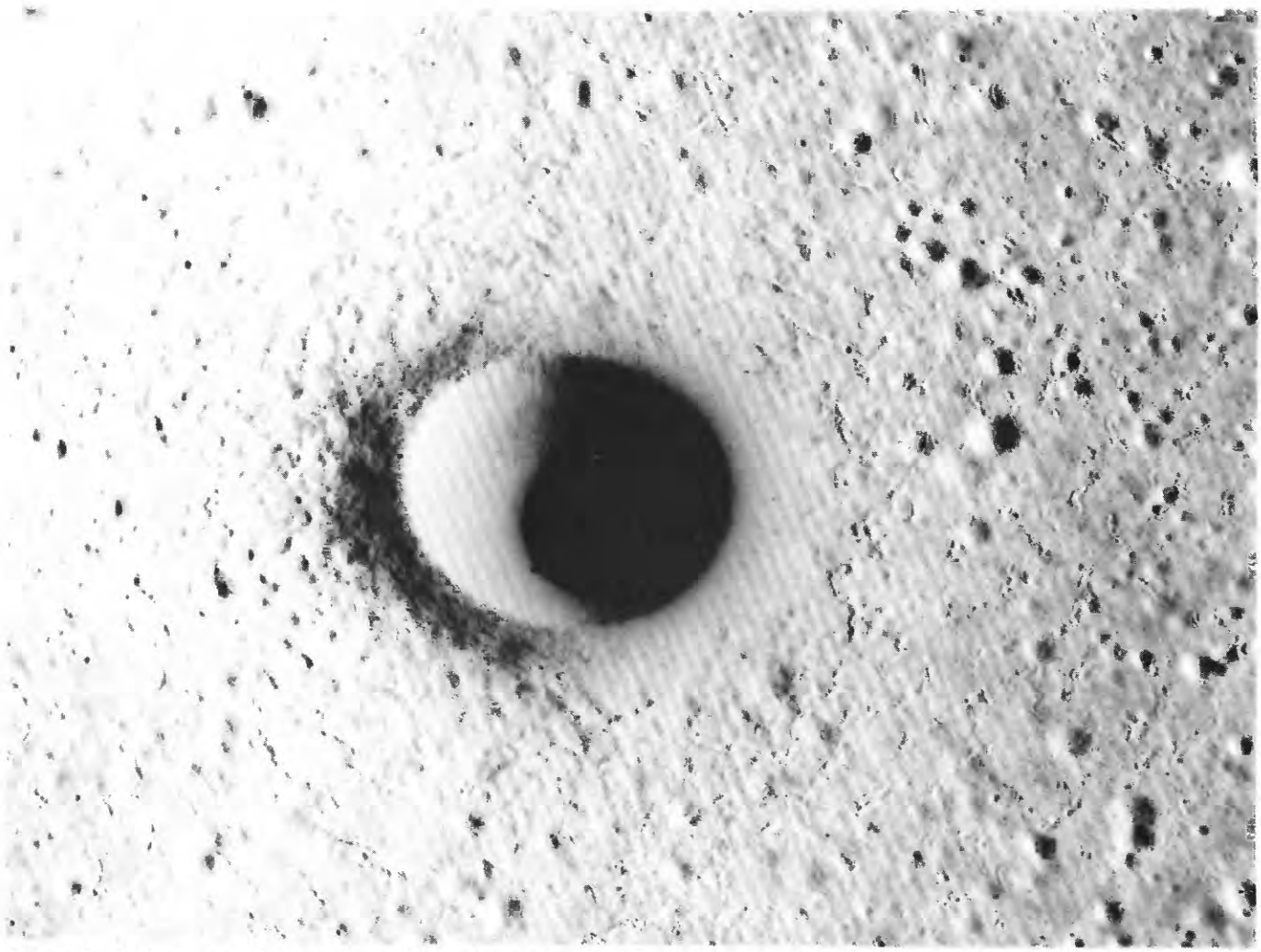

FIGURE 5.—Oblique view of Linné, unusually fresh example of simple impact crater of lunar main sequence, located in northern Mare Serenitatis. Diameter of rim crest is 2,450 m. Note steep interior walls, large blocks of ejecta on rim, dunelike textures on flank, and secondary-impact craters about 1.3 crater radii from rim crest. Compare with much larger fresh crater Aristarchus (fig. 27), which has a complex morphology. View is to north; sun is to right. Apollo 15 panoramic camera photograph 9353.

ing visual observations of Linné, a small crater in western Mare Serenitatis, were responsible for rekindling interest in lunar research during the late nineteenth century and for encouraging belief in recent volcanic eruption on the Moon. Since its initial recognition as a crater in 1823, Linné had been described as a well-formed deep crater between 6 and 11 km in diameter. In 1866, the astronomer Julius Schmidt announced that the crater had vanished and had been replaced by a bright patch surrounding a craterlet only about 500 m across. Reports of still other changes followed, and Linné became one of the most famous "problem" craters on the Moon. Further details of the ensuing controversy and references to the vast literature on this enigma, which accumulated as the misunderstandings were clarified, are available elsewhere (Ashbrook, 1960, 1963b; Moore, 1965; Moore and Cattermole, 1967).

Apollo 15 photographs reveal Linné as an extremely fresh but otherwide quite ordinary impact crater (fig. 5). Two topographic profiles across Linné and a detailed elevation profile on the rim crest from Apollo 15 mapping-camera frames 0407 and 0408 (fig. 6) furnish the following measurements: rim-crest diameter, D_r, 2,450 m; width of the rim flank, W_e, 650 m; depth, R_i, 600 m; height of rim crest above outer surface datum, R_e, 125 m; index of rim-crest circularity, C, 0.89. Although Ashbrook (1963a) obtained good values for depth and height visually, at the telescope, his estimate of diameter was low by a factor of 2. According to the new measurements, the first four of which are averages, the crater interior lies far below the exterior datum; the outer rim flank is both low and narrow, and the rim crest is highly circular. The interior profile is approximately parabolic; the inner wall just below the rim crest is as steep as 40°, and the slope decreases to

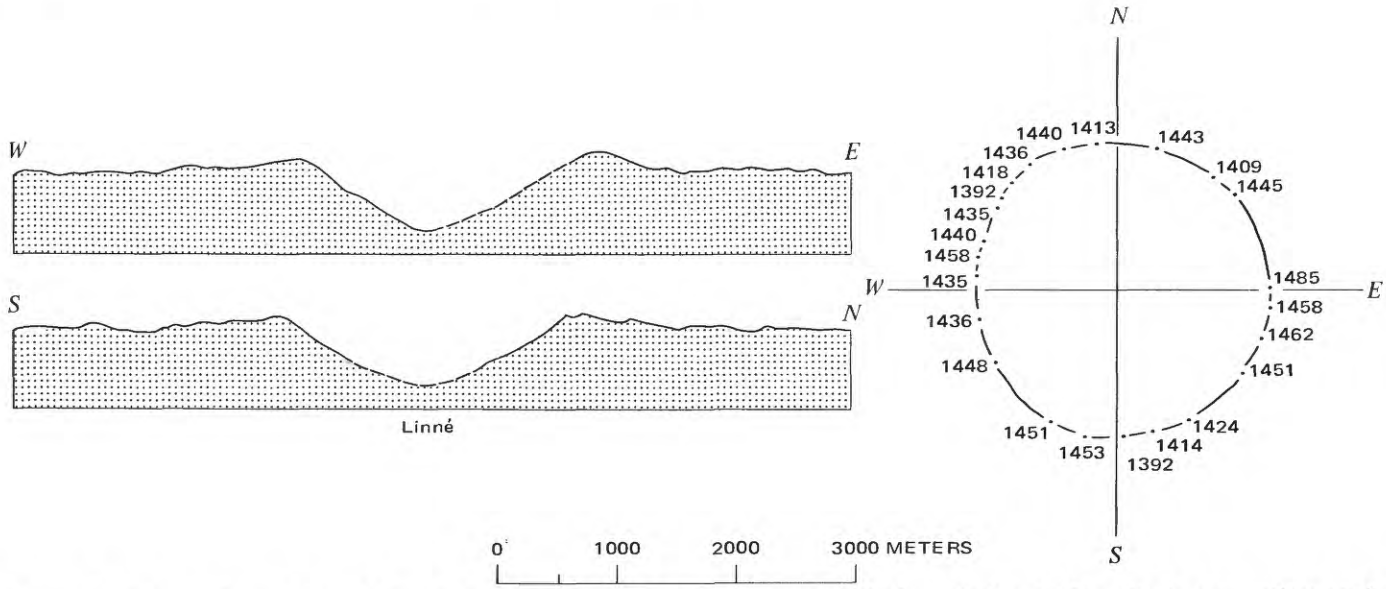

FIGURE 6.—Topographic profiles and rim-crest outline of crater Linné. Profiles dashed where shadowed. No vertical exaggeration; north approximate only. Numbers on rim-crest profile are elevations in meters above arbitrary lunar datum. Data from photogrammetry of Apollo 15 mapping-camera frames 0407 and 0408 by Raymond Jordan, U.S. Geological Survey.

between 25° and 30° about 250 m below the rim. From comparison with shapes of several different types of lunar and terrestrial impact-explosion and volcanic craters (Pike, 1972b), the geometric signature of Linné clearly is that of a very young impact crater, intermediate in size between Meteor Crater (Arizona) and the New Quebec (Canada) crater. It falls into subcluster IC in plate 1 along with both terrestrial meteorite craters.

Linné is perhaps the freshest lunar crater of its size yet photographed in such detail (fig. 7); superposed craters are both scarce and small. Linné has all the features diagnostic of a primary impact crater. Below a crisp and almost circular rim crest lies a hummocky outer rim surface, thickly strewn with boulders up to 35 m across. Boulders distributed singly and in roughly radial rays persist well beyond the topographic break in slope at the base of the rim flank. The surrounding bright patch, seen as coalescing rays on smaller scale high-sun photographs (Pike, 1973b), resolves into an annulus of superbly preserved dunelike structures, formed as ejecta swept out from the impact focus. This deposit may be best interpreted as "ground-surge" (Sparks and Walker, 1973). Radially outward, the morphologic character of Linné's ejecta changes from a coarse pattern of braided hummocks to finer, individually resolvable transverse dunes, and finally to clusters and chains of secondary-impact craters. Relative spectral reflectivity data also show that Linné is very young (McCord and Adams, 1973). The spectral signature of Linné resembles that of (crushed) young mare rock (Apollo 12 site) better than it does the signatures of upland or older mare rock.

Linné is a simple—as opposed to a complex—lunar crater (Quaide and others, 1965; Pike, 1967), in which terraces, central peaks, and a flat floor are characteristically absent. Moreover, little modification appears to have taken place within the crater since the initial impact (fig. 7). Linné's inner walls vary in detailed morphology with distance below the rim crest. About 50 m from the top a discontinuous narrow band of shadow around the visible part of the inner rim suggests an outcrop of relatively resistant material, which might be interpreted as the top of structurally uplifted (bedrock) material underlying the ejecta. Below this possible outcrop, and extending about a third of the way down the inner bowl, the surface is scarred by numerous subradial grooves. Their crudely dendritic pattern suggests shallow debris channels. The many blocks and the deposits of finer loose material present below the grooved zone may indeed indicate mass wasting of the steeper slope above. Radial streaks and bands, which are most conspicuous in the loose material lying below the eroded, fluted zone, may reflect mass-wasted deposits of different ages and textures.

The detailed geometry and morphology of Linné constitute as compelling an argument for primary impact genesis as occurs anywhere on the Moon. There is no evidence that this classic impact crater has ever changed substantially in shape. Totally absent is the rim asymmetry or concentricity which would be expected if, by some bizarre coincidence, a second impact

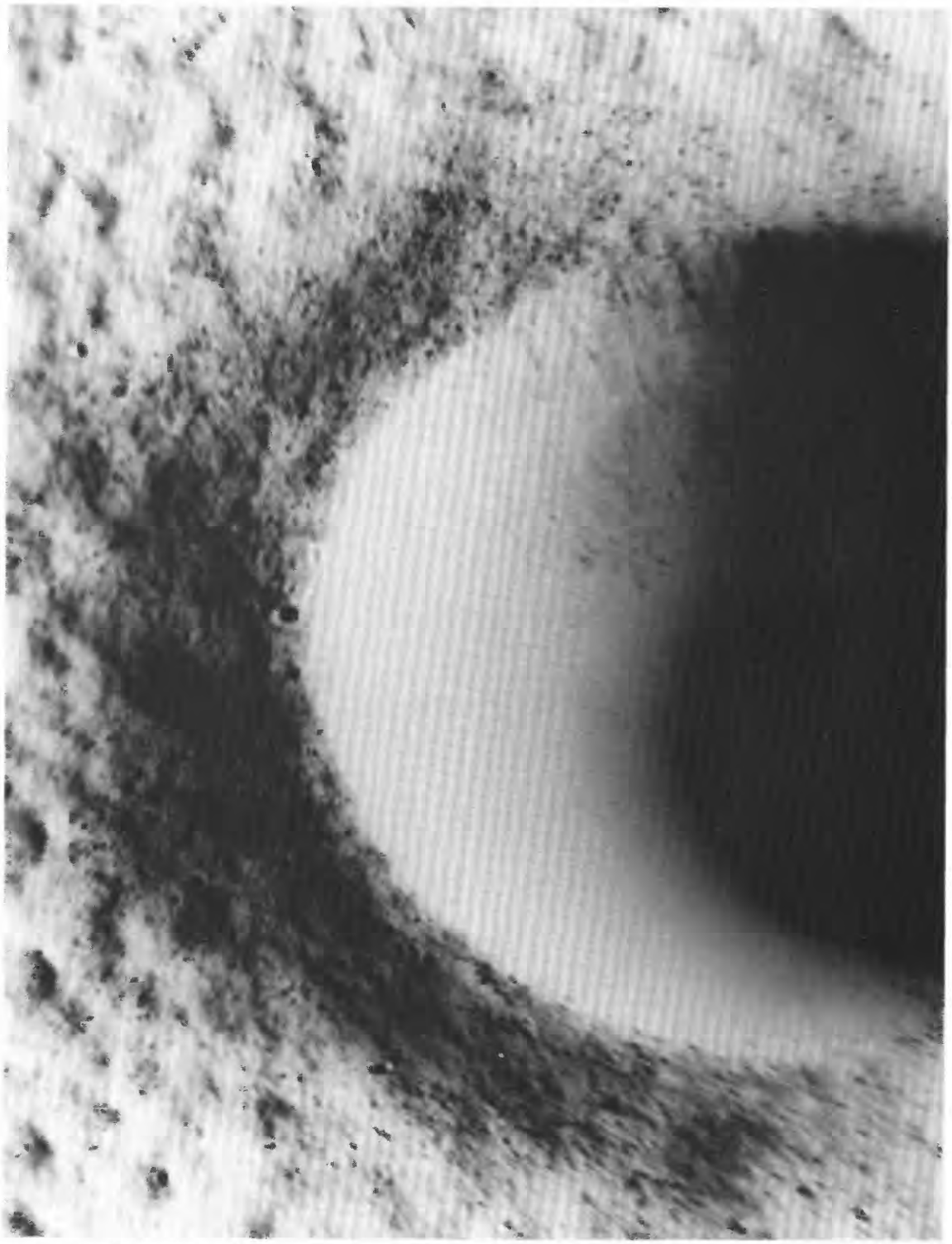

FIGURE 7.—Detail of crater Linné; enlargement of central portion of figure 5. Note large blocks on rim and within crater, suggestion of stratification on upper rim wall, scarcity of superposed impact craters, radial furrows on rim wall, and slump deposit below furrows. Apollo 15 panoramic camera frame 9353.

had been scored directly on the alleged larger crater observed before 1866. Nor is there a trace of endogenic modification to any part of the crater or its ejecta facies; the small craters superposed on Linné look like impact pits, not volcanic vents. Even more unlikely is the possibility that the crater seen before 1866 was a

different small crater in western Mare Serenitatis. Evidently, optical effects were responsible for the enigmatic changes in Linné (Robinson, 1970), an apt testament to the perils of visual lunar observation near the resolution limit of Earth-based telescopes and to the need for more complete coverage of the Moon by data of Apollo quality.

SECONDARY-IMPACT CRATERS

The significance of secondary-impact craters on the Moon to the interpretation of mechanics and ballistics of large primary craters has been recognized for some time (Shoemaker, 1960; Roberts, 1964; Oberbeck and Morrison, 1973), but detailed shape properties of the satellitic craters themselves have been accorded little attention. Apollo photogrammetry now has made it possible to draw some quantitative distinctions between primary and secondary craters on the Moon. Although the morphologic characteristics of the two types of craters have been contrasted (Shoemaker, 1962), the small size of most secondaries and the resulting absence of topographic data have precluded a more exact description of their shape. The 29 secondaries that were measured for this report provide a fair first sampling of satellitic craters in the 450 to 4,000-m-diameter range. Larger older secondaries, particularly those surrounding the Imbrium and Orientale basins (Wilhelms, 1976; Oberbeck and Morrison, 1976), are also common but were not included in this preliminary study. Since the work was completed, I have examined larger secondary craters (Pike and Wilhelms, 1978). The 29 craters used here all are of Copernican age, as nearly as can be determined, and are mostly from Aristarchus (fig. 8) and Catena Davy (fig. 9); a few are from Copernicus and elsewhere (table 9). Many of the craters are clustered and share portions of their rims with adjoining secondaries, although others are single (but not isolated) craters.

The contrast in shape between most impact primaries and most secondaries is clearly evident in averaged values of five ratios of crater dimensions, as shown below for the 29 secondaries and for 44 primary craters in the same diameter size range.

Descriptive variable	Primaries (n=44)	Secondaries (n=29)
Rim-crest circularity, C	0.81	0.57
Height-depth, R_e/R_i	.19	.22
Width/diameter, W_e/D_r	.26	.26
Height/diameter, R_e/D_r	.04	.02
Depth/diameter, R_i/D_r	.19	.13

Mean circularity value for the primaries is 0.81, whereas it is only 0.57 for the secondaries. The latter

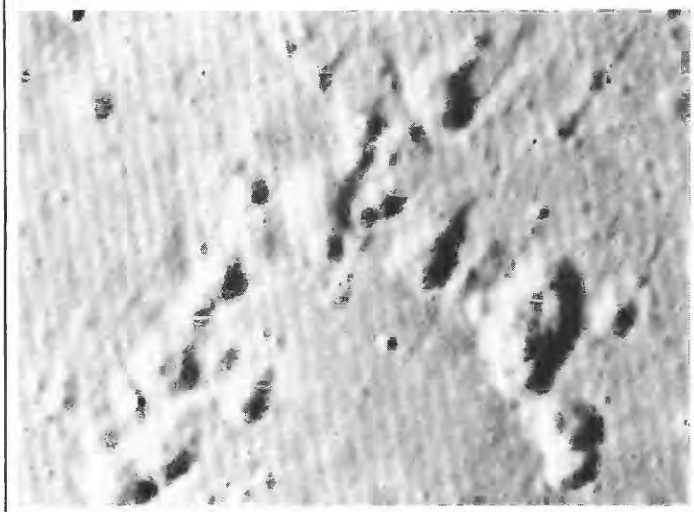

FIGURE 8.—Nearly vertical view of inverted V-shaped cluster of secondary-impact craters in Oceanus Procellarum; formed by material ejected from crater Aristarchus to the south. Legs of V are 4 km apart; north is up. Sun is to right. Compare with craters in figure 9. Apollo 15 panoramic camera photograph 0320. Eleven largest craters were measured on a 1 : 10,000 topographic map compiled from this picture and from frame 0325.

figure is too high, moreover, because the most complex and irregular secondary craters are difficult to measure and hence are underrepresented in the sample. Rim height is another rough indicator of crater genesis (Pike, 1972b). According to the new data shown above, the raised rims of primary craters are about twice as high above the surrounding terrain as those of the satellitic craters. Aside from about a 50 percent greater depth, however, primary craters are rather like secondary craters with respect to the remaining characteristics tabulated above: both the height/depth ratio and the relative width of the rim flank are about the same. Further examination of the data on secondary-impact craters in table 9 at the back of this report reveals that the 11 Aristarchus secondaries exhibit systematically shallower depths and greater rim heights relative to the other larger secondaries in the sample (relation not illustrated here). The explanation for this curious difference, which does not appear to reflect either map accuracy or relative crater age, may lie in the fact that the Aristarchus secondaries (fig. 8) all are clustered in a V-shaped pattern, whereas the larger craters are single or arrayed in a chain (fig. 9). If the Catena Davy craters are Orientale secondaries, they would also have formed in higher velocity impacts. This possible morphologic difference among secondaries may depend upon the angle of impact, the distance from the primary crater, the shape of the projectile, and the nature of the ejected material; it should be examined subsequently in greater detail.

The ability to distinguish primary craters from sec-

FIGURE 9.—Vertical view of Catena Davy, a chain of about two dozen small craters (mostly on floor of large flooded crater Davy Y) that probably formed as a result of secondary impact from large and distant primary crater to the west (unknown but possibly Orientale). These craters also have been interpreted as volcanic vents (Schultz, 1976a). Chain is about 48 km long. Sun is to right. Compare with figure 8. Apollo 16 mapping-camera photograph 2198. Nine of the larger craters were measured for this study on 1 : 50,000 topographic maps compiled from Apollo 16 panoramic camera photographs.

ondaries is useful in assessing the extent and volume of ejecta from lunar impact basins and perhaps the original lengths of ray systems from the basins. Where the secondary craters are alined or clustered, telling them apart from primaries is not difficult, especially when the craters are all fresh. However, the best topographic criteria in attempting this distinction for individual craters, circularity and rim height, become less effective as both types of craters are degraded with time. Because rim height is difficult to measure for a small fresh crater under even the most favorable circumstances, rim-crest circularity may remain the best clue to the origin of an older small isolated crater on the Moon. With appropriate care and allowing for filling of a crater with time, the depth-to-diameter ratio also might be helpful in deciding whether a particular crater is of primary or of secondary origin.

LUNAR CENTRAL VOLCANOES

The frequency of genuine volcanic landforms on the Moon still remains somewhat indefinite (Chapman and others, 1970; Smith, 1973; Fielder and Wilson, 1975; Guest and Murray, 1976; Head, 1976a; Schultz, 1976a). Because lunar volcanic craters are small in size (those measured here do not exceed 3 km in rim diameter) and evidently few in number, almost no data on their shape have been made available. For the first time enough topographic information has been generated for a preliminary quantitative assessment of the morphology of several types of likely volcanoes. The lunar volcanoes for which measurements could be made from Apollo 15–17 data occur on mare surfaces and on the flat floors of a few large craters, the two main loci of endogenic activity on the Moon. Cratered volcanic edifices on the Moon fall into at least three distinct categories: domes, cones, and dark-halo rille craters (figs. 10–13). The dimensions of each feature are listed in the back of this report, and the averaged geometric properties of the three types are summarized in table 2. As the data are few and sometimes of doubtful reliability, I have made little attempt to distinguish morphologic subtypes within any of the three major classes of lunar volcanoes. Other kinds of volcanic edifices familiar from terrestrial experience, such as stratocones with a summit crater or caldera, have not been identified with certainty on the Moon. Although the peculiar crater Hyginus and the chain of smaller pits along the adjacent Rima Hyginus probably are endogenic, little effusive activity appears to have occurred (raised rims are either absent or exceedingly low), and the craters all may be largely collapse pits and not true volcanoes (Pike, 1976a). Other smaller types of volcanoes or pseudovolcanic features may exist on the mare surfaces (Greeley and Schultz, 1975: Schultz and others, 1976), but measurements are not yet available.

CRATERED DOMES

The 15 cratered domes are a small but probably representative sampling of the many similar features that have been recognized and mapped on the Moon, usually on mare surfaces (Jamieson and Rae, 1965;

Smith, 1973). Coverage of domes by Apollo data is poor; only four of the fifteen domes listed in table 9 are measureable on the new photographs and maps. Named domes include Herodotus Omega, Hortensius Sigma, Hortensius Phi, Hortensius Omega, Kies Alpha, and Cauchy Omega. Two unnamed domes are located near the crater Maraldi B (fig. 10), one north of Rima Aristarchus VIII, one west of the crater Milichius (fig. 11), another in the Marius Hills, and three west of the crater Fra Mauro. An enigmatic and very shallow D-shaped depression situated in a patch of mare material between the Montes Haemus and Apenninus (Whitaker, 1972) has been interpreted as a caldera (El-Baz, 1973); its overall form is that of a very low dome or shield. The domes west of Fra Mauro crater conceivably could be only upland hills that have been cratered by chance impacts (Smith, 1973). All domes appear at very low sun angles as low flattish hills, roughly circular to oval in outline with convex margins, and display a more or less centrally disposed, rimless depression at the summit (Figs. 10, 11). A rough model of surface form, comprising values of the arithmetic mean and standard deviation for five topographic variables, is shown below for the 15 lunar domes (see also table 2):

Descriptive variable	Mean	Standard deviation
Rim-crest circularity, C	0.58	0.20
Crater diameter, D_r (m)	1525	640
Crater depth, R_i (m)	160	76
Dome height, R_e (m)	350	175
Flank width, W_e (m)	3525	1750

FIGURE 10.—Vertical view of two small cratered domes in northern Mare Tranquillitatis, just west of crater Maraldi B. Summit craterlets are about 7 km apart. North is up. Apollo 17 mapping-camera photograph 0306. Sun is to right.

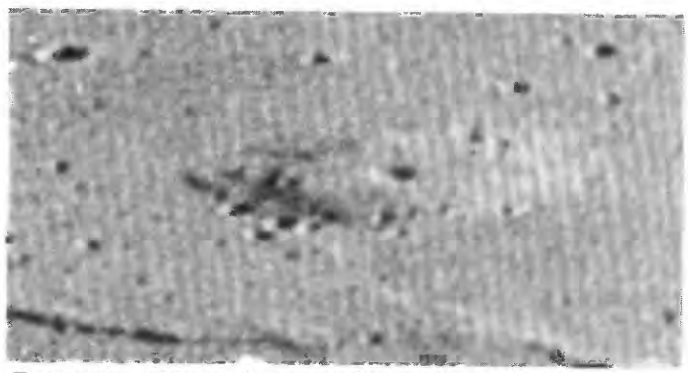

FIGURE 11.—Oblique view to northwest of cratered dome on mare surface between craters Milichius and Milichius A (near Kepler). Dome is nearly 12 km across at base but only 250 m high. Apollo 12 photographs 51–7552 (Hasselblad camera). Sun is to right.

The more complex, perhaps two-stage lunar domes that are found in the Marius Hills region on the Moon (McCauley, 1965, 1968) are not represented in the sample. The simpler domes treated here usually are arranged in groups, although isolated domes (Kies Alpha) are known, and may exhibit some tendency toward alinement along trends of the lunar grid system. Two types of simple dome may exist on the Moon. The larger flat cratered domes, which are restricted in location to the mare surfaces exclusively, are the kind sampled here. A smaller relatively steeper dome that may occur on the floors of some craters (Copernicus) can be confused with cratered cones.

Although it is generally agreed that the lunar domes formed as the result of some type of endogenic activity, several alternative hypotheses have been advanced and the exact mechanism remains in doubt (Baldwin, 1963). The well-established mafic character of the lunar mare rocks suggests that the flat cratered domes considered here could be shield volcanoes of the Hawaiian type (Pickering, 1906; Baldwin, 1949), and their overall geometry lends some support to this interpretation (table 2). However, lunar domes differ from terrestrial shield volcanoes in several respects. The lunar domes are a good deal smaller than most of their alleged terrestrial counterparts, the depth of the summit crater is a larger fraction of the height of the edifice, and the lunar summit craters are not the intersecting and stepped, shallow, pan-shaped depressions commonly found on terrestrial shields. In some ways, the lunar domes are more like the smaller terrestrial lava shields found in the Hawaiian Islands, the western United States especially in southern Idaho and northern California, and Iceland. Although lunar domes usually are quite flat and do not seem to have the conical profile of the classic Icelandic-type lava shields, to which they are often similar in size, the

overall geometry of these two types of features is somewhat more comparable (table 2). The shapes of the summit craters in particular are more alike.

The data presented here tentatively support the analogy first drawn by Rae (1966) and later adopted by Head (1976a) that the lunar mare domes are small flat shield volcanoes, more akin to small terrestrial lava shields with simple craters than to Hawaiian-type volcanic piles with complex summit craters (see also Pike, 1974c). The exceedingly low relief of the lunar domes relative to their areal extent, together with their flat configuration, suggests that the constituent rocks were once highly fluid lava, low in volatile content, emitted in quiet central eruptions with virtually no intercalated pyroclastic material. The lunar mare basalts, which approximately resemble terrestrial tholeiite basalt that is highly enriched in titanium, would have been emplaced in this fashion—almost certainly they are the materials of which the simpler lunar domes were built. The similarity of the domes to the surrounding mare surfaces with respect to albedo and colorimetric properties supports this speculation.

CRATERED CONES

The 14 cratered raised cones are a good sample of a rare lunar feature that has received less attention than the mare domes (Moore, 1971; Mattingly and others, 1972; El-Baz, 1972; Scott, 1973; Scott and Eggleton, 1973). Coverage of cones by Apollo is better than that for domes, half of the sampled ones being measureable on the new photographs and maps. The cones include two in southern Mare Serenitatis, three on the floor of King crater and four on the floor of Copernicus, a single cone west of the crater Lassell (fig. 12), two north of the Aristarchus Plateau, and one located in the Marius Hills. The examples within Copernicus conveivably may be only hillocks cratered by fortuitous impacts (Howard and Wilshire, 1975). No measurements were available for any of the alleged "cinder cones" near the Apollo 17 site (El-Baz and Worden, 1972). A preliminary model of shape, comprising values of the arithmetic mean and standard deviation for five topographic variables, is given below for the 14 raised cones (see also table 2):

Descriptive variable	Mean	Standard deviation
Rim-crest circularity, C	0.55	0.16
Crater diameter, D_r (m)	715	540
Crater depth, R_i (m)	75	65
Cone height, R_e (m)	120	45
Flank width, W_e (m)	440	150

Lunar cones resemble mare domes in that the bottoms of their summit craters tend to lie at or above the surrounding datum, their crater rim crests are quite acircular, and their height/diameter and depth/diameter aspects are similar (table 2); none of these characteristics is typical of impact craters. The summit craters of domes are about three times the diameter of craters atop cones. Moreover, cratered cones have much steeper and narrower rim flanks than lunar domes, and unlike domes, the lunar cones are found on the flat floors of a few large fresh impact craters (Copernicus, King) as well as on mare surfaces. Cones also tend to be disposed in clusters or alinements; isolated cones (Lassell H) are exceedingly rare. Cratered cones tend to have somewhat more subdued morphologies than domes; although cones may be complete and well defined, more often they are breached and highly irregular.

FIGURE 12.—Oblique view to south of cratered cone in Mare Nubium between craters Lassell H and Lassell J. Cone, which is darker than surrounding mare surface, measures about 2,500 m across at its base. Apollo 16 Hasselblad photograph 19237. Sun is to left.

Like mare domes, the cratered lunar cones are directly comparable in both size and shape with specific types of terrestrial volcanoes. Scott (1973) draws an analogy between cones in southern Mare Serenitatis and terrestrial cinder cones. His interpretation is supported by the topographic data presented here (table 9), except perhaps that terrestrial cinder cones tend to be somewhat higher, deeper, and more circular than their possible counterparts on the Moon (table 2). These differences might be ascribed to erosion of the lunar cones. The rim flanks of lunar cones also tend to be slightly narrower than the flanks of the terrestrial cinder cones (table 2), in direct contradiction of calculations predicting the widespread distribution of ejecta around exceedingly low lunar cinder cones (Wright and others, 1963; McGetchin and Head, 1973). However, the observations of "cinder cones" in the Taurus-Littrow area that precipitated these calculations (El-Baz and Worden, 1972) have not yet been verified by detailed measurements of the alleged volcanoes. Two of

these craters, Shorty and Van Serg at the Apollo 17 site, were later interpreted as impact craters (Muehlberger and others, 1973). If in fact the lunar cones described here are pyroclastic volcanoes, then the high rim flanks may have to be explained by taking into account still other differences between lunar and terrestrial eruptive environments. Again, as in the case of the mare domes, if the lunar magmas were exceedingly low in volatiles and the resulting eruptive activity was correspondingly less explosive, then perhaps the ejected material would not travel as far from the vent as it would from a comparable eruption on Earth. All in all, minor pyroclastic eruptions on the Earth and Moon may have yielded fairly comparable landforms despite certain and likely differences in the two physical environments.

DARK-HALO CRATERS

Topographic measurements could be obtained for only three dark-halo craters, Alphonsus KC, Alphonsus MD, and a nearby unnamed crater—all from Apollo data on a 1:50,000 map (fig. 13). The morphology of these craters, which are situated along Rima Alphonsus I on the northeastern part of the flat floor in Alphonsus crater, has been described in detail by Kuiper, Strom, and LePoole (1966) and by Carr (1969). Although this small sample is an inadequate basis for drawing any firm genetic conclusion (no geometric model is give here), the gross geometric characteristics of the three craters do not vary much (table 9). The dark-halo craters are not raised cones (Schultz, 1976a) but rather share some geometric similarities with both lunar secondary-impact craters and with terrestrial maars: low rim-crest circularity, low rims, and low depth/diameter ratio. Their occurrences only along rilles and their wide, dark rim flanks distinguish them readily from lunar secondaries. Hartmann (1967) and Peterfreund (1976) estimated rim and bowl volumes and found that the rim deposits consistently occupy greater volumes than the craters, but preliminary calculations from the new map data suggest rather the reverse. Bowl volumes average about one and a half times the rim volumes. Clearly, good data are needed on the geometry of other craters within Alphonsus.

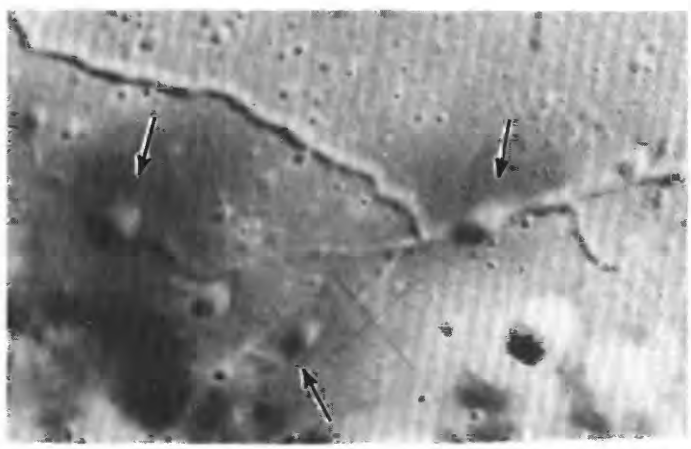

FIGURE 13.—Oblique view of three dark-halo craters, Alphonsus KC (left arrow), Alphonsus MD (right arrow), and unnamed depression (middle arrow) situated along rilles on floor of large impact crater Alphonsus. View is to southwest. Two named craters are 15 km apart. Apollo 16 mapping-camera photograph 2477. Sun is to lower left.

Carr (1969) regarded the dark-halo craters in Alphonsus as volcanoes but did not make a more specific interpretation. Kuiper, Strom, and LePoole (1966) interpreted them as maars. Although these craters are quite similar in surface geometry to terrestrial maars, there are difficulties with the prevalent maar interpretation because of the absence of abundant water on the Moon (Taylor, 1975; Mason and Melson, 1970; Waters and Fisher, 1970; Lorenz, 1973). Conceivably, a nonphreatic maar mechanism could apply (Shoemaker, 1962; Ollier, 1974). The dark-halo craters along the rilles in Alphonsus also are larger than typical terrestrial maars, although this difference could have resulted from the difference in gravity or from their being enlarged by widening of the rilles. Thus, the exact mode of origin—although almost certainly endogenic—remains in doubt. It is possible that a pyroclastic eruption producing volumetrically less, but more widely dispersed, ejecta than lunar cratered cones may occur along a few rilles on the Moon, particularly in the case of features—like the Alphonsus dark-halo craters—situated near the center of the near side (Pike, 1976a). These dark-halo craters could be lunar equivalents of terrestrial cinder cones (Peterfreund, 1976). The morphologic differences between raised cones and dark-halo craters might have arisen from the presence of some fluid lava in the cone eruptions but none in the formation of the dark-halo craters. Alternatively, different magmas may have given rise to the two different types of lunar volcanoes.

SMOOTH-RIMMED CRATERS

Craters such as Ritter, Sabine, Herodotus, and Kopff have been classified on the 1:5,000,000 geologic map of the Moon as a type (Ics) that "may differ sufficiently from main-sequence (impact) craters to suggest a different origin" (Wilhelms and McCauley, 1971). These craters span an usually narrow diameter range, about 20 to 45 km. On Lunar Orbiter images, smooth-rimmed craters lack the well-developed hummocky texture and radial ridges that are characteristic of the rims of other

craters, and conspicuous ejecta blankets are absent. The crater Kopff in Mare Orientale (Lunar Orbiter IV frame H 187) is a particularly good example; unfortunately it was not photographed by Apollo. In addition, they are comparatively shallow; "floors are commonly about level with the surrounding terrain" (Wilhelms and McCauley, 1971). Following Morris and Wilhelms (1967) and especially McCauley (1968), Wilhelms and McCauley suggested a caldera genesis for these craters, an interpretation that seems to have gained some support (Mutch, 1970; DeHon, 1971; Smith and Sanchez, 1973; Short, 1975: Fielder and Wilson, 1975). This idea badly needs to be tested. Nineteen smooth-rimmed craters are included in the sample compiled here, of which five (Langrenus F and B, Yerkes, Lick, and Jansen) have been measured from Apollo photogrammetric data, all on LTO's. The remainder include Vitello, Kopff, Damoiseau, Herodotus, Sabine, Ritter, Grove, Daniell, Gambert, Lassell (fig. 14), McClure D, McClure M, Crozier, and Sosigenes. A crude model of surface form, comprising values of the arithmetic mean and standard deviation for six topographic variables, is shown below for these 19 craters (see also table 2).

Descriptive variable	Mean	Standard deviation
Rim-crest circularity, C	0.78	0.06
Rim diameter, D_r (km)	.31	8
Depth, R_i (km)	1.4	.6
Rim height, R_e (km)	.6	.2
Flank width, W_e (km)	4	2
Floor diameter, D_f (km)	.23	7

FIGURE 14.—Oblique view of Lassell, a smooth-rimmed crater in Mare Nubium. Note shallow floor, absence of radial textures on rim flank. Crater is 23 km across. View is to south. Apollo 16 Hasselblad photograph 19066. Sun is to lower left.

The available data show that smooth-rimmed craters do not differ in shape from ordinary main-sequence craters or from otherwise normal main-sequence craters that have been flooded with mare material to the level of the exterior terrain. This conclusion is evident from the multivariate analysis (figs. 2 and 3; pl. 1) as well as from percentage-frequency distributions for the individual variables circularity, rim height/crater depth, and rim width/diameter (fig. 15). The three graphs contain representative samples of terrestrial volcanic craters, terrestrial meteorite-impact craters and explosive craters, and rimmed main-sequence lunar craters. The five sample smooth-rimmed craters (LTO data) are compared with four extraterrestrial cratered edifices (on Mars) that without doubt are true caldera volcanoes. According to the three criteria, all the smooth-rimmed craters exhibit an impact-crater morphology rather than a volcanic-crater shape and simply do not have the correct shape to be calderas. The somewhat anomalous Jansen is discussed below in greater detail. In all three graphs, the overlap between volcanic and lunar craters mainly reflects the inclusion of 43 maars, many of which tend to resemble lunar craters in their geometry. However, the possibility that smooth-rimmed craters are colossal lunar maars is remote; these craters are roughly 20 to 30 times larger than typical terrestrial maars. On the Moon, where unambiguously volcanic craters are of uniformly small size (none over 3 km across), the maar interpretation of large craters is as tenuous as the caldera hypothesis.

Explanations other than primary volcanic genesis will have to be found for the unusual morphologies of smooth-rimmed craters. Indeed, perhaps these craters should not even be treated uniformly as a single class. A modification of the initial impact process by some unknown perturbation or else some form of secondary postimpact volcanic activity seem to be the most likely prospects for interpreting many of these craters (Pike, 1968; Young, 1972; Brennan, 1975; Schultz, 1976b). Possibly the craters all formed by impact, but some of the target material, probably mare lavas, had not wholly solidified and the characteristic hummocky rims and ejecta aprons never developed. Alternatively, they may have formed as main-sequence impact craters, but some of the later mare lavas partially inundated them, obliterating the ejecta and much of the hummocky rim material. Just such flooding is suggested by the typically low narrow rim flanks and the wide flat interior floors of most smooth-rimmed craters.

The likely involvement of extrusive volcanism in producing the anomalous characteristics of many smooth-rimmed craters is strongly evident in Jansen, perhaps the most unusual of all craters of this type. Contours on LTO sheet 60B–2 (Defense Mapping Agency, 1974–1977) show that the floor of the flooded

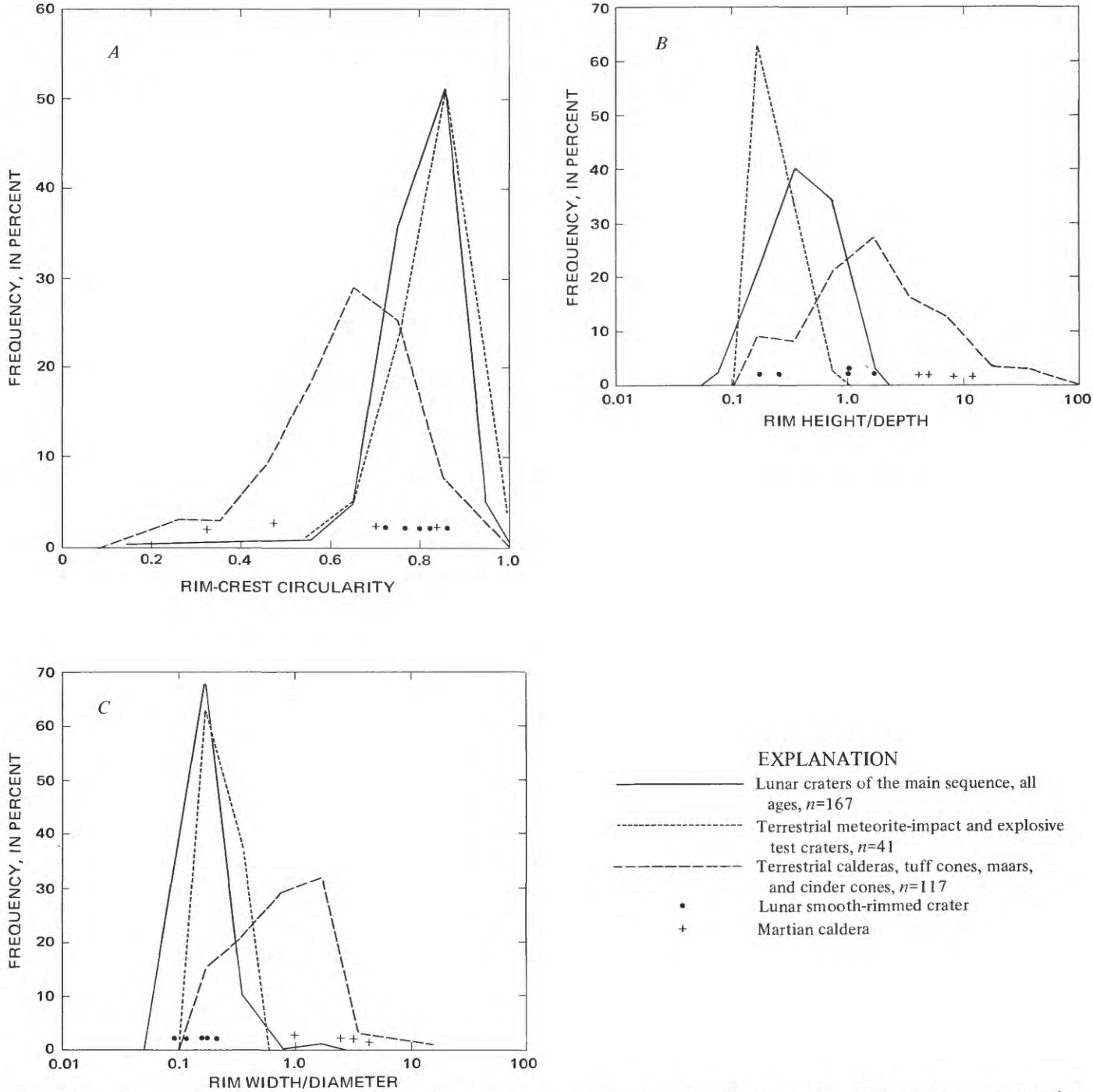

FIGURE 15.—Frequency distributions of three descriptive variables for 325 craters. Apollo measurements used for smooth-rimmed lunar craters Langrenus B, Langrenus F, Lick, Yerkes, and Jansen. Topographic information for martian calderas Olympus Mons, Pavonis Mons, Arsia Mons, and Ascraeus Mons from contoured editions of Mars charts MC–4 and MC–17. Data from Pike (1972a); data used in later analysis (table 2; Pike, 1974c) modified somewhat from those shown here. In each case, curve for volcanic craters differs significantly in shape and location from other two curves. Smooth-rimmed lunar craters resemble impact and explosion craters, not volcanoes, and probably are impact craters that have had an unusual formational or postformational history. *A*, Frequency distribution for index of rim-crest circularity (defined in text). *B*, Frequency distribution for rim height/depth ratio. Displacement of lunar data toward higher ratio values reflects large number of older and hence shallow craters included in sample (Pike, 1971a). *C*, Frequency distribution of rim width/rim-crest diameter ratio. Displacement of lunar data toward lower ratio values reflects diminution of rim width of older lunar craters, or possibly underestimation of rim widths for these objects.

23-km-diameter crater is elevated about 260 m above the main exterior datum. Craters with this odd configuration, the best known of which is Wargentin, are exceedingly rare on the Moon. The raised floor within Jansen, which otherwise has all the characteristics typical of other deeply flooded impact craters, suggests that unusual hydrostatic conditions prevailed locally during the emplacement of basin-filling lavas in this area of Mare Tranquillitatis. Possibly related features in the vicinity of Jansen that seem to reflect true volcanic activity include rilles, a rimless boat-shaped depression 450 m deep, and several 5-km-diameter craters that appear to be buried nearly to the rim crest by mare materials. Although with respect to depth/height, Jansen and Wargentin superficially resemble the lava-filled summit crater of the North Tongariro stratocone in New Zealand, the relatively much wider flank and higher rim of the terrestrial volcano rule out the analogy completely. The data interpreted here suggest that neither lunar crater is of primary volcanic origin, and neither are any of the other smooth-rimmed craters on the Moon. Later contributions to the 1 : 1,000,000 geologic atlas of the Moon (such as Hodges, 1973) have abandoned this interpretation entirely.

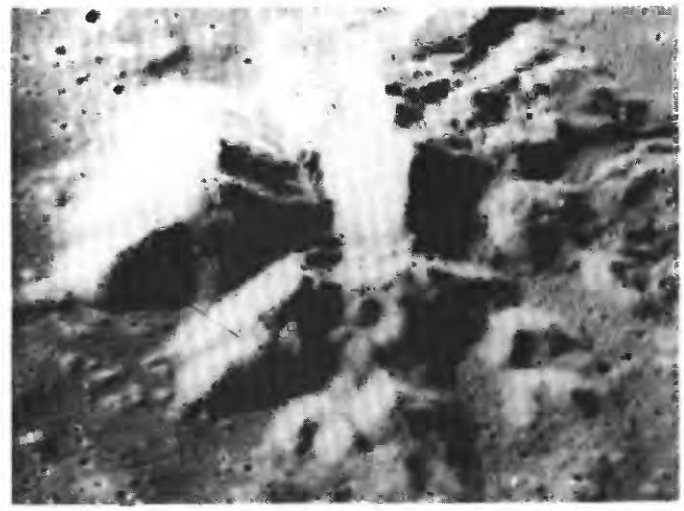

FIGURE 16.—Oblique view of multiple central peaks within young 100-km diameter impact crater Theophilus. Note paucity of well-formed small impact craters on sloping mountain flanks. Craters are common on level terrain of the floor of Theophilus, around peaks. Base of peak complex is about 25 km across. View is to southwest. Apollo 16 mapping-camera photograph 0694. Sun is to left.

SUMMIT CRATERS ON CENTRAL PEAKS

The depressions 1 to 5 km across that have long been observed at or near the tops of some of the central peaks in large lunar craters have been interpreted as the summit craters of stratovolcanoes (Moore, 1953), as chance impact craters on piles of nonvolcanic material (Baldwin, 1963), or as the collapsed summit of a rebound structure (Baldwin, 1963; Schultz, 1976a). Of the 40 or more near-side craters on the Moon once believed to contain central peaks with summit craterlets (Warner, 1962), six are portrayed on the LTO's: Timocharis, Theophilus (fig. 16), Kant, Taruntius, Capella, and Langrenus. Several craters on the far side, including Tsiolkovskiy and Levi-Civita, are also shown on the Apollo pictures (figs. 17 and 18). Although measurements could not be made of these small craters, the new large-scale maps enable at least two of the three contending interpretations to be examined more closely. The collapse hypothesis could not be evaluated from the new data.

Inspection of both contoured and uncontoured versions of the LTO's as well as supplemental maps and photographs from the Apollo and Lunar Orbiter missions, shows not one convincing volcanic crater on the summit of any of the central peaks (figs. 16–18). The photographs and maps do show numerous irregular clefts and protuberances that easily could have

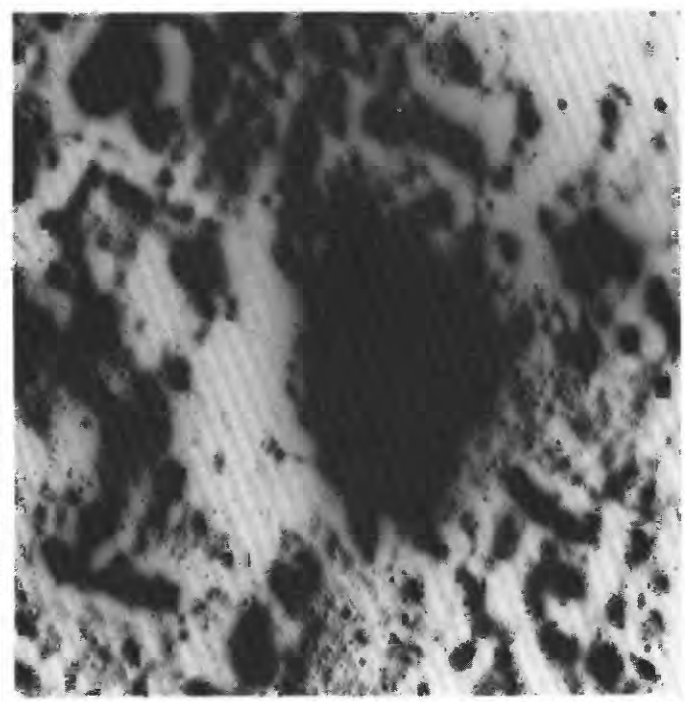

FIGURE 17.—Vertical view of central peak within old upland crater Levi-Civita, at 23° S. and 146° W. on far side. Note double craterlet at summit. Well-formed superimposed impact craters are rare on sloping flanks of peak but common on level surfaces. Base of peak is about 20 km across. Apollo 15 mapping-camera photograph 1019. Sun is to left.

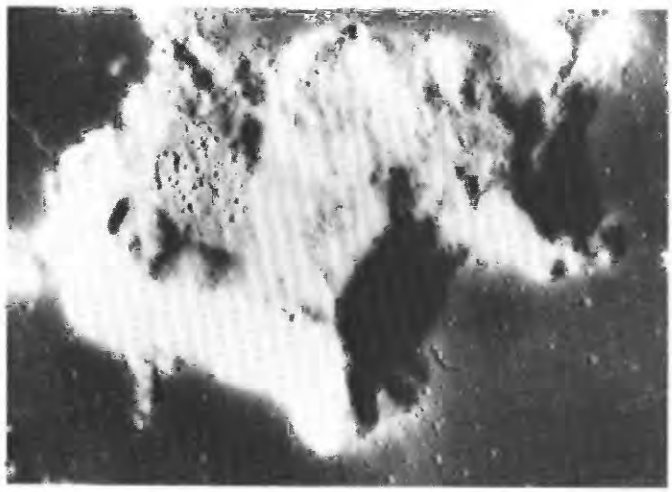

FIGURE 18.—Vertical view of central peaks within very young crater Tsiolkovskiy, at 20° S. and 129° E. on far side. Note scarcity of well-formed impact craters on sloping mountain flanks. Craters are common on level terrain at foot of peaks. Base of peak complex is about 40 by 25 km across. Apollo 15 mapping-camera photograph 0889. Sun is to left.

been mistaken for craters at the telescope or on the small-scale photographs available when such "summit craters" first were recognized. These illustrations also show a great many small, often rimmed, pits that appear to be impact craters. Most of the central peaks in question have been cratered liberally by small impacts, judging from the densities of craters on adjacent level surfaces, but preservation of the craters is highly selective. Impacts on the sloping flanks of central peaks result in misshapen or barely recognizable shallow craters that soon are obliterated by mass wasting. Impact craters formed on the flat floor near the base of the peaks and directly on gently sloping summit areas, on the other hand, are less distorted and tend to persist for a longer time. Impact craters with both degrees of preservation may be seen on central peaks in the craters Timocharis, Capella, Kant, and Theophilus. They also occur on the peaks of Gassendi, Regiomontanus, Tsiolkovskiy, and other large craters (figs. 16–18).

Regiomontanus A, which is located centrally within the old 118-km-diameter crater Regiomontanus, is one of the largest and most striking examples of a cratered central peak on the Moon. The 5.65-km-diameter crater has been interpreted as a caldera, mainly on the strength of Earth-based shadow measurements that put the crater depth at something less than 500 m but the height of the rim above the floor of Regiomontanus at about 680 m (Kopal and others, 1965); width of the rim flank is about 6 km. A more recent determination of the crater's depth that was made from shadow lengths on Lunar Orbiter images (Arthur, 1974), however, reveals that Regiomontanus A is 1,200 m deep. Unfortunately, this crater was not photographed by Apollo (see Lunar Orbiter IV high-resolution frame 107, framelets 398–400), but for most small craters Arthur's measurements are comparable in accuracy to those made later from Apollo photogrammetry (Pike, 1974b); there is no reason to question the 1,200-m figure, which now places the bottom of the crater some 700 m below the floor of Regiomontanus, not above it. The gross morphology of the crater and central peak no longer suggests a caldera origin, but rather indicates fortuitous superposition of a fresh, comparatively large impact crater on the summit of a central peak within a large, old lunar crater. This interpretation may hold for most other such features on the Moon, although other alternatives may better explain the observations for some craters (Allen, 1975).

SIZE-DEPENDENCE IN THE SHAPE OF FRESH IMPACT CRATERS

Fresh craters on the Moon form a continuous morphologic sequence within which they display greater complexity with increasing size. A general size continuum of lunar crater shapes has been known to exist for some time (Gilbert, 1893). Results of the Ranger, Orbiter, Surveyor, and Apollo missions have since confirmed that the sequence extends over at least 11 orders of magnitude (Hörz and Ronca, 1971). Most of the craters throughout this remarkably broad size range, from microscopic pits to the largest basins, share some overall characteristics (such as radial symmetry, a depressed cavity, and ejecta) and probably originated by impact. Variations in 33 morphologic properties of craters between 1 and 1,000 km across have been reviewed and summarized in considerable detail by Howard (1974).

The size-morphology sequence is not perfectly continuous, however, in that craters of adjacent size ranges differ significantly with respect to characteristics such as the proportion of depth to diameter and the presence or absence of central peaks. Some of the more apparent changes of crater shape with size were described and illustrated briefly by Gilbert (1893) for craters that could be resolved telescopically from Earth. Seventy-five years later, Mackin (1969, p. 743) wrote of the same continuum of larger lunar craters, which he described aptly as "a single genetic series, with simple bowl-shaped impact-explosion craters at one end and the largest maria [that is, multiringed

basins] at the other. There are two breaks in the series, both transitional, but both well-defined and meaningful: (a) at a diameter of 20±5 km between craters that show no slumping and those bounded by a wreath of slumps ***, and (b) between the latter and *** the maria [that is, basins]."

The first of these two discontinuities is elucidated here; other morphologic thresholds, such as the crucial change from large craters to small basins (Stuart-Alexander and Howard, 1970), interrupt the size continuum of lunar craters but will not be treated further in this report.

Fresh impact craters on the Moon exhibit changes in no fewer than 11 attributes of shape in the diameter range between about 10 and 30 km. At this size there is a transition from smaller, simple craters to larger, more complex craters. The changes usually are described as being either morphologic (qualitative) or geometric or morphometric (quantitative) in character, but the distinction is artificial; some are just measured more exactly than others (Griffiths, 1960). Four differences in crater shape are documented here at the nominal and interval levels of measurement: the restriction of swirl-textured floors mostly to craters bridging the simple-to-complex transition, and presence and elaborateness of central peaks, flat interior floors, and terraces on the rim wall. Seven size-dependent contrasts in crater geometry are defined at the ratio level of measurement (Griffiths, 1960): graphs of rim-crest diameter (D_r) against crater depth (R_i), rim height (R_e), flank width (W_e), floor diameter (D_f), rim-wall slope, circularity of the rim crest (C), and (profile) evenness of the rim crest (V_c) all inflect at values of rim diameter ranging from about 10 to about 30 km. The first four ratio relations are logarithmic and the last three semilogarithmic. The last five relations are evident only from the new topographic data available from the Apollo missions. Three quantities for which an inflection with increasing crater size has not yet been found are width of continuous ejecta, length of rays, and perhaps relative height of the central peak.

The value of average crater diameter at which the 11 changes in shape occur is 17.5 km, in excellent agreement with earlier estimates of the threshold size (Baldwin, 1968b; Pike, 1972b), although it is more realistic to think in terms of a diameter range (about 10–20 km) because the scatter of data points in the depth/diameter and other diagrams can be quite severe. Moreover, flat floors and other features do not appear all at once in craters exactly 17.5 km across. The seven ratio-level changes occur over an interval of about 10 km, and the four other changes are transitional over a diameter interval of about 40 km. The seven inflections in plotted distributions differ in crispness: those of diameter with depth, rim height, and slope are quite obvious, but the remaining four are more subtle. Analogous size-morphology thresholds that separate simple from complex craters have been identified in terrestrial impact structures (Dence, 1964, 1968; Lozej and Beales, 1975) and are evident in craters on Mercury (Gault, Guest, and others, 1975) and Mars as well (Pike, 1971a; Hartmann, 1972b).

RATIO-LEVEL VARIATIONS

The relation of depth and other geometric attributes of lunar craters to their overall size, as expressed by the rim-crest diameter or radius, can best be ascertained on bivariate graphs with both quantities plotted as logarithms (Baldwin, 1949; 1963; Pike, 1968, 1972b). The high quality of the Apollo photogrammetric data enable depth/diameter and other plots to be determined with more accuracy for craters between about 400 m and 300 km across than they could from the old shadow-length data. Fresh craters, Copernican and Eratosthenian in age as mapped by the U.S. Geological Survey, predominate in all graphs so as to avoid contaminating resulting trends with the topographic effects of crater degradation. The largest craters in the sample, such as Gagarin and Mendeleev, are substantially older, but they also are so large that their gross form may not have changed very much since their formation; no harm is done by including them. According to the new data, seven geometric properties of fresh lunar craters exhibit some sort of change or inflection at a crater diameter of about 10 to 30 km: depth, rim height, width of rim flank, slope angle of the rim wall, diameter of the flat floor, circularity of the rim crest, and evenness of the rim crest.

Seven of the 10 ratio-level relations of crater rim diameter to other dimensions are linear regressions of the form $\log y = \log b + a \log x$, with four of them—depth/diameter, height/diameter, width/diameter, and rim diameter/floor diameter—requiring two such expressions. This form does not apply to the semilogarithmic plots of rim slope, circularity, and evenness against diameter, although the constituents of rim slope (crater depth and rim-wall width) do plot exponentially as two linear fits. Calculated least-squares fits to data in the graphs are presented where applicable. All equations written for the new data are summarized in table 6, which gives values of a (slope) and b (intercept on the y axis at 1-km rim diameter) for 11 exponential equations (variables in kilometers), along with the sample size and the standard error of estimate of y on x (x always being the rim diameter). Because these fits are statistical relations rather than physical laws, the y value calculated for a particular x

TABLE 6.—*Numerical data for geometric model of fresh lunar craters*

Relation	Symbol	Size range (km)	N	Slope	Intercept at 1-km diameter (km)	Standard error (km)	Source
Depth/diameter	R_i/D_r	<15	171	1.010	0.196	+0.038 −.027	(1)
		>15	33	.301	1.044	+.067 −.063	(1)
Height/diameter	R_e/D_r	<15	124	1.014	.036	+.0075 −.0062	
		>15	38	.399	.236	+.036 −.031	
Width/diameter	W_e/D_r	<15	117	1.011	.257	+.055 −.046	
		>15	46	.836	.467	+.081 −.069	
Floor diameter/ rim diameter	D_f/D_r	<20	38	1.765	.031	+.011 −.009	
		>20	53	1.249	.187	+.012 −.011	
Width continuous ejecta/diameter	W_{ej}/D_r	All	84	1.001	.674	−.162 −.157	(2)
Relief of central peak/diameter	R_{cp}/D_r	>27	22	.900	.032	+.011 −.008	
Length (radius) of rays/diameter	R_r/D_r	All	50	1.25	4.41	+2.94 −1.76	(3)

[1]Pike (1974b).
[2]Moore and others (1974).
[3]Moore and others (1974); data from Baldwin (1963), table 32.

from any of the equations is not unique but only lies within a range of probable values. The dependability of each estimate of y varies according to the severity of scatter in the original data. To provide some measure of this variability to users of the equations, the standard error (Croxton and others, 1967, p. 395) was calculated for each fit.

The new equations (table 6) constitute fairly complete models, or average representations, of the geometry of both simple and complex fresh craters on the Moon that may be helpful in estimating the initial dimensions of multi-ring basins and large craters as well as the volume and distribution of their ejecta. They also serve as standards of comparison for the shapes of craters on Earth, Mars, Mercury, and other planets and their satellites. For some purposes, it will be found more convenient to convert crater diameter to radius (Quaide and others, 1965; McGetchin and others, 1973; Pike, 1974a). The equations supplant and revise older models of crater shape (Baldwin, 1963; Pike, 1972b) and should not change very much with additional data. The seven size-dependent changes in crater geometry indicate a qualitative increase in the complexity of fresh lunar craters that correlates with other types of size-dependent changes at the threshold diameter of about 10 to 20 km. An interpretation of the geometric changes in terms of dimensional analysis and allometry has appeared elsewhere (Pike, 1967; 1972b).

DEPTH

The relation of depth to diameter for craters on the Moon has a long history, reviewed in detail elsewhere (Baldwin, 1949; Pike, 1968). Previous work, commencing recently with that of Baldwin (1963, p. 141–142) and Quaide and others (1965), but actually going back to Ebert (1889), has shown statistically that lunar craters less than 20 to 30 km across are significantly deeper per unit diameter than are larger craters. Using more abundant and refined measurements than had been available before, I have located the inflection at a crater diameter near 15 km and fit separate linear equations to the data for craters both above and below the size threshold (Pike, 1967). The depth/diameter plot recently was revised (Pike, 1974b) from Apollo photogrammetric data for 204 craters between 60 m and 275 km across. A similar graph—with eight additional craters (fig. 19)—shows a sharp diminution in the rate of increase of depth as crater diameter increases beyond 20 km.

The distribution of 171 craters smaller than about 15 km across (excluding the eight new craters) is described by the expression

$$R_i = 0.196\, D_r^{1.010}, \quad (1)$$

where R_i is crater depth (km) and D_r is rim-crest diameter (km). Equation (1), a regression line that was calculated by the method of least squares, applies equally to fresh mare and to fresh upland craters. The eight added craters follow this trend. The depth/diameter distribution of the 33 craters over about 15 km in diameter follows the least-squares expression

$$R_i = 1.044\, D_r^{0.301}. \quad (2)$$

Large mare craters in figure 19 do not appear to differ systematically from large upland craters. The two linear fits intersect at a crater diameter of about 10.6 km. Equation (1), which resembles depth/diameter expressions for experimental-explosion and meteorite-impact craters on Earth, reveals that small lunar craters are about 50 percent deeper than older telescopic data showed them to be. The difference between old and new depth data is much less for the larger craters. The new depth/diameter equations have been compared with earlier expressions and discussed in greater detail elsewhere (Pike, 1974b).

The two subgroups of fresh craters in figure 19 overlap somewhat between 12 km and about 25 km in diameter. First noticed independently in 1965 by both R. B. Baldwin and myself, the trend established for smaller craters—here, equation (1)—extends well beyond the inflection diameter of about 11 km (see also David, 1975). The 13 largest craters that are described by equation (1) are Proclus, Alfraganus, Macrobius A

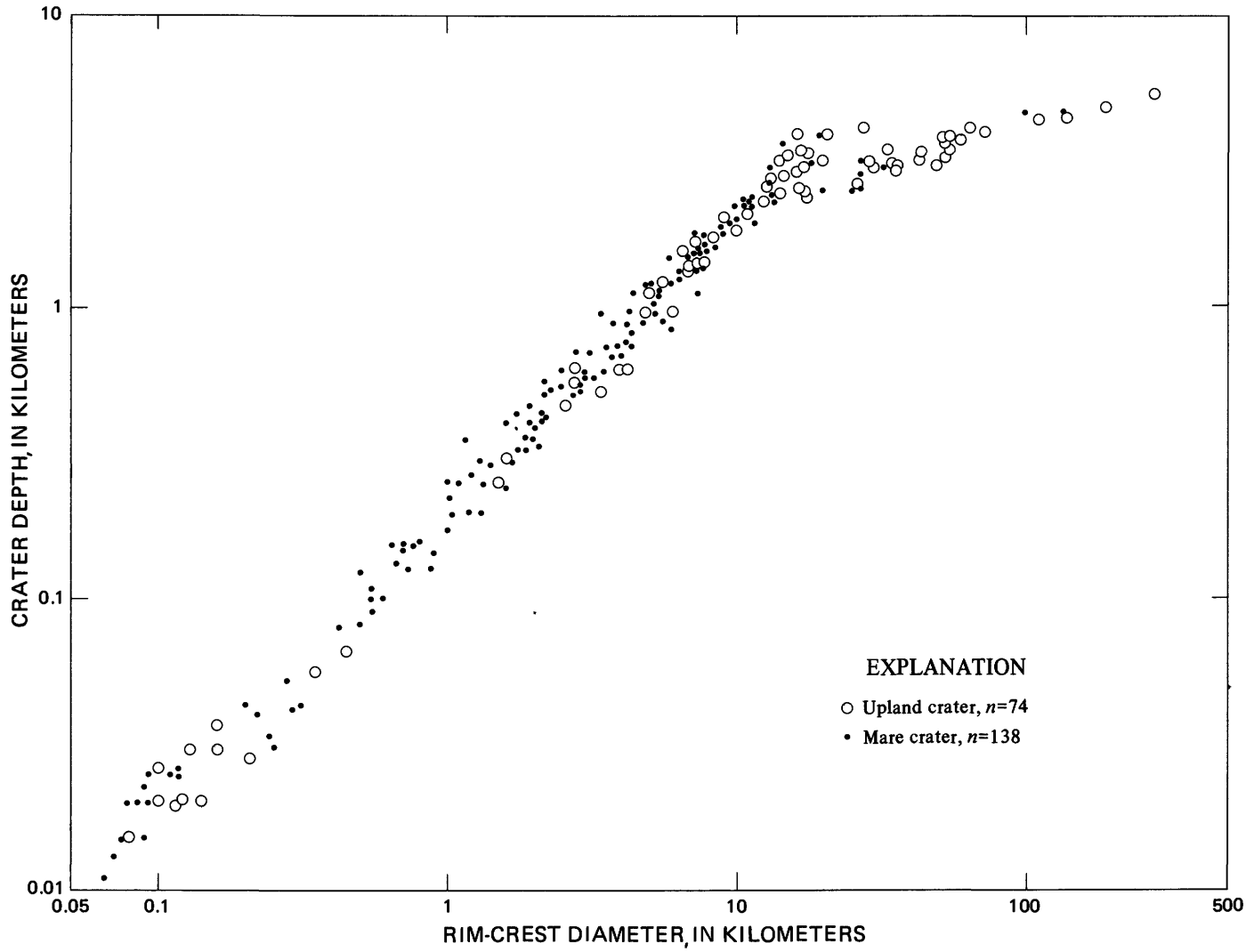

FIGURE 19.—Relation between depth, R_i, and diameter, D_r, for 204 fresh lunar craters from Pike (1974b) and eight additional craters. All data from maps and topographic profiles compiled photogrammetrically from Apollo 15, 16, and 17 photographs. Distribution inflects sharply at a diameter of about 15 km, marking transition from simple to complex, or modified, craters on the Moon. This 15-km inflection appears in several of the following figures. Simple craters extend beyond transition diameter (see text).

and B, Kästner F, Diophantus, Dario, Vitruvius A, Dubyago S, Isidorus D, Li Po, Benedict, and Langrenus C. All of these anomalous craters are exceptionally deep for their size (see table 9). Only one, Diophantus, has a central mound, and only Proclus has rim-wall terraces; in neither crater are these features well developed. The flat interior floors are quite small, especially in those craters under 18 km across. Clearly these are simple, rather than complex craters, despite their comparatively large size. It is not clear why these 13 craters and others like them have turned out differently from most lunar craters in the 13- to 28-km size range. About as many of them have formed on mare or upland-plains surfaces as have formed on uneven upland terrain, and so geographical location—and any material strength or other contrasts related to mare-upland differences—evidently was not a factor. Probably the anomalously deep craters reflect chance variations in the transition from simple to complex morphologies on the Moon, rather than any systematic physical influence on crater shape or internal structure.

RIM HEIGHT

Before the Apollo missions, the relation of rim height to crater size on the Moon was less certain than the depth/diameter relation, because rim height could not be measured with as much accuracy as crater depth. Baldwin (1963, p. 143) first recognized that rim height also is significantly greater per unit diameter for lunar craters below about 30-km diameter than it is for larger craters. Although I placed the inflection nearer

to 15-km diameter and derived linear equations for rim height/diameter that had much the same form as the depth/diameter fits (Pike, 1967, 1972b), the greater scatter in the height/diameter data and the vagueness of the inflection at about 10–20-km diameter left the true form of the relation tenuous. Any doubts now are dispelled. The height/diameter relation has been revised from the latest Apollo photogrammetric data, including most of the 212 craters plotted in figure 19. The resulting graph for 162 fresh craters between 400 m and 320 km across (fig. 20) indisputably establishes a well-defined inflection of rim height at a crater diameter between 10 and 20 km.

The 162 craters divide into two groups at a diameter of about 17 km, and each distribution was fitted with a regression line. The two linear fits intersect at a diameter of about 21.3 km. The 124 smaller craters follow the expression

$$R_e = 0.036\, D_r^{1.014}, \tag{3}$$

where R_e is crater rim height and all units are in kilometers. Fresh upland and mare craters do not appear to differ. Unlike the case with depth/diameter (fig. 19), smaller craters do not extend beyond the inflection

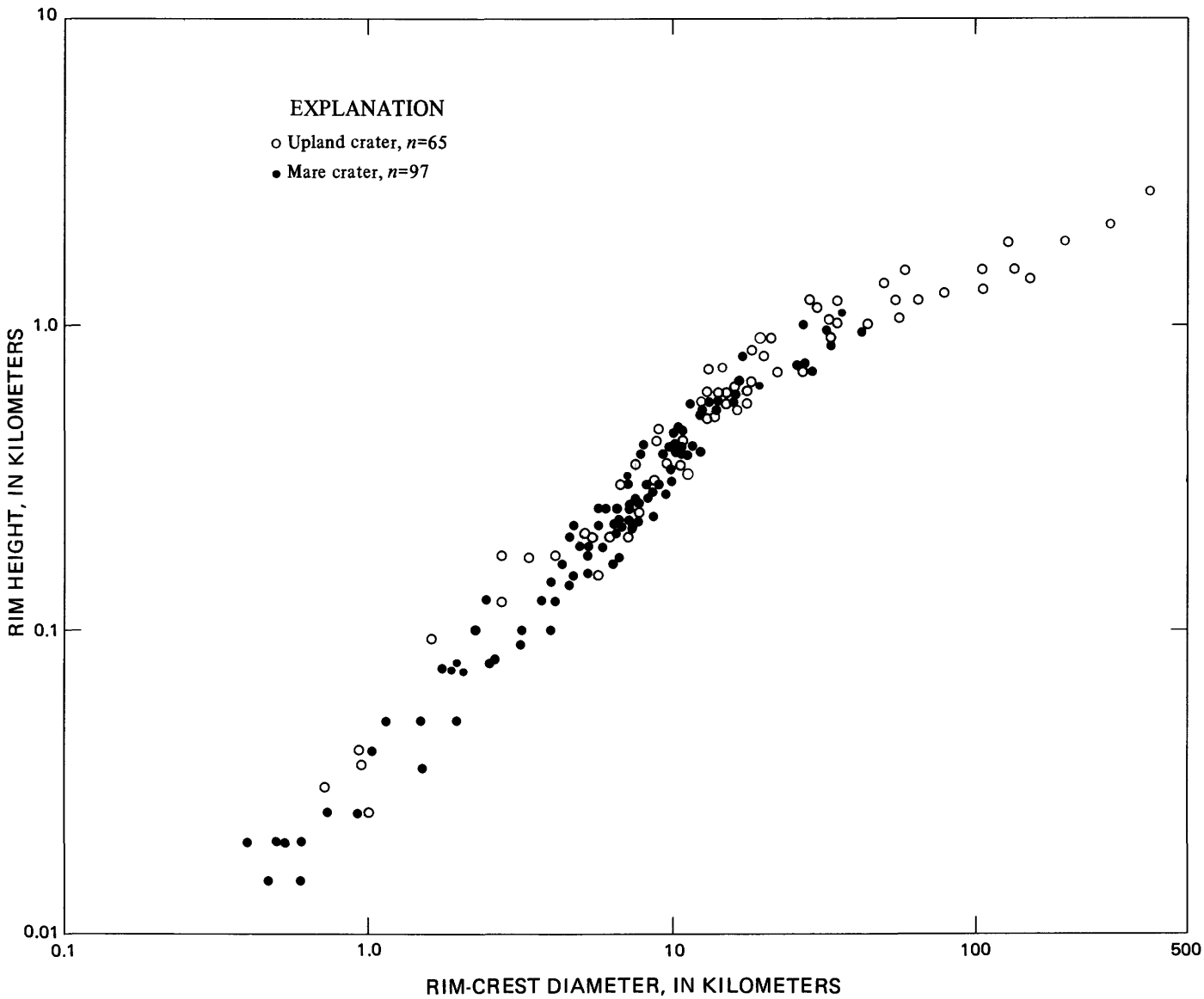

FIGURE 20.—Relation between rim height, R_e, and diameter, D_r, for 162 of the 212 fresh lunar craters plotted in figure 19. Data from photogrammetry of Apollo 15–17 pictures. Distribution inflects at diameter of about 15 km. Equations fitted to two linear segments of distribution supplant previous expressions for height/diameter (see text).

diameter. The height/diameter distribution of the 38 larger craters follows the expression

$$R_e = 0.236\, D_r^{0.399}. \quad (4)$$

Neither of these expressions differs radically from the visually fitted regression lines given previously for fresh craters on the Moon (Pike, 1967, 1972b), although the slope of equation (3) is now essentially 1.0, the value expected from dimensional theory (Pike, 1967, 1968). Equations (3) and (4) provide a new standard of accuracy that defines the rim height/diameter of fresh lunar craters better than do the equations currently in use (Baldwin, 1963; Pike, 1972b). Equation (3) now should be used instead of earlier expressions in applications where the height/diameter relation of craters under 15 km across is deemed appropriate for modeling the transient (pre-slump) profile geometry, interval volumes, and ejecta volumes of fresh impact basins and craters over 15 km across. Although further improvement in the quantity and quality of topographic measurements on the Moon may result in equations (3) and (4) being refined, neither expression is likely to change appreciably from that given here.

The rim height/diameter relation described for fresh lunar craters in figure 20 by equation (3) is quite consistent with the height/diameter characteristics of fresh experimental-explosion and meteorite-impact craters on Earth. Equation (3) is very much like an expression derived previously for a sample of 28 freshly formed (or reexcavated) terrestrial meteorite craters (Pike, 1972b),

$$R_e = 0.033\, D_r^{0.94}, \quad (5)$$

and also resembles an expression derived for a sample of 100 experimental-explosion craters (Pike, 1972b),

$$R_e = 0.042\, D_r^{0.98}; \quad (6)$$

variables for both equations are in kilometers. Equation (3) differs only somewhat more from the height/diameter expression describing 35 laboratory craters formed in loose particulate material by hypervelocity impact of small projectiles (Gault and others, 1966),

$$R_e = 0.022\, D_r, \quad (7)$$

variables converted to kilometers. The new lunar height/diameter data do not appear to require any qualitative revisions of hypotheses or conclusions that had been based on older rim-height measurements, now obsolete.

WIDTH OF RIM FLANK

According to earlier studies over a wide size range of craters on the Moon, the relation of flank width to diameter was linear throughout (Baldwin, 1963; Pike, 1968, 1972b; Guest and Murray, 1969). The apparent absence of any inflection in the width/diameter relation posed a problem, because diminution of crater depth at a diameter of about 15 km customarily has been attributed to slumping of the rim and formation of terraces (Quaide and others, 1965; Mackin, 1969). The substantial increase in crater diameter believed to result from slumping would require a commensurate retreat of the rim flank. Although earlier I appealed to isostatic compensation to lower the rim height of craters over 15 km in diameter without substantially increasing crater diameter and suggested that horizontal dimensions such as rim width were less susceptible to postimpact modifications than were vertical dimensions such as rim height (Pike, 1967), this interpretation probably is incorrect. Gravity data (Phillips and others, 1975; Moore and others, 1979) have shown that isostatic movements are insignificant for all but the largest craters.

The width-diameter relation has been reexamined using the same 162 craters as in figure 20. The resulting graph (fig. 21) shows a perceptible diminution of rim-flank width as crater diameter increases beyond 20 km, although the inflection is not as strong as those evident for depth/diameter and rim height/diameter. Evidently earlier studies did not show this subtle change, because flank width is especially susceptible to errors in visual measurements on photographs. The inflection in the width/diameter data at the same crater diameter as the height/diameter inflection suggests strongly that diminution in rim height at the threshold diameter of 10–20 km occurs through retreat of the rim, probably by slumping, rather than through isostatic subsidence.

The 162 craters in figure 21 fall into two linear segments at a crater diameter of about 17 km; each segment has been fitted with a least-squares regression. Again, the distribution of smaller craters does not extend beyond the inflection diameter, as it does in the depth/diameter plot (fig. 19). The 116 smaller craters follow the trend

$$W_e = 0.257\, D_r^{1.011}, \quad (8)$$

and the 46 larger craters are described by the expression

$$W_e = 0.467\, D_r^{0.836}, \quad (9)$$

where W_e is rim-flank width and both variables are in

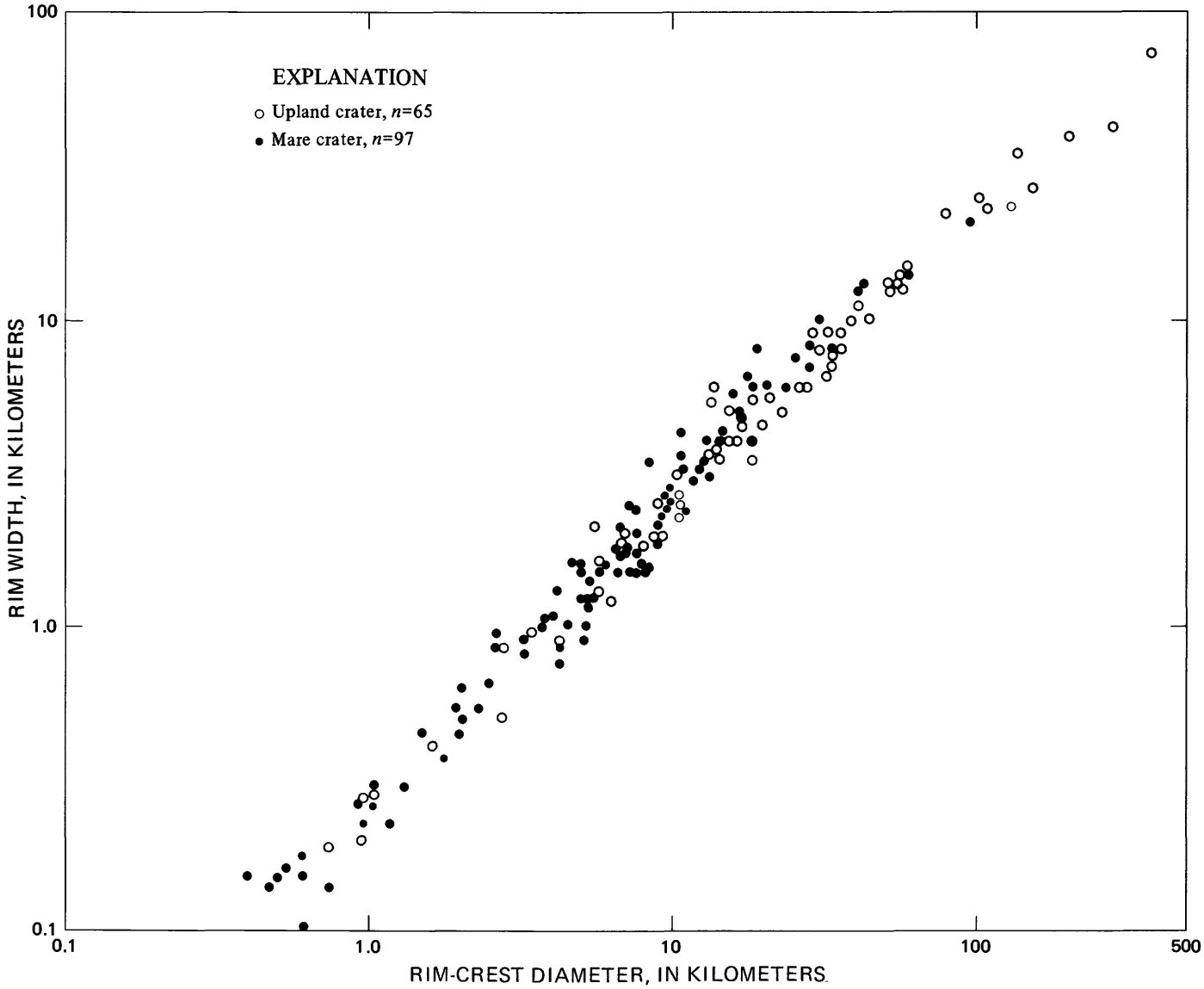

FIGURE 21.—Relation between width of rim flank, W_e, and rim-crest diameter, D_r, for same 162 fresh lunar craters as in figure 20. Distribution inflects at diameter of about 15 km rather than remaining linear for craters of all sizes. Equations fitted to two linear segments of distribution supplant previous expressions for width-diameter, all of which were linear throughout (see text).

kilometers. The two linear fits intersect at a crater diameter of about 30.4 km, although visually the inflection seems closer to 20 km. The discrepancy probably reflects some nonlinearity in the data, particularly those describing smaller craters. As in the case of depth/diameter and rim height/diameter, fresh upland craters do not appear different from mare craters.

Equation (8) shows that the rim flanks of fresh lunar craters under about 20 km diameter are between 25 and 30 percent wider than had been ascertained from pre-Apollo observations by Baldwin (1963, fig. 22) for about 100 craters:

$$W_e = 0.206\, D_r \quad (10)$$

and by Pike (1972b) for 400 craters:

$$W_e = 0.170\, D_r. \quad (11)$$

The latter measurements all were visual estimates from photographs, which tend to result in narrower rim flanks because terrain of the outer rim is not sufficiently steep or rugged to cast perceptible shadows on photographs. The new values of W_e for smaller craters on the Moon also are systematically higher by 30 percent or so than rim-flank widths of 15 terrestrial meteorite-impact craters:

$$W_e = 0.200\, D_r^{0.97} \quad (12)$$

and 20 experimental-explosion craters:

$$W_e = 0.190\, D_r^{0.98} \quad (13)$$

(both from Pike, 1972b). The explanation for these latter discrepancies may involve effects of differences in gravity scaling that favor slightly broader blankets of ejecta on the topographic rim and subjacent annular zones of uplifted bedrock on the Moon than on Earth.

RIM-WALL SLOPE

Fauth (1894) discovered that inner walls (between rim crest and floor) of lunar craters under about 30 km across did not vary significantly in "effective" slope with changing diameter, whereas the slope angle decreased appreciably with increasing diameter for craters above this size. On the supposition that rim-wall slopes should reflect the several changes in rim and floor geometry that had been shown to occur in lunar craters at a diameter of 10 to 20 km, I examined slopes for a small sample of far-side craters from the first Apollo 15 and 17 photogrammetric data and identified a possible discontinuity in the relation between rim-wall slope and crater size at a diameter of about 17 km (Pike, 1973a). The slope/diameter relation has been studied more thoroughly for this report for 107 craters, mostly fresh, from the recently published Apollo photogrammeteric maps.

The latest graph of rim-wall slope against diameter (fig. 22) shows the tangent of slope increasing gradually for small craters from about 0.34 (19°) in craters 0.5 km across to a maximum of about 0.55 (29°) at a diameter of about 10–20 km, then dropping sharply for larger craters to a value of about 0.25 (14°) at 50–60 km diameter, and then declining somewhat less rapidly to a value of 0.12 (7°) for the largest crater. The revised relation confirms the thrust of Fauth's original findings but places the change in slope angle at a crater diameter of about 15 km rather than 30 km. Craters that have flat floors and central peaks have been so indicated in figure 22. In this sample, flat floors develop at a much smaller crater diameter, 7 km, than do central peaks, 18 km. On the slope/diameter diagram, craters with flat floors and craters without flat floors occupy all but mutually exclusive fields. The steepest interior walls all occur in craters that have small flat floors. The relation between slope of the rim flank and crater size, which led to no conclusive results in the preliminary test (Pike, 1973a), has not been redone here.

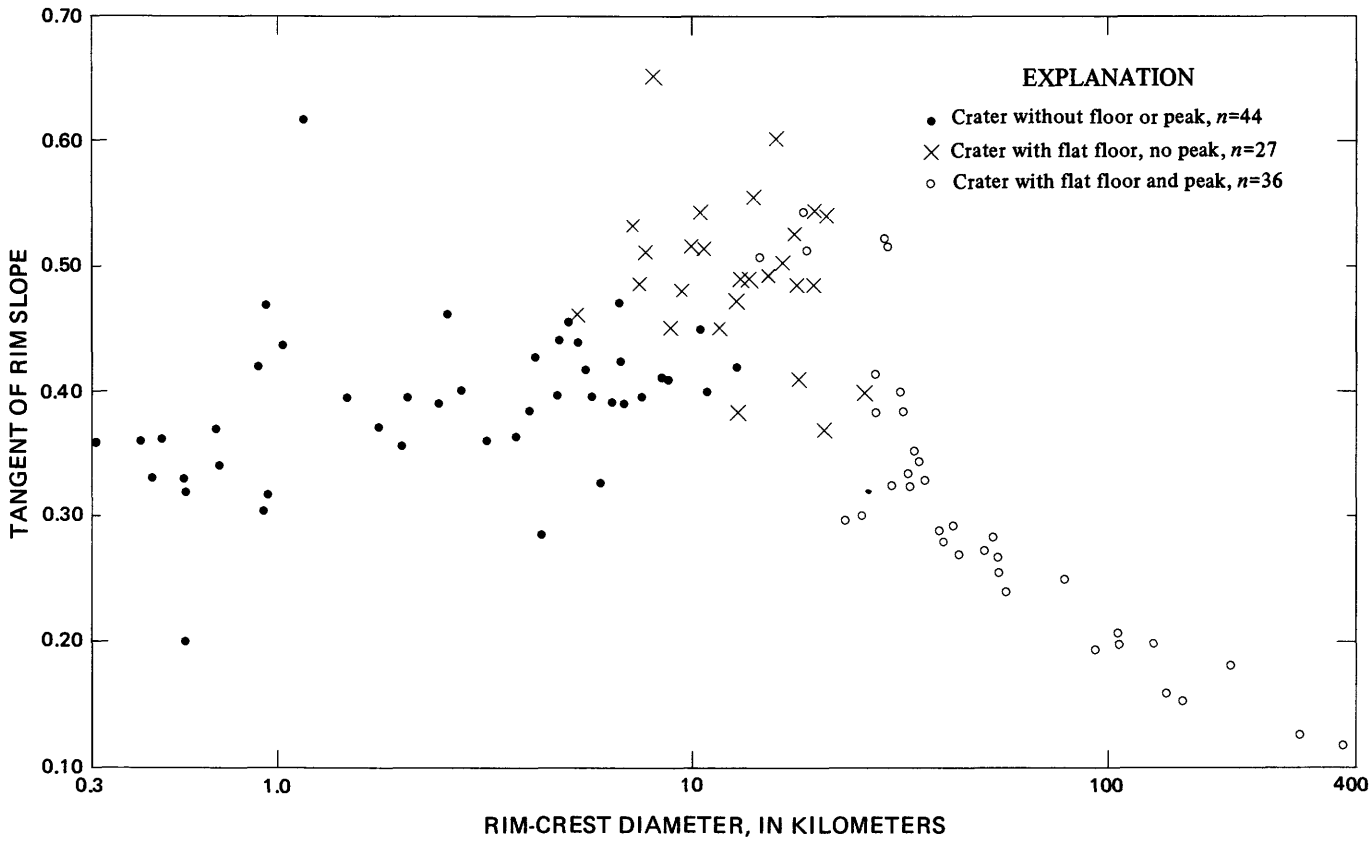

FIGURE 22.—Relation between tangent of slope of rim wall and rim-crest diameter, D_r, for 107 fresh lunar craters. Data from photogrammetry of Apollo 15–17 pictures. Slope values increase with crater diameter to maximum of about 29° (0.55) for craters about 15 km across, and then decrease sharply (see text).

FLOOR DIAMETER

Although the size of the flat floor within larger craters on the Moon has been studied in little detail, the ratio of floor diameter to rim-crest diameter correlates inversely with depth/diameter and thus roughly indicates the relative age of a crater (Warner, 1961; Pike, 1968). Warner's raw data, which he fit with a single linear equation, also suggested that the floor diameter/rim-crest diameter relation for fresh craters inflected at a rim diameter of about 10 km; my data (Pike, 1968), which were fit with two linear equations, seemed to suggest a very slight inflection at 80 km. The new photogrammetric data show that the floor diameter/rim-crest diameter plot for fresh craters (fig. 23) inflects perceptibly at a rim diameter of about 20 km and a floor diameter of about 8 km. Craters smaller than this threshold value have increasingly narrow floors, down to about a kilometer across in craters 7 km or so in diameter. There is considerable scatter in the latter data, possibly because floors are more difficult to measure in the smaller craters; floors occur quite infrequently in craters much under 5 km across. Flat floors make up increasingly larger fractions of the rim diameter in fresh craters over 20 km across, the proportion reaching nearly 75 percent for Tsiolkovskiy, with very little scatter in the data.

The 91 craters in figure 23 were divided by inspection into two linear segments at a diameter of roughly 20 km; each segment has been fitted with a least-squares equation. The 51 smaller craters are described by the trend

$$D_f = 0.031\, D_r^{1.765} - K, \tag{14}$$

and the 40 larger craters follow the expression

$$D_f = 0.187\, D_r^{1.249}, \tag{15}$$

where D_f is diameter of the flat floor, K is some constant between 2 and 5 km, and the two variables are in kilometers. The equations intersect at a crater diameter of 33 km, again a higher figure than visual inspection would lead one to expect. The difference is ascribed to curvature in the field of smaller craters (fig. 23). Both relations now are more clearly defined than they had been from the older data. Equation (14), which does not extend to craters less than 2 to 5 km across (approximately where D_f goes to zero), differs entirely from my previous expression for smaller craters (Pike, 1968). Equation (15) is much less different from the equations fit to larger craters by me (Pike, 1968) and by Warner (1961) and also seems to fit data for the flooded mare basins up to a diameter of 900 km. Upland craters have been distinguished from mare craters in figure 23, but again, no difference in the two subsamples is evident in the plot.

Unlike the other logarithmic relations between linear variables that describe lunar impact craters, the new D_f/D_r equation describing smaller craters does not follow the slope of 1.0 that normally would be expected from dimensional theory for an isometric phenomenon (Pike, 1968). However, if a flat floor is not present in the transient phase of an impact or explosion cratering event (Pike, 1967), floor size should not be expected to relate similarly to rim-crest diameter and other variables that describe primary features of craters in both transient and fresh postimpact configurations. A slope of 1.0 is found in all logarithmic plots of linear variables describing primary morphologic aspects: those that always are present in craters or that reflect no changes in crater shape. Measurements for other types of morphologic aspects, such as flat floors and central peaks or the depths of modified craters (see table 6), characteristically do not plot with a slope of 1.0. Thus, Siegal and Wickman (1973) are mistaken when they contend that allometry—actually Gibrat's law of proportionate effect (see Aitchison and Brown, 1957)—does not apply to empirical relations among crater dimensions. Linear measurements of crater geometry graph logarithmically with a slope of 1.0 only if the craters all have a similar shape. Deviations from a slope of unity are important indications of differences in shape and hence suggest differences or complications in mode of origin (Pike, 1967).

RIM-CREST CIRCULARITY

The planimetric symmetry of craters on the Moon—expressed by circularity or polygonality of the rim crest—has been examined quantitatively by several investigators, but the findings disagree. Ronca and Salisbury (1966), Adler and Salisbury (1969), and Murray and Guest (1970) found no functional relation between crater size and the value of a circularity index. Similar negative results are evident for Mars from Mariner 6 and 7 pictures (Oberbeck and others, 1972). However, Fielder (1961) and Quaide and others (1965) both observed that craters more than 20 km across are more polygonal than are smaller craters, and Schultz (1976a) judged the rims of most craters over 15 km across to be either scalloped or polygonal. I found increases, statistically, in the frequency of rim-crest polygonality and in strength of polygonality with increasing crater size (Pike, 1968). Pohn and Offield (1970) divided the size continuum of fresh lunar craters over 8 km across into three morphologic classes "on the basis of the planimetric shape of their rim crests" as determined by inspection from Lunar Orbiter IV images. The diagnostic criterion was the presence or absence of polygonality. Fresh craters between about 16

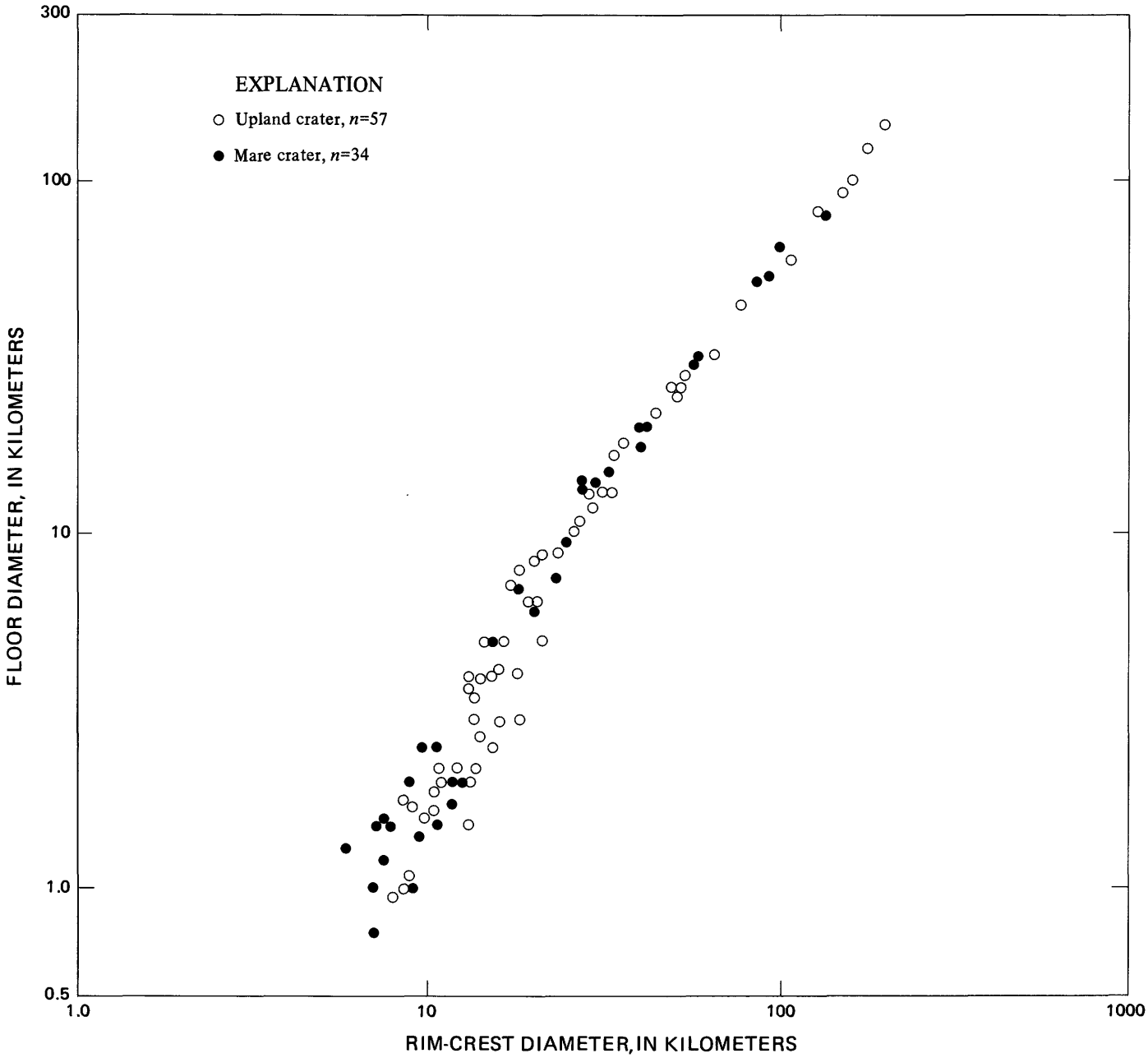

FIGURE 23.—Relation between diameter of the inner flat floor, D_f, and rim-crest diameter, D_r, for 91 fresh lunar craters. All but a half-dozen points from photogrammetry of Apollo 15–17 pictures. Distribution inflects at diameter of about 20 km. Equations fitted to two linear segments of distributions supplant earlier expressions.

and 48 km across were observed by Pohn and Offield (1970) to have markedly polygonal rim crests, whereas the rim crests of fresh craters both larger and smaller than this size range were observed to be more nearly circular. The qualitative tripartite classification can be tested to some extent quantitatively, using an index of crater circularity. Although circularity, the two-dimensional equivalent of sphericity, is not the same as polygonality, the two-dimensional equivalent of roundness, a polygonal crater nonetheless must be somewhat less circular than a similar-sized crater that has perfect radial symmetry.

The relation between rim-crest circularity and crater size was reexamined for this report using data from Apollo photogrammetric maps and orthophotomaps. The outcome for 201 fresh lunar craters between 400 m and 370 km across is a graph (fig. 24) that shows a systematic dependence of the circularity index—discussed earlier in this paper—on diameter: circularity is not constant with crater size. Despite the consid-

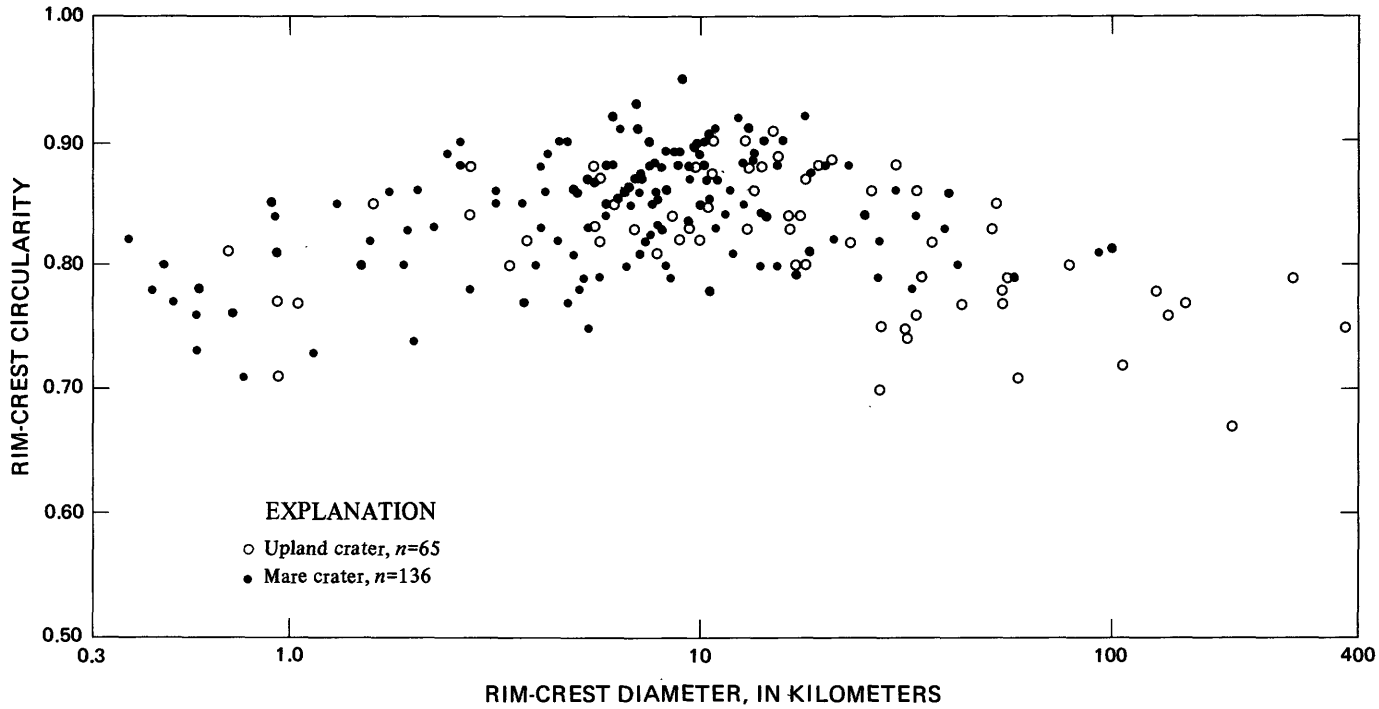

FIGURE 24.—Relation between index of crater circularity, C—defined as ratio of area of inscribed circle to area of circumscribed circle fitted to outline of rim crest—and diameter, D_r, for 201 fresh lunar craters. Data from photogrammetry of Apollo 15–17 pictures. Average circularity increases with rim diameter to maximum of 0.85–0.90 in craters about 10 km across, and then decreases (see text).

erable scatter in the diagram, it is evident that fresh lunar craters have maximum planimetric symmetry at a rim diameter of 10 km or so, in much the same way as rim-wall slope (see fig. 22). Circularity declines in both larger and smaller craters, but the decrease is more perceptible among the larger craters. Fresh craters on the upland do not appear to differ significantly from fresh mare craters in circularity, save where rims of upland craters have been distorted by uneven terrain. Although these results do not expressly contradict the observations of Pohn and Offield (1970), their contention that fresh craters in the 16- to 48-km size range are markedly more polygonal than are either larger or smaller craters is not supported by circularity data. Of the sample of craters plotted in figure 24, those in the class I size interval of Pohn and Offield (over 45 km) have a median circularity of 0.78; class II craters (16–48 km) have a median circularity of 0.83; and class III craters (under 20 km, but restricted to craters between 8 and 20 km to assure a similar sample to that of Pohn and Offield) have a median circularity of 0.87. Hence the three size classes of craters adopted by Pohn and Offield on the basis of rim-crest polygonality may be artificial. As in the case of the new rim width/diameter and floor diameter/rim-crest diameter results, a functional relation between circularity and crater size has become evident now only because the Apollo data portray lunar landforms with the requisite accuracy. Interpretation of the results in figure 24 remains speculative. Fulmer and Roberts (1963) earlier had suggested an explanation of noncircular crater rims in terms of regolith thickness, but the observations here seem to require a more complex mechanism or combination of mechanisms.

EVENNESS OF RIM CREST

High-quality data resulting from the last three Apollo missions have made it possible to examine quantitatively a neglected aspect of a crater shape—configuration of the rim-crest profile. Millman (1956) made a detailed numerical analysis of the raised rim of the New Quebec meteorite crater, but excepting the work of MacDonald (1929), earlier evaluations of rim-crest evenness for lunar craters have been qualitative. I previously studied two different aspects of rim-crest configuration from a small sample of 15 lunar craters (Pike, 1973a); here, the sample is increased to 30, and the two problems are reexamined in greater detail. The relation of rim-crest roughness to crater size is taken up here, and azimuth-dependent tendencies are treated later in the paper. A common telescopic observation has been that rim crests of lunar craters below a certain diameter appeared to be relatively even and smooth, whereas rim crests of larger craters were significantly rougher (Baldwin, 1949). The critical di-

ameter has been placed at 15 km by Firsoff (1959) and at 50 to 60 km by Shoemaker (1965). Dependence of rim-crest evenness upon crater size was treated using rim-crest relief and standard deviation of rim-crest elevation.

Relative relief, the vertical distance between highest and lowest elevation, was measured along the rim crest for 46 fresh-looking lunar craters from 1:250,000 LTO and larger scale published Apollo maps as well as from unpublished rim-crest profiles (Pike, 1973a). The sample is evenly divided between mare and upland craters 1.6 to 275 km across. Rim-crest relief increases linearly with crater diameter (fig. 25) and does not change significantly at any well-marked threshold diameter. The upland craters have systematically rougher rim crests than mare craters, as might be expected from their having formed on a rougher surface. The slope of each logarithmic distribution is about 1.0 throughout, and no inflection or discontinuity can be detected at any discrete range of crater diameters. Relative relief has shortcomings as a roughness parameter, however, because of its undue sensitivity to extreme altitudes along the rim crest. Statistically it is the equivalent of the range, the crudest of all measures of dispersion (Croxton and others, 1967, p. 191).

The standard deviation of elevation along the rim-crest, a far more comprehensive measure of dispersion, was calculated for 35 of the 46 craters in an attempt at a more sensitive test of the supposed dependency of rim-crest roughness upon crater size. Thirty-six elevations were determined along the rim crest of each crater at intervals of 10° from due north. Interpolation of elevation values is easy on the circular topographic profiles obtained specifically for the purpose (Pike, 1973a, 1973b) and for LTO's and other published maps where the contour interval was relatively small compared to the crater size. Interpolation is less certain on LTO's for craters between 6.5 and 11 km across, although the problem was minimized by using craters with the maximum number of observed contours and spot heights along the rim crest. Some bias toward greater roughness thus may have been introduced for the latter craters. Because the 35 sampled craters lie at different lunar elevations, each resulting standard deviation was divided by its mean elevation to measure relative rather than absolute dispersion (Croxton and others, 1967, p. 198). The resulting statistic, the coefficient of variation, provides a fairly sensitive index of rim-crest evenness for the 35 selected craters.

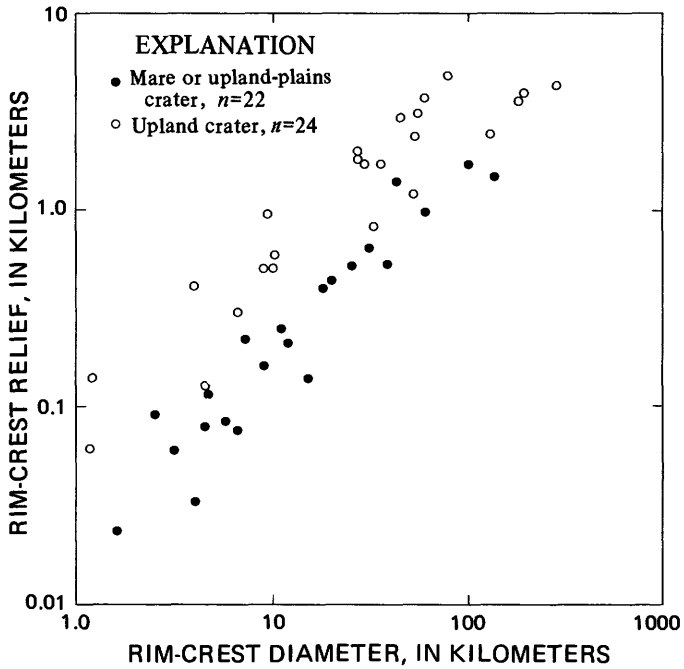

FIGURE 25.—Relation between relief along rim crest and crater diameter, D_r, for 46 fresh lunar craters. Data from photogrammetry of Apollo 15–17 photographs. Distribution is linear throughout, and much of the scatter can be accounted for by less even surfaces upon which upland craters formed. Upland craters have about three times the rim-crest relief of mare craters.

A plot of the coefficient of variation for rim-crest elevation (V_c) against the logarithm of crater diameter (fig. 26) indicates a significant increase in rim-crest roughness for craters over 10–20 km across. For 13 of the 21 mare craters (15 km in diameter and less), V_c remains relatively constant, at a value of about 0.006, whereas the statistic increases systematically to a maximum of about 0.05 for the eight mare craters over 15 km across. The 14 upland craters have less even rim crests than the mare craters. V_c values for the upland craters also increase with the crater size, but the relation is not very systematic and any size-dependent inflection is much less evident than that shown by the mare craters. The sample of small upland craters may not be large enough to show an inflection, if indeed one exists. Most of the scatter among the larger upland craters in figure 26 is attributed to the inherently less even surface upon which they formed. Apollo data appear to show that evenness of the crater rim crest starts to increase at a diameter of 10 to 20 km for craters that formed on surfaces with a similar (flat and even) configuration, thus supporting the older qualitative observations of yet another size-dependent change in crater shape.

NONRATIO VARIATIONS

At least four discontinuities or transitions in more qualitatively expressed aspects of shape also interrupt the morphologic continuum of lunar craters in the same size range indicated by the seven changes in crater geometry described above. Gilbert (1893) was perhaps the first to recognize that well-developed flat

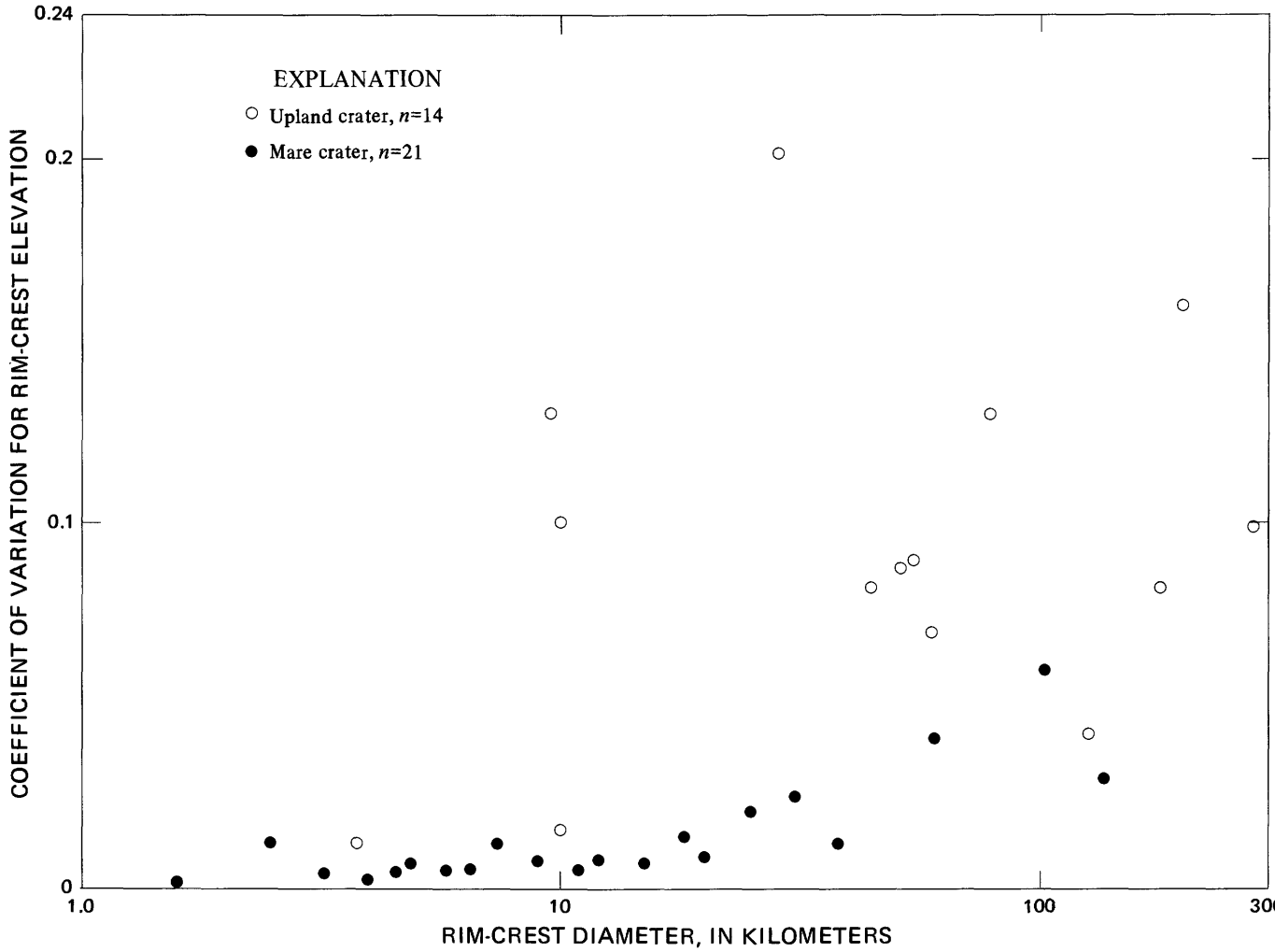

FIGURE 26.—Relation between evenness of rim crest, expressed by coefficient of variation for 36 measured rim-crest elevations per crater, V_c, and diameter, D_r, for 35 fresh lunar craters. Data from photogrammetry of Apollo 15–17 pictures. Upland craters have much more irregular rims than mare craters. Values of V_c for mare craters remain constant at small diameters but begin to increase with crater size at diameter of about 10–20 km.

floors, rim-wall terraces, and central peaks (not related to regolith thickness) all are relatively rare in fresh craters on the Moon under about 10–20 km in diameter, such as Linné (fig. 5), but are common in larger craters, such as Aristarchus (fig. 27). His observations have been confirmed repeatedly by independent telescopic, photointerpretive, and statistical work (Baldwin, 1949; Firsoff, 1959; Levin and Ruskol, 1962; Quaide and others, 1965; Pike, 1968). Morphologies of the larger and smaller craters have been described in detail by Howard (1975) and Pike (1973b), respectively, and the contrasts were nicely summarized by Mutch (1970). One recent study (Smith and Sanchez, 1973) at first appears to contradict the size-dependent onset of occurrence of crater floors, terraces, and peaks but in fact strongly supports the morphologic discontinuity at a crater diameter of 10–20 km. The same paper also documented the existence of a fourth size-dependent feature: the presence on crater floors of a distinctive morphologic characteristic that has been termed "swirl texture."

From an analysis of four semiquantitative index numbers that reflect the degree of complexity of crater floors, terraces, and central peaks, Smith and Sanchez (1973) concluded that fresh lunar craters between 4 km and about 150 km across make up a continuous morphologic sequence. Although their data show convincingly that the morphologies of lunar craters between about 10–20 km and about 100 km in diameter gradually become more complex with increasing size, smaller craters do not belong to this unbroken sequence. Upon further analysis, the data of Smith and Sanchez documented a size threshold that divides their sample of 115 fresh craters into two contrasting shape

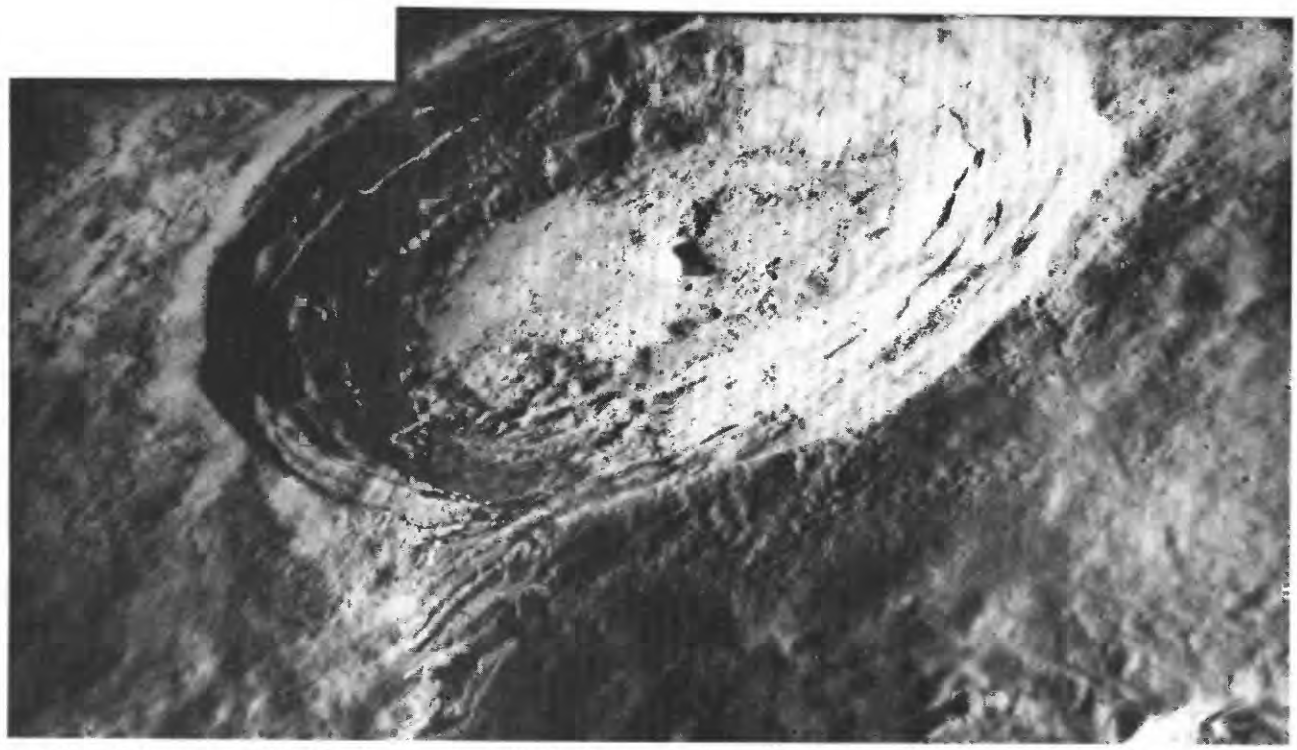

FIGURE 27.—Oblique view of Aristarchus, an especially fresh example of a well-defined complex or modified impact crater of lunar main sequence, in Oceanus Procellarum. Rim crest is about 40 km across. Compare with small simple crater Linné (fig. 5) and with craters that fall between Aristarchus and Linné in both size and morphology (fig. 31). View is to south. Mosaicked from Apollo 15 panoramic camera photographs 0331 and 0333. Sun is to left.

categories at a diameter of 10–20 km (Pike, 1975). The two types of data, index numbers and frequencies of occurrence (figs. 28 and 29), gathered by Smith and Sanchez from Lunar Orbiter and Apollo photographs are examined at some length here because they provide an especially systematic and comprehensive body of observations showing changes in crater morphology at this size range.

INDEX DATA

Smith and Sanchez (1973) obtained a semiquantitative description of crater terraces, floors, and peaks by assigning numerical values to specific morphologic characteristics in a way such that more complex craters bear proportionately higher values. The index numbers derived from this information reveal a significant morphologic change in lunar craters within the same narrow size range over which seven geometric changes also occur (fig. 28). This result differs from that obtained initially by Smith and Sanchez, but the use of arithmetic scales on the diagrams and the inclusion of too few small craters prevented the inflection in the size-morphology continuum from being recognized in the original investigation. First, the arithmetic scale is unsuited to most graphical analyses of the dimensions of natural and experimental craters; it unduly compresses smaller values and thus conceals possible variations in the data. Use of the logarithmic scale, which accommodates the great size range over which lunar craters occur, has been conventional practice for some time (see MacDonald, 1931; Baldwin, 1949), although it does tend to obscure some constants. Second, Smith and Sanchez did not examine enough small craters. Only 3 of their 115 sample craters lie below the 5–10-km diameter range where the pronounced differences in morphology start to become evident. Similarly, because the sample was limited to only three craters larger than 100 km in diameter, their conclusions do not necessarily apply to craters larger than about 100 km across.

The Smith-Sanchez conclusions were tested by additional data. A representative sample of fresh primary craters in the 0.1- to 10-km diameter range (table 7) was obtained to determine whether or not extension of the sample to smaller craters would continue to show a gradual sequence of shape characteristics. Expansion of the sample to larger craters was not attempted. The 37 small craters were selected primarily from published maps and reports prepared for, or resulting from, the Apollo missions. According to the morphologic-index (MI) criteria listed in table 2 of

TABLE 7.—*Morphologic index numbers of selected lunar craters*

Crater identification	Diameter (km)	TSI[1]	CPI[1]	FI[1]	MI[2]
Sunrise (Apollo 14)	0.18	5	5	10	20
L.O. III H 133	.20	5	5	5	15
Cone (Apollo 14)	.34	5	5	5	15
AS16, PAN-5400	.43	5	10	5	20
Horatio (Apollo 17)	.45	5	5	5	15
Sherlock (Apollo 17)	.50	5	5	5	15
L.O. III H 189	.51	10	5	5	20
Near Rima Prinz I	.60	5	5	5	15
Emory (Apollo 17)	.65	5	5	5	15
South Ray (Apollo 16)	.65	5	10	5	20
Cochise (Apollo 17)	.70	5	5	5	15
Camelot (Apollo 17)	.73	5	5	5	15
Kiva (Apollo 16)	.85	5	10	5	20
North Ray (Apollo 16)	.93	5	10	5	20
L.O. III H 143	1.05	15	5	5	25
Near Apollo 17 site	1.30	5	5	5	15
L.O. III H 143	1.50	15	5	5	25
In Sklodowska[3]	1.60	5	5	5	15
NW of Krieger C	1.96	5	5	5	15
Linné	2.45	5	5	5	15
Near Gagarin[3]	2.75	5	5	5	15
In Sklodowska[3]	2.75	5	5	5	15
In Hirayama[3]	3.45	5	5	5	15
Censorinus	3.82	5	5	5	15
Littrow BD	4.05	5	5	5	15
In Curie[3]	4.25	5	5	5	15
Krieger C	4.30	5	5	5	15
Secchi X	4.80	5	5	5	15
In Tsiolkovskiy[3]	4.90	5	5	5	15
Hyginus B	5.20	5	5	5	15
Hadley C	5.82	5	5	5	15
In Hilbert[3]	6.00	5	5	5	15
Censorinus A	6.52	5	5	5	15
Moltke	6.80	5	5	5	15
Littrow B	7.00	5	5	5	15
AS10–29–4207[3]	8.00	10	10	5	25
Messier B	8.00	5	5	10	20

[1]Index numbers that reflect, from left to right, the morphology of crater-wall terraces, central peaks, and floors, according to criteria in table II of Smith and Sanchez (1973).
[2]Sum of these index numbers.
[3]Far-side craters; all but AS10–29–4207 from Pike (1973a).

Smith and Sanchez (1973), most of the additional craters (MI values were taken from photographs) are quite similar in shape and have the minimum possible value, 15, of the cumulative morphology index. For craters under 2 km in diameter, cumulative MI values over 15 may indicate complexities in shape imparted by a thin regolith on the Moon (Oberbeck and Quaide, 1967). Figure 28 is the resulting revision of Smith and Sanchez's figure 1, with crater diameter plotted on a logarithmic scale. The morphologic contrast provided by the added smaller craters in table 7 reveals a sharp inflection, rather than a gradual change, in the trend of the cumulative morphology index at about 10-km diameter. Most lunar craters larger than this size clearly are much more complex than are the smaller craters. Although each of the constituent index numbers—TSI, CPI, and FI of the Smith and Sanchez (1973) cumulative morphology index, MI, shows a similar inflection at about 10-km diameter, the sudden change in shape is adequately illustrated by the MI/diameter data alone.

FREQUENCY DATA

Data on the prevalence of certain features in craters on the Moon also support the existence of a marked morphologic change in craters at the restricted diameter range in which the seven geometric changes occur. Smith and Sanchez (1973) show that crater-wall terraces, textured (flat) floors, and central peaks increase gradually in frequency of occurrence from nearly zero in craters under 5 km in diameter until they are present universally in fresh lunar craters that exceed 55 km in diameter. Replotting their data for all three features (fig. 29) reveals a parallel transition from simple to complex crater morphologies within a diameter range of about 50 km. This interval is remarkably narrow in view of the 11 orders of magnitude spanned by lunar impact features. As craters increase in size, statistically a flat floor is the first complication in the simple bowl shape of the smaller craters. Development of a floor is followed by the appearance of central peaks and finally terraced walls.

The frequency data of Smith and Sanchez (1973) show that the transition between 100 percent absence and 100 percent presence of peaks, terraces, and flat floors in all craters falls within a restricted size range, about 9 to 22 km in diameter (fig. 29), and averages 15 km for the three features. Corroboration appears in figures 7, 9, and 11 of Smith and Sanchez (1973), wherein percentages of craters possessing terraces, floors, or peaks within each of the 10 discrete diameter intervals are plotted against crater diameter. Presence of these features in craters is transitional and does not happen at one diameter value. Thus the threshold or transitional diameter is statistical in nature and requires a measure of central tendency. The center of the transition from a preponderance of craters not having these features to one of craters having them is located correctly at the crater diameter at which the frequency of occurrence of each feature is 0.5 (fig. 29). This median diameter marks the focal point of each transition statistically. It lends greater precision to the qualitative statements of earlier workers such as Gilbert (1893) and Quaide and others (1965) that various features tend to appear or disappear within fresh lunar craters above or below some particular size. The crater diameter marking the 0.5 frequency of occurrence is preferable to the diameters at which features begin to occur (the "onset diameter"; see Cintala and others, 1976) or stop occurring, because the latter two values are based wholly on single occurrences of peaks, floors, or terraces and hence are susceptible to large errors.

According to figure 7 of Smith and Sanchez (1973), the transition from unterraced to terraced craters is centered at a crater diameter of 22 km. Next, their figure 9 shows that at a diameter range centered at about 9 km, 50 percent of the sampled fresh craters exhibit no floor texturing. This curve also describes data that mark the presence or absence of flat interior floors within 749 lunar craters (Pike, 1968, table 14).

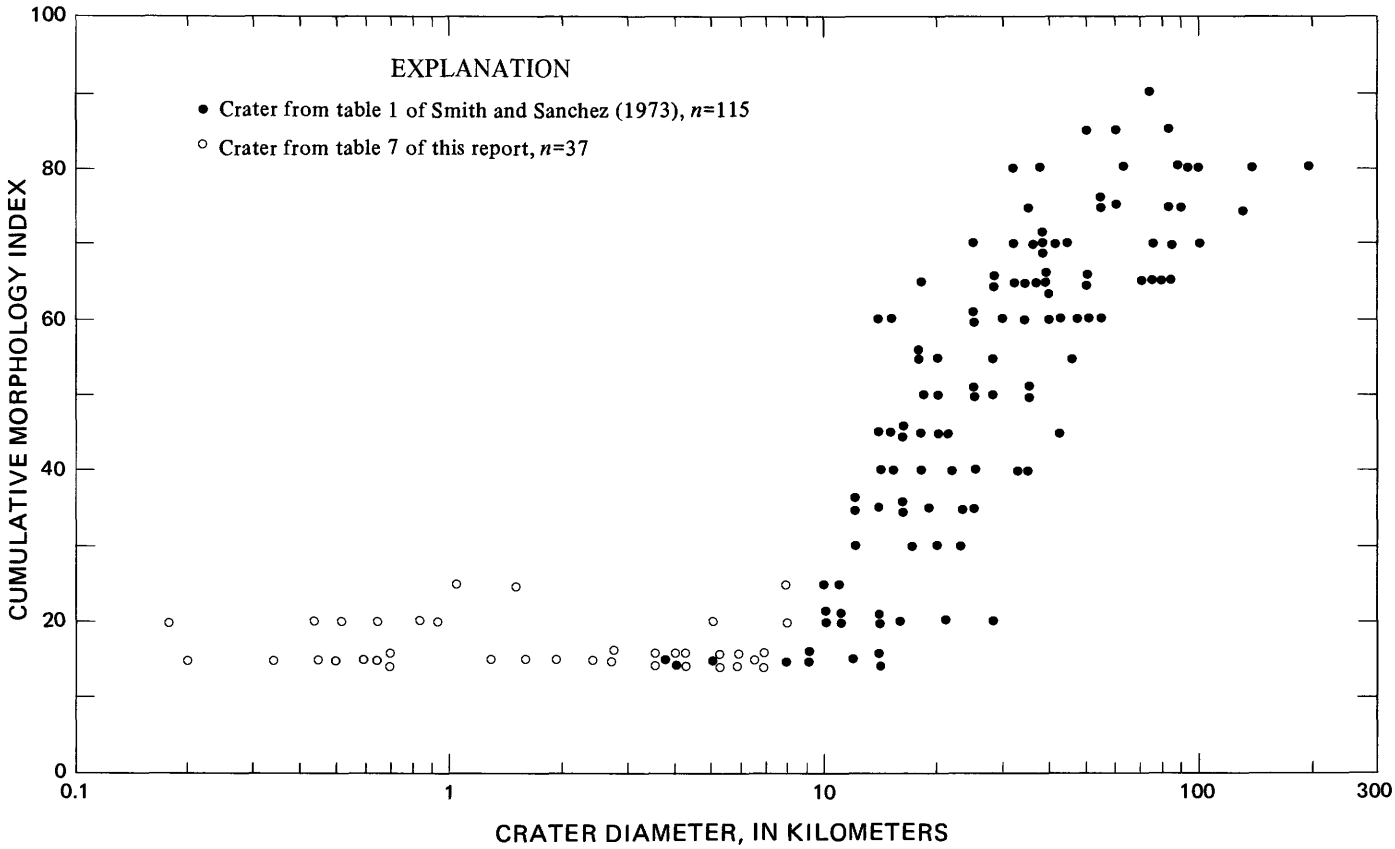

FIGURE 28.—Inflection in complexity with size of large lunar impact craters. Relation between cumulative morphology index, MI, of Smith and Sanchez (1973) and crater diameter for 152 fresh lunar craters ranging in diameter from 180 m to 195 km. Abrupt elbow in distribution at about 10-km diameter marks transition from simple to complex craters on the Moon.

Finally, figure 11 of Smith and Sanchez (1973) shows that the transition from craters without central peaks to craters with peaks is centered at a crater diameter of 14 km. These three values can be read from figure 29. The average of the three transition-center diameters, 15 km, indicates a characteristic size that divides most craters with a relatively uncomplicated shape from most craters with relatively complex shapes, however continuous the change in morphology (from simple to complex or modified) may appear to be. The value of 15 km, although based on only three morphologic criteria and hence approximate, agrees well with the 10–20-km diameter range containing the seven geometric inflections.

Moreover, a crater diameter of 15 km exactly bisects the frequency distribution derived by Smith and Sanchez (1973) for the occurrence of "swirl texture" on the floors of certain lunar craters (their fig. 9). The texture, which is particularly well developed in the craters Dawes and Bessel, is significant because it may arise from the transition of relatively smooth crater walls to terraced walls. "Swirl texture" may simply describe the surface configuration of material that has slumped from the crater walls: not cohesive terraces that have separated from the upper wall, but rather unconsolidated material that has slid down the walls rapidly in rock slides and spread across the flat floor in festooned piles of debris. Unlike flat floors, central peaks, and terraced walls, "swirl texture" does not increase in prevalence from zero to 100 percent over the crater-diameter range of about 4 to 55 km (fig. 29). Rather, it is most common in craters about 20 km across and is not observed at all in craters under 5 km or over 40 km in diameter. Location of the median frequency of occurrence of "swirl texture" at 15-km diameter, the average of the three transition-center diameters (fig. 29), suggests strongly that this feature is yet another manifestation of the fundamental change from simple craters to complex craters on the Moon.

DISCUSSION

Inflections in the plot of morphology index and diameter (fig. 28) and in the four morphologic transitions evident from the frequency data of Smith and Sanchez (fig. 29) coincide with seven size-dependent differences in the geometry of lunar craters (figs. 19–26). It is likely that all 11 shape changes—which occur at an average crater diameter of 17.5 km—have a common

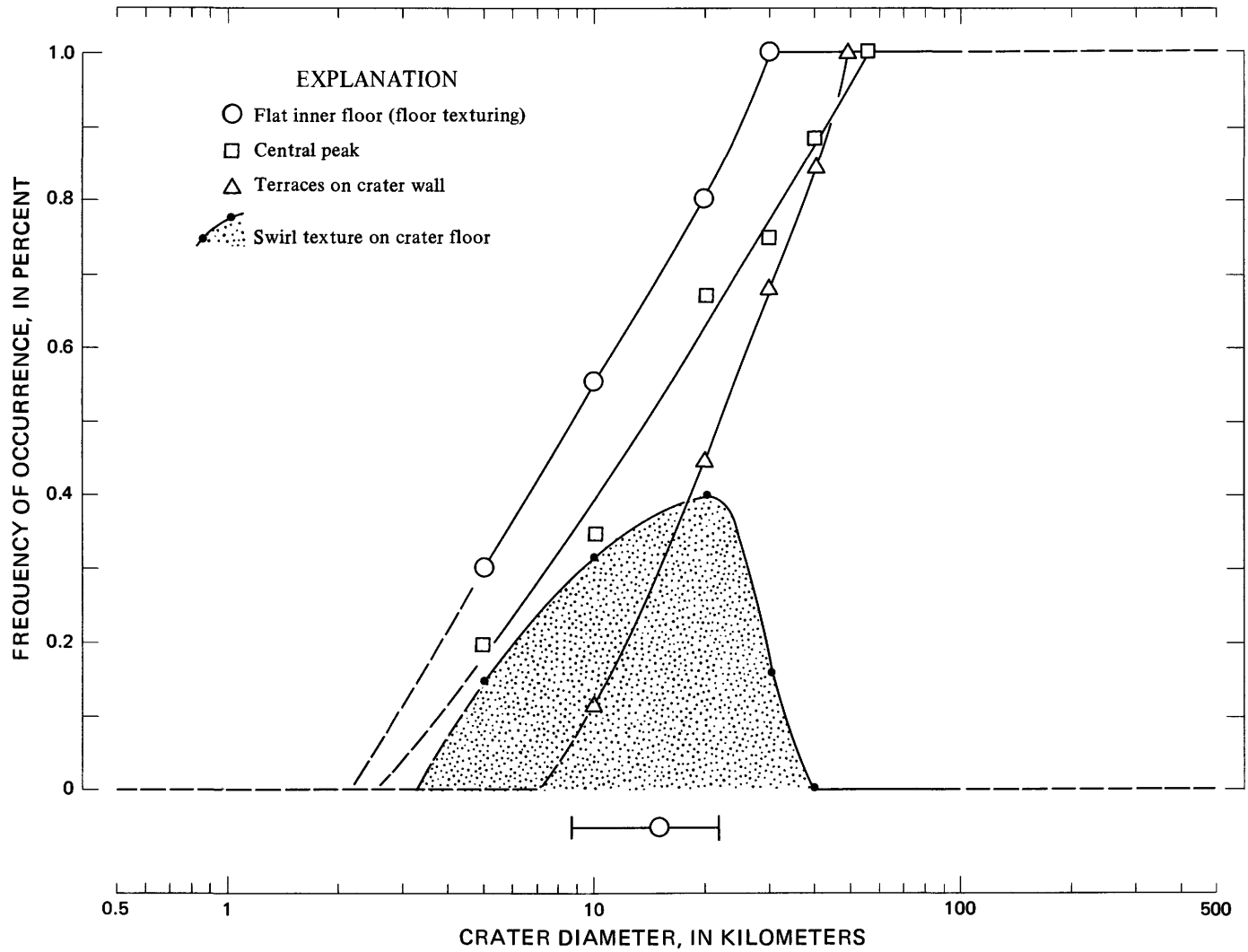

FIGURE 29.—Transition from simple to complex morphologies in fresh lunar craters at approximately 10- to 20-km diameter. Frequencies of occurrence, at various diameter intervals, for four salient features in craters between 0.5 and 500 km in diameter. Solid curves are data from Smith and Sanchez (1973). Dashed curves used where data are sparse or obtained elsewhere (Pike, 1968). Barred circle shows range and mean diameter for first three features at 50 percent frequency (see text).

origin related to formation of central peaks, a flat floor, and rim-wall terraces in fresh craters of a critical size (Gilbert, 1893; Shoemaker, 1959; Quaide and others, 1965; Pike, 1967: Mackin, 1969; Schultz, 1976a). The changes in crater geometry reflect two principal effects. First, diminution of rim height and flank width indicate lowering of the rim crest and enlargement of the crater rim diameter, almost certainly as the result of terracing of the rim wall. This wholesale slumping probably has decreased slope, depth, circularity, and evenness as well. Second, changes in slope, floor diameter, and depth reflect emplacement and widening of the flat floor in larger craters—in part probably from uplift accompanying formation of the central peak. The net result of these changes is to reduce both rim and crater volumes for craters exceeding some threshold size, that is, to diminish the topographic disturbance created at the Moon's surface by the original impact. The changes in impact-crater shape mark the transition from one type of equilibrium landform to another (Pike, 1967): simple craters seem to be stable only up to 15-20 km across. The larger complex craters evidently cannot reach equilibrium with the postimpact environment without departing significantly from the geometry of the smaller simple craters.

DEPTH VERSUS RIM-WALL WIDTH

The inflected relation between depth and rim-wall width (fig. 30) provides further insight into the transition from simple to complex craters. The two variables are components of rim-wall slope (fig. 22) for a sample of 107 craters ranging in size from 400 m to 370 km across. The presence of flat floors and central peaks, which generally are accompanied by rim terraces, is

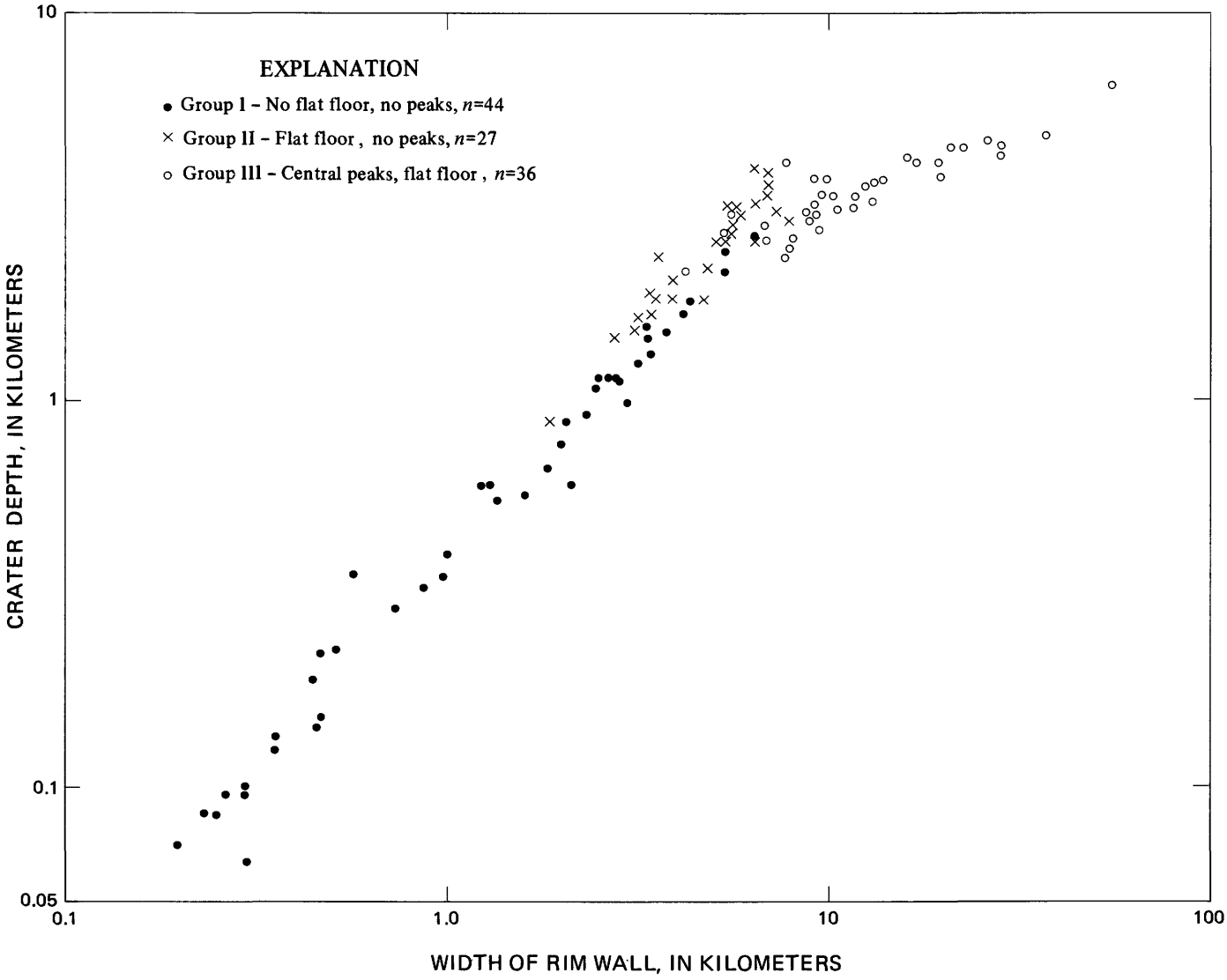

FIGURE 30.—Relation between crater depth, R_i, and width, W_i, of rim wall for 107 fresh lunar craters. Data and crater types same as in figure 22. The sample of craters divides into three fields (see text). Terraces usually present in craters with peaks. Transition from group II to group III craters marks change from simple to complex or modified craters.

indicated for each crater. The depth/wall-width data lie in three relatively discrete fields on the graph, each of which is dominated by morphologic characteristics that mark the transition from simple to complex impact craters. For convenience in discussing the data in figure 30, the three fields are referred to as group I (no special features), group II (small flat floors only), and group III (conspicuous flat floors and central peaks). Group I meets group III at a rim width of about 5 km and a depth of about 2.5 km, but group II (with craters as deep as 3.9 km) spans this inflection without any change in slope on the graph. Although flat floors are the first complication of the simple shape as craters increase in size, depth does not diminish with increasing width of the wall until central peaks begin to appear (group III).

Group I contains 44 craters and exhibits a positive slope of about 1.0 (fig. 30). The simple impact craters in the group I sample, which range from 400 m to 12.8 km in diameter, have no terraces, peaks, or flat floors. Wall slopes typically are between 18° and 24°, averaged from rim crest to crater center, but reach 30° and more on upper slopes of the wall. Cauchy, at 2,675 m, is the deepest crater in the group; the slope of its wall (6.4 km long) averages about 23°. The depth of Cauchy approaches the 3.0 km upper limit proposed on the basis of older data by Quaide and others (1965) for the depth of a stable crater landform on the Moon. A more typical

example of a group I crater is Linné (fig. 7). The symmetrical simple shapes of group I craters and their similarity to much smaller experimental impact and explosion craters suggest that they differ little in form from the transient craters that developed at the climax of the original impact event, except for the addition of some fallback ejecta and minor rockslides on the walls. Group II and III craters are increasingly complex and evidently have not retained the simple pre-slump morphology.

Group II in figure 30 contains 27 craters and lies above and parallel to group I. The craters range from about 5 to 29 km in diameter and have no prominent central peaks or rim terraces. Group II craters have very small flat floors (the same craters less than 20 km across in fig. 23) and are comparatively deep for their size; their rim walls are narrow and steep. Evidently moderate infilling, not accompanied by terrace slumping, has formed a small floor that reduces the rim-wall width substantially without much reducing crater depth. Four group III craters, which plot with the group II craters, contain central peaks, Proclus, Peirce, Diophantus, and an unnamed far-side crater 14.6 km across, but their peaks are abnormally small for the size of the crater (fig. 32). These four anomalous craters also are among the smallest craters that have measurable peaks (excepting, of course, the much smaller craters excavated in thin regolith), and their rim walls are among the steepest in the sample. Some craters within the group II size range—such as Messier B (Pike, 1971b) and Taruntius E—have small flat floors, but only low hummocks instead of well-developed central peaks. These observations and floor-frequency data in figure 29 suggest that emplacement of small flat floors is the first manifestation (with respect to increasing crater size) of the change in shape at the 10–20-km diameter threshold. The small peaks within larger craters in the group may be large blocks of fallback ejecta or rocks that fell from the upper crater wall onto the crater bottom but were not buried in the flat floor. Alternatively, these protuberances may be blocks of material that have been thrust up from depth by recoil from the impact. The flat floor in these smaller craters is interpreted as a more or less leveled deposit of impact fallback and loose rock debris that moved rapidly in sheetlike slides down the crater walls, probably right after impact, until the slope stabilized (Pike, 1971b). The deposit probably is not impact melt (Howard and Wilshire, 1975). Typically, the floor forms a gently sloping conical surface that is not quite flat and level, but inclined 4° to 5°, as can be seen in the 18-km crater Gilbert D on LTO sheet no. 81A2. The floor material covers the originally concave crater bottom, which can still be seen in group I craters, and in most cases any small central mounds or peaks; only a few peaks protrude above the surface of the floor deposit. The maximum depth for group II craters is about 4 km, corresponding to a crater diameter of about 20 km (equation 1)—deeper craters on the Moon all are much larger and more complex. The limiting slope angle of the crater wall is about 31°. The largest craters in the group II sample appear to contain the longest steep slopes on the Moon, 6 km to nearly 8 km. By way of comparison using measurements from the 1:50,000 Apollo contour maps, the steepest slopes measured on Mons Hadley—which is considerably older than the fresh group II craters—are about 7 km long and lie at about 29° or less. Thus, the limiting conditions for stability of partly constructional and partly excavational slopes on the Moon may be about 7 km and 30°, presumably in badly fractured basalt or similar material.

Group III in figure 30 contains 36 craters and slopes positively away from the other two fields at about 0.40. The craters in group III, which range in diameter from 18 to 370 km, are full-fledged complex or modified craters, with well-developed terraces, flat floors, and central peaks. The large floors in group III craters are considerably more complicated topographically than the small floors in group II craters and may consist of uplifted material veneered with impact melt (Pike, 1971a; Howard and Wilshire, 1975). Compared with group II craters, the floors are wider, the peaks (if present at all in group II) are larger (fig. 32), and the depths are significantly less per unit diameter. Walls slope at only 17° to 22° for the smaller group III craters, and slopes are much less in larger craters (fig. 22). Small craters in group III are only about 2.7 km deep; the larger group III craters all are over 4.0 km deep (the maximum for group II) once rim-wall slopes are wider than 15 km. The limiting depth of the largest crater exceeds 6.0 km, but its sloping walls are stable owing to their great width. Three group II craters, which lack well-developed central peaks—Conon, Vitruvius A, and an unnamed crater on the far side—and appear to mark the transition from group II to group III, plot at the lower end of the group III field. These somewhat anomalous craters have low hummocks on their small flat floors, tend to be deeper than other group III craters of similar size, and are the three smallest craters in the group III sample; their walls, which are only 6.5 km to 8.0 km wide, slope at 20° to 22°.

With respect to surface geometry, the change from simple to complex, or modified, craters on the Moon at the 10–20-km size may be defined as the change from group II to group III craters in figure 30. Two good illustrations of craters that are intermediate in the transition are Diophantus and Delisle (fig. 31). Both

FIGURE 31.—Vertical views of fresh impact craters in western Mare Imbrium. Larger craters contain features that illustrate transition from simple to complex craters on the Moon (see text, fig. 30). *A*, Diophantus C (5 km across), a simple impact crater in group I (fig. 30), is much like the crater Linné (fig. 5). Diophantus (18 km across), in group II, is between Diophantus C and Delisle in morphology. *B*, Delisle (25 km across), in group III (fig. 30), is a complex impact crater but lacks the well-formed slump terraces that characterize full-fledged complex craters such as Aristarchus (fig. 27). Apollo 15 mapping-camera photograph 2738. Sun is to right.

craters have small peaks and floors with these features better developed in the larger crater but differ significantly in that Delisle has several massive terraces on the rim wall, whereas Diophantus has only one or two slump blocks.

Figure 30 suggests that for fresh lunar craters less than 10 km or so across and 3 km deep (group I), the observed and presumably stable form might not differ much from that of the transient cavity reached at the height of the impact. The profile of this cavity may be parabolic (Dence, 1973), but it could be hemispherical or even hemielliptical (Pike, 1968). Although the observed configurations of the larger craters (groups II and III) probably are not like those of the transient craters, the degree of difference between the two forms remains unknown. Figure 30 might provide one way to estimate the size and shape of transient cavities for these larger craters. Group II craters differ only slightly from those in group I. Hence the group II field probably could be shifted up to about 0.5 km and to the right on figure 30 until it is alined with the upper part of group I, in order to obtain a fair approximation of the shape of the transient cavities for group II craters. An analogous restoration of group III craters would involve rotating the field counterclockwise about an origin marked by a rim width of 6 km and a depth of 2.5 km. Such a restoration for the larger group III craters would involve very great differences between observed and hypothesized depths (Pike, 1968). Whether or not this practice is justified remains one of the more intriguing questions concerning craters on the Moon, because of possible extrapolation to initial cavities of excavation of large basins and the radial distribution of their ejecta (Pike, 1967, 1974a; McGetchin and others, 1973).

SOME ALTERNATIVE EXPLANATIONS

The problem of explaining the break at 10–20 km within the crater continuum now lies less in relating changes in crater geometry to the appearance of various morphologic features than in determining the underlying physical mechanisms and how and why they operate. The latter are difficult if not impossible to judge from a scrutiny of lunar topography alone, so some recourse to experimental work, computer modeling and simulation, and especially analogies with terrestrial impact structures is necessary. However, the best known terrestrial impact craters are small features compared to the larger craters on the Moon, and the fundamental cause of the related features in lunar craters 10–20 km across remains uncertain and controversial. Currently the issue seems to hinge upon origin of central peaks and rim-wall terraces, for which there are two main interpretations in contention: centripetal collapse and elastic recoil.

Various hypotheses for the discontinuity in crater shape—including the cometary-impact model developed by Roddy and others (1969), isostasy (Baldwin, 1963), and variable depths of impact focus (Baldwin, 1963)—have been summarized by Quaide and others (1965) and reviewed more recently by Allen (1975). The layered-substrate idea of Wegener (1921) has been revived (Head, 1976b). Quaide and his colleagues concurred with Shoemaker's (1959, 1962) view that deep-seated slumping of the crater rim to form terraces also converged at the crater center to thrust up a peak (see also Gilbert, 1893). Subsequently this model was adopted by Dence (1968), Mackin (1969), Gault, Quaide, and Oberbeck (1968), and Gault, Guest, and others (1975). Centripetal collapse of the rim and uplift of the central peak, likened to formation of a central jet in a liquid splash (Harlow and Shannon, 1967), are presumed to result from gravitational instability of lunar rock materials making up long slopes that exceed some critical value, shown here to be about 30°, in transient craters larger than 10–20 km across and deeper than 4 km (fig. 30). According to the collapse hypothesis, peak-forming energy is potential energy that is stored momentarily in the mass of the rim of the transient crater and then released in a late stage of the cratering event. This mechanism would produce most of the size-dependent changes in crater shape, with a veneer of impact melt perhaps accounting for the level floors in larger craters such as Tycho and Aristarchus (Howard and Wilshire, 1975). Explanations for the increase of rim-crest circularity and rim-wall slope in craters up to 10–20 km across are less evident and may not even be related to the main shape discontinuity. Quantitative evaluation of the gravity-collapse hypothesis currently is underway (Melosh, 1977).

Geologic evidence from impact structures on Earth, however, suggests that central peaks within lunar craters did not result from deep-seated centripetal collapse of the crater rim but are rebound phenomena as Baldwin (1963) suggested (see also Gilbert, 1893). Elastic recoil depends upon crater-forming energy—as manifested by compression of the ground surface by the shock wave—rather than upon potential energy stored in the rim of the transient cavity. Data of Wood (1973) imply that the amount of uplift estimated to have occurred in the centers of terrestrial impact craters is directly proportional to the size of the crater and hence to impact energy (fig. 32). Theoretical calculations by Dent (1973) are consistent with this view.

Study of the Gosses Bluff, Australia, and Sierra Madera, Texas, structures on Earth shows that rocks of the central uplifts came from stratigraphic horizons well below those that could have been affected by rim slumping (Milton and Brett, 1968; Milton and others, 1972; Wilshire and others, 1972). Additionally, the central uplift appears to develop in early, not late, stages of a cratering event (Milton and Roddy, 1972). The centripetal movement that seems to accompany formation of a central uplift may have caused the rims of these structures to collapse into slump terraces with attendant loss of crater depth, not vice versa. If the terrestrial analogy can be extended to large craters on the Moon, then rim terraces and flat floors with "swirl-texture" material (Smith and Sanchez, 1973) probably develop consequent to central peaks rather than the other way around. Much of the shallowness of large craters may result from accompanying (and instantaneous) uplift of the floor area between the peaks and the rim (Offield and Pohn, 1977), rather than exclusively from terracing of the rim. This structural shallowing also would enable a comparatively small volume of impact melt and fallback material to form a broad flat floor in large craters. Great volumes of fill might not be required except where it can be shown that central peaks have been completely buried, usually in subsequent events unrelated to formation of the crater.

Although the mechanisms responsible for central uplifts in lunar craters according to the recoil, or rebound, hypothesis remain conjectural, the geology of terrestrial impact craters and analyses of experimental-explosion craters imply that peaks result from reflection of the impact-rarefaction waves by target material at the excavated ground surface (Milton and Roddy, 1972, Roddy, 1976). Laboratory experiments with small impact craters had suggested earlier that a stratified target—comprising a less cohesive surface layer and a more cohesive substrate—is required for central peaks to form. From the results of experiments, first Wegener (1921, 1975) and later Sabaneyev (1962) applied this interpretation to large lunar craters. Similar results were obtained in more elaborate series of tests by Oberbeck and Quaide (1967) and Quaide and Oberbeck (1968), who explained only the central mounds in small (less than 250 m across) craters on the lunar mare surfaces in terms of the strength-discontinuity mechanism. I subsequently suggested (Pike, 1971a) that Oberbeck and Quaide's interpretation might be scaled up to account for the transition from simple to complex morphologies in lunar craters over 1 km across. Head (1976b) proposed more specifically that the "megaregolith" believed to veneer the lunar highlands (Hartmann, 1973) is the low-cohesion surface layer by which the strength-discontinuity mechanism can effect the shape transition in craters in the 10–20-km diameter range. However, the highland "megaregolith," about 2.5 km deep (Head, 1976b), is two orders of magnitude thicker than typical

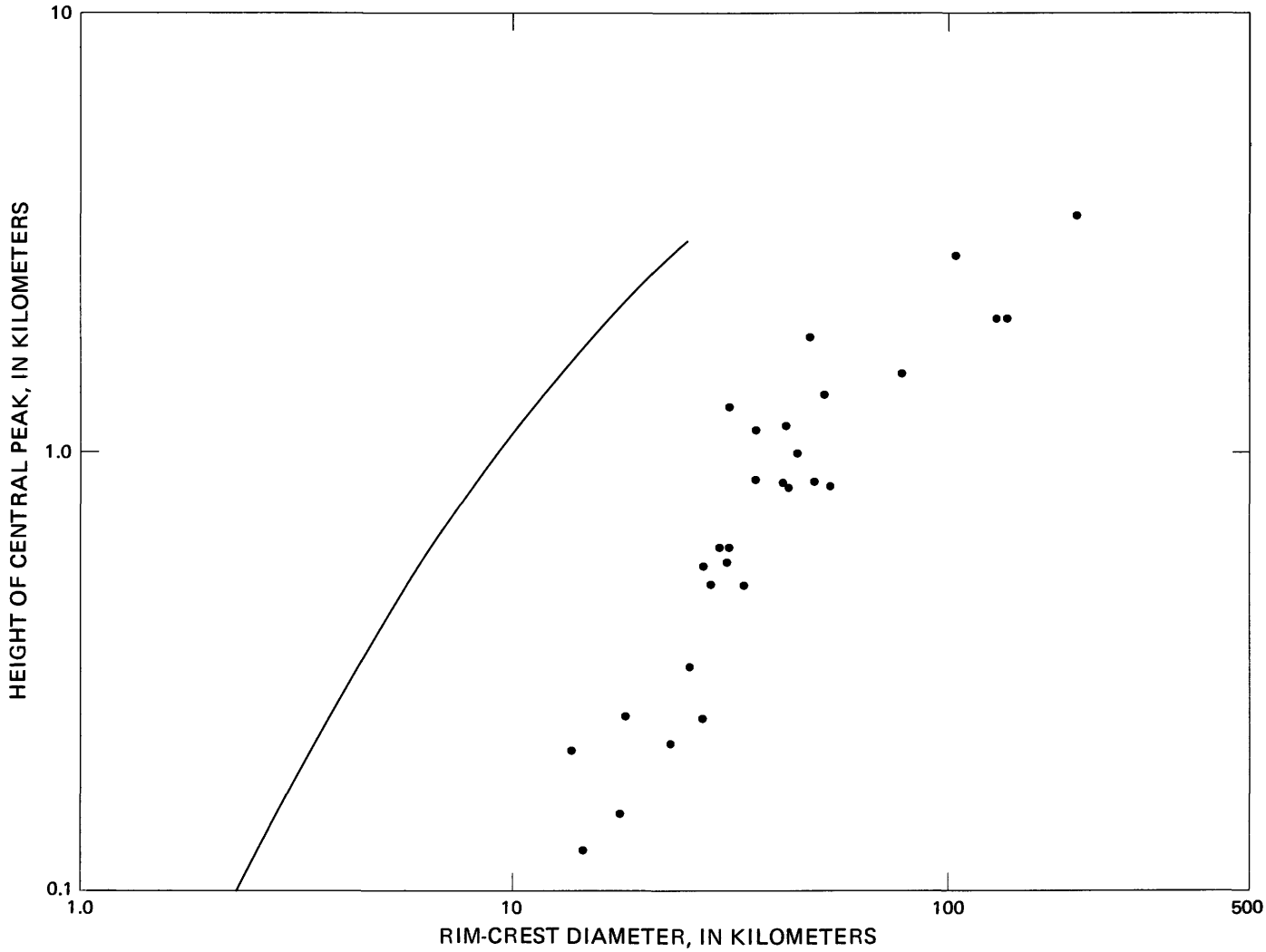

FIGURE 32.—Relation between relative height of central peak and rim diameter for 29 fresh lunar craters. Peaks in seven craters under 28 km across are systematically lower than peaks in the 22 larger craters, for which an equation has been fit (table 6), supplanting the fit to shadow data done by Wood (1973). Solid curve is Wood's (1973) fit to central uplifts estimated within terrestrial impact structures. All data points from photogrammetry of Apollo pictures.

mare regolith, about 10 m (Oberbeck and Quaide, 1967; Quaide and Oberbeck, 1968), a difference that should be reflected by a dramatic contrast between maria and uplands in the crater size ranges at which the shape transition occurs. The absence of any such difference in the geometric data presented in this report suggests that the strength-discontinuity hypothesis for the formation of peaks in large lunar craters requires further evaluation.

Critical to explaining the existance of central peaks or uplifts according to any process is their obvious dependence upon crater size. Why peaks form only in craters above a particular diameter is not clear, but two influences, an energy threshold and gravitational acceleration, may be involved. The role of increased energy in changing crater form was addressed implicitly by Gilbert (1893), discussed briefly by Baldwin (1963, p. 184), and still is speculative. A threshold in the relation between impact energy and strength of the target materials could provide physical circumstances that favor development of central peaks and other structural displacements. It is suggested that the mechanics of impact cratering change qualitatively once energy exceeds some critical value. Perhaps beyond this level, a significant fraction of the target material—some of which becomes impact melt—behaves as a fluid rather than as fractured and comminuted rock (Baldwin, 1963). The energy level at which the postulated change in shock-hydrodynamic regime occurs on the Moon is unknown, but it may not be far from the 10^{24} to 10^{25} ergs (Innes, 1961; Baldwin, 1963) thought to be required for development of a central

uplift in terrestrial meteorite craters. Chao's (1976) suggestion that the basic mechanism producing shallow (complex) impact craters such as the Ries may differ substantially from that responsible for bowl-shaped (simple) craters such as the Arizona Meteor Crater is consistent with the existence of a critical energy threshold.

Gravity almost certainly affects the way energy couples with the target materials to form peaks, because central uplifts (Dence, 1968) and diminished depth/diameter ratios (fig. 33, see also David, 1975; Losej and Beales, 1975) first appear in terrestrial impact craters 2 to 4 km across, or about one-sixth the crater size at which similar changes take place on the Moon. Some influence of gravity also is indicated for the appearance of central peaks in craters on Mars (Hartmann, 1972b) and Mercury (Gault, Wedekind, and others, 1975; Gault, Guest, and others, 1975) and possibly for the relative height of peaks and uplifts in terrestrial and lunar craters (fig. 32; Wood, 1973; Gault, Wedekind, and others, 1975; Gault, Guest, and others, 1975). Recently I have summarized observations showing that the simple-to-complex transition is an inverse function of gravitational attraction on Earth, the Moon, Mars, and Mercury (Pike, 1978b). Although the influence of gravity has been interpreted in the context of the centripetal-collapse hypothesis (Quaide and others, 1965; Gault, Wedekind, and others, 1975; Gault, Guest, and others, 1975), it has not yet been evaluated in terms of elastic recoil. Currently the role of elastic recoil in forming peaks is being reexamined by computer-modeling large experimental craters from more elaborate hydrodynamic and material-strength assumptions than have been used in past simulations of this type (Ullrich, 1976; Ullrich and others, 1977).

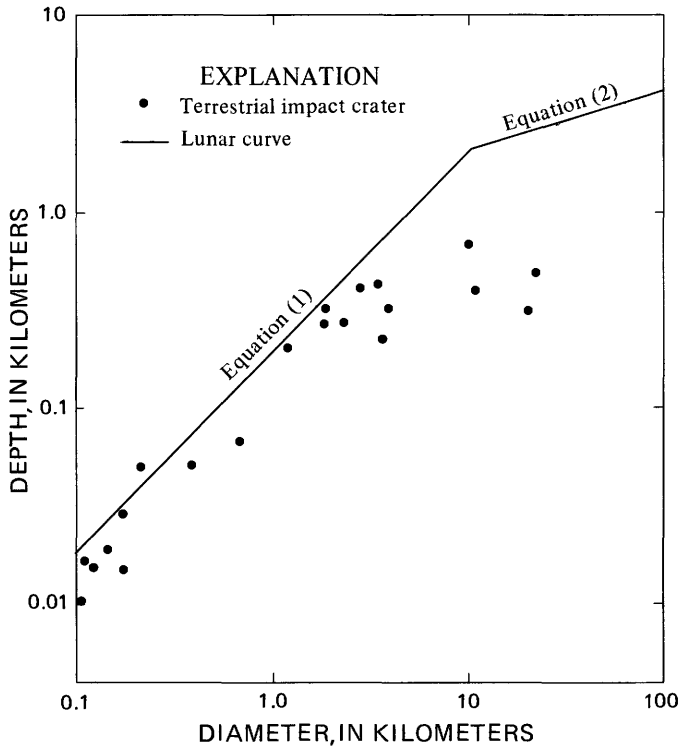

FIGURE 33.—Depth/diameter plot for 21 terrestrial impact craters (some unpublished data, but most from Pike, 1972b). Craters tend to be relatively fresh, otherwise depths were determined from results of drilling or gravity work. Solid curves are equations (1) and (2) for fresh lunar craters, simple and complex, respectively. Array of terrestrial craters inflects at about one-sixth of the diameter at which curve inflects for lunar craters, a consequence of the sixfold difference in gravitational acceleration at the planetary surface.

A third explanation for the size- or energy-dependent occurrence of central peaks might be systematic decrease of scaled depth of burial with increasing crater size, although the role of gravity scaling in such a scheme is difficult to follow at this time. There are at least two ways this might occur. Baldwin (1963) contended that larger meteoroids flatten more upon impact and disintegrate at correspondingly shallower depths of burial. He also suggested that if central peaks are rebound phenomena, then they must result from relatively shallow releases of energy or else be buried by fallback. The work of Roddy (1968), Roddy and others (1969), and Ullrich (1976) now suggests that only shallow impacts are capable of producing central peaks in terrestrial craters. If the cometary impact hypothesis for peak formation can be dismissed, then the occurrence of central uplifts may instead be governed by depth of penetration of the projectile. This depth in turn could relate directly to the bulk of the impacting body and its flattening, as discussed previously by Baldwin and several others (see Baldwin, 1963, p. 167). However, cometary impact may not be so easily ignored, despite the seeming illogic that only comets (low density) can make large craters and only meteoroids (high density) can make small craters. At this time there is no evidence on which to test the idea. Until more is known about the composition of impact-producing projectiles in the solar system (Wetherill, 1977), the possibility of size-dependency in the density distribution of impacting bodies remains open.

Other gravity-driven mechanisms for modifying craters operate at a more leisurely pace than those above. Much of the diminution of crater depth and rim height at the 10–20-km size range has been attributed to isostatic compensation (Daneš, 1962; Baldwin, 1963; 1968c, 1971; Scott, 1967) and to isostasy plus consequent volcanism (Pike, 1967). There seems little doubt that viscous flow of the substrate has raised the floors of the multi-ringed basins and is intimately involved with mare volcanism (Wise and Yates, 1970).

Isostasy also has deformed some large craters such as Taruntius (Masursky, 1964) and Humboldt (Baldwin, 1968c), where the central peak appears to have been carried up along with the uplifted, cracked crater floor. Many of these craters are located along the margins of basins (Pike, 1968, 1971a). However, inflection of the statistical relation between flank width and rim diameter suggests that crater rims generally lose height by retreat of the rim crest through slumping. Thus, isostasy probably does not affect most craters as small as 10 to 30 km across, and indeed, with few exceptions (such as Taruntius) only craters over about 150 km across have the substantial positive Bouguer gravity anomalies that indicate deformation of the lunar mantle, as in response to isostasy (Phillips and others, 1975). The minor negative gravity anomalies that typically accompany the smaller complex craters, like Copernicus, can be accounted for entirely by their topography (Sjogren and others, 1973; Bowin, 1975); isostasy does not seem to have been involved. The 200-km crater Humboldt (fig. 34) has a bulged and cracked floor that does suggest some isostatic uplift (Baldwin, 1968c), along with annular deposits of presumably volcanic material that may have accompanied the deformation (Pike, 1968), but the central peak complex does not appear large enough to have been uplifted rather than partially buried. Moreover, Schultz (1976a, b) has identified over 200 craters that possess similar or nearly similar modified floors. These "floor-fractured craters" range in size from about 10 km to over 200 km across and may reflect post-impact modification in which isostasy has not played a major role (see also Brennan, 1975). Under normal circumstances isostasy does not appear to explain enough of the size-dependent morphologic observations summarized here, especially emplacement of the central peak.

MINOR DIFFERENCES IN CRATER SHAPE

The most conspicuous contrasts in morphology among craters on the Moon reflect mode of origin, size, and relative age. Genetic and size-dependent variations among craters have been treated here, whereas age-related differences have been analyzed elsewhere (Baldwin, 1949; Pike, 1971; Pohn and Offield, 1970; Schubert and others, 1977) and some of them recently reviewed by Head (1975). Other kinds of contrasts among lunar craters have been recognized by observers at different times, but they are of less importance, where real. Three of these variations are briefly examined here from Apollo 15–17 data: results from the new information show that craters on mare surfaces are much like craters on uplands, except for the expected differences in evenness of the rim imparted by irregular upland terrain; there are no differences between far-side and near-side craters on the Moon; and the

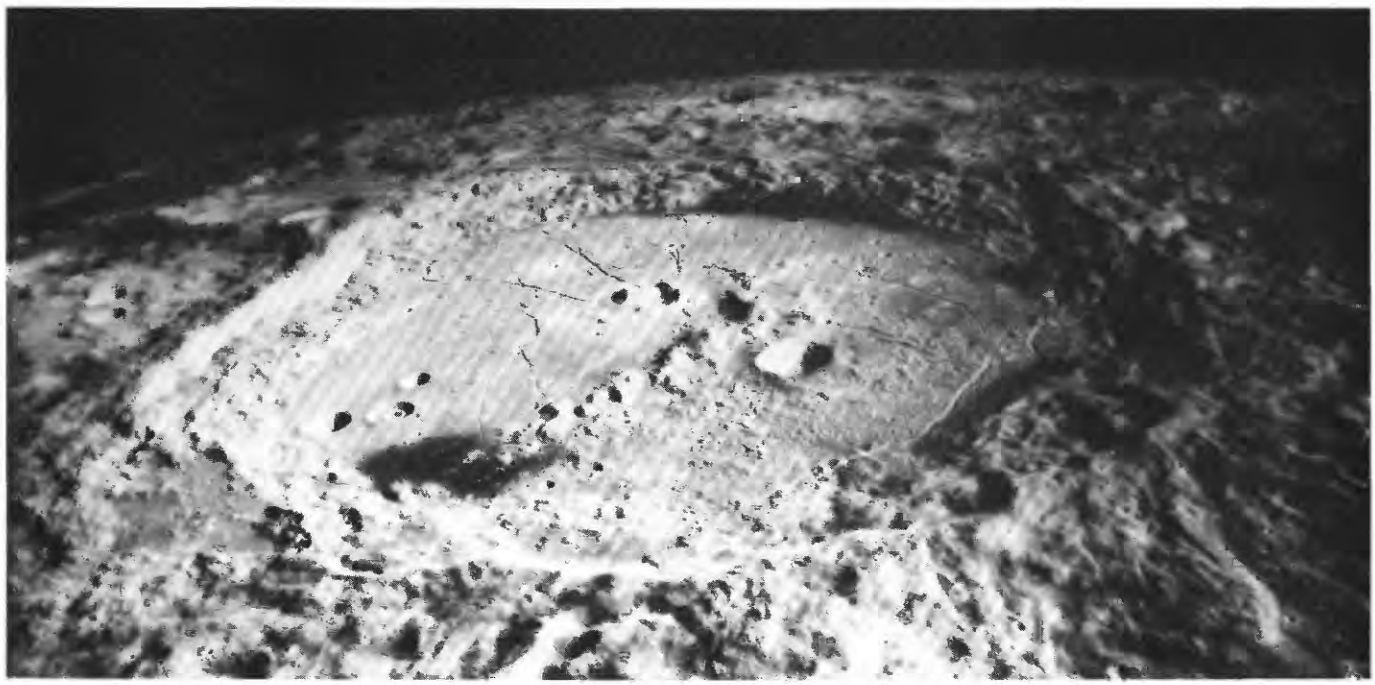

FIGURE 34.—Oblique view of large crater Humboldt on far eastern limb of the Moon. Cracks and dark patches on floor of this 200-km-diameter crater indicate isostatic compensation (Pike, 1968; Baldwin, 1968c). Note unusual double-rimmed crater on floor of Humboldt. View is to south. Apollo 15 mapping-camera photograph 2513. Sun is to right.

height of crater rims does not appear to vary systematically with azimuth.

MARE-TERRA CONTRASTS

Some older Earth-based measurements of lunar craters over 20 km across have suggested that craters formed on mare surfaces are systematically shallower than craters formed on upland surfaces (MacDonald, 1929, 1931; Marcus, 1967; Pike, 1972c). These data appear to have been inaccurate or unrepresentative. There is no such contrast in the new photogrammetric depth/diameter data (fig. 19), and a difference so small as to be negligible and readily explained is evident in a second set of new depth/diameter data, which resulted from updating of a standard catalog, the System of Lunar Craters (Arthur and others, 1963, 1964, 1965, 1966). The latter depths, which were generated from measurements of shadow lengths on Lunar Orbiter IV high-resolution images of the near side, already have been described in detail (Wood, 1972; Arthur, 1974). Nearly half of the depths from the first section of the revised catalog (Arthur, 1974) are plotted against their diameters in figure 35 (see also Pike, 1974b). The sample of 950 craters was stratified according to conventions adopted in the System of Lunar Craters (Arthur and others, 1963). Only the freshest looking (Class 1) craters are included, and craters on mare surfaces are plotted separately from craters on upland surfaces.

Depth/diameter distributions of mare and upland craters less than about 15 km across barely differ from each other (fig. 35). Visually this minor contrast is evident only upon overlaying the two plots. The equations (fitted by inspection only) for mare and upland craters are, respectively,

$$R_i \approx 0.18\, D_r^{1.03} \tag{16}$$

and

$$R_i \approx 0.15\, D_r^{1.09} \tag{17}$$

(variables in kilometers). The two distributions are only slightly lower and steeper than the distribution in figure 19, a small difference that also can be seen only by overlaying the three graphs. The significance, if any, of differences between mare and upland craters suggested by the new shadow-length data may be obtainable subsequently from more exact regression and an analysis of variance. The contrast could well reflect the slightly greater scatter in the upland data. Some such scatter is to be expected from inadvertent classification of Class 2 upland craters (somewhat older looking; rims less crisp than Class 1) as Class 1 objects, and from a greater variance in the depths of the upland craters relative to that of mare-crater depths. Unevenness of the lunar upland terrain almost certainly introduces some minor scatter from both these sources.

Unlike all other aspects of crater geometry, none of which show any significant differences between fresh upland and mare craters, evenness of the rim crest is markedly less for upland than for mare craters. The contrast is evident both in the plot of rim-crest relief against crater diameter (fig. 25) and in the graph showing coefficient of variation for rim-crest elevation (V_c) as a function of crater size (fig. 26). The influence of pre-crater topography upon this difference is obvious from perusal of the LTO's. For example, relief along the rim of the 27-km-diameter crater Menelaus is 2,000 m, more than twice the average rim height and nearly equal to the depth, because the crater formed on the slopes of Montes Haemus rather than on a mare surface or on less irregular upland terrain. In contrast, relief along the rim crest of Mädler, a mare crater similar to Menelaus in size and relative age but located on much smoother and more level terrain, is only 700 m. These two craters lie on opposite margins of the rim-crest relief/diameter distribution (fig. 25); there are numerous other examples.

The uneven upland terrain also is responsible for the marked contrast between mare and upland craters in figure 26. The inflection in the V_c/diameter distribution would not be as recognizable without the mare/upland distinction. Within the larger sample of figure 26, the mare craters serve as a control group by which rim-crest roughness that is the result of irregular background terrain can be separated from roughness that is related only to crater size. Among the larger upland craters Proclus, followed by King and Tsiolkovskiy, is the most seriously affected by an irregular background, whereas Sklodowska has not been distorted at all. Particular care must be taken when measuring the dimensions of the more deformed among such craters in the lunar uplands in order to secure only representative data for subsequent analysis. It is conceivable that the mare/terra contrast in rim evenness may accompany analogous differences in the crater sizes at which central peaks and rim-wall terraces begin to occur in mare and highland craters (Cintala and others, 1977). If real, these differences may reflect only the difference in pre-crater topography rather than any significant contrasts in properties of the target materials.

FAR SIDE-NEAR SIDE CONTRASTS

Through photometric processing of Zond 3 images, Mironova (1970a, b) generated the first topographic measurements ever made of craters on the Moon's far

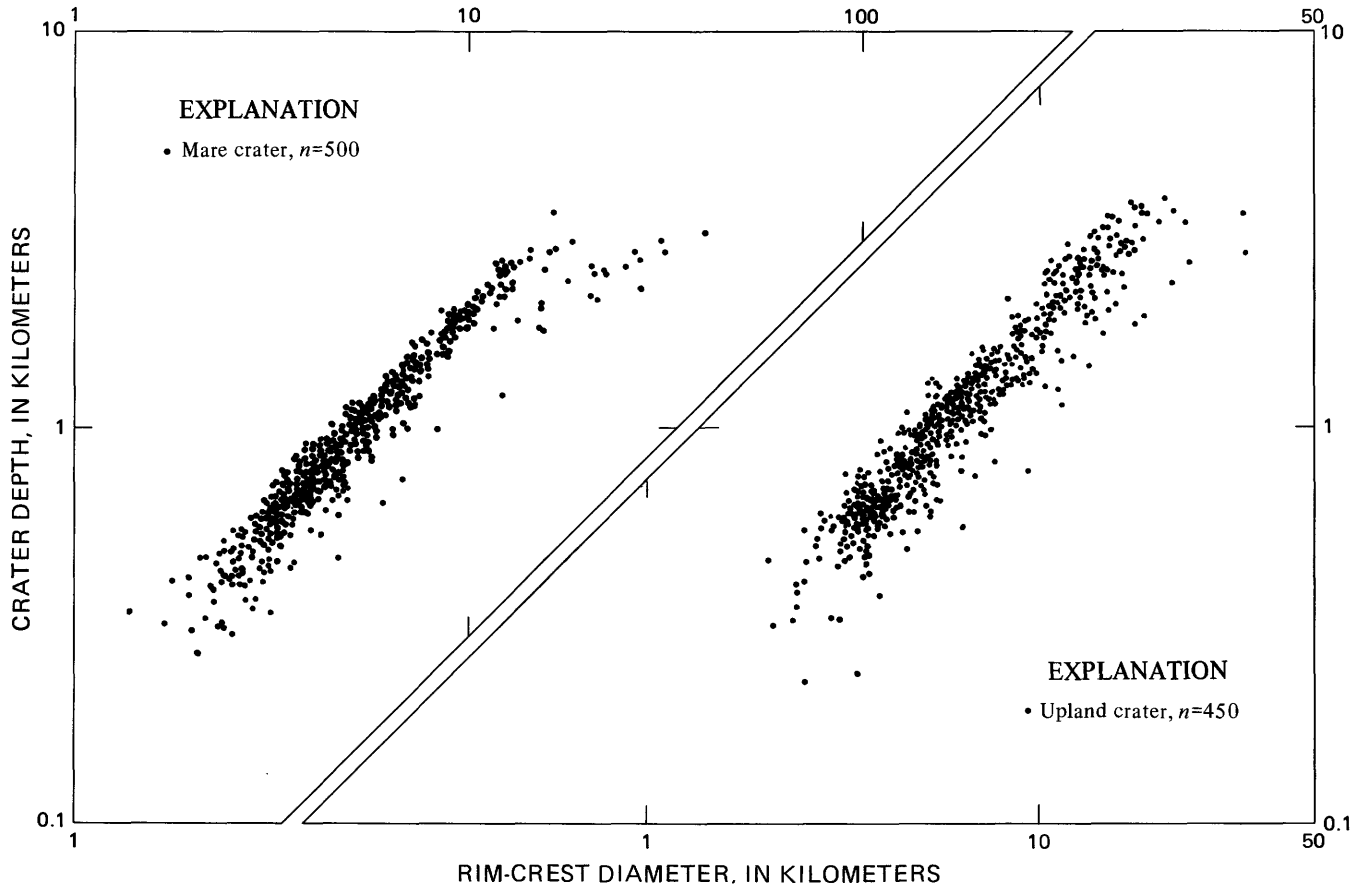

FIGURE 35.—Relation between depth and diameter for 950 fresh (Class 1) lunar craters from Pike (1974b). All data from Arthur (1974). Crater depths measured from shadow lengths on Lunar Orbiter IV high-resolution images. Distributions differ only slightly from one another and from that for small craters in figure 19 (see text).

side. The 29 craters that were profiled and measured range in diameter from 16 to 100 km and vary in relative age. From a brief analysis of surface geometry, Mironova concluded that the far-side craters were similar in shape to near-side craters and were volcanic in origin. I examined both conclusions using preliminary photogrammetric measurements of 25 different far-side craters (Pike, 1972a, 1974c). Although the Apollo craters and the Zond craters are not the same, the statistics of each group are judged to adequately represent the larger population of far-side craters. My two studies revealed neither any distinction between far-side and near-side craters nor evidence for a volcanic origin of the craters. The more abundant Apollo data on fresh far-side craters that were collected to update the preliminary work (figs. 36 and 37) are consistent with these conclusions.

Compared to the new photogrammetric data on far-side craters, the photoclinometric measurements of Mironova are not very accurate. Depth measurements from the Zond 3 data generally represent craters as being excessively shallow, even when taking relative age into consideration (fig. 36). The rim-height data from Zond 3, which also are inconsistent with photogrammetric measurements, are too low for smaller craters and too high for larger craters (fig. 37). Despite the absolute error, photometric analysis of the Zond 3 imagery at least preserved the relative proportion between crater depth and rim height for many of the craters. The height/depth ratio for fresh lunar craters over 15 km across varies between 0.32 and 0.38 (figs. 19 and 20, equations 2 and 4); for the 18 far-side craters in the fresh and intermediate-age categories of Mironova, the ratio averages 0.34; however, the Zond data do range widely, from 0.09 to 1.20. Under favorable circumstances, useful information can be extracted from the photoclinometric technique (Lambiotte and Taylor, 1968; Leighton, 1966), but the low-quality measurements obtained by Mironova reflect problems that need to be overcome before photoclinometry can be applied confidently to large topographic features of other planets.

Using the depth/diameter proportion, Mironova (1970a) deduced a volcanic genesis for both near-side

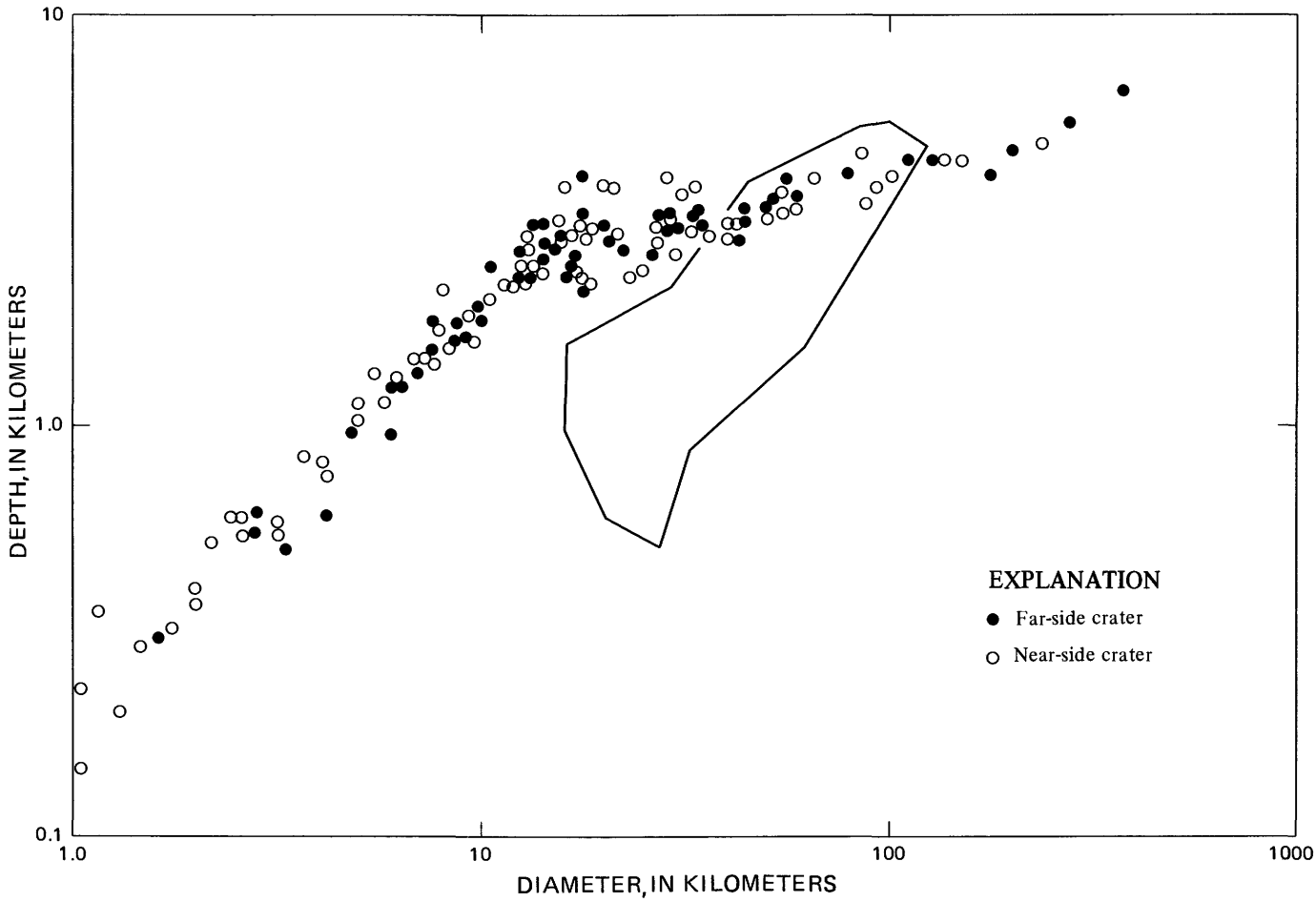

FIGURE 36.—Depth/diameter plot for 58 far-side and 78 near-side craters on the Moon. Most craters are fresh-looking and were measured from photogrammetric data. Polygon contains Zond 3 photoclinometric data for 29 far-side craters, which do not coincide with newer data (see text).

and far-side craters from the same type of analog argument by which Baldwin (1949) originally inferred an impact origin for near-side craters. Although the depth/diameter relation has become the most often-used morphometric criterion of crater genesis, the generous overlap among depth/diameter fields describing all types of lunar and terrestrial craters demonstrates that it is also the least reliable of all available geometric discriminants (Green, 1959; Steinberg, 1968; Baldwin, 1968a: Pike, 1972b) and cannot support any genetic hypothesis. Crater-depth measurements are better applied to the analysis of relative age or post-impact modification (Baldwin, 1949: Pike, 1968). Rim height is a more reliable—although still imperfect—indicator of crater genesis, but the Zond 3 rim height/diameter data in figure 37 are characteristic of impact craters rather than volcanoes (Pike, 1973a, 1974c).

According to photogrammetric measurements of lunar craters, (1) differences between near-side and far-side craters are negligible and (2) far-side craters more probably formed by the impact of large cosmic bodies than by volcanism. Mironova (1970a) also reached the first conclusion, but as shown here, not for the same reasons. Evidently the photoclinometric method, the only way to obtain quantitative data from Zond images, did not yield topographic information as accurate as that of even the older shadow-length crater measurements. Mironova's conclusions that the lunar craters formed from volcanic eruptions is not supported by the available data. Instead, the results obtained from Apollo metric cameras, and indeed the Zond 3 measurements themselves, are more consistent with an impact genesis for craters on the Moon's far side.

AZIMUTH-DEPENDENT DIFFERENCES

According to early morphometric work by MacDonald (1929) on data collected and published by Schmidt (1878), the rim crests of large craters on the Moon generally are much higher along the eastern and western parts of their walls than along northern and southern segments. Although photointerpretation and

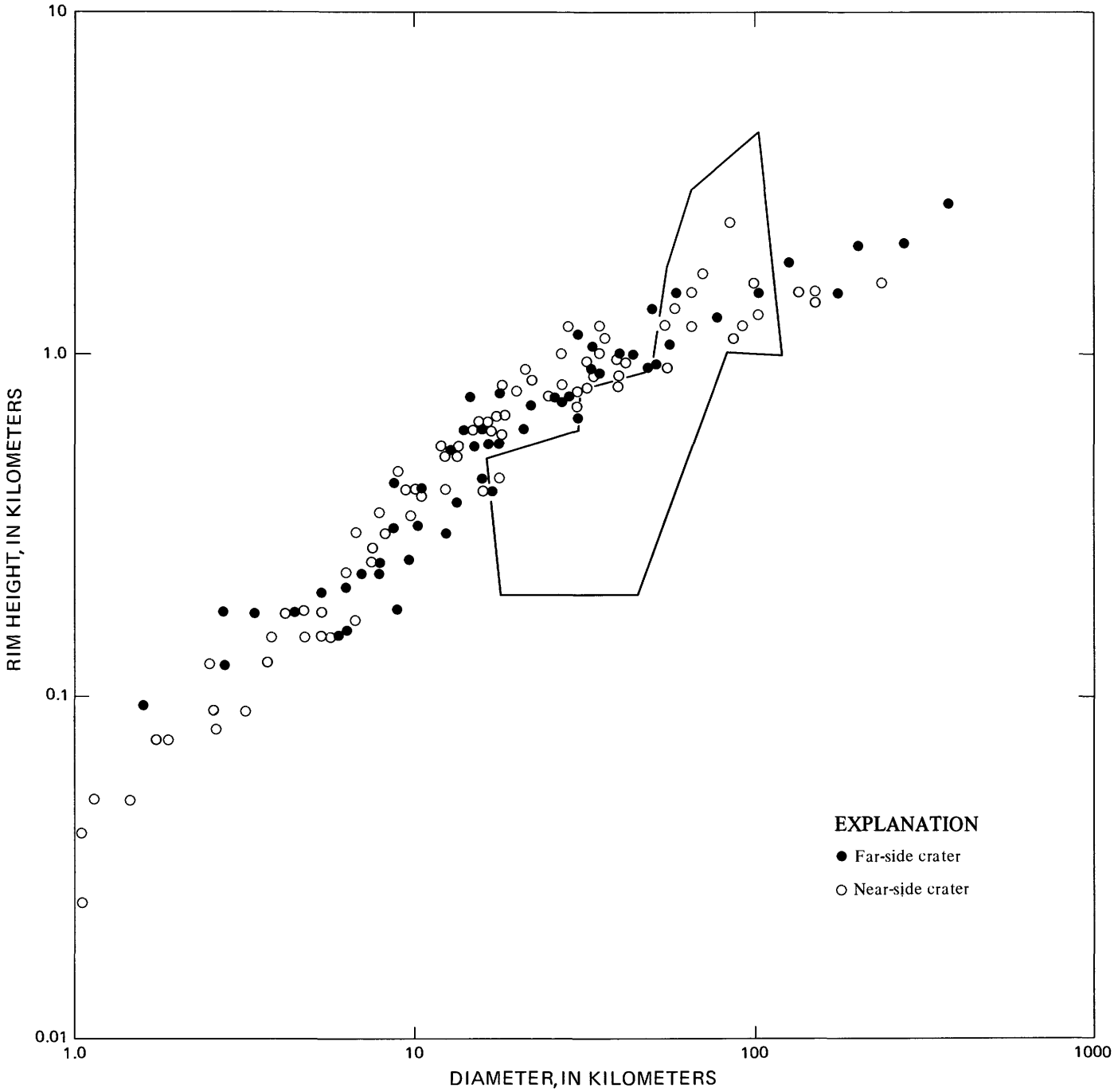

FIGURE 37.—Rim-height/diameter plot for 54 far-side and 78 near-side craters on the Moon. Most craters are fresh-looking and were measured from photogrammetric data. Polygon contains Zond 3 photoclinometric data for 29 far-side craters, which do not coincide with newer data (see text).

visual observation of the lunar surface do not show such a strong azimuth-related tendency, certain pre-Apollo contour maps of the Moon indeed portray many craters with a systematic excess in height of the east and west walls (Pike, 1968). The 1:5,000,000 U.S. Army Map Service Topographic Lunar Map and various 1:1,000,000 U.S. Air Force Lunar Aeronautical Charts both show this tendency. A contour map of the crater Aristarchus from stereophotogrammetry of Lunar Orbiter V images clearly carried this systematic difference in rim height (unpublished U.S. Geological Survey data, 1968), although the difference was much reduced in another map of the same area from the same data by the U.S. Air Force Aeronautical Chart and

Information Center (1972). If real, the systematic rim-height relation could have interesting structural implications—possibly involving influence of broad-scale fracture networks—and would further complicate mensuration of crater average depths and rim heights. The considerable importance ascribed by some investigators to lineament patterns and possible planetwide grid systems of tectonic features (Fielder, 1965) prompted a test for systematic dependence of crater rim-crest profile on lunar azimuth.

The existence of the height excess in the east-west direction was tested with an updated sample of 36 rim-crest elevations from each of 34 craters used previously in this report for examining the comparative roughness of crater rim crests (table 8). Following procedures used in a preliminary test (Pike, 1973a), six quantities were calculated for each crater: (1) total relief along the rim crest, (2) mean elevation of the rim crest, and (3–6) deviation from mean elevation of the heights of eastern, western, northern, and southern walls, expressed as a plus or minus percentage of total rim-crest relief. Deviations were averaged from three elevations centered on the four cardinal directions and tabulated as in Pike (1973a) for each of the craters, which range in diameter from 1.6 to 197 km.

Except for a slight tendency for crater rims to be higher in the south and lower in the north, there is no systematic relation among the rim-crest results. When averaged for all 34 craters, the four percentage deviations from mean elevation are +0.02 (east), −0.01 (west), −0.04 (north), and −0.05 (south). The absolute values average even lower than the deviations resulting from the preliminary study (Pike, 1973a). The essential randomness of rim-crest height-azimuth also is evident in table 8. The systematic arrangement suggested by the data of MacDonald and the early contour maps, + + − − in table 8, occurs only in Linné, Euler K, and Littrow BD, three of the 12 small mare craters examined in this analysis. Summed plus and minus deviations confirm that southern segments of crater rims tend to be somewhat higher than average and northern rims tend to be lower, whereas east and west rims are roughly comparable in elevation. The significance, if any, of this contrast is not evident. The results, which do not change if only mare craters are included in the tabulation, imply that variation in height along the rim crest of a lunar crater occurs more or less randomly with respect to azimuth. Croft and Kaula (1976) reached similar conclusions from their analysis of rim-crest ellipticity and azimuth for nearly 300 craters portrayed on the LTO's. The systematic variations in height found by MacDonald and observed by compilers of the earlier contour maps and charts probably are not real. They may have resulted from the high-contrast, east-west illumination of the lunar surface and from inadequate photogrammetric separation in the available Earth-based photographs.

TABLE 8.—*Qualitative deviations from mean rim-crest elevation*

Azimuth				*n*
90°	270°	360°	180°	(34 craters)
+	+	+	+	0
+	+	+	−	2
+	+	−	+	2
+	+	−	−	3
+	−	+	+	2
+	−	+	−	3
+	−	−	+	6
+	−	−	−	1
−	+	+	+	3
−	+	+	−	1
−	+	−	+	5
−	+	−	−	2
−	−	+	+	1
−	−	+	−	0
−	−	−	+	3
−	−	−	−	0
19+	18+	12+	22+	71+
15−	16−	22−	12−	65−

SUMMARY AND CONCLUSIONS

This report samples the variety of results obtained by statistical analysis of the topography of the Moon's craters, principally using new data reduced photogrammetrically from Apollo orbital pictures. Many of these results have been published elsewhere as separate contributions. The systematic measurements of rim and floor diameter, rim height and flank width, and crater depth and circularity for some 500 lunar craters between about 400 m and about 300 km across provide the planetary science community with a new data set. The new information supplants earlier compilations of telescopic measurements, and is more complete and precise than data sets compiled from Lunar Orbiter results. The new data emphasize freshly formed craters and are more accurate than the older measurement. The principal aim of this series of investigations was to reevaluate several old problems that might benefit from the application of improved data. The work addresses four overall areas of possible influences on the variation in shape of lunar craters: mode of origin, size, geography, and azimuth.

The new data confirm quite conclusively the thesis of Gilbert (1893) that different modes of origin produce distinctively different crater shapes. The most fundamental contrast is that between volcanic craters and impact craters. According to multivariate statistical models of dimensionless variables, the two processes yield crater shapes that are all but mutually exclusive. With respect to the distribution of mass, most vol-

canoes are positive landforms, whereas impact craters are always negative features in the terrain. To some extent, results of the multivariate analysis can be used to discriminate impact craters from volcanoes on the basis of their gross geometry. Although maar volcanoes on Earth share some geometric characteristics with impact craters, they differ sharply in others. Secondary-impact craters on the Moon differ similarly in geometry from primary craters of the lunar main sequence and somewhat resemble terrestrial maars. The closest terrestrial volcanic analog of lunar impact craters is the maar, not the caldera. Of the several categories of calderas examined here, only the large ash-flow plains even remotely approach lunar impact craters in shape. Calderas are particularly poor analogs of lunar craters of any type. Some special classes of lunar landforms evidently are true central volcanoes, but they are small and rare. The low domes on mare surfaces probably are a type of shield volcano; the small raised cones on mare and crater-floor surfaces could be some sort of spatter-cinder edifice. The dark-halo craters along rilles on the floor of Alphonsus are negative landforms, but probably did not form in phreatic eruptions like most terrestrial maars. One class of lunar craters roughly 20 to 40 km across, often described as smooth-rimmed craters, may have had an atypical impact origin or may have been modified by mare lavas after their formation. These craters almost certainly are not calderas. The depressions atop summits of central peaks within many large craters on the Moon likewise do not seem to be volcanic vents, but rather superposed and distorted impact craters or collapse depressions in the irregular peak topography. The small, mysterious crater Linné turns out to be a quite ordinary—if exceedingly young—impact crater; it appears to have undergone none of the several "volcanic changes" that were ascribed to it by classical selenologists. Most of the volcanism associated with craters on the Moon is post-impact modification, especially on the flat floors of large craters, and does not arise from primary crater genesis.

Aside from the fundamental contrast between impact craters and multi-ring basins, the outstanding size-dependent variation among fresh lunar craters between 400 m and about 300 km across is the transition from small simple craters to large complex craters at a threshold diameter of 10 to 20 km. Eleven of the constituent changes in shape are documented here in considerable detail: the appearance of central peaks, flat floors, rim-wall terraces, and swirl texture, and the variation with rim diameter of crater depth, rim height, flank width, rim-wall slope, floor diameter, rim-crest circularity, and rim evenness. Observations of some of these changes in craters on Earth, Mars, and Mercury suggest that the transition is a widespread and fundamental phenomenon of planetary impact cratering. There are several contending explanations for the onset of these features, especially peaks, two of the more attractive being centripetal collapse and elastic recoil of target rocks. Size-dependence in the density distribution of impacting bodies is a third alternative. Gravitational acceleration, an impact-energy/strength-of-materials threshold, and layering of the target material may modulate the initiating process—which remains uncertain. Future research in this area should concentrate on developing criteria for testing all of the alternative hypotheses. A solution to the problem may eventually emerge from some combination of theoretical modeling of the impact process, interplanetary comparison of crater shapes, and the geologic investigation of terrestrial impact structures and experimental-explosion craters.

The variation of several of the crater dimensions with crater size, as represented by rim-crest diameter, has been expressed in linear power functions and standard errors of the estimate of the dependent variable on rim diameter. These new relations from Apollo measurements of depth/diameter, rim height/diameter, floor diameter/rim diameter, and flank width/diameter constitute an average geometric model for fresh craters on the Moon. Separate calculations have been made for simple and for complex craters. These models serve as standards of comparison for older degraded lunar craters, for both fresh and eroded impact craters on the other planets, and for experimental-impact and explosion craters excavated on Earth in both the field and the laboratory. If simplifying assumptions are allowed concerning the shape of the crater interior and the extent of ejecta beyond the edge of the topographic rim flank, then these models also can be used to estimate volumes for lunar impact craters.

The generalized statistical analysis—mainly curve fitting—carried out in this report suggests that fresh impact craters on the lunar uplands do not differ significantly in shape from craters on the mare surfaces and further, that craters on the Moon's far side are similar to near-side craters. The rim crests of upland craters are systematically less even than those of craters formed on mare and upland plains surfaces, it is true, but this difference is ascribable wholly to the more uneven surfaces on which the upland craters formed rather than to any contrast in substrate composition, strength properties, or structure. It is possible that differences in the shapes of mare and upland craters may emerge from more detailed types of analysis than those carried out here, but the evidence thus far indicates no important differences. In light of current knowledge of impact cratering, it would have been sur-

prising indeed to have found any significant disparity between craters located on the lunar near side and on the far side. There are no such differences according to the analysis done here, but it was still advisable to address the issue in case an unexpected variation might have turned up.

The test for systematic dependence of crater rim-crest profile on lunar azimuth shows that the relative height of rim crests is distributed randomly with respect to compass direction. Rims are not systematically higher or lower along preferred orientations. It is also well known, however, that segments of crater rim crests in plan—as opposed to profile—often appear to follow local and regional lineament patterns. These two results do not necessarily conflict and in any case demonstrate that structural patterns are pervasive enough to influence the planimetric outline of a crater, but insufficiently strong to effect a preferential distribution of mass in the rim.

The work reported here suggests that impact craters are among the most orderly of all landforms. Impact craters have an even more uniform surface geometry than sand dunes, drumlins, alluvial fans, fluvial watersheds, and other landscape features. This orderliness arises from the brief duration and high energy of the formational process. Unlike most other planetary landforms, craters form instantanously, by a shock-wave mechanism that within limits is fairly uniform over a very wide range of formational energies. An equilibrium geometry—that of a "landform of explosion"—is imparted to impact craters at the outset, whereas most landforms reach an equilibrium configuration only after prolonged operation of less energetic geomorphic processes. The geomorphic history of an impact crater is one of degradation of a pristine and geometrically a very well defined shape, rather than one of gradual development of a characteristic morphology as the end product.

The analysis of degradational histories of lunar craters is only one of many different problems that might well be examined in further analysis of the new quantitative data now available from the orbital cameras of the last three Apollo flights to the Moon. Other problem areas in crater geometry include a reevaluation of volumetric models, more detailed study of flat floors, relations between apparent crater dimension, better information on the size and location of central peaks, testing various models of rim-wall slumping, more detailed evaluation of any relation between rim-crest planimetry and planetary lineaments, regional variations in degree of crater infilling, improved geometric models of the shape of secondary-impact craters from multi-ring basins, and more precise models of ejecta distribution.

REFERENCES CITED

Adam, D. P., 1974, Palynological applications of principal components and cluster analyses: U.S. Geol. Survey Jour. Research, v. 2, p. 727–741.

Adler, J. E., and Salisbury, J. W., 1969, Circularity of lunar craters: Icarus, v. 10, p. 37–52.

Aitchison, J., and Brown, J. A. C., 1957, The log-normal distribution: London, Cambridge Univ. Press, 176 p.

Allen, C. C., 1975, Central peaks in lunar craters: The Moon, v. 12, p. 463–474.

Anderson, A. J. B., 1971, Numeric examination of multivariate soil samples: Math. Geology, v. 3, p. 1–14.

Arthur, D. W. G., 1974, Lunar crater depths from Orbiter IV long-focus photographs: Icarus, v. 23, p. 116–133.

Arthur, D. W. G., Agnieray, A. P., Horvath, R. A., Wood, C. A., and Chapman, C. R., 1963, The system of lunar craters, quadrant I: Tucson, Arizona Univ. Lunar and Planetary Lab. Commun., v. 2, no. 30, 68 p.

———1964, The system of lunar craters, quadrant II: Tucson, Arizona Univ. Lunar and Planetary Lab. Commun., v. 3, no. 40, 59 p.

Arthur, D. W. G., Agnieray, A. P., Pellicori, R. H., Wood, C. A., and Weller, T., The system of lunar craters, quadrant III: Tucson, Arizona Univ. Lunar and Planetary Lab. Commun., v. 3, no. 50, 146 p.

Arthur, D. W. G., Pellicori, R. H., and Wood, C. A., 1966, The system of lunar craters, quadrant IV: Tucson, Arizona Univ. Lunar and Planetary Lab. Commun., v. 5, no. 70, 208 p.

Ashbrook, Joseph, 1960, Linné in fact and legend: Sky and Telescope, v. 19, p. 87–88.

———1963a, Dimensions of the Linné craterlet: Strolling Astronomer, v. 17, p. 26–28.

———1963b, An analysis of Schmidt's observations of Linné: Strolling Astronomer, v. 17, p. 85–89.

Atchley, W. R., Gaskins, C. T., and Anderson, D., 1976, Statistical properties of ratios; I, empirical results; Systematic Zoology, v. 25, p. 137–148.

Baldwin, R. B., 1949, The face of the Moon: Chicago, Univ. Chicago Press, 239 p.

———1963, The measure of the Moon: Chicago, Univ. Chicago Press, 488 p.

———1968a, Comments on Letter by G. Steinberg, "Inapplicability of Baldwin's relation for determining the causes of formation of lunar craters": Jour. Geophys. Research, v. 73, p. 6133–6135.

———1968b, A determination of the elastic limit of the outer layer of the Moon: Icarus, v. 9, p. 401–404.

———1968c, Rille pattern in the lunar crater Humboldt: Jour. Geophys. Research, v. 73, p. 3227–3230.

———1971, The question of isostasy on the Moon: Physics Earth and Planetary Interiors, v. 4, p. 167–179.

Bowin, C., 1975, Negative gravity anomalies on the Moon, *in* Abstracts submitted to the Sixth Lunar Science Conference: Houston, Lunar Sci. Inst., p. 66–68.

Boyce, J. L., 1976, Ages of flow units in the lunar nearside maria based on Lunar Orbiter IV photographs: Lunar Sci. Conf., 7th, Proc., p. 2717–2728.

Brennan, W. J., 1975, Modification of premare impact craters by volcanism and tectonism: The Moon, v. 12, p. 449–461.

Bronowski, Jacob, and Long, W. M., 1951, Statistical methods in anthropology: Nature, v. 168, p. 794.

Burt, J., Veverka, J., and Cook, K., 1976, Depth-diameter relation for large Martian craters determined from Mariner 9 UVS altimetry: Icarus, v. 29, p. 83–90.

Carr, M. H., 1969, Geologic map of the Alphonsus region of the Moon:

U. S. Geol. Survey Misc. Geol. Inv. Map I–599, scale 1:250,000.
———1973, Volcanism on Mars: Jour. Geophys. Research, v. 78, p. 4049–4062.
Cattell, R. B., 1952, Factor analysis: New York, Harper and Bros., 462 p.
Chao, E. C. T., 1976, Mineral-produced high-pressure striae and clay polish; Key evidence for nonballistic transport of ejecta from Ries Crater: Science, v. 194, p. 615–618.
Chapman, C. R., 1976, Chronology of terrestrial planet evolution: The evidence from Mercury: Icarus, v. 28, p. 523–536.
Chapman, C. R., Mosher, J. A., and Simmons, G., 1970, Lunar cratering and erosion from Orbiter 5 photographs: Jour. Geophys. Research, v. 75, p. 1445–1466.
Chapman, R. P., 1976, Some consequences of applying lognormal theory to pseudolognormal distributions: Math. Geology, v. 8, p. 209–214.
Chayes, Felix, 1964, A petrographic distinction between Cenozoic volcanics in and around the open ocean: Jour. Geophys. Research, v. 69, p. 1573–1588.
———1971, Ratio correlation: A manual for students of petrology and geochemistry: Chicago, Univ. Chicago Press, 99 p.
Chayes, Felix, and Velde, D., 1965, On distinguishing basaltic lavas of circumocean and oceanic-island type by means of discriminant functions: Am. Jour. Science, v. 263, no. 3, p. 206–222.
Chernoff, Herman, 1973, The use of faces to represent points in K-dimensional space graphically: Jour. Am. Statistical Assoc., v. 68, p. 361–368.
Cintala, M. J., Head, J. W., and Mutch, T. A., 1976, Characteristics of fresh Martian craters as a function of diameter: Comparison with the Moon and Mercury: Geophys. Research letters, v. 3, p. 117–120.
Cintala, M. J., Wood, C. A., Head, J. W., and Mutch, T. A., 1977, Interplanetary comparison of fresh crater morphology: preliminary results, *in* Abstracts submitted to the Eighth Lunar Science Conference: Houston, Tex., Lunar Sci. Inst., p. 181–183.
Croft, S. K., and Kaula, W. M, 1976, Lunar crater dimensions and statistics, *in* Lunar photo and altimetry analysis: Final Report Natl. Aeronautics and Space Admin./Johnson Spacecraft Center Contract NAS–9–12757, May 5, 1972–October 1, 1975, p. H1–H21.
Croxton, F. E., Cowden, D. J., and Klein, S., 1967, Applied general statistics: Englewood Cliffs, N. J., Prentice-Hall, 754 p.
Dana, J. D., 1846, On the volcanoes of the Moon: Am. Jour. Sci., v. 2, series 2, p. 335–353.
Daneš, Z. F., 1962, Isostatic compensation of lunar craters: Tacoma, Wash., Univ. Puget Sound Research Inst. Rept. RIR–GP–62–1, 11 p.
David, E. J. H., 1975, Scaling law for impacts on different planets or satellites [abs.]: Meteoritics, v. 10, p. 389–390.
Defense Mapping Agency (DMA), 1974–1977, Lunar topographic orthophotomaps (LTO), scale 1:250,000: Washington, D.C., Topographic Center.
DeHon, R. A., 1971, Cauldron subsidence in lunar craters Ritter and Sabine: Jour. Geophys. Research, v. 76, p. 5712–5718.
Dence, M. R., 1964, A comparative structural and petrographic study of probable Canadian meteorite craters: Meteoritics, v. 2, p. 249–270.
———1968, Shock zoning at Canadian craters: Petrography and structural implications, *in* French, B. M., and Short, N. M., eds., Shock metamorphism of natural materials: Baltimore, Mono Book Corp., p. 169–184.
———1973, Dimensional analysis of impact structures [abs.]: Meteoritics, v. 8, p. 343–344.
Dent, Brian, 1973, Gravitationally induced stresses around a large impact crater [abs.]: Am. Geophys. Union Trans., v. 54, p. 1207.
Ebert, H., 1889, Über die Ringgebirge des Mondes: Astron. Nachrich., v. 122, p. 263–264.
El-Baz, Farouk, 1972, King crater and its environs, *in* Apollo 16 preliminary science report: Natl. Aeronautics and Space Adm. Spec. Pub. SP–315, p. 29–62 to 29–70.
———1973, "D-caldera": New photographs of a unique feature, *in* Apollo 17 preliminary science report: Natl. Aeronautics and Space Adm. Spec. Pub. SP–330, p. 30–13 to 30–17.
El-Baz, Farouk, and Worden, A. M., 1972, Visual observations from lunar orbit, *in* Apollo 15 preliminary science report: Natl. Aeronautics and Space Adm. Spec. Pub. SP–289, p. 25–1 to 25–27.
Erlich, E. N., Melekestsev, I. V., and Steinberg, G. S., 1974, General peculiarities of lunar volcanism: Modern Geology, v. 5, p. 31–43.
Fauth, Philip, 1894, Neue Beitrage zur Begrundung einer Modernen Selenologie: Astron. Nachrich., v. 137, p. 17–26.
Fielder, Gilbert, 1961, Structure of the Moon's surface: London, Pergamon Press, 266 p.
———1965, Lunar geology: London, Lutterworth Press, 184 p.
Fielder, Gilbert , and Wilson, L., eds., 1975, Volcanoes of the Earth, Moon, and Mars: New York, St. Martin's Press, 126 p.
Firsoff, V. A., 1959, Strange world of the Moon: New York, Basic Books, 226 p.
———1961, Surface of the Moon: Its structure and origin: London, Hutchinson and Co. Ltd., 128 p.
Fudali, R. F., 1979, Gravity investigation of Wolf Creek Crater, Western Australia: Jour. Geology, v. 87, p. 55–67.
Fulmer, C. V., and Roberts, W. A., 1963, Rock induration and crater shape: Icarus, v. 2, p. 452–465.
Gault, D. E., Guest, J. E., Murray, J. B., Dzurisin, D., and Malin, M. C., 1975, Some comparisons of impact craters on Mercury and the Moon: Jour. Geophys. Research, v. 80, p. 2444–2460.
Gault, D. E., Quaide, W. L., and Oberbeck, V. R., 1968, Impact cratering mechanics and structures, *in* French, B. M., and Short, N. M., eds., Shock metamorphism of natural materials: Baltimore, Mono Book Corp., p. 87–99.
Gault, D. E., Quaide, W. L., Oberbeck, V. R., and Moore, H. J., 1966, Luna 9 photographs: Evidence for a fragmental surface layer: Science, v. 153, p. 985–988.
Gault, D. E., Wedekind, J.A., Nakata, Gary, and Jordan, Raymond, 1975, Effects of gravitational acceleration on hypervelocity impact craters formed in quartz sand [abs.]: EOS, Am. Geophys. Union Trans., v. 56, p. 1015.
Gilbert, G. K., 1893, The Moon's face—A study of the origin of its features: Philos. Soc. Washington Bull., v. 12, p. 241–292.
Gewer, J. C., 1970, A note on Burnaby's character-weighting similarity coefficient: Math. Geology, v. 2, p. 39–45.
Greeley, Ronald, and Schultz , P. H., 1975, Lunar ring-moat structures in Letronne and the Flamsteed Ring [abs.]: EOS, Am. Geophys. Union Trans., v. 56, p. 1015.
Green, Jack, 1959, Geochemical implications of lunar degassing: Lunar and Planetary Explor. Colloquium Proc., v. 1, no. 4, p. 1–18.
———1971, Copernicus as a lunar caldera: Jour. Geophys. Research, v. 76, p. 5719–5731.
Green, Jack, and Poldervaart, Arie, 1960, Lunar defluidization and its implications: Internat. Geol. Cong., 21st, Copenhagen, Rept. of Sessions, pt. 21, p. 15–33.
Griffiths, J. C., 1960, Some aspects of measurement in geosciences: Mineral Industries, v. 29, no. 4, p. 1, 4, 5, 8.
———1966, Application of discriminant functions as a classification tool in the geosciences, *in* Merriam, D. F., ed., Computer applications in the earth sciences: Colloquium on classification procedures: Lawrence, Kans., Geol. Survey, Univ. Kansas, Computer Contr., p. 48–52.

Guest, J. E., and Murray, J. B., 1969, Nature and origin of Tsiolkovsky Crater, lunar farside: Planetary and Space Sci., v. 17, p. 121–141.

———1976, Volcanic features of nearside equatorial lunar maria: Jour. Geol. Soc., v. 132, p. 251–258.

Harbaugh, J. W., and Merriam, D. F., 1968, Computer applications in stratigraphic analysis: New York, John Wiley and Sons, 282 p.

Harlow, F. H., and Shannon, J. P., 1967, Distortion of a splashing liquid drop: Science, v. 157, p. 547–550.

Harman, H. H., 1967, Modern factor analysis: Chicago, Univ. Chicago Press, 474 p.

Hartmann, W. K., 1967, Lunar crater counts, I: Alphonsus: Tucson, Univ. Ariz. Lunar and Planetary Lab. Commun. 6, p. 31–38.

———1972a, Paleocratering of the Moon: Review of post-Apollo data: Astrophysics and Space Sci., v. 17, p. 48–64.

———1972b, Interplanet variations in scale of crater morphology—Earth, Mars, Moon: Icarus, v. 17, p. 707–713.

———1973, Ancient lunar mega-regolith and subsurface structure: Icarus, v. 18, p. 634–636.

Head, J. W., 1975, Processes of lunar crater degradation: Changes in style with geologic time: The Moon, v. 12, p. 299–329.

———1976a, Lunar volcanism in space and time: Rev. Geophysics and Space Physics, v. 14, p. 265–300.

———1976b, The significance of substrate characteristics in determining morphology and morphometry of lunar craters: Lunar Sci. Conf., 7th, Proc., p. 2913–2929.

Hodges, C. A., 1973, Geologic map of the Langrenus quadrangle of the Moon: U.S. Geol. Survey Misc. Geol. Inv. Map I–739, scale 1 : 1,000,000.

Hörz, F., and Ronca, L. B., 1971, A classification of impact craters: Modern Geology, v. 2, p. 65–69.

Howard, K. A., 1973, Avalanche mode of motion: Implications from lunar samples: Science, v. 80, p. 1052–1055.

———1974, Fresh lunar impact craters: Review of variations with size: Lunar Science Conf., 5th, Proc. p. 61–69.

———1975, Geologic map of the crater Copernicus: U.S. Geol. Survey Misc. Geol. Inv. Map I–840, scale 1 : 250,000.

Howard, K. A., Wilhelms, D. E., and Scott, D. H., 1974, Lunar basin formation and highland stratigraphy: Rev. Geophysics and Space Physics, v. 12, p. 309–327.

Howard, K. A., and Wilshire, H. G., 1975, Flows of impact melt at lunar craters: U.S. Geol. Survey Jour. Research, v. 3, p. 237–251.

Howarth, R. J., 1973, Preliminary assessment of a nonlinear mapping algorithm in a geological context: Math. Geology, v. 5, p. 39–57.

Innes, M. J. S., 1961, The use of gravity methods to study underground structure of meteorite craters: Jour. Geophys. Research, v. 66, p. 2225–2239.

Jamieson, H., and Rae, W. L., 1965, The joint A.L.P.O.-B.A.A. dome project: British Astron. Assoc. Jour., v. 75, p. 310–314.

Katterfeld, G. N., 1967, Types, ages, and origins of lunar ring structures: Statistical and comparative geologic approach: Icarus, v. 6, p. 360–380.

Kopal, Zdĕnek, Klĕpsta, J., and Rackham, T. W., 1965, Photographic atlas of the Moon: New York, Academic Press, 277 p.

Kuiper, G. P., Strom, R. G., and LePoole, R. S., 1966, Interpretation of the Ranger records, Chapter III, *in* Ranger VIII and IX, Part II, Experimenters' analyses and interpretations: Natl. Aeronautics and Space Adm. Tech. Rept. No. 32–800, p. 35–248.

Lambiotte, J. J., and Taylor, G. R., 1968, A photometric technique for deriving slopes from Lunar Orbiter photography, *in* Enzmann, R. D., ed., Use of space systems for planetary geology and geophysics: Am. Assoc. of Space Sci. and Technology ser., v. 17, Proc. of Symposium, Boston, Mass., 1967, p. 205–224.

Leighton, R. B., 1966, The photographs from Mariner IV: Sci. American, v. 214, p. 54–68.

Leonardi, Piero, 1976, Volcanoes and impact craters on the Moon and Mars: Amsterdam, Elsevier, 432 p.

Leopold, L. B., and Langbein, W. B., 1963, Association and indeterminacy in geomorphology, *in* Albritton, C. C., Jr., ed., The fabric of geology: Reading, Mass., Addison-Wesley, p. 184–192.

Levin, B. I., and Ruskol, E. L, 1962, Review of current knowledge about the Moon: Problems in cosmogony, v. 8, p. 109–144 (in Russian); 1965, Natl. Aeronautics and Space Admin. Tech. Translation, F–119, p. 127–169.

Lindqvist, L., 1976, SELLO, a FORTRAN IV program for the transformation of skewed distributions to normality: Computers and Geosciences, v. 1, p. 129–145.

Lorenz, Volker, 1973, On the formation of maars: Bull. Volcanol., v. 37, p. 183–204.

Lozej, G. P., and Beales, F. W., 1975, The unmetamorphosed sedimentary fill of the Brent meteorite crater, southeastern Ontario: Canadian Jour. Earth Sci., v. 12, p. 606–628.

McCall, G. J. H., 1966, The concept of volcano-tectonic undation in selenology, *in* Ordway, F. I., ed., Advances in space science and technology (v. 8): New York, Academic Press, p. 1–64.

McCammon, R. B., 1969, Aspects of classification, *in* Models of geologic processes—An introduction to mathematical geology: Am. Geol. Inst. Rept., p. RM–C–1–42.

McCammon, R. B., and Wenninger, Guenther, 1970, The dendrograph: Lawrence, Kans., State Geol. Survey, Univ. Kansas, Computer Contr. 48, 28 p.

McCauley, J. F., 1965, The Marius Hills volcanic complex: Astrogeol. Studies Ann. Prog. Reht., July 1964–July 1965, pt. A, p. 115–122.

———1968, Geologic results from the lunar precursor probes: Am. Inst. Aeronautics and Astronautics Jour., v. 6, p. 1991–1996.

McCord, T. B., and Adams, J. B., 1973, Progress in remote optical analysis of lunar surface composition: The Moon, v. 7, p. 453–474.

MacDonald, T. L., 1929, The altitudes of lunar craters: British Astron. Assoc. Jour., v. 39, p. 314–324.

———1931, The distribution of lunar altitudes: British Astron. Assoc. Jour., v. 41, p. 172–183 and 228–239.

McGetchin, T. R., and Head, J. W., 1973, Lunar cinder cones: Science, v. 180, p. 68–71.

McGetchin, T. R., Settle, Mark, and Head, J. W., 1973, Radial thickness variation in impact crater ejecta: Implications for lunar basin deposits: Earth and Planetary Sci. Letters, v. 20, p. 226–236.

Mackin, J. H., 1969, Origin of lunar maria: Geol. Soc. America Bull, v. 80, p. 735–748.

Marcus, A. H., 1967, A stochastic model of the formation and survival of lunar craters; VI, Initial depth, distribution of depths, and the lunar history: Icarus, v. 6, p. 56–74.

Mason, B., and Melson, W. G., 1970, The lunar rocks: New York, Wiley Interscience, 179 p.

Masursky, Harold, 1964, A preliminary report on the role of isostatic rebound in the geologic development of the lunar crater Ptolemaeus: Astrogeol. Studies, Ann. Prog. Rept., July 1963-July 1964, pt. A, p. 102–134.

Masursky, Harold, Colton, G. W., and El-Baz, Farouk, 1978, Apollo over the Moon: A view from orbit: Natl. Aeronautics and Space Admin. Spec. Pub., SP–362, 255 p.

Mattingly, T. K., El-Baz, Farouk, and Laidley, R. A., 1972, Observations and impressions from lunar orbit, *in* Apollo 16 preliminary science report: Natl. Aeronautics and Space Admin. Spec. Pub. SP–315, p. 28–1—28–16.

Melosh, H. J., 1977, Crater modification by gravity: A mechanical

analysis of slumping, *in* D. J. Roddy, R. O. Pepin, and R. B. Merrill, eds., Impact and explosion cratering: New York, Pergamon, p. 1245–1260.

Millman, P. M. 1956, A profile study of the New Quebec crater: Dominion Observatory Ottawa Pubs., v. 18, p. 61–82.

Milton, D. J., Barlow, B. C., Brett, Robin, Brown, A. R., Glikson, A. Y., Manwaring, F. A., Moss, F. J., Sedmik, E. C. E., VanSon, J., and Young, G. A., 1972, Gosses Bluff impact structure, Australia: Science, v. 175, p. 1199–1207.

Milton, D. J., and Brett, Robin, 1968, Gosses Bluff astrobleme, Australia—The central uplift region [abs.]: Geol. Soc. America, 64th Ann. Mtg., Tucson, Ariz. p. 82.

Milton, D. J., and Roddy, D. J., 1972, Displacements within impact craters: Internat. Geol. Cong., 24th, Montreal, 1972, Sec. 15, p. 119–124.

Mironova, M. N., 1970a, Structural characteristics of some craters on the far side of the Moon, *in* Astronometry and Astrophysics, No. 1: Physics of the Moon and planets: Natl. Aeronautics and Space Adm., TT F–566, p. 33–45.

———1970b, Height profiles of twenty-nine craters on the far side of the Moon, *in* Astronometry and Astrophysics, No. 1: Physics of the Moon and planets: Natl. Aeronautics and Space Adm., TT F566, p. 46–57.

Moore, H. J., 1971, Geologic interpretation of lunar data: Earth Sci. Rev., v. 7, p. 5–33.

Moore, H. J., Boyce, J. M., Schaber, G. G., and Scott, D. H., 1980, Lunar remote sensing and measurements: U.S. Geol. Survey Prof. Paper 1046–B., 78 p.

Moore, H. J., Hodges, C. A., and Scott, D. H., 1974, Multiringed basins—Illustrated by Orientale and associated features: Lunar Science Conf., 5th, Proc., p. 71–100.

Moore, P. A., 1953, Lunar summit craters: British Astron. Assoc. Jour., v. 64, p. 34–36.

———1965, An evaluation of the reported lunar changes: New York Acad. Sci. Ann., v. 123, art. 2, p. 797–810.

Moore, P. A., and Cattermole, P., 1967, The craters of the Moon: London, Lutterworth Press, 160 p.

Morris, E. C., and Wilhelms, D. W., 1967, Geologic map of the Julius Caesar quadrangle of the Moon: U. S. Geol. Survey Misc. Geol. Inv. Map I–510, scale 1:1,000,000.

Muehlberger, W. R., and others, 1973, Preliminary geologic investigation of the Apollo 17 landing site, *in* Apollo 17 preliminary science report: Natl. Aeronautics and Space Admin. Spec. Pub. SP–330, p. 6–1 to 6–91.

Murray, J. B, and Guest, J. E., 1970, Circularities of craters and related structures on Earth and Moon: Modern Geology, v. 1, p. 149–159.

Mutch, T. A., 1970, Geology of the Moon—A stratigraphic view: Princeton, N.J., Princeton University Press, 324 p.

Oberbeck, V. R., Aoyagi, M., and Murray, J. B, 1972, Circularity of martian craters: Modern Geology, v. 3, p. 195–199.

Oberbeck, V. R., and Morrison, R. H., 1973, The lunar herringbone pattern, *in* Apollo 16 preliminary science report: Natl. Aeronautics and Space Admin. Spec. Pub. SP–330, p. 32–15—32–28.

———1976, Candidate areas for in situ ancient lunar materials: Lunar Sci. Conf., 7th, Proc., p. 2983–3005.

Oberbeck, V. R., and Quaide, W. L., 1967, Estimated thickness of a fragmental surface layer of Oceanus Procellarum: Jour. Geophys. Research, v. 72, p. 4697–4704.

Offield, T. W., and Pohn, H. A., 1970, Lunar crater morphology and relative-age determination of lunar geologic units—Part 2. Applications: U.S. Geol. Survey Prof. Paper 700–C, p. C163–C169.

———1977, Deformation at the Decaturville impact structure, Missouri, *in* D. J. Roddy, R. O. Pepin, R. B. Merrill, eds., Impact and explosion cratering: New York, Pergamon, p. 321–341.

Ollier, C. D., 1974, Phreatic eruptions and maars, *in* Gasparini, P., Civetta, L., Rapolla, A., and Luongo, G., eds., Physical volcanology: Amsterdam, Elsevier, p. 289–311.

Parks, J. M., 1966, Cluster analysis applied to mutivariate data: Jour. Geology, v. 74, p. 703–715.

———1969, Classification of mixed mode data by R-mode factor analysis and Q-mode cluster analysis on distance function, *in* Cole, A. J., ed., Numerical taxonomy: London, Academic Press, p. 216–223.

———1970, Fortran IV program for Q-mode cluster analysis on distance function wtith printed dendrogram: Lawrence, Kans., State Geol. Survey, Univ. Kansas, Computer Contr. 46, 32 p.

Peterfreund, A. R., 1976, Alphonsus dark-haloed craters: Examples of isolated dark mantle sources [abs.]: EOS, Trans. Am. Geophys. Union, v. 57, p. 275.

Peyve, A. V., ed., 1969, Problemy geologii Luny (in Russian): Moscow, Nauka, translated as "Problems of lunar geology," 1973, Natl. Aeronautics and Space Admin. TT F–689.

Philips, R. J., Conel, J. E., Johnson, T. V., Saunders, R. S., and Zisk, S. H., 1975, Lunar crater Bouguer gravity anomalies [abs.]: EOS, Am. Geophys. Union Trans., v. 56, p. 1012.

Pickering, W. H., 1906, Lunar and Hawaiian physical features compared: Am. Academy Arts and Sci. Mem., v. 13, p. 149–179.

Pike, R. J., 1967, Schroeter's Rule and the modification of lunar crater impact morphology: Jour. Geophys. Research, v. 72, p. 2099–2106.

———1968, Meteoritic origin and consequent endogenic modification of large lunar craters—A study in analytical geomorphology: Ann Arbor, Univ. Michigan, Ph.D. thesis, 404 p.

———1971a, Genetic implications of the shapes of martian and lunar craters: Icarus, v. 15, p. 384–395.

———1971b, Some preliminary interpretations of lunar mass-wasting processes from Apollo 10 photography, *in* Analysis of Apollo 10 photography and visual observations: Natl. Aeronautics and Space Admin. Spec. Pub. SP–232, p. 14–20.

———1972a, Crater morphometry, *in* Apollo 16 preliminary science report: Natl. Aeronautics and Space Admin. Spec. Pub. SP–315, p. 29–56 to 29–61.

———1972b, Geometric similitude of lunar and terrestrial craters: Internat. Geol. Cong., 24th, Montreal, 1972, Proc., Sec. 15, p. 41–47.

———1973a, Lunar crater morphometry, *in* Apollo 17 preliminary science report: Natl. Aeronautics and Space Admin. Spec. Pub. SP–330, p. 32–1 to 32–7.

———1973b, The lunar crater Linné: Sky and Telescope, v. 46, p. 364–366.

———1974a, Ejecta from large craters on the Moon: Comments on the geometric model of McGetchin et al: Earth and Planetary Sci. Letters, v. 23, p. 265–271.

———1974b, Depth/diameter relations of fresh lunar craters: Revision from spacecraft data: Geophys. Research Letters, v. 1, p. 291–294.

———1974c, Craters on Earth, Moon, and Mars: Multivariate classification and mode of origin: Earth and Planetary Sci. Letters, v. 22, p. 245–255.

———1975, Size-morphology relations of lunar craters: Discussion: Modern Geology, v. 5, p. 169–173.

———1976a, Geologic map of the Rima Hyginus region of the Moon: U.S. Geol. Survey Misc. Geol. Inv. Map I–945, scale 1:1,250,000.

———1976b, Ejecta thickness, rim uplift, energy type, and depth of energy release [abs.]: Papers presented to the symposium on planetary cratering mechanics, Flagstaff, Ariz., Sept. 13–17, 1976, Lunar Sci. Inst. Contr. 259, Houston, Texas, p. 105–107.

———1976c, Crater dimensions from Apollo data and supplemental sources: The Moon, v. 15, p. 463–477.

———1978a, Volcanoes on the inner planets: Some preliminary comparisons of gross topography: Lunar Sci. Conf., 9th, Proc., p. 3239–3273.

———1978b, A geomorphic threshold for impact craters on the terrestrial planets [abs.], *in* program and abstracts: Ninth Ann. Geomorphology Symposium, Binghamton, State Univ. New York, p. 20.

Pike, R. J., and Wilhelms, D. E., 1978, Secondary-impact craters on the Moon: Topographic form and geologic process [abs.], *in* Abstracts submitted to the Ninth Lunar and Planetary Science Conference: Houston, Tex., Lunar Sci. Inst., p. 907–909.

Pohn, H. A., and Offield, T. W., 1970, Lunar crater morphology and relative age determination of lunar geologic units—Part 1, Classification: U.S. Geol. Survey Prof. Paper 700–C, p. C153–C162.

Quaide, W. L., Gault, D. E., and Schmidt, R. A., 1965, Gravitative effects on lunar impact structures: New York Acad. Sci. Ann. v. 123, Art. 2, p. 563–572.

Quaide, W. L., and Oberbeck, V. R., 1968, Thickness determinations of the lunar surface layer from lunar impact craters: Jour. Geophys. Research, v. 73, p. 5247–5270.

Rae, W. L., 1966, Lunar domes: British Astron. Assoc. Jour., v. 76, p. 319–327.

Roberts, W. A., 1964, Secondary craters: Icarus, v. 3, p. 348–364.

Robinson, J. H., 1970, The Linné affair: British Astron. Assoc. Jour., v. 81, p. 34–36.

Roddy, D. J., 1968, The Flynn Creek crater, Tennessee, *in* French, B. M., and Short, N. M., eds., Shock metamorphism of natural materials: Baltimore, Mono Book Corp., p. 31–42.

———1976, High explosive cratering analogs for bowl-shaped, central uplift, and multiring impact craters: Lunar Sci. Conf., 7th, Proc. p. 3027–3056.

Roddy, D. J., Jones, G. H. S., and Diehl, C. H. H., 1969, Similarities of 100-and 500-ton TNT explosion craters and proposed comet impact craters [abs.]: Trans. Am. Geophys. Union, v. 50, p. 220.

Ronca, L. B., and Salisbury, J. W., 1966, Lunar History as suggested by the circularity index of lunar craters: Icarus, v. 5, p. 130–138.

Ross, H. P., 1968, A simplified mathematical model for lunar crater erosion: Jour. Geophys. Research, v. 73, p. 1343–1354.

Sabaneyev, P. F., 1962, Some results deduced from simulations of lunar craters, *in* Kopal, Zděnek, and Mikhailov, Z. K., eds., The Moon, Symposium no. 14 of the International Astronomical Union: London, Academic Press, p. 419–431.

Schmidt, J. F. J., 1878, Die Charte der Gebirge des Mondes: Berlin, Dietrich Reimer, 303 p.

Schubert, G., Lingenfelter, R. E., and Terrile, R. J., 1977, Crater evolutionary tracks: Icarus, v. 32, p. 131–146.

Schultz, P. H., 1976a, Moon morphology: Austin, Univ. Texas Press, 626 p.

———1976b, Floor-fractured lunar craters: The Moon, v. 15, p. 241–273.

Schultz, P. H., Greeley, R., and Gault, D. E., 1976, Degradation of small mare surface features [abs.], *in* Abstracts submitted to the Seventh Lunar Science Conference: Houston, Tex., Lunar Sci. Inst., p. 782–784.

Scott, D. H., 1973, Mare Serenitatis cinder cones and terrestrial analogs, *in* Apollo 17 preliminary science report: Natl. Aeronautics and Space Admin. Spec. Pub. SP–330, p. 30–7 to 30–8.

Scott, D. H., and Eggleton, R. E., 1973, Geologic map of the Rümker quadrangle of the Moon: U.S. Geol. Survey Misc. Geol. Inv. Map I–805, scale 1: 1,000,000.

Scott, R. F., 1967, Viscous flow of craters: Icarus, v. 7, p. 139–148.

Shoemaker, E. M., 1959, Address to earth sciences session: Proceedings Lunar and Planetary Explor. Colloquium, v. 2, no. 1, p. 20–28.

———1960, Ballistics of the Copernican ray system: Proc. Lunar and Planetary Explor. Colloquium, v. 2, no. 2, p. 7–21.

———1962, Interpretation of lunar craters, *in* Kopal, Zděnek, ed., Physics and astronomy of the Moon: London, Academic Press, p. 283–359.

———1965, Preliminary analysis of the fine structure of the lunar surface: Natl. Aeronautics and Space Adm. Tech Rept. 32–700, p. 75–134.

Short, N. M., 1975, Planetary geology: Englewood Cliffs, N.J., Prentice-Hall, 361 p.

Siegal, B. S., 1973, Crater morphology: An indicator of origin?: Pennsylvania State Univ., Ph.D. thesis, 176 p.

Siegal, B. S., and Griffiths, J. C., 1974, Multivariate analyses of crater parameters and the classification of craters: The Moon, v. 9, p. 397–413.

Siegal, B. S., and Wickman, F. E., 1973, Geometric interpretation of the ratio of overall diameter to rim crest diameter for lunar and terrestrial craters: Jour. Geophys. Research, v. 78, p. 5593–6000.

Sjogren, W. L., Wollenhaupt, W. R., and Wimberly, R. N., 1973, S-band transponder experiment, *in* Apollo 17 preliminary science report: Natl. Aeronautics and Space Adm. Spec. Pub. SP–330, p. 14–1 — 14–4.

Smith, E. I., 1971, Determination of origin of small lunar and terrestrial craters by depth-diameter ratio: Jour. Geophys. Research, v. 76, p. 5683–5689.

———1973, Identification, distribution and significance of lunar volcanic domes: The Moon, v. 6, p. 3–31.

Smith, E. I., and Sanchez, A. G., 1973, Fresh lunar craters: Morphology as a function of diameter, a possible criterion for crater origin: Modern Geology, v. 4, p. 51–59.

Sokal, R. R., 1974, Classification: Purposes, principles, progress, prospects: Science, v. 183, p. 1115–1123.

Sokal, R. R., and Michener, C. D., 1958, A statistical method for evaluating systematic relationships: Kansas Univ. Sci. Bull., v. 38, p. 1409–1438.

Sokal, R. R., and Sneath, P. H. A., 1963, Principles of numerical taxonomy: San Francisco, W. H. Freeman, 359 p.

Sparks, R. S. J., and Walker, G. P. L., 1973, The ground surge deposit: A third type of pyroclastic rock: Nature, v. 241, p. 62–64.

Steinberg, G. S., 1968, Inapplicability of Baldwin's relation for determining the causes of formation of lunar craters: Jour. Geophys. Research, v. 73, p. 6125–6132.

Stuart-Alexander, D. E., and Howard, K. A., 1970 Lunar maria and circular basins—A review: Icarus, v. 12, p. 440–456.

Taylor, S. R., 1975, Lunar science: A post-Apollo view: New York, Pergamon, 372 p.

Ullrich, G. W., 1976, The mechanics of central peak formation in shock wave cratering events: U.S. Air Force Rept. AFWL–TR–75–88, Kirtland Air Force Base, N. Mex., 138 p.

Ullrich, G. W., Roddy, D. J., and Simmons, G., 1977, Numerical simulations of a 20-ton TNT detonation on the Earth's surface and implications concerning the mechanics of central uplift formation, *in* Roddy, D. J., Pepin, R. O., and Merrill, R. B., eds., Impact and explosion cratering: New York, Pergamon, p. 959–982.

U.S. Air Force Aeronautical Chart and Information Center, 1972, Lunar topographic map of Aristarchus, Orbiter V Site 48.

Warner, Brian, 1961, Accretion and erosion on the surface of the Moon: Planetary and Space Sci., v. 5, p. 321–325.

———1962, Some problems of lunar orogeny: British Astron. Assoc. Jour., v. 72, p. 280–285.

Waters, A. C., and Fisher, R. V., 1970, Maar volcanoes, *in* Gilmour, E. H., and Stradling, Dale, eds., Proceedings of the Second Columbia River Basalt Symposium: Cheney, Wash., East Washington State Coll. Press, p. 157–170.

Wegener, Alfred, 1921, Die Entstehung der Mondkrater: Samml. Vieweg, No. 55, Braunschweig, Vieweg & Sohn, 48 p.

———1975, The origin of lunar craters: The Moon, v. 14, p. 211–236 (translation by A. M. Celal Şengör of 1921 paper).

Wetherill, G. W., 1977, The nature of the present interplanetary crater-forming projectiles, *in* Roddy, D. J., Pepin, R. O., and Merrill, R. B., eds., Impact and explosion cratering: New York, Pergamon, p. 613–615.

Whitaker, E. A., 1972, An unusual mare feature, *in* Apollo 15 preliminary science report: Natl. Aeronautics and Space Adm. Spec. Pub. SP–289, p. 25–84 to 25–85.

Wilhelms, D. E., 1976, Secondary impact craters of lunar basins: Lunar Sci. Conf., 7th, Proc., p. 2883–2901.

Wilhelms, D. E., and McCauley, J. F., 1971, Geologic map of the near side of the Moon: U.S. Geol. Survey Misc. Geol. Inv. Map I–703, scale 1:5,000,000.

Wilshire, H. G., Offield, T. W., Howard, K. A., and Cummings, D., 1972, Geology of the Sierra Madera cryptoexplosion structure, Pecos County, Texas: U.S. Geol. Survey Prof. Paper 599–H, 42 p.

Wise, D. U., and Yates, M. T., 1970, Mascons as structural relief on a lunar 'Moho': Jour. Geophys. Research, v. 75, p. 261–268.

Wishart, David, 1969, Fortran II programs for 8 methods of cluster analysis (CLUSTAN I): Lawrence, Kans., State Geol. Survey, Univ. Kansas, Computer Contr. 38, 112 p.

Wood, C. A., 1972, The system of lunar craters, revised: The Moon, v. 3, p. 408–411.

———1973, Moon: Central peak heights and crater origins: Icarus, v. 20, p. 503–506.

Wright, F. E., Wright, F. M., and Wright, Helen, 1963, The lunar surface: Introduction, *in* Kuiper, G. P., and Middlehurst, B. M., eds., The Moon, meteorites, and comets: Univ. Chicago Press, p. 1–56.

Young, R. A., 1972, Lunar volcanism: Fracture patterns and rilles in marginal premare craters, *in* Apollo 16 preliminary science report: Natl. Aeronautics and Space Admin. Spec. Pub. SP–315, p. 29–89 to 29–90.

SUPPLEMENTAL INFORMATION

MEASURING CRATER DIMENSIONS

Previous work has established at least six quantities that adequately specify the overall surface geometry of a lunar crater (MacDonald, 1931; Ronca and Salisbury, 1966): (1) rim-crest diameter (or radius); (2) width of exterior rim flank; (3) diameter (radius) of flat inner floor, if present; (4) depth; (5) height of rim crest above surrounding terrain; and (6) degree of circularity of the rim crest (fig. 1). Average values of the first five quantities (only four if there is no flat floor) were calculated for the 504 lunar craters studied here and all but 17 of the 119 craters added later. Other variables can be derived from the first five: average slope of the rim flank, width and average slope of the wall between the rim crest and the crater bottom or flat floor, and the depth of the crater below the pre-crater datum. Volumes of a crater and its raised rim can be estimated with fair accuracy from average values of these variables, although contour planimetry always yields more reliable results. Two additional quantities that are useful in the analysis of lunar craters, the radius of the bright rays surrounding the crater (Baldwin, 1963, table 32) and the diameter of the continuous deposit of ejecta material (Moore and others, 1974), can be obtained from photointerpretation rather than from measurement of contours but were not gathered specifically for this report. The six quantities and combinations of them provide a comprehensive geometric signature by which lunar craters can be described, compared with each other, and then compared with craters on the Earth and elsewhere.

Similar techniques of mensuration were applied to craters of all sizes, although they became exceedingly time-consuming for the largest features. The procedure is given in detail here so that other workers can more easily supplement the present sample with uniform data of their own. First, the planimetric outline of the rim crest was carefully traced on an overlay (a step sometimes dispensed with for small sharp craters). The rim crest is defined as the marked break in slope where the (typically gentler) rim-flank or rim-summit topography—the latter is the "wreath" described by Gilbert (1893)—meets the (typically steeper) rim wall. Especially for larger complex craters (over 30 km across), the rim crest does not necessarily coincide with maximum elevations along the rim topography, which may occur on overlapping segments of concentric ridges located a short distance outward from the rim crest as defined here.

After the circumference of the rim crest was traced, it was fitted with circumscribed and inscribed circles of known diameter, using a set of transparent templates. The two circle diameters were averaged and multiplied by a factor appropriate to the map scale to yield the crater rim-crest diameter, D_r, in kilometers. The index of circularity, which is defined as the ratio of area of the inscribed circle to area of the circumscribed circle, is obtained by dividing the squared diameter of the smaller circle by the squared diameter of the larger. First used by the author on lunar craters in unpublished experiments in 1967, this method yields rapid and reasonably sensitive results, especially for very small craters that would be less amenable to the more elaborate techniques. More sophisticated measures of circularity were judged not to warrant the considerable effort required for their calculation (Murray and Guest, 1970; Oberbeck and others, 1972).

Average width of the rim flank, W_e, was obtained by subtracting rim-crest diameter from the diameter at the base of the rim flank and halving the result, or it was measured directly with a compass at intervals along the circumference. The latter technique is more practicable for larger craters. The base of the rim flank commonly can be located without difficulty in terrain of low relief at a topographic break in slope (Baldwin, 1963), which may in fact represent the outer limit of structurally upthrust bedrock beneath the ejecta blanket (Pike, 1968). The topographic inflection is difficult to locate accurately on LTO's for the larger craters without close scrutiny of the terrain, especially in the uplands, and in some few cases it was necessary to draw several (radial) topographic profiles. Although this break in slope defines a convenient outer limit to the main structure of an impact crater, it omits some of the crater's ejecta and thus should not be used in volumetric calculations (Pike, 1967) without provision for including ejecta beyond the rim flank of the crater.

If a flat floor was present within a crater, its diameter (D_f) was measured by fitting a circle to the topographic break at the foot of the inner wall slope. In cases where slump blocks from the walls above produced an irregular floor outline, then an average diameter was calculated from readings at several azimuths. In some craters within the 10–20-km diameter range, the inflection at the juncture of floor and inner wall is poorly defined, and the floor diameter must be estimated from changes in contour spacing near the bottom of the crater.

Average crater depths (R_i) were obtained in one of two ways. For craters with no flat floors, the spot height shown on the map at the crater bottom (unless that elevation did not represent the lowest within the crater) was subtracted from the average elevation of the rim crest, or for very small craters, from the spot height given for the rim crest. The number of elevation readings along the rim crest was increased considerably for large craters or for craters of any size where the rim crest appeared irregular. For craters with flat floors, the mean elevation of the floor was determined either from several spot elevations or by inspection of contours and then subtracted from the mean rim-crest elevation. Craters that evidently formed on sloping surfaces, such as Menelaus, posed a special problem because average elevations of the highly variable levels of rim crest and floor are misrepresentative. Wherever possible in such cases, the relief measurements were referenced to a level pre-crater datum. Where such adjusted values could not be obtained, the crater was omitted from further analysis to avoid contaminating the sample.

Average height of the crater rim above the surrounding terrain (R_e) was calculated by subtracting the mean elevation at the foot of the rim flank from the rim-crest elevation. The former figure is obtained easily once the width of the rim flank has been determined. Many elevation readings are essential if the crater is large or situated in irregular topography. In calculating rim height for many overlapping craters in the uplands, it is necessary to distinguish floors of large adjacent craters from the actual pre-crater datum, as the two figures may differ considerably in elevation. In such cases, indiscriminately measuring elevations at the foot of the rim flank all around a large crater can lead to gross overestimates of its rim height. Also, the rim flanks of some large craters appear to have little or no relief at all along parts of their circumferences, because the crater formed on a highly irregular surface. Upland craters in which the rim height could not be determined accurately or objectively were omitted from the sample.

TABULATION OF THE NEW DATA

Descriptive data on the 504 lunar craters and the 59 terrestrial impact and experimental craters that have been included for comparison are listed in tables 9 and 10, respectively. Data on 119 lunar craters that were measured after the work had been completed also are given in table 9. Following the precedent of MacDonald (1931) and Baldwin (1963), craters in each of the various categories are tabulated in order of decreasing size (rim diameter). All in all, this arrangement is thought to be more convenient than an alphabetical array (Arthur, 1974) or a listing by position on the Moon (Arthur and others, 1963), although each has its advantages for specific purposes. Information on primary impact craters of the lunar main sequence is arranged in twelve columns; there are only six or seven columns for other types of craters.

The first column (Moon only) gives the crater's identification number, which is an exact function of geographic location, from the University of Arizona catalog prepared under the direction of Arthur (Arthur and others, 1963, 1964, 1965, and 1966). To date only the near-side lists, quadrants A–D, have been published, but the far-side listing is in an advanced state of preparation (E. A. Whitaker, personal communication). No numbers have been assigned the very smallest craters, however. Names are given, where possible, in the second column; (IS) denotes a smooth-rimmed crater and (IC) denotes a crater that probably has undergone considerable isostatic compensation. Diacritical marks are absent from the names because a computer-printout format was used. The third column lists sources of the measurements. Besides the 1:250,000-scale topographic orthophotomaps (designated LTO plus the sheet number, or only the sheet number for larger scale maps), these are primarily Earth-based shadow-length measurements from the LAC program (SHADOW DATA), topographic profiles compiled stereoscopically by the U.S. Geological Survey from Apollo pictures (USGS PHOTOGRM), and large-scale contour maps made from Apollo pictures (for example, USGSMAP 1/100). A "P" in the fourth column denotes presence of a well-defined central peak, and "R" a ridge. The numbers 1–4 in the fifth column denote the relative-age classification of the Arthur catalog (Arthur and others, 1963), 1 being youngest in appearance and 4 oldest; "F" denotes flooding of the crater by dark mare material. The sixth column gives the "background," or type of surface on which the crater formed, usually mare (M) or uplands (C), as indicated in the Arthur catalog.

The next five columns list, respectively, the crater rim diameter, depth, rim height, width of the rim flank, diameter of the flat floor (where present), and circularity of the rim-crest as defined above. Secondary impact craters, cratered cones, dark-halo craters, and cratered domes are distinguished from fresh and modified impact craters of the main sequence. Measurements generally are given to a precision that accords with accuracy of the raw data, but some figures for the smallest craters have been rounded off. Although the bulk of the data are from Apollo photographic sources, many of the better known near-side craters that were not included in the new photogrammetric coverage are listed here where the old shadow-length relief data are much better than average. Shadow data for the domes and cones are less reliable than for the normal craters.

Users of the data in table 9 are cautioned that grouping craters for analysis according to the classification of morphology by Arthur and others (1963) (or any similar type of classification, for that matter) does not necessarily guarantee uniform subsamples. Considerable variance in the different dimensions, especially depth and rim height, has been found in the course of analyzing this information, and it is clear that the original relative-age ranking on the basis of morphology will require some systematic updating. Misclassified craters tend to be more common in the lunar uplands (Pike, 1974b).

Measurements of terrestrial meteorite-impact and experimental-explosion craters were compiled from more than three dozen scattered sources (not all listed in the references), and some unevenness in the quality of the data is to be expected. Virtually all of the impact craters have been degraded to some extent. Wherever possible, depth values were determined from subsurface data in order to approximate the original topography. The depth given for Wolf Creek Crater is not that used in the analysis (pl. 1) but rather an older figure that included a considerable thickness of sedimentary fill (Fudali, 1979). Some caution is advised in comparing the dimensions of impact craters on either Earth or the Moon with those of the experimental-explosion craters. The scaled depths of burst for these test craters (see discussion by Baldwin, 1963) vary considerably, resulting in systematically different structures within the raised rim (Pike, 1974a, 1976b), and only the most shallow experiments may have produced suitable analogs for meteorite craters (Roddy, 1968, 1976).

Finally, mistakes invariably find their way into a numerical listing of the magnitude and detail undertaken here even when, as in this case, all measurements were made or compiled by one individual and photographed directly from a computer listing that has been carefully checked. Although every effort has been made to assure that the data are correct, some errors almost certainly remain and are the sole responsibility of the author. Doubtful entries or outright mistakes that are found by users of this listing should be called to the author's attention so that corrected figures can be promptly published. Since the initial release of these data (Pike, 1976c), entries for the following 21 craters in table 9 have been revised: Gagarin, Tsiolkovskiy, Neper, Sklodowska, Abul Wafa, Brunner, Schubert B, Ctesibius, Proclus, Pytheas, Vitruvius A, Dawes, Richards, Macrobius B, Jansen B, Langrenus N, D'Arrest, Lebesgue, Le Monnier B, one unnamed lunar crater, and Wolf Creek Crater. Additionally, entries for 12 named primary craters have been inserted in table 9—Aitken, Chaplygin, La Pérouse, Langrenus A, Kapteyn E, Euler, Langrenus M, La Pérouse D, Pytheas A, Jansen K, Picard Y, and Cauchy CA; there are nine unnamed craters as well. Data for the Siberian crater El 'Gygtgyn have been added to table 10. Five lunar craters that I listed as primary (Pike, 1976c) have since been identified as large secondaries: Zöllner, Schröter, D'Arrest, Secchi, and Capella M. Finally, table 9 includes data for the 118 additional secondary craters that I analyzed after this work had been completed (Pike and Wilhelms, 1978).

TABLE 9.—*Dimensions of 623 lunar craters*
[See text for table explanation]

I.D.	CRATER		DATA	P	CL	BGD	DIAM.	DEPTH	HT.	WIDTH	FLOOR	CIRC
			PRIMARY IMPACT CRATERS									
	M. SERENITATIS		LASER PROFILE			C	680.	2.5	1.2	120.	600.	.80
	M. CRISIUM		LASER PROFILE			C	480.	3.75	1.2	150.	400.	.83
	M. SMYTHII		LASER PROFILE			C	450.	3.5	1.5	120.	400.	.80
	MENDELEEV		LASER PROFILE	P	3	C	370.	6.5	2.7	75.	260.	.75
	GAGARIN		LTO102B3	P		C	275.	5.3	2.1	43.	200.	.79
C1835	CLAVIUS		SHADOW DATA	P	3	C	235.	4.90	1.6	40.0	190.0	.76
	TSIOLKOVSKIY		LTO101B2.3	P	1	C	197.	5.0	1.9	40.	145.	.67
	HILBERT		USGS PHOTOGRM	P	2	C	178.	4.1	1.5	35.	125.	.80
	CURIE		USGS PHOTOGRM	P	3	C	158.	3.85	1.5	29.	100.	.73
D0089	HIPPARCHUS		SHADOW DATA	P	4	C	150.	1.10	.99	15.	139.0	.78
A9185	NEPER		LTO63B3,4C1,2	P	2	PMC	148.5	3.97	1.15	27.0	91.0	.76
D8248	VENDELINUS		SHADOW DATA		3F	AMC	147.	2.2	1.5	12.	132.	.77
	AITKEN		LTO86D4/104A1	P		C	137.1	4.90	1.90	30.0	85.7	.77
D8165	LANGRENUS		LTO80C1	P	2	PMC	136.	4.50	1.50	35.	80.	.76
D0179	ALBATEGNIUS		SHADOW DATA	P	3	C	135.	3.2	.98	28.	93.	.87
	SKLODOWSKA		LTO100A1-2	P		C	128.	4.28	1.40	23.0	77.0	.76
	CHAPLYGIN		LTO84B3/LOC-4	P		C	127.9	5.10	1.75	26.0	85.3	.74
C3798	SCHILLER		SHADOW DATA	P	3	C	125.	2.5	1.5	15.	94.	.18
C6310	GASSENDI	(IC)	ORBITER 5 MAP	P	3F	AMC	110.	1.42	1.04	5.	103.	.84
	LANGEMAK		LTO83D2/C1	P		C	106.	4.50	1.5	23.	60.	.72
	BABCOCK		LTO64D1			C	102.5	2.3	1.1	13.	75.	.72
D4139	THEOPHILUS		LTO78C2	P	1	PMC	102.	4.10	1.3	25.	65.	.80
A4522	POSIDONIUS	(IC)	SHADOW DATA	P	3	AMC	101.	1.37	.82	10.	90.	.75
C2500	PITATUS	(IC)	SHADOW DATA	P	3F	AMC	100.	.68	.53	9.	87.	.76
B0798	PLATO		SHADOW DATA		2F	C	100.	2.0	1.6	19.	87.	.83
C2180	FRA MAURO		SHADOW DATA		4	AMC	95.	.83	.80	10.	90.	.76
B3136	COPERNICUS		SHADOW DATA	P	2	PM	93.	3.80	1.10	21.	54.	.82
A1796	ARISTOTELES		SHADOW DATA	P	2	PM	87.3	3.50	1.25	17.	52.	.76
C1648A	TYCHO		SHADOW DATA	P	1	C	85.	4.6	2.4	20.	46.	.84
C5766	WARGENTIN		SHADOW DATA		3F	C	85.	.3	.6	12.	82.	.85
D9158	LA PEROUSE		LTO81D2	P	2	C	81.	4.18	1.44	20.0	42.5	.85
B0469	ARCHIMEDES		SHADOW DATA		2F	AMC	80.	1.6	1.6	13.	66.	.86
	KING		LTO65C1	P	1	C	78.2	4.15	1.28	22.0	45.0	.80
	KIESS	(IC)	LTO81B4/3	P	4F	AMC	72.1	.80	.55	7.0	70.0	.75
D6540	REICHENBACH		SHADOW DATA	P	3	C	71.4	3.2	1.7	9.5	38.	.86
D6154	GUTENBERG		SHADOW DATA	P	3	AMC	71.	1.75	1.0	15.5	59.	.81
D0457	WERNER		SHADOW DATA	P	1	C	71.	4.2	.83	12.	40.	.86
	ERRO		LTO64D2			C	70.	1.98	1.03	10.0	48.0	.65
C0615	HUGGINS		SHADOW DATA	P	3	C	68.	1.85	.99	6.	50.	.86
C5487	DOPPELMEYER	(IC)	SHADOW DATA	P	4F	AMC	65.	1.1	.4	3.	58.	.80
A6376	MACROBIUS		USGS PHOTOGRM	P	2	C	64.5	4.05	1.2	8.2	32.5	.86
A3576	CAPUANUS		SHADOW DATA		3F	AMC	64.	1.6	1.5	9.	51.	.78
D0432A	BLANCHINUS		SHADOW DATA		3	C	62.	1.16	.66	5.5	52.0	.70
D6197A	GOCLENIUS		SHADOW DATA	P	3	AM	60.	2.2	.85	5.	37.	.41
A8182	FIRMICUS		LTO62C1		3F	C	59.8	2.14	.90	11.5	43.8	.80
	RITZ		USGS PHOTOGRM		3	C	59.	3.75	1.5	15.5	24.	.71
C2230	GUERICKE		SHADOW DATA		4	AM	59.	.74	.66	3.	55.	.76
C2194	BONPLAND		SHADOW DATA		4	AMC	59.	.73	.69	4.	52.	.75
A7029	TARUNTIUS	(IC)	LTO61C2	P	2F	PMC	58.5	1.10	.80	14.	42.	.79
B1295	ERATOSTHENES		SHADOW DATA	P	2	PM	58.3	3.43	1.35	19.	31.5	.83
A4552	HIPPALUS	(IC)	SHADOW DATA		4F	AMC	57.	.9	.9	2.	51.	.84
D1072	LADE		SHADOW DATA		4F	C	56.	.82	.57	4.	50.	.64
	ABUL WAFA		LTO65D3	P	2	C	55.9	3.7	1.05	12.5	22.0	.79
A0515	ARISTILLUS		SHADOW DATA	P	1	PM	55.3	3.30	1.00	14.	30.	.80
A1899	KANE		SHADOW DATA		3F	AMC	55.	.57	.74	4.	47.	.85
D2427	PONTANUS		SHADOW DATA	P	3	C	54.0	1.80	1.06	7.5	39.0	.76
A9084	SCHUBERT		LTO63C4	P	1	C	53.9	3.35	1.2	13.0	28.	.78
	SCHORR		USGS PHOTOGRM	P	2	C	53.5	3.7	.73	13.	26.	.77
	MAUNDER		ORBITER DATA		1	PMC	53.5	3.2	1.1	10.4	32.8	.81
D0014	REAMUR		SHADOW DATA		4F	AMC	53.	.82	.74	3.5	46.	.79
A8077	APOLLONIUS		LTO62C1	P	3F	C	52.6	2.75	.93	10.0	32.5	.79
D9023	MACLAURIN		LTO80B2	P	3	C	52.5	3.38	.85	8.0	25.	.77
	BRUNNER		LTO82D1	P		C	51.6	3.63	1.35	13.	26.	.85
A9037	DUBIAGO		LTO62C2		2F	AMC	50.6	2.7	.70	8.0	30.0	.72
	SO OF SAHA		USGS PHOTOGRM	P	2	C	50.5	3.64	1.38	13.2	24.0	.83
B0029	PALLAS		SHADOW DATA	P	3	C	50.	1.5	.77	5.2	35.	.71
D2260	DESCARTES		SHADOW DATA		4	C	49.	.85	.66	5.	43.	.79
	TOLSTOY		LTO82A4	P	2	C	48.	3.00	.90	9.0	23.	.81
C4416	CAMPANUS		SHADOW DATA		2F	PM	48.	2.	1.2	7.	28.	.73
D5163A	CAPELLA		LTO79A3/4	P	3	C	47.0	3.5	.9	8.	20.	.60
C3488	MERCATOR		SHADOW DATA		2F	AMC	47.	1.1	.7	6.	35.	.80
D9213	KAPTEYN C		USGS PHOTOGRM		3F	C	46.	.5	.35	6.8	39.	.75

TABLE 9.—Continued

I.D.	CRATER		DATA	P	CL	BGD	DIAM.	DEPTH	HT.	WIDTH	FLOOR	CIRC
A0080	RHAETICUS		SHADOW DATA	P	4	C	46.	1.2	.87	3.	32.	.72
C2163	PARRY		SHADOW DATA		3F	AMC	46.	.87	.86	4.	40.	.82
A1087	AGRIPPA		SHADOW DATA	P	2	C	46.	3.0	.80	5.5	27.	.80
D8120	LANGRENUS F	(IS)	LTO80A3		3	CM	45.12	1.75	.30	8.0	29.	.76
C5520	VITELLO	(IS)	SHADOW DATA		2	C	45.	1.7	.61	6.4	37.	.80
C2448	HESIODUS		SHADOW DATA		3F	AMC	45.	.45	.38	3.	34.	.67
D1057	SAUNDER		SHADOW DATA		4F	C	45.	.64	.55	2.5	40.	.80
A3657	PLANA		SHADOW DATA	P	3	AMC	45.	1.8	.73	3.	32.	.76
B3085	REINHOLD		SHADOW DATA	P	1	PM	44.7	2.70	.78	13.	27.	.83
	DELPORTE		LTO83C4	P	2	C	43.38	3.19	1.0	9.	18.	.77
	GANSKIY		LTO82D2	P		C	43.38	3.37	1.0	10.	19.	.77
D9108	LANGRENUS A		LTO80C2	P	2	C	43.25	2.91	1.11	10.5	18.5	.72
A5333	MARALDI		LTO43D4		3F	C	43.1	1.5	.55	4.5	31.	.67
	KOPFF	(IS)	ORBITER DATA		F	PMC	43.0	2.0	0.9	6.0	27.0	.80
A3286	PLINIUS		LTO60B1	P	1	PM	42.1	3.07	.95	13.	20.	.80
D5143	ISIDORUS		LTO79A4/D1		2	C	41.8	2.5	.9	8.	24.	.79
C0039	W. HERSCHEL		USGS AS12 PGM	P	1	C	41.6	3.33	.90	10.0	19.0	.89
B7250	MARIUS		SHADOW DATA		2F	AM	41.	1.5	.6	8.	33.	.88
	LITKE		LTO101B1	P	2F	C	40.5	2.70	1.0	8.	19.	.78
D	RUNGE		LTO81B2		F	C	40.25	.23	.13	6.0	36.0	.84
B6470	ARISTARCHUS		ORBITER 5 MAP	P	1	PMC	40.2	3.15	.80	15.	17.5	.84
	HALDANE	(IC)	LTO81B1	P	F	AMC	40.12	.325	.300	7.0	36.0	.83
C8078	DAMOISEAU	(IS)	SHADOW DATA	P	3	C	40.	1.25	.6	3.	33.	.73
C4040	LANSBERG		USGS PHOTOGRM	P	1	PM	40.0	2.75	.65	12.5	20.	.83
A5432	ROMER		SHADOW DATA	P	1	C	39.6	3.5	1.1	10.	20.	.70
A3730	BURG		SHADOW DATA	P	1	PM	39.6	3.07	.85	9.	20.	.80
	VIVIANI		LTO65D2			C	39.50	2.51	.45	5.0	10.5	.83
D9125	KAPTEYN E		LTO80C2	P	3	C	39.13	1.75	.52	8.0	22.0	.73
B8434	BRIGGS	(IC)	SHADOW DATA	P	2	PM	39.	1.2	.9	6.5	29.	.74
	BALZAC		LTO82D1	P	2	C	38.88	2.57	.80	9.5	22.	.78
D2133	DOLLOND B		SHADOW DATA		4F	C	37.	.88	.66	4.	31.	.78
D2089	TAYLOR		LTO78A3	P	3	C	36.25	3.1	.85	6.0	17.	.68
A1836	C. MAYER B		SHADOW DATA	P	3	C	36.	1.12	.87	4.	25.	.71
A9082	SCHUBERT B		LTO63C4	P	1	C	35.8	2.9	.75	8.0	18.	.82
	MILTON		LTO82A1		F	AM	35.38	.43	.30	3.5	31.	.74
A7255	YERKES	(IS)	LTO62A1	P	4F	AMC	35.25	.62	.62	4.0	31.5	.84
B7309	HERODOTUS	(IS)	SHADOW DATA		2F	AMC	35.	1.3	.94	4.5	28.	.83
D1104	HALLEY		SHADOW DATA	P	3F	C	35.	2.47	1.11	4.	22.	.80
A6396	TISSERAND		USGS PHOTOGRM		3	C	35.	2.93	1.05	6.	16.	.77
A1073	GODIN		SHADOW DATA	P	2	C	34.8	3.2	.73	5.	10.	.72
D	WARNER	(IC)	LTO81B2	P	F	C	34.75	.25	.20	5.0	31.5	.84
D9073	GILBERT M		LTO81A2	P	1	C	34.5	3.03	1.00	9.0	17.0	.79
	KATCHALSKY		LTO65D2	P		C	34.12	3.06	.88	8.0	13.0	.63
D2118	ANDEL		LTO78D1	P	3	C	34.0	1.35	.79	6.0	24.0	.74
	NECHO		LTO83B4		1	C	33.75	3.3	.50	11.0	15.0	.62
A7271	LICK	(IS)	LTO62A1	P	4F	AMC	33.7	.30	.30	3.0	29.	.72
D8048	LANGRENUS B	(IS)	LTO80A3		3	C	33.6	1.87	.47	5.	19.	.80
B2404	TIMOCHARIS		LTO40B3	P	1	PM	33.50	3.00	.85	8.0	15.	.84
	CTESIBIUS		LTO65D3	P		C	33.25	3.06	.83	7.0	14.0	.76
	IZSAK		USGS PHOTOGRM	P	2	C	33.2	3.4	1.03	7.7	13.0	.86
D9072	GILBERT N		LTO81A2		2	C	33.0	2.58	.60	5.0	15.0	.78
C6216	GASSENDI A		ORBITER 5 MAP	P	2	C	33.	2.9	.9	8.	20.	.81
D2122	DOLLOND C		SHADOW DATA		4F	C	32.	.62	.57	3.	28.	.66
B6104	KEPLER		SHADOW DATA	P	2	PMC	32.	2.7	.85	9.	19.	.86
A8187	AUZOUT		LTO62B4	P	2	C	31.75	3.85	.95	6.5	12.0	.75
D3148	KANT		LTO78C1	P	1	C	31.63	3.72	.8	9.	13.	.74
A3023	RITTER	(IS)	SHADOW DATA		2F	AM	31.	1.3	.57	3.	23.	.79
A3042	SABINE	(IS)	SHADOW DATA		2	AM	31.	1.4	.61	4.	24.	.83
D	DOYLE		LTO63C4/3		F	C	30.88	.42	.32	3.0	26.5	.86
D5047	ISIDORUS B		LTO79A4	P	3	C	30.63	1.6	.77	6.5	12.	.71
	FISCHER		LTO66C1			C	30.38	3.1	.65	9.0	11.5	.86
A4390	VITRUVIUS		LTO43D4	P	2F	AMC	30.10	1.88	.46	4.0	19.0	.74
D6217	BOHNENBERGER	(IS	SHADOW DATA	P	2	PMC	30.	2.4	.68	7.7	24.	.84
B3423	LAMBERT		LTO40A3	P	2	PM	29.9	2.60	.70	10.	14.	.86
D	CELLINI		LTO81B4/C1	R		C	29.63	2.99	1.14	8.0	12.0	.88
D8140	LANGRENUS K		LTO80A3	P	3	C	29.25	2.50	.63	8.0	19.	.81
A4614	GROVE	(IS)	SHADOW DATA	P	1	PM	29.	2.37	.61	4.7	17.	.80
A4527	DANIELL	(IS)	SHADOW DATA		1	PM	28.5	1.9	.8	2.	20.5	.64
A7207	PROCLUS		LTO43C3	P	1	C	28.5	4.04	1.19	9.0	13.0	.75
	MONTESQUIEU		LTO82A4		2	C	28.38	3.06	.71	6.5	9.	.74
	AUSTIN		LTO82D1		2	C	27.75	3.05	.70	7.0	12.5	.84
A2268	MENELAUS		LTO42D3	P	1	PM	27.40	2.6	.80	7.00	14.0	.82
D4189	MADLER		LTO78C2	P	1	PM	27.13	2.80	1.00	7.5	13.5	.76
D4078	TORRICELLI		LTO78B3		3	PM	27.0	2.5	.6	4.5	10.	.44
A3726	BAILY		SHADOW DATA		4F	AMC	27.	.52	.45	2.5	20.	.60

TABLE 9.—Continued

I.D.	CRATER	DATA	P	CL	BGD	DIAM.	DEPTH	HT.	WIDTH	FLOOR	CIRC
	N. OF KATCHALSKY	LTO65D2			C	26.88	2.71	.71	6.0	12.	.70
B4349	EULER	LTO40D1/LO-4	P	1	PM	26.63	2.24	.74	11.5	12.0	.84
C1001	MOSTING	SHADOW DATA	P	2	PMC	26.5	2.80	.55	4.3	10.	.78
A3160	ARAGO	SHADOW DATA	P	2	PM	26.0	2.68	.73	5.5	15.	.76
	NEAR GAGARIN	USGS PHOTOGRM		2	C	26.	2.6	.73	6.0	13.0	.86
B2061	GAMBART (IS)	SHADOW DATA		2F	AMC	25.6	1.1	.57	1.5	21.	.79
B4499	DELISLE	LTO39B2	P	2	PM	25.38	2.42	.72	7.5	9.5	.84
B3067A	REINHOLD B	SHADOW DATA		3F	AM	25.	.8	.51	3.	21.	.86
D	SWASEY	LTD81B3		F	C	25.0	.45	.20	2.5	22.5	.82
C4544	RAMSDEN	SHADOW DATA		2F	AM	24.	1.9	.7	3.	15.	.72
A5003	MASKELYNE	SHADOW DATA	P	2	PM	23.8	2.50	.80	4.	15.	.69
	W OF NEUJMIN	LTO101C1		3	C	23.5	2.65	.4	4.25	9.	.84
A7076	TARUNTIUS M	LTO61C1		3	AMC	23.50	.85	.50	5.5	19.	.84
A7285	PICARD	LTO62A1	P	1	PMC	23.00	2.32	.54	6.0	7.5	.88
C1236	LASSELL (IS)	SHADOW DATA		2F	AM	23.	.9	.5	4.3	17.	.80
A4263	JANSEN (IS)	LTO60B2		2F	AM	22.88	.34	.60	4.75	17.5	.82
B6428A	KRIEGER	LTO39A1		3F	AM	22.88	.95	.70	3.5	19.	.75
D8061	WEBB	LTO80A2/B1	P	2F	PMC	22.56	1.85	.60	4.0	14.0	.76
	BERGMAN	LTO66D2			C	22.3	2.7	.70	5.0	8.	.74
C6225	GASSENDI B	ORBITER 5 MAP	P	2	C	22.	1.36	.40	3.5	12.	.83
D7255	MCCLURE D (IS)	SHADOW DATA		3F	C	22.	1.1	.72	3.4	16.	.73
	UNNAMED	LTO83C3 ODD				21.88	2.77	.32	4.50	7.0	.51
D7253	CROZIER (IS)	SHADOW DATA		2F	MC	21.5	1.3	.94	2.	16.	.74
	MOISSAN	LTO66D2			C	21.3	2.9	.60	4.8	4.	.71
D7254	MCCLURE M (IS)	SHADOW DATA		4F	C	21.	.74	.52	1.5	16.	.67
A0336	CONON	LTO41C1		1	C	20.75	2.93	.90	5.3	5.0	.82
	IN GAGARIN (OLD)	LTO102B3			C	20.66	2.0	.35	4.3	8.5	.81
C6097	FLAMSTEED	SHADOW DATA	P	2	PM	20.6	2.16	.66	3.5	12.5	.80
D3029	ALFRAGANUS	LTO78A3		1	C	20.38	3.8	.78	5.5	6.5	.88
A9176	NEPER G	LTO63B4		2	PMC	20.0	1.5	.60	7.0	10.5	.74
A6313	MACROBIUS A	LTO43C4		1	PM	19.88	3.80	.90	6.00	6.	.88
D9176	KASTNER F	LTO81C1		1	C	19.6	3.17	.57	4.5	6.5	.88
B3325	PYTHEAS	LTO40D2/LO4	P	1	PM	19.56	2.54	.765	7.0	(5.0)	.76
C4082	LANSBERG C	SHADOW DATA		2F	M	19.	.78	.57	2.	14.5	.82
A7361	PEIRCE	LTO44D4	P	2	PM	18.5	2.16	.64	8.	10.	.81
D9106	LANGRENUS M	LTO80C2		1	C	18.25	3.685	.785	5.	5.5	.90
B4496	DIOPHANTUS	LTO39B3	P	1	PM	18.13	3.02	.82	6.0	7.	.87
B6370	ARISTARCHUS F	ORBITER 5 MAP		3F	AM	17.9	.29	.29	2.5	15.3	.84
A5330	VITRUVIUS A	LTO43D4	R	1	C	17.88	2.93	.66	5.50	4.0	.87
	DARIO	LTO82D1		1	C	17.88	3.33	.55	3.5	4.	.92
A2195	SOSIGENES (IS)	SHADOW DATA		1F	AMC	17.8	1.5	.4	2.5	11.	.88
D9074	GILBERT D	LTO81A2		1	C	17.75	2.97	.60	4.0	0.	.80
	ON NW RIM ERRO	LTO64D2			C	17.75	2.17	.42	4.5	5.6	.84
D	ELMER	LTO81C1			C	17.5	2.35	.8	4.5	7.	.80
A4229	DAWES	42C3S4(50)	P	1	PM	17.40	2.31	.585	6.5	(8.0)	.80
	RICHARDS	LTO66C1			C	17.25	3.94	.64	4.0	3.5	.84
	UNNAMED	LTO82A4			C	17.13	2.45	.35	4.0	4.5	.82
	IN HILBERT	USGS PHOTOGRM		2	C	17.0	1.8	.40	3.0	5.0	.79
C1338	BIRT	SHADOW DATA		1	PM	17.	3.47	.66	3.	4.	.80
A6326	MACROBIUS L	LTO43C1		3F	AMC	17.0	.59	.31	2.3	14.	.61
A9054	DUBIAGO S	LTO63D4		1	C	16.5	2.91	.61	4.8	5.	.83
A7232	GLAISHER	LTO61B2		1	C	16.37	3.29	.65	2.8	4.5	.81
	SE OF DANJON	LTO83C4			C	16.25	2.51	.54	3.5	6.	.83
	W RIM FLANK ERRO	LTO64D2			C	16.19	2.33	.40	4.0	4.0	.84
41025	E. PICKERING	SHADOW DATA		1	C	16.	2.74	.70	4.	6.	.88
A6315	MACROBIUS B	LTO43C1		1	PM	15.9	3.83	.60	5.	3.	.90
A4148	JANSEN B	LTO60B3		2	PM	15.88	2.19	.510	4.5	0.	.75
	IN SAHA	USGS PHOTOGRM		3	C	15.7	.88	.28	3.6	9.0	.80
	IN GAGARIN (OLD)	LTO102B3			C	15.63	1.45	.30	3.0	6.0	.85
A2387	BESSEL	LTO42D2		1	PM	15.50	1.77	.61	5.75	3.5	.88
	NO. OF ABUL WAFA	LTO65D3			C	15.37	2.73	.35	3.5	2.5	.80
D5057	ISIDORUS D	LTO79A4		1	C	15.25	3.22	.60	5.0	0.	.88
	HARDEN	LTO66C1			C	15.13	2.75	.55	4.0	4.0	.91
	KOSBERG	LTO102B3			C	15.06	1.25	.60	3.5	9.0	.86
	UNNAMED	LTO100A2			C	15.05	2.635	.535	4.2	5.0	.86
B4029	HORTENSIUS E	SHADOW DATA		3F	AM	15.	.20	.20	1.2	12.5	.86
B4161	HORTENSIUS	SHADOW DATA		1	PM	14.7	2.86	.43	2.6	8.	.85
A6253	PROCLUS A	LTO61B1		1	C	14.63	3.01	.42	4.0	3.9	.84
	BAUDELAIRE	LTO101B4	P	2	C	14.63	2.69	.4	3.5	4.0	.90
B5365	BRAYLEY	LTO39C1/LO4		1	PM	14.47	2.84	.48	3.25	0.	.88
	LI PO	LTO82A1		1	PM	14.38	3.59	.74	4.3	5.	.84
	BENEDICT	LTO66C1			C	13.99	3.14	.60	3.5	2.7	.88
D7099	MESSIER G	LTO80A4		1	PM	13.81	1.89	.31	3.2	0.	.79
A7272	LICK D	LTO62A1		1	PMC	13.88	2.41	.56	4.06	5.0	.80
D1198	ANDEL A	LTO78D1	P	2	C	13.75	.80	.30	1.8	9.5	.69

TABLE 9.—Continued

I.D.	CRATER	DATA	P	CL	BGD	DIAM.	DEPTH	HT.	WIDTH	FLOOR	CIRC
A8189	ISIDORUS E	LT079A4		1	C	13.75	3.05	.50	2.5	2.0	.75
A0016	CHLADNI	SHADOW DATA		1	PM	13.6	2.63	.38	2.7	5.	.92
C2176	PARRY A	LT076C1		2F	PM	13.5	.98	.45	2.75	7.60	.89
A9381	MACROBIUS D	LT043C3		2	C	13.5	2.56	.54	4.0	3.0	.86
D9105	LANGRENUS N	LT080C2	P	2	C	13.38	1.65	.23	3.1	2.5	.71
D7026	MESSIER A	LT079B2		1	PM	13.25	2.24	.53	2.50	3.5	.43
	NO. OF FOX	LT064D3			C	13.19	3.01	.38	3.45	1.5	.91
D8069	LANGRENUS C	LT080B4		1	C	13.13	2.90	.71	4.0	4.	.83
	UNNAMED	LT084B3			C	13.13	2.3	.40	2.7	3.0	.83
C0095	MOSTING A	SHADOW DATA		1	C	13.05	2.70	.43	3.	0.	.90
C1161	LALANDE A	USGS PHOTOGRM		1	C	13.	2.7	.6	3.6	2.	.88
A	PEEK	LT063C3		1	PM	13.0	2.34	.52	3.5	3.75	.86
D6005	CENSORINUS F	LT079A2		1	C	12.85	1.80	.48	3.5	3.5	.90
A6116	CAUCHY	LT061A3		1	PM	12.80	2.67	.51	3.0	0.	.88
A7152	TARUNTIUS A	LT061C2		1	PMC	12.75	2.55	.40	4.0	2.0	.85
D	TALBOT	LT081B2		F	C	12.6	.30	.20	1.6	9.4	.86
	E OF PURKYNE	LT082A2			C	12.5	2.59	.29	3.5	3.2	.85
	NW OF TSIOLKOVSK	LT0101B2		1	C	12.5	2.27	.3	2.75	0.	.79
A3234	TACQUET A	LT060B1		1F	AMC	12.4	1.04	.36	2.6	7.0	.92
A6229	PROCLUS D	LT043C4		1	PMC	12.0	2.40	.26	2.3	2.2	.85
D	SLOCUM	LT081B2		F	C	12.3	.48	.18	1.6	9.0	.84
D	LEBESGUE	LT081B3		F	C	12.25	.35	.25	1.6	9.5	.85
D5340	ROSSE	SHADOW DATA		1	PM	12.1	2.42	.34	2.	0.	.92
D4097	TORRICELLI A	LT078B3		1	PM	11.94	2.16	.54	3.2	0.	.86
A1393	SULPICIUS GALLUS	LT042D4		1	PM	11.88	2.17	.32	3.80	0.	.81
A5338	ROMER K	LT043D3		1	PM	11.75	2.60	.30	3.62	2.0	.84
D7033	MESSIER	LT079B2		1	PM	11.63	1.90	.40	2.0	0.	.36
A6049	TARUNTIUS E	LT061C1		1	PM	11.50	2.20	.40	3.0	1.75	.84
D2148	DOLLOND	LT078D1		1	C	11.0	2.04	.30	2.5	2.0	.83
A7110	TARUNTIUS C	LT061C2		1	PMC	10.88	2.19	.35	3.0	2.5	.87
A8019	APOLLONIUS K	LT062D1		1	C	10.78	2.07	.35	2.5	2.0	.90
A7053	TARUNTIUS G	LT061C3		1	PM	10.75	2.22	.38	2.4	1.5	.91
A4361	VITRUVIUS E	LT042C3		1	PMC	10.75	2.15	.45	2.5	3.0	.91
	GILBERT U	LT081B1			PM	10.75	2.08	.38	3.75	2.5	.91
D8063	WEBB H	LT080A2		1F	PM	10.75	2.02	.08	.88	0.	.87
C1290	GUERICKE C	LT076C2		1	PM	10.56	2.41	.38	3.2	0.	.85
A6046	TARUNTIUS F	LT061C4		1	PM	10.56	2.2	.40	3.1	0.	.85
	ZASYADKO	LT064D4			PM	10.54	2.4	.4	3.6	0.	.78
D3100	ALFRAGANUS C	LT078A3		1	C	10.44	2.30	.32	2.2	2.2	.85
A7353	PEIRCE B	LT044D4		1	PM	10.4	2.04	.46	4.3	2.5	.87
C4290	EUCLIDES B	LT075C2		1	PM	10.28	2.15	.45	3.10	0.	.90
A0470	ARATUS	LT041C1		1	C	10.19	1.88	.35	2.3	3.3	.88
	UNNAMED	LT0100A1			C	10.13	1.985	.285	2.935	2.8	.86
A5329	ROMER L	LT043D1		1	C	10.04	2.34	.40	2.5	0.	.85
	UNNAMED	LT082D1		1	C	10.	1.81	.31	2.5	3.	.82
A8171	FIRMICUS F	LT062C1		1	C	10.0	1.93	.20	2.0	1.6	.89
	IN PASTEUR	USGS PHOTOGRM		3	C	9.9	1.1	.11	1.75	2.75	.79
B6520	WOLLASTON	LT039A1		1	PM	9.75	2.22	.38	2.7	0.	.90
A5479	ANGSTROM	LT039A2		1	PM	9.75	2.00	.40	2.3	0.	.90
	UNNAMED	LT082A1		F	AM	9.75	.30	.20	2.0	7.8	.90
A8035	APOLLONIUS C	LT062D3		1	C	9.69	1.87	.34	2.4	0.	.88
	UNNAMED	LT064D1			C	9.69	1.97	.25	2.95	1.6	.79
B1445A	FEUILLET	LT041A4		1	PM	9.56	1.89	.18	2.0	1.5	.88
	UNNAMED	LT082A4			C	9.5	1.1	.23	1.75	4.	.81
B6428	KRIEGER B	39A1S01(50)		1	PM	9.48	1.61	.40	3.0	0.	.84
B1445	BEER	LT041A4		1	PM	9.44	1.67	.28	2.5	2.5	.83
A6137	CAUCHY D	LT061B4		1	PM	9.42	1.90	.20	2.0	1.4	.83
D1194	ANDEL F	LT078D1		1	C	9.0	1.8	.45	2.5	1.7	.82
A6201	CAUCHY A	LT061A2		2F	PM	9.00	.40	.05	1.0	6.0	.95
A0476	HADLEY B	LT041B4		1	C	9.0	2.0	.20	1.88	0.	.76
A5201	JANSEN F	LT061A1		1	PM	8.94	1.81	.35	1.88	1.0	.87
	UNNAMED	LT064D1			C	8.94	1.76	.18	1.8	0.	.78
	UNNAMED	LT066D2			C	8.80	1.75	.42	1.50	1.0	.84
A7060	TARUNTIUS H	LT061C3		1	PM	8.75	1.90	.30	1.9	2.0	.89
A5368	ROMER J	LT043D2		1	PMC	8.75	1.83	.25	3.0	0.	.80
A3281	ROSS D	LT060B1		1	PM	8.75	1.8	.24	2.13	0.	.88
	UNNAMED	LT066C1			C	8.63	1.63	.30	1.95	0.	.84
A4267	JANSEN C	LT042C3		1	PM	8.62	1.07	.20	2.5	3.5	.84
C0114	PTOLEMAEUS A	LT077D?		1	C	8.5	1.82	.22	3.0	1.8	.89
B5396A	BRAYLEY C	LT039C1/LO4		1	PM	8.50	1.66	.35	2.75	0.	.89
D2114	DOLLOND D	LT078D1		1	C	8.5	1.56	.20	2.2	1.0	.79
A7168	LICK E	LT062A4		1	C	8.3	1.73	.15	1.75	0.	.81
A0279	MANILIUS F	LT041C4		2F	PMC	8.25	.60	.18	1.13	5.0	.89
A6300	MARALDI M	LT043D3		1	PM	8.25	1.69	.28	3.4	0.	.80
B5426	DIOPHANTUS A	LT039B4		1	PM	8.18	2.01	.30	1.56	0.	.86

TABLE 9.—Continued

I.D.	CRATER	DATA	P	CL	BGD	DIAM.	DEPTH	HT.	WIDTH	FLOOR	CIRC
D9020A	NO. MACLAURIN	LTO80B2		1	PMC	8.0	2.32	.40	1.5	0.9	.83
D7026	MESSIER D	LTO79B2		1	PM	8.00	1.46	.35	1.3	1.0	.88
A8004	TARUNTIUS N	LTO62D4		1	PM	7.88	.95	.15	1.6	0.	.83
	UNNAMED	LTO66D2			C	7.84	1.84	.24	1.83	0.	.81
A5354	MARALDI A	LTO43D2/D3		2	PM	7.81	.50	.19	1.85	4.	.85
D	TUCKER	LTO81B3		1	PM	7.75	1.6	.23	1.6	1.5	.86
A3203	AUWERS A	LTO60A2		1	C	7.63	1.64	.20	1.59	0.	.82
	SW OF HOUTERMANS	LTO81C2			C	7.63	1.4	.10	1.2	0.	.82
A4285	JANSEN L	LTO61A1		1	PM	7.57	1.49	.20	1.9	0.	.90
A4257	JANSEN D	LTO60B2		1	PM	7.56	1.34	.27	2.0	0.	.85
A4254	JANSEN E	LTO60B2		1	PM	7.50	1.50	.25	1.75	0.	.88
A6380	PROCLUS W	LTO43C3		1	C	7.50	1.57	.20	1.25	0.	.88
A3421	BESSEL A	LTO42B4		1	PM	7.5	1.73	.35	2.4	0.	.88
A7025	TARUNTIUS B	LTO61C3		1	PM	7.38	1.5	.22	1.5	1.2	.82
A6279	PROCLUS Y	LTO43C4		2	C	7.38	1.00	.09	1.0	0.	.54
B4468	DIOPHANTUS B	LTO39B2		1	PM	7.38	1.10	.19	1.0	0.	.82
A7080	TARUNTIUS P	LTO62D4		1	PM	7.38	1.46	.25	1.80	0.	.82
D	UNNAMED	LTO81D2			C	7.35	1.62	.395	3.075	1.4	.80
D8141	LANGRENUS KA	LTO80A3		2	PM	7.12	1.37	.15	1.6	1.6	.70
B3500	CARLINI B	LTO40A2		1	PM	7.12	1.60	.30	1.5	1.5	.81
B2441	TIMOCHARIS A	LTO40B4		1	PM	7.1	1.46	.23	2.54	1.6	.87
D8101	LANGRENUS FF	LTO80A4		1	PM	7.0	1.14	.25	1.25	0.	.87
A5284	MARALDI B	LTO61A2		1	PM	7.00	1.54	.25	1.8	.75	.87
A8013	TARUNTIUS O	LTO62D4		1F	PM	7.0	1.35	.08	.8	0.	.86
A3218	TACQUET	LTO42D3		1	PM	7.00	1.10	.10	1.0	0.	.75
D8044	WEBB D	LTO80A2		1	PM	7.0	1.33	.18	1.2	0.	.91
D7041	MESSIER B	LTO79B2		1	PM	7.06	1.37	.15	1.25	1.7	.90
A0480	ARATUS B	LTO41B3		2	C	7.00	.93	.10	1.75	0.	.84
D	UNNAMED	LTO81B3			C	7.0	1.40	.23	1.0	0.	.80
B6456	ARISTARCHUS C	LTO39A4.1		1	PM	7.0	1.30	.20	1.25	0.	.77
D9158	LA PEROUSE D	LTO81D2		2	C	6.85	1.615	.265	1.95	0.	.85
	UNNAMED	LTO102D1		2	C	6.81	1.35	.3	1.85	0.	.83
D4001	MOLTKE	USGS PHOTOGRM		1	PM	6.8	1.30	.30	2.0	0.	.85
A4366	LITTROW B	LTO42C2		1	PM	6.75	1.44	.25	2.10	0.	.86
A8252A	PICARD X	LTO62B1		1	PM	6.62	1.5	.23	1.7	0.	.86
C3176	BONPLAND E	LTO76D2		1	PM	6.59	1.55	.17	1.7	0.	.80
A2229	MENELAUS A	LTO42D4		1	PMC	6.50	1.11	.21	1.50	1.75	.86
D7010	SECCHI K	LTO79B2		1	PM	6.5	1.33	.13	.75	0.	.86
A3326	DESEILLIGNY	LTO42C1		1	PM	6.38	1.25	.23	1.81	0.	.91
A2353	BESSEL E	LTO42D3		1	PM	6.25	1.26	.11	1.0	0.	.85
B3344	PYTHEAS A	LTO40D2		1	PM	6.20	2.54	.280	1.65	0.	.73
A4189	JANSEN K	LTO60B3		1	PM	6.19	1.425	.345	1.91	0.	.82
A	PICARD Y	LTO62B1			PM	6.19	.90	.145	.56	0.	.82
C4126	EUCLIDES D	LTO76D1		1	PM	6.13	1.26	.13	1.19	0.	.92
	UNNAMED	LTO64D1			C	6.12	1.25	.15	1.4	0.	.78
	N. OF KATCHALSKY	LTO65D2			C	6.1	1.28	.21	1.2	0.	.85
A6370	PROCLUS X	LTO43C3		1	C	6.0	1.24	.11	1.2	0.	.85
A7081	TARUNTIUS K	LTOL2D4		1	PM	6.0	1.0	.25	1.6	0.	.85
	IN HILBERT	USGS PHOTOGRM		2	C	6.0	.95	.15	1.0	0.	.79
A6078	TARUNTIUS EA	LTO61C1		1	PM	5.90	.83	.10	1.1	0.	.86
A0472	HADLEY C	41B4S02(50)		1	PM	5.80	1.16	.14	1.70	1.3	.84
A1303	SULPIC. GALLUS G	LTO41C3		1	PM	5.81	1.22	.20	1.15	0.	.88
B5561	ANGSTROM A	LTO39A2		1	PM	5.75	1.46	.13	1.38	0.	.88
	REGIOMONTANUS A	SHADOW DATA				5.65	1.2	.68	5.80	.0	.74
D2167	DOLLOND E	LTO78D2		1	C	5.56	1.11	.2	1.62	1.5	.87
A1402	HADLEY A	LTO41B3		1	C	5.5	1.20	.15	1.3	0.	.82
A6182	TARUNTIUS MA	LTO61C1		2	PM	5.50	.90	.15	1.0	0.	.85
A6066	SECCHI B	LTO61C4		1	PM	5.5	1.15	.15	1.25	0.	.83
D0167A	ALBATEGNIUS C	LTO77C1		1	C	5.5	1.35	.2	2.1	0.	.88
A3405	BESSEL D	LTO42A3		1	PM	5.44	1.07	.13	1.25	0.	.79
A2454	LINNE E	LTO42A3		1	PM	5.44	1.13	.25	1.50	0.	.87
A5254	VITRUVIUS G	LTO61A1		1	PM	5.31	1.01	.13	.85	0.	.87
B1486	TIMOCHARIS B	LTO40B3		1	PM	5.25	1.16	.18	1.4	0.	.83
	FLOOR TSIOLKOVSK	LTO101B2		2	PMC	5.25	.88	.20	1.25	1.5	.74
A3483	LE MONNIER B	LTO42B3		1	PM	5.19	.93	.20	1.15	1.5	.79
A6065	SECCHI A	LTO61C4		1	PM	5.10	1.02	.15	1.2	0.	.85
B3447	LA HIRE A	LTO40A2		2	PM	5.06	1.21	.20	.90	0.	.78
A7167	LICK G	LTO62A4		2	C	5.02	1.1	.10	1.2	0.	.82
B5405	DIOPHANTUS C	LTO39B3		1	PM	5.0	1.14	.22	1.25	0.	.86
D7015	MESSIER E	LTO79B2		1	PM	4.94	.85	.20	1.03	0.	.86
A	UNNAMED	LTO63B3		1	PM	4.9	1.04	.125	1.8	0.	.83
A4318	LE MONNIER C	LTO42C2		1	PM	4.88	1.09	.20	1.56	0.	.81
A6059	TARUNTIUS EB	LTO61C1		1	PM	4.81	.65	.08	1.0	0.	.77
B4395	EULER K	39C2 S1(50)		1	PM	4.72	.73	.15	1.55	0.	.90
B6418	KRIEGER D	39AISI(50)		1	PM	4.63	.92	.18	1.60	0.	.90

TABLE 9.—Continued

I.D.	CRATER	DATA	P	CL	BGD	DIAM.	DEPTH	HT.	WIDTH	FLOOR	CIRC
A7060A	SE OF TARUNT. H	LT062D4		2	PM	4.3	.71	.06	.70	0.	.80
B6426	KRIEGER C	LT039A3		1	PM	4.3	.85	.10	1.01	0.	.82
	IN CURIE	USGS PHOTOGRM			C	4.25	.60	.18	.88	0.	.64
A1431	ARATUS D	LT041B3		1	PM	4.13	.96	.18	.88	0.	.89
A1450	ARATUS C	LT041B3		1	PM	4.13	.88	.10	.75	0.	.88
B2401	TIMOCHARIS E	LT040B4		1	PM	4.10	.84	.13	1.33	0.	.83
A4364	LITTROW BD	42C3S3(50)		1	PM	4.05	.76	.10	1.00	0.	.86
B0374	WALLACE B	LT041D2		1	PM	4.00	.77	.15	1.10	0.	.80
C6300	GASSENDI N	ORBITER 5 MAP		1	C	3.9	.6	.05	0.45	0.	.88
D5030	CENSORINUS	USGS PGM AS10		1	C	3.79	1.039	.15	1.2	0.	.82
B2421	TIMOCHARIS C	LT040B3		1	PM	3.75	.86	.13	1.0	0.	.77
A3403	BESSEL H	LT042A3		1	PM	3.7	.67	.08	1.0	0.	.85
	IN HIRAYAMA	USGS PHOTOGRM		2	C	3.45	.50	.18	.96	0.	.84
B6591	WOLLASTON V	LT038B2		2	PM	3.2	.58	.09	.80	0.	.86
B	UNNAMED	39A1S1(50)			PM	3.18	.58	.10	.90	0.	.85
	WOLLASTON U	LT038B2 IRREG		F	PM	3.1	.50	.02	.10	.0	.68
	PICARD Z	LT062A2		1	PM	3.00	.62	.13	.8	0.	.80
A	LEMONNIER LB	LT042C2		1	PM	2.90	.60	.08	.95	0.	.90
A	CAUCHY CA	61D2S1(50)		1	PM	2.85	.578	.072	1.025	.6	.87
A	ESE DESEILLIGNY	LT042C1		1	PM	2.75	.57	.05	.50	0.	.78
	IN SKLODOWSKA	USGS PHOTOGRM	P	1	C	2.75	.55	.13	.50	0.	.88
	NEAR GAGARIN	USGS PHOTOGRM		1	C	2.75	.63	.18	.85	0.3	.83
C	12D20'S/358D04'E	7703S0(50)			C	2.600	.54	.09	.75	.0	.80
A	LITTROW BB	42C2S1(50)		1	PM	2.60	.50	.08	.85	0.	.88
A1486	LINNE	USGS PHOTOGRM		1	PM	2.45	.60	.13	.65	0.	.89
B	39.6KM SSW WOLLV	USGSMAP 1/100			PM	2.25	.53	.10	.53	0.	.83
B	4.9 KM ESE WOLLU	USGSMAP 1/100			PM	2.03	.40	.08	.64	0.	.86
B	28D30'N/325D42'E	39B2S1(25)	P		PM	2.025	.373	.065	.70	.65	.74
B	N. OF DIOPHANTUS	USGSMAP 1/50M			PM	2.00	.39	.08	.50	0.	.74
B	NW OF KRIEGER C	USGSMAP 1/250			PM	1.96	.35	.05	.44	0.	.83
A	17D32'N/25D55'E	42C3S4(50)			PM	1.95	.370	.040	.775	0.	.80
B	57.8KM SSE WOLLV	USGSMAP 1/100			PM	1.90	.45	.08	.55	0.	.80
B	22.5KM SW WOLLV	USGSMAP 1/100			PM	1.75	.33	.08	.38	0.	.86
	IN SKLODOWSKA	USGS PHOTOGRM		2	C	1.6	.3	.1	.4	0.	.85
B	51.7KM S WOLLV	USGSMAP 1/100			C	1.50	.30	.04	.25	0.	.80
B	NE OF KRIEGER	39A1S1(50)			PM	1.48	.29	.05	.45	0.	.82
A	29D25'N/334D20'E	40A1S1(50)			PM	1.375	.260	.030	.39	0.	.86
B	30D40'N/325D37'E	39B2S2(25)			PM	1.363	.235	.019	.344	0.	.77
A	APOLLO 17 SITE	USGS MAP1/50M			PM	1.30	.20	.03	.30	0.	.85
	SW AS16 SITE-E.	APOLLO PGM			C	1.200	.160	.011	.250	.0	.81
B	12.9 KM SW WOLLV	USGSMAP 1/100			PM	1.15	.35	.05	.23	0.	.73
	NE AS16 SITE	APOLLO PGM			C	1.050	.094	.009	.250	.0	.70
B	23.2 KM E WOLL.V	USGSMAP 1/100			PM	1.03	.23	.04	.30	0.	.77
	KIVA (APOLLO 16)	APOLLO 14 MAP		2	C	1.03	.15	.03	0.28	0.	.72
	SW AS16 SITE-W	APOLLO PGM			C	.95	.14	.007	.160	.0	.71
	PALMETTO AS16	APOLLO PGM			C	.950	.120	.008	.225	.0	.80
B	19.5KM SSE WOLLU	USGSMAP 1/50M			PM	.95	.15	.02	.23	0.	.81
B	60 KM SW WOLL U	USGSMAP 1/50M			PM	.95	.14	.03	.25	0.	.81
	NO.RAY APOLLO 16	APOLLO 14 MAP	P	1	C	.95	.22	.04	.21	0.	.71
	GATOR APOLLO 16	APOLLO 14 MAP		2	C	.95	.14	.04	.28	0.	.77
B	31.3KMSSE WOLL.V	USGSMAP 1/50M			PM	.92	.14	.03	.27	0.	.84
B	24D33'N/329D15'E	39B3S/U(50)			PM	.910	.190	.019	.270	.0	.85
B	24.2KM SE WOLL V	USGS 1/50MMAP			PM	.78	.13	.01	.21	0.	.71
B	28D28'N/325D47'E	39B2S1(25)			PM	.766	.118	.018	.207	0.	.84
B	N. OF DIOPHANTUS	USGSMAP 1/50M			PM	.73	.13	.03	.14	0.	.76
	SO.RAY APOLLO 16	78D1S1(50)		1	C	.70	.13	.03	.19	0.	.81
B	NEAR RIMA PRINZ	USGSMAP 1/50M			PM	.60	.06	.01	.10	0.	.78
B	32.1KM SSE WOLLV	USGSMAP 1/50M			PM	.60	.10	.02	.15	0.	.76
B	25.7KM SSE WOLLU	USGS 1/50MMAP			PM	.60	.10	.02	.18	0.	.73
	NE AS16 SITE	APOLLO PGM			C	.550	.064	.006	.100	.0	.73
A53	50.5KM SSE WOLLU	USGS 1/50MMAP			PM	.53	.10	.02	.16	0.	.77
B	N. OF DIOPHANTUS	USGSMAP 1/50M			PM	.50	.08	.02	.15	0.	.80
B	34.0KM SSW WOLLU	USGS 1/50MMAP			PM	.47	.09	.02	.14	0.	.78
B	24.2KM SSW WOLLU	USGS 1/50MMAP			PM	.40	.07	.02	.15	0.	.82
A	3D29'N/36D46'E	TM-ORBIIS2(2)		2	PM	.064	.007	.002	.008	.0	.76
A	3D26'N/36D45'E	TM-ORBIIS2(2)		2	PM	.048	.005	.001	.008	.0	.75
A	3D28'N/36D46'E	TM-ORBIIS2(2)		2	PM	.042	.005	.001	.008	.0	.66
		SECONDARY-IMPACT CRATERS									
D3123	ZOELLNER	LT078A3/D2	P	4	C	42.75	2.50	.620	8.60	26.0	.53
A7250	GLAISHER C	LT062A1		4	C	35.88	4.13	1.180	8.000	0.	.35
B1024	SCHROETER	SHADOW DATA		4F	AMC	35.	.83	.81	4.	29.	.57
D3087	HYPATIA	LT078B4		3	C	34.50	1.50	1.10	7.50	21.0	.31

TABLE 9.—Continued

I.D.	CRATER	DATA	P	CL	BGD	DIAM.	DEPTH	HT.	WIDTH	FLOOR	CIRC
D0296	VOGEL	SHADOW DATA		2	C	34.00	2.40	.	7.00	15.5	.43
A2054	D'ARREST	LAC 60 (NEW)		3	C	31.5	1.90	.99	6.0	20.0	.58
A7169	LICK B	LTO62A4		4F	C	30.625	.965	.640	4.69	22.50	.40
A7231	GLAISHER E	LTO61B2		3	C	30.25	2.560	.650	8.000	0.	.33
D1149	RITCHEY	LTO77C2	P	3	C	29.00	1.400	.400	6.00	20.0	.43
C0440	PURBACH G	SHADOW DATA		2	C	26.70	1.67	.	.	19.0	.61
C0483	PURBACH H	SHADOW DATA		3	C	26.10	1.35	.	.	15.0	.63
D0308A	LA CAILLE AB	SHADOW DATA		3F	C	24.45	1.33	.	5.50	13.0	.58
A6084	SECCHI	LTO61C4	R	3	C	24.0	1.35	.73	4.0	15.	.58
A2033A	D'ARREST M	LAC 60 (NEW)		4	C	23.50	.900	.750	6.0	15.0	.39
A2286	AUWERS	LTO62A2		3F	C	23.40	1.07	.46	6.2	11.0	.51
D3243	TACITUS D	LAC 78 (NEW)		3	C	22.60	1.275	.375	5.20	8.0	.55
D0133	MUELLER	LTO77B4		3	C	21.63	2.030	.445	6.20	8.0	.59
A2167	JULIUS CAESAR G	LAC 78 (NEW)		4F	C	21.50	1.05	.35	5.75	8.5	.43
D1262	ABULFEDA D	SHADOW DATA		3F	C	21.50	1.63	.665	6.75	13.5	.63
D0167	ALBATEGNIUS B	LTO77C1		2	C	19.00	1.435	.400	3.50	9.0	.53
D5078A	IMBRIUM 2NDARY	LTO79A3		3	C	18.69	.825	.300	5.50	7.0	.35
D0320	PARROT H	SHADOW DATA		3F	C	18.00	1.36	.	.	7.0	.62
D5047	ISIDORUS B (SO.)	LTO79A4		3	C	18.00	1.670	.500	6.500	0.	.51
D1509	KAISER A	SHADOW DATA		2	C	17.35	2.330	.500	.	0.	.43
C0476	PURBACH C	SHADOW DATA		3	C	17.30	1.31	.	.	6.0	.72
D6103	CAPELLA E	LTO79A3		2	C	16.44	1.960	.385	2.675	5.0	.55
D0465	PURBACH B	SHADOW DATA		1	C	16.20	2.250	.600	.	0.	.80
D5182	CAPELLA GA/N	LTO79A3		2	C	16.20	1.750	.306	4.100	0.	.38
D5195	IMBRIUM 2NDARY	LTO79D2		2	C	16.00	1.135	.245	3.250	8.0	.38
D5175	CAPELLA F	LTO79D2		2	C	15.70	1.595	.657	4.600	0.	.63
D0136	ALBATEGNIUS G	LTO77C1		2	C	15.63	1.750	.470	4.700	5.0	.66
D0153	HIPPARCHUS J	LTO77B4		1	C	14.38	2.45	.68	3.3	3.9	.73
D5161	CAPELLA TA	LTO79A4		3	C	14.00	1.465	.423	4.500	0.	.70
A6099	TARUNTIUS L	LTO61C1		2	C	13.250	.750	.350	2.625	8.0	.50
D5097	CAPELLA M	LTO79A3		2F	C	12.75	.80	.08	1.9	6.5	.62
D5089	CAPELLA RA	LTO79A3		3	C	12.000	.838	.075	1.875	0.	.36
D5191	CAPELLA G	LTO79A3		2	C	11.875	.990	.225	1.250	6.25	.68
C1144	PALISSA T	LTO77D1		2	C	11.50	1.819	.440	3.250	0.	.54
D0132	HIPPARCHUS K	LTO77B4		1	C	11.40	2.535	.247	1.810	0.	.80
B7435	HERODOTUS D	LTO38B4		3	C	10.625	.660	.160	2.500	5.80	.36
D0143	MUELLER O	LTO77B4		2	C	10.50	1.690	.200	2.750	0.	.68
D5099	CAPELLA C	LTO79A3		3	C	10.500	.853	.100	2.250	0.	.46
D5049	POSS.IMBR.2NDARY	LTO79A4		3	C	10.500	.714	.225	3.500	0.	.31
	TSIOLKOV. 2ND	LTO66D2	04D50'N/138D30'E			10.50	1.844	.120	1.750	0.	.46
	AITKEN 2NDARY	LTO85C1	08D55'S/162D00'E			10.38	1.745	.200	2.060	0.	.59
	TSIOLKOV 2NDY	LTO66C1	05D35'N/140D10'E			10.16	1.007	.207	2.400	3.60	.57
D5181	CAPELLA CA	LTO79A3		2	C	9.94	1.168	.143	2.030	2.50	.43
D5196	CAPELLA B	LTO79D2		1	C	9.90	1.475	.380	2.560	0.	.63
	TSIOLKOV 2NDY	LTO66A3	08D25'N/138D55'E			8.940	.735	.075	2.000	2.50	.49
D0134	MUELLER A	LTO77C1		2	C	9.69	1.676	.250	3.150	0.	.61
D8037	LANGRENUS 2NDARY	LTO80A3		2	PM	9.625	.688	.235	2.435	0.	.37
D8028	LANGRENUS FB	LTO80A3		1	PM	9.50	1.240	.200	2.500	0.	.42
	TSIOLKOV 2NDY	LTO66C1	06D35'N/143D15'E			8.375	.910	.320	2.300	0.	.46
D8059	LANGRENUS BB	LTO80A3		2	PM	8.315	.836	.130	2.590	0.	.39
	TSIOLKOV. 2ND	LTO66D2	06D00'N/138D55'E			7.88	1.005	.305	2.810	0.	.43
	TSIOLKOV. 2ND	LTO66A3	08D30'N/139D10'E			7.875	.620	.075	1.800	0.	.60
	TSIOLKOV. 2ND	LTO66D2	07D40'N/139D35'E			7.75	.900	.100	1.625	0.	.46
	TSIOLKOV 2NDY	LTO66C1	06D45'N/143D25'E			7.750	.726	.184	2.125	0.	.52
	TSIOLKOV 2NDY	LTO66C1	06D45'N/141D25'E			7.685	.470	.120	1.660	0.	.38
D6101A	CAPELLA DA	LTO79A3		2	C	7.625	.332	.100	1.935	0.	.63
D5170	CAPELLA R	LTO79A3		2	C	7.57	1.040	.363	3.775	0.	.53
	TSIOLKOV. 2ND	LTO66A3	08D35'N/138D55'E			7.000	.419	.069	1.750	0.	.36
D8028A	LANGRENUS 2NDARY	LTO80A3		1	PM	6.375	.725	.100	1.560	0.	.42
D8037A	LANGRENUS 2NDARY	LTO80A3		2	PM	6.280	.846	.150	1.735	0.	.63
	AITKEN 2NDARY	LTO85C1	08D45'S/161D50'E			6.190	.990	.075	1.400	0.	.64
	TSIOLKOV 2NDY	LTO66C1	05D00'N/140D30'E			6.125	.600	.150	1.560	0.	.40
	TSIOLKOV. 2ND	LTO66D2	05D25'N/138D45'E			6.00	1.112	.075	1.750	0.	.72
D8035	LANGRENUS 2NDARY	LTO80A2		2	PM	5.960	.650	.125	1.270	0.	.52
	TSIOLKOV 2NDY	LTO66C1	06D55'N/141D40'E			5.940	.605	.085	1.150	0.	.58
D8027	LANGRENUS FC	LTO80A3		2	PM	5.690	.765	.102	1.700	0.	.43
	AITKEN 2NDARY	LTO85C1	08D37'S/161D20'E			5.560	.780	.185	1.470	0.	.51
	TSIOLKOV. 2ND	LTO66D2	05D10'N/138D38'E			5.310	.400	.075	1.345	0.	.30
D8028C	LANGRENUS 2NDARY	LTO80A3		2	PM	5.190	.665	.100	1.650	0.	.59
D8113	LANGRENUS 2NDARY	LTO80A3		2	PM	5.160	.507	.100	.920	0.	.43
D8045A	LANGRENUS 2NDARY	LTO80A2		2	PM	4.940	.631	.133	1.030	0.	.46
	TSIOLKOV. 2ND	LTO66D2	06D32'N/139D07'E			4.910	.400	.150	1.300	0.	.36
D8028B	LANGRENUS 2NDARY	LTO80A3		2	PM	4.875	.542	.125	1.065	0.	.54
D	LANGRENUS 2ND	LTO80A2	03D20'S/ 58D55'E			4.690	.531	.056	.780	0.	.44
D8038F	LANGRENUS 2NDARY	LTO80A3		2	PM	4.625	.670	.119	1.600	0.	.58

TABLE 9.—Continued

I.D.	CRATER DATA	P CL BGD	DIAM.	DEPTH	HT.	WIDTH	FLOOR	CIRC
D8028D	LANGRENUS 2NDARY LT080A3	2 PM	4.500	.415	.065	1.190	0.	.45
	TSIOLKOV. 2ND LT066D2 06D40'N/139D10'E		4.440	.300	.075	.780	0.	.42
	TSIOLKOV. 2ND LT066D2 07D15'N/139D25'E		4.375	.500	.050	.900	0.	.35
D8057	LANGRENUS 2NDARY LT080A3	3 PM	4.125	.525	.075	1.060	0.	.69
	UNNAMED LT062D4 POSS. SECONDARY		4.0	.530	.075	.500	.0	.38
D	LANGRENUS 2ND LT080A3 04D32'S/ 55D31'E		3.940	.475	.075	1.090	0.	.56
	AITKEN 2NDARY LT085C1 08D33'S/160D25'E		3.750	.626	.100	1.000	0.	.58
	CATENA DAVY 1 SECONDARY USGS AS16 PGM		3.5	.607	.088	.900	.0	.77
D	THEOPHIL. 2ND LT078B3 07D03'S/ 29D16'E		3.440	.300	.	.	0.	.52
	TSIOLKOV. 2ND LT066A3 08D20'N/139D23'E		3.440	.525	.075	1.400	0.	.80
	CATENA DAVY 2 SECONDARY USGS AS16 PGM		3.4	.497	.074	.900	.0	.48
	CATENA DAVY 3 SECONDARY USGS AS16 PGM		3.2	.541	.072	.900	.0	.78
D	THEOPHIL. 2ND LT078B3 07D23'S/ 29D34'E		3.19	.400	.	.	0.	.42
	TSIOLKOV. 2ND LT066A3 08D12'N/139D27'E		3.150	.275	.050	.675	0.	.28
	SECONDARY 100C1S1(50) 25D56'S/102D59'E		3.125	.220	.040	.700	.0	.42
	TSIOLKOV. 2ND LT066D2 07D05'N/139D21'E		3.060	.500	.050	.850	0.	.66
D	THEOPHIL. 2ND LT078B3 07D15'S/ 29D56'E		2.750	.225	.	.	0.	.69
D	THEOPHIL. 2ND LT078B3 06D59'S/ 29D08'E		2.750	.200	.075	.	0.	.44
D	THEOPHIL. 2ND LT078B3 07D13'S/ 29D50'E		2.750	.250	.050	.	0.	.69
D	THEOPHIL. 2ND LT078B3 06D50'S/ 29D10'E		2.66	.300	.075	.	0.	.73
D	THEOPHIL. 2ND LT078B3 07D38'S/ 29D26'E		2.475	.200	.	.	0.	.69
D	THEOPHIL. 2ND LT078B3 07D04'S/ 28D29'E		2.375	.225	.	.	0.	.53
D	THEOPHIL. 2ND LT078B3 06D55'S/ 28D49'E		2.325	.200	.	.	0.	.62
	COPERNICUS SECONDARY 40A4S01(10)1		2.265	.367	.045	.500	.0	.62
B	SECONDARY 39C2S1(50) 20D26'N/328D00'E		2.160	.200	.015	.440	.0	.59
	CATENA DAVY 5 SECONDARY USGS AS16 PGM		2.1	.316	.045	.600	.0	.68
B	COPERN 2ND. 39C2S1(50) 20D27'N/328D00'E		2.100	.193	.015	.750	0.	.56
	CATENA DAVY 7 SECONDARY 77D1S01(10)		1.97	.275	.040	.550	.0	.60
	CATENA DAVY 8 SECONDARY 77D1S01(10)		1.85	.300	.040	.650	.0	.46
	CATENA DAVY 6 SECONDARY USGS AS16 PGM		1.85	.206	.040	.550	.0	.68
B	DIOPHAN 2ND 39B2S0125 28D02'N/326D11'E		1.850	.119	.061	.760	0.	.39
B	EULER 2NDY. 39B3S1(50) 25D18'N/329D42'E		1.740	.270	.015	.500	0.	.73
	CATENA DAVY 4 SECONDARY USGS AS16 PGM		1.7	.195	.050	.500	.0	.79
B	SECONDARY 39C2S1(50) 20D24'N/328D11'E		1.675	.265	.030	.430	.0	.74
B	SECONDARY 41A3S1(50) 25D24'N/359D52'E		1.650	.145	.025	.360	.0	.42
	COPERNICUS SECONDARY 40A4S01(10)3		1.580	.343	.040	.500	.0	.84
	CATENA DAVY 9 SECONDARY 77D1S01(10)		1.50	.180	.030	.500	.0	.34
B	DIOPHAN 2ND 39B2S0125 28D10'N/325D55'E		1.490	.151	.057	.480	0.	.64
	COPERNICUS SECONDARY 40A4S01(10)2		1.410	.218	.040	.350	.0	.58
B	COPERN 2ND. 39C2S1(50) 20D20'N/328D12'E		1.325	.182	.015	.290	0.	.63
B	SECONDARY 39B3S1(50) 25D08'N/329D11'E		1.290	.200	.020	.280	.0	.76
B	COPERN 2ND. 40A1S1(50) 29D45'N/333D38'E		1.175	.149	.022	.300	0.	.65
B	ARISTARCHUS SECONDARY-7 USGS 1/10M MAP		1.120	.109	.023	.240	.0	.36
B	KEPLER 2ND. 39B3S1(50) 25D03'N/328D51'E		1.100	.131	.020	.360	0.	.27
B	COPERN 2ND. 39C2S1(50) 20D55'N/328D08'E		1.100	.119	.020	.425	0.	.76
B	ARISTARCHUS SECONDARY-4 USGS 1/10M MAP		1.045	.077	.039	.225	.0	.49
B	EULER 2NDY. 39B3S1(50) 24D25'N/329D06'E		1.025	.097	.010	.225	0.	.27
B	KEPLER 2ND. 39B3S1(50) 25D13'N/329D02'E		.975	.174	.015	.290	0.	.73
B	COPERN 2ND. 39C2S1(50) 20D57'N/328D20'E		.940	.118	.014	.280	0.	.62
B	ARISTARCHUS SECONDARY-11USGS 1/10M MAP		.930	.076	.026	.235	.0	.44
B	EULER 2NDY. 39B3S1(50) 25D19'N/329D07'E		.890	.102	.010	.230	0.	.75
B	EULER 2NDY. 39B3S1(50) 25D12'N/329D13'E		.875	.155	.015	.260	0.	.80
B	ARISTARCHUS SECONDARY-2 USGS 1/10M MAP		.740	.060	.025	.180	.0	.37
B	ARISTARCHUS SECONDARY-1 USGS 1/10M MAP		.735	.072	.030	.135	.0	.56
B	KEPLER 2ND. 39B3S1(50) 25D12'N/328D34'E		.725	.113	.020	.210	0.	.66
B	EULER 2NDY. 39B3S1(50) 24D21'N/329D01'E		.700	.095	.006	.275	0.	.74
B	KEPLER 2ND. 39B3S1(50) 25D06'N/328D53'E		.675	.131	.020	.235	0.	.74
B	ARISTARCHUS SECONDARY-6 USGS 1/10M MAP		.665	.073	.024	.165	.0	.76
B	ARISTARCHUS SECONDARY-8 USGS 1/10M MAP		.660	.078	.020	.170	.0	.54
B	KEPLER 2ND. 39B3S1(50) 25D15'N/329D04'E		.640	.063	.010	.140	0.	.67
B	ARISTARCHUS SECONDARY-3 USGS 1/10M MAP		.605	.063	.020	.210	.0	.46
B	ARISTARCHUS SECONDARY-5 USGS 1/10M MAP		.550	.066	.022	.175	.0	.60
B	ARISTARCHUS SECONDARY-9 USGS 1/10M MAP		.470	.053	.010	.090	.0	.46
B	ARISTARCHUS SECONDARY-10USGS 1/10M MAP		.445	.060	.015	.113	.0	.61
B	ARISTARCHUS SECONDARY-15 USGS 1/10M MAP		.390	.047	.013	.130	0.	.68
B	ARISTARCHUS SECONDARY-20 USGS 1/10M MAP		.365	.039	.009	.140	0.	.68
B	ARISTARCHUS SECONDARY-16 USGS 1/10M MAP		.355	.030	.010	.150	0.	.54
B	ARISTARCHUS SECONDARY-18 USGS 1/10M MAP		.320	.029	.005	.110	0.	.43
B	ARISTARCHUS SECONDARY-13 USGS 1/10M MAP		.285	.028	.005	.080	0.	.46
B	ARISTARCHUS SECONDARY-14 USGS 1/10M MAP		.265	.027	.005	.070	0.	.59
B	ARISTARCHUS SECONDARY-17 USGS 1/10M MAP		.220	.028	.010	.060	0.	.42
B	ARISTARCHUS SECONDARY-12 USGS 1/10M MAP		.220	.021	.005	.080	0.	.48
B	ARISTARCHUS SECONDARY-19 USGS 1/10M MAP		.210	.027	.008	.065	0.	.78

TABLE 9.—Continued

I.D.	CRATER DATA	P CL BGD	DIAM.	DEPTH	HT.	WIDTH	FLOOR	CIRC
	CRATERED CONES							
B	ARISTARCH.CONE 1 ORBITER 4 SHADOW DATA		1.865	.194	.145	.655	.0	.28
B	ARISTARCH.CONE 2 ORBITER 4 SHADOW DATA		1.505	.136	.116	.523	.0	.41
	LASSELL MJ CONE 15D00'S/10D50'W		1.5	.240	.175	.525	.0	.80
	SERENITAT.CONE 1 18D38'N/27D38'E.42C3S2		.925	.060	.072	.700	.0	.53
B	MARIUS HILLS CONE L.0.4-157 SHADOW DATA		.750	.030	.200	.273	.0	.52
	SERENITAT.CONE 2 18D57'N/27D28'E.42C3S1		0.635	.030	.060	.550	.0	.55
	KING FLOOR CONE NE 5D35'N/120D51'S		.500	.056	.152	.450	.0	.35
	KING FLOOR CONE C. 5D32'N/120D48'E		.488	.050	.147	.430	.0	.48
B	COPERNICUS FLOOR CONE L05-154 SHADOWS		.475	.060	.160	.440	.0	.67
	KING FLOOR CONE SO 5D27'N/120D45'E		.440	.062	.068	.380	.0	.79
	KING FLOOR CONE W. 5D31'N/120D43'E		.330	.038	.145	.510	.0	.54
B	COPERNICUS FLOOR CONE L05-152 SHADOWS		.260	.030	.090	.270	.0	.69
B	COPERNICUS FLOOR CONE L05-153 SHADOWS		.240	.040	.125	.285	.0	.41
B	COPERNICUS FLOOR CONE L05-152 SHADOWS		.120	.015	.055	.180	.0	.65
	DARK-HALO CRATERS							
C	ALPHONSUS KC 77D3S0150 12D52'S/358D23'E		2.550	.376	.050	1.725	.0	.58
C	ALPHONSUS MD 77D3S0150 12D31'S/358D03'E		2.250	.336	.050	.875	.0	.64
C	IN ALPHONSUS 77D3S0150 12D33'S/358D17'E		1.725	.212	.015	.900	.0	.47
	CRATERED DOMES							
B	HERODOTUS OMEGA DOME L04-150 SHADOWS		2.90	.300	.460	5.460	.0	.15
	"D-CRATER" DOME 18D40'N/05D20'E		2.650	.050	.200	6.175	2.25	.54
C	DOME WEST OF KIES L04-125 SHADOWS		1.830	.265	.690	5.590	.0	.71
B	DOME WEST OF MILICHIUS L04-133 SHADOWS		1.730	.165	.260	4.700	.0	.75
A	MARALDI B DOME 2 NW. 61A2S01		1.70	.185	.090	3.4	0.	.49
B	HORTENSIUS PHI DOME L04-133 SHADOWS		1.670	.190	.370	2.260	.0	.66
B	CAUCHY OMEGA DOME L04-225 SHADOW DATA		1.650	.180	.300	4.150	.0	.59
A	MARALDI B DOME 1 SE. 61A2S01		1.60	.070	.130	3.4	0.	.45
B	HORTENSIUS OMEGA DOME L04-133 SHADOWS		1.530	.190	.590	3.240	.0	.71
B	HORTENSIUS SIGMA DOME L04-133 SHADOWS		1.485	.180	.350	2.770	.0	.73
B	RIMA ARIS.B DOME 30D30'N/49D10'W USGS		1.275	.025	.065	2.235	.0	.30
C	DOME W.OF FRA MAURO-S. L04-120 SHADOWS		1.200	.210	.540	1.500	.0	.50
B	MARIUS HILLS DOME L04-157 SHADOW DATA		.950	.120	.270	6.030	.0	.88
C	DOME W.OF FRA MAURO-W. L04-120 SHADOWS		.670	.070	.425	1.070	.0	.65
C	DOME W.OF FRA MAURO-E. L04-120 SHADOWS		.470	.095	.400	1.100	.0	.80

TABLE 10.—*Dimensions of 59 terrestrial craters*

CRATER	DATA		DIAM.	DEPTH	HT.	WIDTH	FLOOR	CIRC
METEORITE-IMPACT CRATERS								
RIESKESSEL	BAVARIA,GER.		22.5	.500	.125	5.0	0.0	.77
EL'GYGTGYN	E. SIBERIA, USSR		18.0	.620	.200	5.0	0.0	.77
LAKE BOSUMPTWI	GHANA		10.42	.400	.135	2.0	0.0	.79
FLYNN CREEK	TENNESSEE,USA		3.600	.225	.075	.500	0.0	.72
NEW QUEBEC	UNGAVA, CAN.		3.44	.415	.152	.610	0.0	.88
ROTER KAMM	NAMIBIA		2.438	.425	.110	.670	0.0	.85
TENOUMER	MAURETANIA		1.920	.329	.100	.300	0.0	.90
LONAR LAKE	INDIA,DECCAN		1.830	.275	.025	.125	0.0	.81
METEOR CRATER	ARIZONA, USA		1.21	.207	.055	.248	0.0	.74
WOLF CREEK	W. AUSTRALIA		.875	.145	.043	.145	0.0	.75
TEMIMICHAT G.	MAURETANIA		.686	.069	.023	.100	0.0	.80
AOUELLOUL	MAURETANIA		.389	.051	.021	.074	0.0	.85
BOXHOLE	NT, AUSTRALIA		.175	.015	.004	.034	0.0	.77
ODESSA-1	TEXAS, USA		.168	.029	.003	.030	0.0	.68
KAALIJARV	ESTONIA		.097	.016	.006	.020	0.0	.80
ILUMETSA-1	ESTONIA		.080	.012	.004	.015	0.0	.78
CAMPO D. CIELO-2	ARGENTINA		.070	.015	.002	.015	0.0	.86
HENBURY-8	NT, AUSTRALIA		.070	.004	.002	.012	0.0	.85
HENBURY-3	NT, AUSTRALIA		.061	.005	.002	.012	0.0	.80
ILUMETSA-2	ESTONIA		.050	.005	.002	.015	0.0	.85
DALGARANGA	W. AUSTRALIA		.025	.005	.001	.006	0.0	.78
ODESSA-2	TEXAS, USA		.021	.005	.001	.006	0.0	.83
SIKHOTE-ALIN-60	SIBERIA,USSR		.010	.002	.0004	.001	0.0	.83
EXPERIMENTAL-EXPLOSION CRATERS								
SEDAN THERMONUCL	NEVADA	1962	.408	.110	.015	.062	0.0	.93
CABRIOLET NUCL	2.3 KT	1968	.135	.047	.012	.027	0.0	.85
LACROSSE THERM.	ENIWETOK	1956	.123	.015	.002	.015	0.0	.85
CACTUS THERMONUC	ENIWETOK	1958	.113	.017	.006	.030	0.0	.89
TEAPOT-ESS NUCL.	NEVADA	1955	.107	.033	.006	.031	0.0	.81
JANGLE-U NUCL.	NEVADA	1951	.091	.019	.0025	.008	0.0	.80
DANNY BOY NUCL.	NEVADA	1962	.085	.026	.007	.028	0.0	.84
JOHNIE BOY NUC	0.5 KT	1963	.045	.0126	.0035	.010	0.0	.86
FAULD (UK)	CHEM.	1944	.243	.033	.006	.061	0.0	.66
SCOOTER TNT	NEVADA	1960	.104	.027	.004	.022	0.0	.75
PRE-SCHOONER-II	NITROMET	1965	.070	.024	.005	.018	0.0	.83
STAGECOACH-3	20-TON	1960	.042	.0109	.0020	.0095	0.0	.82
CINDER LAKE-3	ARIZONA	1967	.041	.003	.0003	.016	0.0	.95
BUCKBOARD-12 TNT	NEVADA	1960	.041	.013	.0027	.010	0.0	.75
PRE-SCHOONER-D	NITROMET	1965	.037	.010	.003	.007	0.0	.79
STAGECOACH-2	20-TON	1960	.036	.0089	.0017	.0075	0.0	.84
DISTANT PLAIN	CANADA	1966	.035	.006	.001	.008	0.0	.84
CINDER LAKE-2	ARIZONA	1967	.035	.003	.0003	.011	0.0	.99
CINDER LAKE-5	ARIZONA	1967	.034	.003	.0004	.009	0.0	.94
BUCKBOARD-11 TNT	NEVADA	1960	.034	.009	.0015	.007	0.0	.78
CINDER LAKE-1	ARIZONA	1967	.033	.002	.0003	.011	0.0	.98
PRE-MINE THROW-4	100-TON/6	'74	.026	.0055	.0011	.007	0.0	.83
CINDER LAKE-4	ARIZONA	1967	.020	.001	.0001	.006	0.0	.90
CHARIOT TNT	ALASKA	1960	.011	.003	.0008	.002	0.0	.79
SANDIA 256-LB-8	TNT	1959	.0095	.0028	.0006	.0024	0.0	.85
SANDIA 256-LB-9	TNT	1959	.0088	.0023	.0004	.0024	0.0	.86
PRE-MINE THROW-4	7.1-TON/3	'73	.0087	.0017	.0002	.002	0.0	.82
SANDIA 256-LB-2	TNT	1959	.0082	.0027	.0004	.004	0.0	.75
EUNGARD CRATER	PENNA.	1970	.0076	.0036	.00078	.0024	0.0	.74
TONOPAH 211-56	0.5 TON	1968	.0075	.0017	.00027	.0021	0.0	.80
TONOPAH 211-52	0.5 TON	1967	.0069	.0015	.0002	.0018	0.0	.81
TONOPAH 211-40	64 LBTNT	1966	.0051	.0015	.00023	.0021	0.0	.83
TONOPAH 211-51	64 LBTNT	1967	.0026	.0006	.00010	.00058	.0	.78
TONOPAH 211-53	64 LBTNT	1968	.0024	.0006	.00011	.00055	.0	.85
TULALIP W2.5B	TNT	1964	.0014	.0002	.00005	.0002	0.0	.82
TULALIP D2A-E	TNT	1964	.0013	.0001	.00002	.0003	0.0	.83